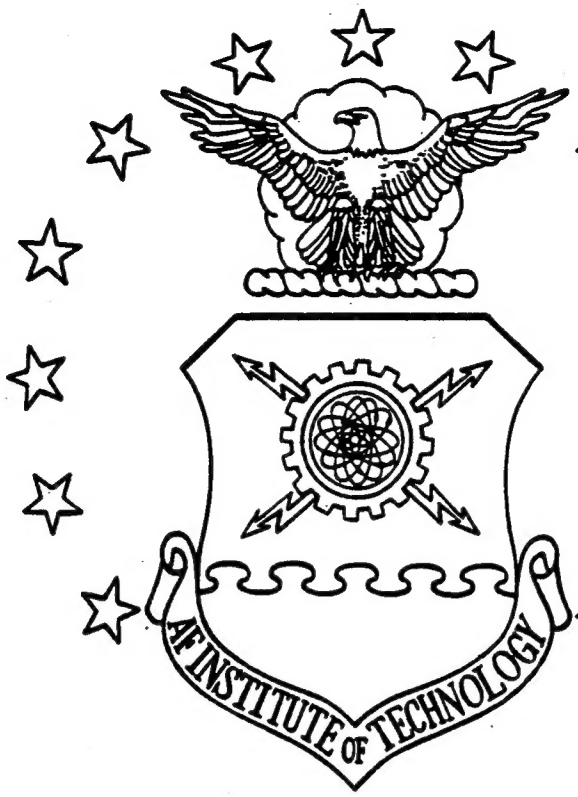

COMPRESSIBLE TURBULENCE MEASUREMENTS IN A SUPERSONIC FLOW WITH ADVERSE PRESSURE GRADIENT

THESIS

Jon William Dotter
Second Lieutenant, USAF

AFIT/GAE/ENY/94D

DEPARTMENT OF THE AIR FORCE
AIR UNIVERSITY
AIR FORCE INSTITUTE OF TECHNOLOGY

Wright-Patterson Air Force Base, Ohio

AFIT/GAE/ENY/94D-10

COMPRESSIBLE TURBULENCE MEASUREMENTS IN A SUPERSONIC FLOW WITH ADVERSE PRESSURE GRADIENT

THESIS
Jon William Dotter
Second Lieutenant, USAF

AFIT/GAE/ENY/94D

Approved for public release; distribution unlimited

The views expressed in this thesis are those of the author and do not reflect the official policy or position of the Department of Defense or the U.S. Government.

AFIT/GAE/ENY/94D-10

COMPRESSIBLE TURBULENCE MEASUREMENTS IN A SUPERSONIC FLOW WITH ADVERSE PRESSURE GRADIENT

THESIS

Presented to the Faculty of the School of Engineering
of the Air Force Institute of Technology
Air University
In Partial Fulfillment of the
Requirements for the Degree of
Master of Science in Aeronautical Engineering

Jon William Dotter, B.S.
Second Lieutenant, USAF

December 1994

Acknowledgments

I would first like to thank my advisor, Dr. Rodney Bowersox, for his support and never-ending patience. Without his open-door policy and willingness to answer my many questions, this work would have never been completed.

I would also like to thank Major Tom Buter for his help on this thesis as well. He was also just as willing to answer my questions and offer guidance. And Capt. Ray Miller, who answered just as many questions.

Most of all I would like to thank my parents and sister for their love and words of encouragement throughout my time in graduate school.

Jon William Dotter

Table of Contents

List of Figures

List of Tables

List of Symbols

a,b	Hot-wire calibration constants
f,g	Hot-wire sensitivities
k	Thermal conductivity
M	Local Mach number
Nu	Nusselt number
P,p	Pressure
Pr	Prandtl number
q	Heat flux
Re	Reynolds number
T	Temperature
u,v,w	Velocity components
x,y,z	Cartesian coordinates
α,β	Functions of Mach number
γ	Ratio of specific heats, Klebanoff intermittency factor
δ	Boundary layer thickness
μ	Viscosity
ρ	Local density
ϕ	Hot-wire incidence angle
τ	Shear stress

Subscripts

e	Effective
n	Normal component
o	Reference condition

T	Turbulent
t	Total condition or tangential component
w	Wire or wall
∞	Infinity

Superscripts

T	Turbulent
( )'	Fluctuating component
$\overline{(\ )}$	Mean component

Abstract

Mean flow and compressible turbulence measurements have been obtained upstream and in the vicinity of a compression ramp in a Mach 3.0 flow ($Re/m \approx 1.5 \times 10^7$). Mean flow data was also acquired for a shock boundary layer (same freestream conditions). Data were collected using conventional Pitot and cone-static probes, single and multiple overheat cross-wire anemometry, and flow visualization techniques (shadowgraphs and schlierens). Direct measurements of the total Reynolds shear stress were obtained using a turbulence transformation. Results indicate that compressibility effects, as evidenced by the density fluctuations, are large relative to the velocity fluctuations and should be rigorously accounted for in new turbulence models. The results also indicate that compressibility also manifests itself in the total Reynolds shear stress, accounting for as much as 75% of the total Reynolds shear.

Compressible Turbulence Measurements in a Supersonic Flow with Adverse Pressure Gradient

I. Background

1.1 Requirement for Turbulence Modeling

It is generally accepted that all of the properties of a turbulent, continuum flow can be described by the solution of the unsteady Navier-Stokes equations [1]. That is, given a computer with sufficient speed and storage capability, a solution of the time-dependent Navier-Stokes equations would yield instantaneous values of the flow properties (u, v, w, P, T, and ρ). Although full aircraft configurations using the Reynolds averaged Navier-Stokes equations and available turbulence models have been made [2], current and next-generation computers have neither the speed nor storage capacity necessary to fully resolve the full-scale turbulent motion that is the goal of direct numerical simulations. The problem arises because turbulent flows are characterized by a range of time and length scales that vary over several orders of magnitude. Based on current trends in computer resources, it will probably be well into the next century before computers posses the speed and memory requirements necessary to calculate turbulent flow properties from first principles (the unsteady, Navier-Stokes equations). And there is some disagreement as to whether or not the smallest turbulent motion will ever be resolved by numerical methods for practical problems [3]. Due to the difficult nature in obtaining instantaneous flow properties over the full range of time and spatial scales associated with turbulent flows, direct solutions of the unsteady, Navier-Stokes equations may be required before the physics of turbulent flow are understood.

As an example, Tannehill et al [3] note that ten grid points are usually required to resolve the motion of the smallest turbulent eddies, and that eddies are normally 10^{-3} times the size of the flow domain. This would require approximately 10^5 grid points to adequately capture the turbulence in just 1 cm^3 of the flowfield. Consider a 10 cm section of a typical airfoil of chord 1m. If only ten turbulent times

scales are required, and assuming a computer speed of 1 nsec/operation, it would take on the order of 200 years (a conservative estimate) to yield a solution of the unsteady, Navier-Stokes! Thus, engineers must rely on approximate methods to provide acceptable solutions that admittedly do not account for all of the physics of turbulent flow.

The two most prevalent approximate methods include the Reynolds-averaged (or time-averaged) Navier-Stokes equations (RANS) and the Favre-averaged (or mass-averaged) Navier-Stokes equations (FANS). Both of these methods will be discussed in greater detail in Chapter 2.

When the Navier-Stokes equations are time-averaged, the number of unknowns outnumber the number of equations, resulting in a closure problem. Turbulence modeling is the process of reducing the number of unknowns to equal the number of equations. In the past, researchers have made judicious use of oftentimes ad hoc assumptions to arrive at turbulence models. These assumptions, which usually are not based on the actual physics of the flow, are known to be rigorously incorrect [4]. While these simplified turbulence models do serve a purpose and have had a degree of success (especially for incompressible flows), they are inaccurate for predictions of compressible flow phenomena such as shock wave/boundary layer interactions, supersonic shear mixing layers, and high-speed attached boundary layers with pressure gradient [4].

1.2 Importance of Accurate Flowfield Predictions For Compressible Flows

In the design of supersonic and hypersonic vehicles, CFD has played and will play an ever-increasing role. A major reason is that wind tunnels and ground facilities do not exist that can simulate the high Mach number and large Reynolds number ranges, coupled with high temperatures, in which future supersonic and hypersonic vehicles will operate [5]. For cases where facilities do exist, testing often proves too expensive or difficult to justify (both economically and politically) when compared to a CFD study of the same problem. With this greater dependence on CFD solutions, the qualitative and quantitative accuracy of all high-speed solutions becomes paramount.

Although not the only limitation to further advances in CFD predictions, turbulence modeling is a crucial one [4]. Since all Navier-Stokes and boundary layer calculations rely on turbulence models for

closure, the accuracy of such predictions depends on how well the turbulence models reflect the actual flow physics. For example, in the case of complex shock/boundary layer interactions, turbulence modeling is a significant pacing issue in further CFD advancements for high-speed flows.

The accurate modeling of shock boundary layer interactions is crucial due to the common occurrence of such phenomena in practical applications in both internal and external aerodynamics. For supersonic and hypersonic vehicles, shock waves are always present. When shock waves interact with boundary layers (such as an engine inlet system, or externally, on a deflected control surface), a strong adverse pressure gradient acts on the boundary layer [6]. This interaction is a complex flow phenomena that is difficult to numerically model. These flows are governed by both elliptic and hyperbolic partial differential equations (with different domains of dependence) with boundary conditions that are just as difficult to determine and impose.

In addition to shock-induced adverse pressure gradients, examples abound where high-speed boundary layers are subjected to adverse pressure gradients that are not strong enough to cause separation. Or the turbulent boundary layer could become reattached further downstream of a shock boundary layer interaction.

1.3 Status of Current Compressible Turbulence Models

In the past, incompressible turbulent boundary layers have received a great deal of attention, especially those with no pressure gradient. Much of the hope of extending incompressible models to compressible flows stems from Morkovin's hypothesis, which was proposed in 1964. Morkovin's hypothesis states that "the turbulence structure is unaffected by compressibility as long as the fluctuation Mach number is much less than unity" [7]. As Liou and Shih (1991) report, extensions to incompressible models have had some success with wall shear layers, but not when applied to flows with adverse pressure gradients, shock waves, and expansion fans [7].

Most current compressible turbulence models, even for flows with pressure gradients, shock waves, and expansion waves, are based on extensions to incompressible models. Effective-viscosity models (mixing length and eddy viscosity) are a common choice for compressible Navier-Stokes calculations. But

they are also inadequate for shock boundary layer interactions [8], and are not valid for adverse pressure gradient flows [9,10].

In addition to algebraic models, much of the turbulence modeling community uses the two-equation κ-ε model as the foundation for complex turbulent flow calculations [9]. But it has been known for quite some time that κ-ε models are very inaccurate for flows with adverse pressure gradients [9]. Many researchers have employed what basically amounts to ad hoc extensions (adjusting constants, adding "compressibility" terms, and allowing density to vary) with limited success. But, as Clauser writes, these corrections "do little more than correlate the set of data on which they were originally based" [11].

Marvin (1982) used a Reynolds stress model for a Mach 2.3 flow with adverse and favorable pressure gradients [12]. The correct trends were predicted, but the effect of the pressure gradients was overestimated. As with the algebraic and two-equation turbulence models, the Reynolds stress turbulence models suffer from a lack of experimental data.

Until recently, there has been little research that attacks compressibility directly. Also, as Liou and Shih mention, there is still no consensus regarding which terms in either the RANS or the FANS that compressibility manifests itself [7]. At the crux of the compressible turbulence modeling problem lies the lack of quality compressible turbulence data for use in validating CFD codes and developing compressible turbulence models.

1.4 Need For Compressible Turbulence Data

The development of a new turbulence model is a long process that involves significant intellectual effort, experience, and creative genius. Although primarily a theoretical problem, some insight can be gleaned from data from simple experiments. This was recognized over twenty years ago by Tennekes and Lumley when they commented that "one must be willing to use (and capable of using) simple physical concepts based on experience to bridge the gap between the equations and actual flows" [13]. But even today there is still a lack of compressible turbulence data of sufficient quality to validate CFD codes and guide the development of improved turbulence models.

There have been hundreds of experiments which have considered compressible turbulent flows. But most of these pre-1970 experiments only reported mean flow results [4]. And for most of the experiments that reported turbulence measurements, the results have been of questionable quality [15]. A few researchers have made compressible turbulence measurements in supersonic, turbulent boundary layers, including Waltrup and Schetz [32], and Sturek and Danberg [33]. But these experiments were conducted in the 1970s, without the benefit of recent hot-wire anemometry and data reduction developments.

In order for turbulence measurements to be useful to the turbulence modeler, they must be of sufficient quality to validate CFD codes and offer guidance for new models. This means that experimental geometries must be simple enough so that they can be modeled accurately without undue difficulty [4]. In other words, there is still a need for "building-block" experiments. In addition, compressible turbulence studies should provide an initial plane of data, consisting of both mean flow and turbulence quantities, to provide CFD codes with a reference starting point. A recent search of available supersonic and hypersonic compressible turbulence data ($M_\infty \geq 3.0$) revealed that only nineteen experiments were found to be of sufficient quality to validate CFD codes and guide new turbulence model development [4].

In particular, the available experimental data for Reynolds stress are extremely scarce. In compressible thin layer type flows, the largest stress component takes on the following form [12]:

$$\tau_{xy}^{T} = -\overline{\rho}\,\overline{u'v'} - \overline{u}\,\overline{\rho'v'} - \overline{v}\,\overline{\rho'u'} - \overline{\rho'u'v'} \tag{1.1}$$

The last term in (1.1) can be safely neglected--it is a triple correlation and is usually very small [12]. For thin layer type flows (e.g. boundary layers), $\overline{v}$ is small compared to $\overline{u}$; thus the third term on the right-hand side can usually be neglected. But most researchers also neglect the second term on the right-hand side of (1.1), which is harder to justify. Very little data exists to justify neglecting this term.

1.5 Scope of Present Study

The present study proposes to expand the understanding of supersonic, adverse pressure gradient shock boundary layer interactions by obtaining compressible turbulence data prior to, in, and aft of a shock

boundary layer interaction and a compression ramp. These data will provide a better understanding of which terms in the RANS are important for compressible flows, which may lead to a better understanding of the physics associated with these flows. Also, the data are intended to validate existing CFD codes and may lead to improved compressible turbulence modeling.

1.6 Document Roadmap

Chapter 2 reviews the governing equations for turbulent flow and presents them in a format that is experimentally convenient. Chapter 3 describes the wind tunnel facilities and instrumentation, as well as the factors affecting the model design and fabrication. Chapter 4 contains the data reduction techniques used to arrive at the compressible turbulence measurements, which are presented in Chapter 5. Conclusions and recommendations for further study are presented in Chapter 6. The results are presented in tabular form in Appendix A.

II. Equation Development

This chapter begins by presenting the unsteady Navier-Stokes equations. Since a closed-form solution of the exact equations is not yet possible, the two most common averaging techniques ("Reynolds", or time averaged, Navier-Stokes [RANS] equations and the Favre, or mass averaged Navier-Stokes [FANS] equations) are briefly presented and their applicability to the flows of this study discussed. Finally, a turbulence transformation is applied to the RANS to present them in an experimentally convenient form.

2.1 Compressible Navier-Stokes Equations

As a starting point to the development of the equations relevant to turbulent flow, the compressible, Navier-Stokes equations are given below for a Cartesian coordinate system (in conservative form):

$$\frac{\partial \rho}{\partial t}+\frac{\partial}{\partial x_j}\left(\rho u_j\right)=0 \tag{2.1}$$

$$\frac{\partial}{\partial t}\left(\rho u_i\right)+\frac{\partial}{\partial x_j}\left(\rho u_i u_j\right)=-\frac{\partial P}{\partial x_i}+\frac{\partial}{\partial x_j}\left(\tau_{ij}\right) \tag{2.2}$$

$$\frac{\partial}{\partial t}\left(\rho h_o\right)+\frac{\partial}{\partial x_j}\left(\rho u_j h_o\right)=\frac{\partial P}{\partial t}+\frac{\partial}{\partial x_j}\left(u\tau_{ij}-q_j\right) \tag{2.3}$$

where

$$h_o=h+\frac{1}{2}u_i u_i \tag{2.4}$$

$$\tau_{ij}=\mu\left(\frac{\partial u_i}{\partial x_j}+\frac{\partial u_j}{\partial x_i}\right)+\delta_{ij}\lambda\frac{\partial u_k}{\partial x_k} \tag{2.5}$$

$$q_j=-k\frac{\partial T}{\partial x_j}\,. \tag{2.6}$$

$$\lambda = -\frac{2}{3}\mu \quad \text{(bulk viscosity)} \tag{2.7}$$

As discussed in Chapter 1, the solution of the unsteady, Navier-Stokes equations, for problems of engineering interest, are not yet obtainable. Therefore, approximate (average) methods must be relied upon. One of the most prevalent averaging techniques leads to the RANS equations.

2.2 *Reynolds-Averaged Navier-Stokes (RANS) Equations*

A standard procedure for analyzing turbulent flows is to separate the instantaneous flow properties into a mean and fluctuating component. The instantaneous flow properties then become

$$\begin{aligned} u_i &= \overline{u_i} + u_i' & h_o &= \overline{h_o} + h_o' \\ P &= \overline{P} + P' & q_i &= \overline{q_i} + q_i' \\ \rho &= \overline{\rho} + \rho' & \tau_{ij} &= \overline{\tau_{ij}} + \tau_{ij}' \end{aligned} \tag{2.7}$$

The overbar values represent the mean flow quantities obtained by time-averaging over a period that must be both longer then the period of the longest fluctuation but shorter than any period of unsteadiness of the flow, and the prime values which represent deviations from the average values [16]. The flow variables are time-averaged in the following manner

$$\overline{u} = \int_{0}^{t_o+T} u(x,y,z,t)\, dt. \tag{2.8}$$

When the mean and fluctuating components (2.7) are substituted into the governing equations (2.1) - (2.3), and the rules of time-averaging applied, the RANS equations result

$$\frac{\partial \overline{\rho}}{\partial t} + \frac{\partial}{\partial x_j}\left(\overline{\rho u_j} + \overline{\rho' u_j'}\right) = 0 \tag{2.9}$$

$$\frac{\partial}{\partial t}\left(\overline{\rho}\,\overline{u_i} + \overline{\rho' u_i'}\right) + \frac{\partial}{\partial x_j}\left(\overline{\rho}\,\overline{u_i}\,\overline{u_j}\right) = -\frac{\partial \overline{P}}{\partial x_i} + \frac{\partial}{\partial x_j}\left(\tau_{ij} + \tau_{ij}^{T}\right) \tag{2.10}$$

$$\frac{\partial}{\partial t}\left(\overline{\rho}\,\overline{e_o} + \overline{\rho' h_o'}\right) + \frac{\partial}{\partial x_j}\left(\overline{\rho}\,\overline{h_o}\,\overline{u_j}\right) = -\frac{\partial}{\partial x_j}\left(\overline{u_i}\,\overline{\tau_{ij}} + \overline{u_i'\tau_{ij}'} - q_j - q_j^{T}\right). \tag{2.11}$$

The compressible terms in (2.9)-(2.11) can be written as

$$m_i^T = -\overline{\rho' u_i'} \tag{2.12}$$

$$\tau_{ij}^T = -\bar{\rho}\,\overline{u_i' u_j'} - \bar{u}_i\,\overline{\rho' u_j'} - \bar{u}_j\,\overline{\rho' u_i'} - \overline{\rho' u_i' u_j'} \tag{2.13}$$

$$q_i^T = \bar{\rho}\,\overline{h_o' u_i'} + \bar{h}_o\,\overline{\rho' u_i'} + \bar{u}_i\,\overline{\rho' h_o'} + \overline{\rho' h_o' u_i'} \tag{2.14}$$

where m^T is the turbulent apparent mass, τ^T is the turbulent compressible shear, and q^T is the turbulent compressible heat flux. It should be noted that the averaging process eliminates several important characteristics of the turbulent flow, including the frequency, phase, and wavelength [17].

For incompressible flows, the apparent mass is zero, as well as the last three terms in (2.13) and (2.14). It is now easier to understand why extensions of incompressible turbulence models to compressible flows have met with little success. Compressibility terms are included in each of the continuity, momentum, and energy equations (2.9) - (2.11). By not including these terms in compressible turbulence models, significant flowfield physics are neglected, or at least not accounted for in a rigorous, complete manner. A major goal of this study is to determine the relative importance of the terms of the right-hand side of (2.13) and (2.14) for supersonic, turbulent boundary layers with adverse pressure gradients.

2.3 Favre-Averaged Navier-Stokes Equations

A second averaging technique is the mass (or Favre) averaged Navier-Stokes equations. The detailed description of the FANS development can be found in Ref. [19]. As a result of Favre-averaging, moments of the density fluctuation are eliminated and the FANS bear a close resemblance to the incompressible RANS, with no explicit density-velocity correlation [17]. Researchers have found that the application of the FANS to compressible flows, using extensions to incompressible turbulence models, has had some degree of success with wall shear layers, but has failed when applied to free shear layers and in the presence of shock, compression, and expansions waves [17].

Because this study includes shocks and compression waves, limited compressible turbulence measurements will be obtained for terms within the FANS. But compressible turbulence measurements will be obtained for the complete Reynolds averaged form.

2.4 Turbulence Transformation

As mentioned above, the complete compressible Reynolds averaged equations (2.12) - (2.14) will primarily be considered in this experiment. The terms on the right-hand side of (2.12) - (2.14), though, cannot be directly measured. Therefore, a turbulence transformation must be used. This section presents a method developed by Bowersox [18].

The transformation begins by using the following identity

$$\rho\,\phi = \left(\overline{\rho\,\phi}\right) + \left(\rho\,\phi\right)' \tag{2.15}$$

$$\rho\,\phi = \left(\overline{\rho} + \rho'\right)\left(\overline{\phi} + \phi'\right) \tag{2.16}$$

where ϕ is a generic variable. Equating the right-hand sides of (2.15) and (2.16) yields the following relationship

$$\overline{\rho\,\phi} + \left(\rho\,\phi\right)' = \left(\overline{\rho} + \rho'\right)\left(\overline{\phi} + \phi'\right) \tag{2.17}$$

When (2.17) is time averaged, the following results

$$\overline{\rho\,\phi} = \overline{\rho}\,\overline{\phi} + \overline{\rho'\,\phi'}, \tag{2.18}$$

a preliminary step in the FANS development [18]. The next step is to subtract (2.18) from (2.17), resulting in the following fluctuation relation

$$\left(\rho\,\phi\right)' = \overline{\rho}\,\phi' + \overline{\phi}\,\rho' + \left(\rho'\,\phi' - \overline{\rho'\,\phi'}\right). \tag{2.19}$$

When $\phi = u_i$ and $\phi = u_j$ are substituted into (2.19) and the products of $\left(\rho\,u_i\right)'$ with $\left(\rho\,u_j\right)'$ are formed, the terms appearing in the Reynolds shear (2.13) can be collected on one side of the equation to yield the following Reynolds shear transformation

$$\tau_{ij}^{T} = -\frac{\overline{\left(\rho\,u_i\right)'\left(\rho\,u_j\right)'}}{\overline{\rho}} + \overline{\rho}\,\overline{u_i}\,\overline{u_j}\left(\frac{\rho'}{\overline{\rho}}\right)^2, \tag{2.20}$$

where the triple correlation term $\overline{\rho' u_i' u_j'}$ and fourth order terms have been neglected. By a similar process, it can be shown [18] that the Reynolds heat flux terms are equal to the following

$$q_i^T = \overline{(\rho u_i)' h_o'} + \overline{h_o}\,\overline{\rho' u_i'} \tag{2.21}$$

All of the terms appearing in (2.20) and (2.21) can be measured directly or estimated by separating cross-wire variables [18]. This process will be presented in further detail in Chapter 4.

III. Facilities and Instrumentation

This chapter describes the experimental facilities and instrumentation used for the present study. The AFIT Mach 3.0 (6.35 cm x 6.35 cm test section) pressure-vacuum wind tunnel and test section models will be discussed, as well as the equipment and configuration for flow visualization. Also, the instrumentation and data acquisition procedures will be discussed for both the mean flow data and the turbulence (hot-wire) data.

3.1 Experimental Facility

The present experimental work was conducted in the AFIT Mach 3.0 pressure-vacuum wind tunnel. This section describes the wind tunnel facilities and flow visualization configurations.

3.1.1 Supersonic Wind Tunnel

The wind tunnel is a pressure-vacuum facility. The tunnel currently has a Mach 3.0 nozzle section and a variable area diffuser section. The 0.69 MPa air pressure was provided by two Atlas Copco GAU 807 air compressors at a mass flow rate of 0.5 kg/s. The air was dried by two Pioneer Refrigerant Air Dryers. Three 7.5 hp, 230 V Stokes MicroVac Pumps provided a vacuum, typically around 14 mm of mercury (approximately 0.27 atm) at the beginning of each run. The pressure-vacuum system provided run times of approximately twenty seconds.

The settling chamber contains a flow straightener, a Pitot pressure probe, and a thermocouple. The thermocouple used to monitor $T_{t\infty}$ was an Omega Engineering, Inc., Type K (chromel-alumel) thermocouple, constructed of Type 316 stainless steel, with a 3.18 mm diameter probe [19]. An Endevco 0-100 psig pressure transducer, connected to a Pitot probe in the settling chamber, monitored the stagnation pressure.

3.1.2 Shadowgraph Configuration

Shadowgraphs were taken of both the compression ramp model (CRM) and the wedge model. The light source was a Cordin Model 5401 arc light, whose spark provided an exposure time of 600 nanoseconds. The light source was powered by a Cordin Model 5205 power supply that was set to approximately 5000 V dc for all of the shadowgraphs and schlierens. A 100 cm focal length mirror was used to collimate the light into a beam and to aim the light through the test section. Polaroid Type 52 film was used for both the shadowgraphs and schlierens.

3.1.3 Schlieren Configuration

Schlierens were also taken of both the CRM and the wedge model. The same light source, power supply, mirrors, and film were used to take the schlierens. The configuration was essentially the same as the shadowgraph configuration, except that the collimated light beam, after passing through the test section, was bounced off another 100 cm focal length mirror and partially obstructed with a knife edge before it reached the exposed film.

3.2 Test Section Models

As discussed in Chapter 1, the purpose of this study was to obtain supersonic compressible turbulence measurements in flows with adverse pressure gradients. In order to do this, two models were designed and fabricated: a compression ramp model and a wedge model.

3.2.1 Compression Ramp Design Considerations

The design of the compression ramp model (CRM) centered around two primary issues. The first consideration was to produce an adverse pressure gradient that was mild enough to allow the boundary layer to remain attached. Since the purpose of the present study was to obtain compressible turbulence measurements for basic, building-block configurations, unseparated boundary layers were desired. Separation adds a much higher level of complexity, both experimentally and numerically, even for simple geometries.

The second consideration was to create an adverse pressure gradient without a shock wave (within the boundary layer). The CRM was, therefore, designed so that the shock wave, formed by the coalescing of compression waves, formed outside the boundary layer.

3.2.2 Compression Ramp Model Design

The cross-sectional area of the CRM was fixed by the wind tunnel nozzle exit geometry (6.35 cm x 6.35 cm cross-section). The length of the model was somewhat arbitrarily chosen at 33.02 cm (13.0 inches) and involved coordinating between other users of the wind tunnel for ease of exchanging test section models. To minimize blockage effects, the height of the CRM was set at 6.35 mm, or 10% of the test section height. The CRM was designed to be symmetric about the midplane for ease of manufacturing. A cubic polynomial was generated from the four boundary conditions. A curve fit of the actual (machined) coordinates is given by

$$h(x)=\begin{Bmatrix} 0, & x\in[0,5.08] \\ a_0+a_1x+a_2x^2+a_3x^3, & x\in[5.08,13.081] \\ 0.335, & x\in[13.081,16.51] \end{Bmatrix} \tag{3.1}$$

where $a_0 = 1.1858$, $a_1 = -0.541019$, $a_2 = 0.0747755$, $a_3 = -0.0028$ and all dimensions are cm. Eqn (3.1) is valid for the first half of the model; the model is symmetric about the midplane. The CRM was machined out of standard aluminum, and the probe location was approximately 71 cm downstream of the nozzle throat, or 11.113 cm from the front edge of the test section. See Fig. 3.1 below for a schematic of the CRM.

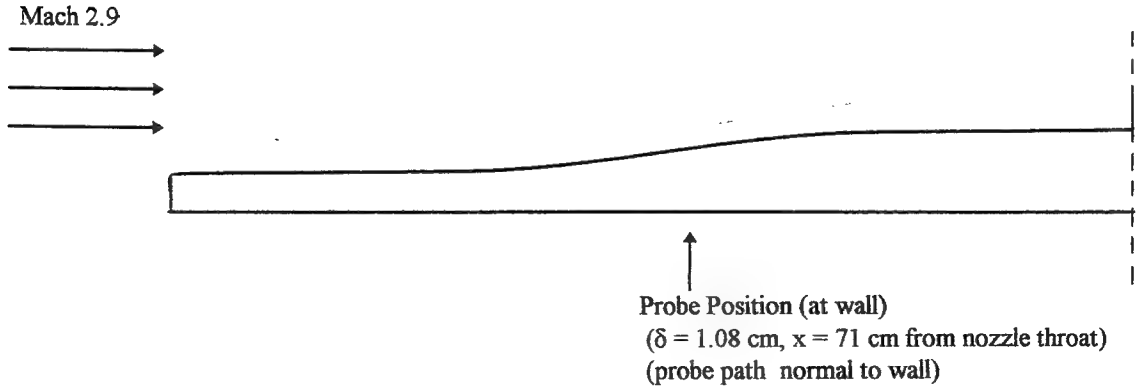

Figure 3.1: Schematic of Compression Ramp Model

3.2.3 Shock Boundary Layer Model

The design of the shock boundary layer wedge model was driven by two factors. The first design consideration was to create a shock wave that would be within the boundary layer. Using a wedge that spanned the test section would provide a strong enough initial oblique shock wave, and several reflected shock waves, behind which turbulence measurements could be made.

The second design consideration involved the specification of the wedge angle. This angle dictates the strength of the shock wave and the downstream Mach number. The downstream Mach number is important because the present cross-wire anemometry techniques require that the Mach number be greater than approximately 1.4 [19].

3.2.4 Shock Boundary Layer Model Design

Using normal/oblique shock relations [21], for $M_\infty = 3.0$ and a flow turning angle of 10°, the Mach number behind the initial and reflected shocks is approximately 2.09 (see Fig. 3.2). It is contended that a freestream Mach number of approximately two is large enough to keep the Mach number above 1.4 at the lowest point in the boundary layer measured in this study ($y/\delta \approx 0.1$). Therefore, a 10° symmetric wedge was used. The height of the wedge was designed to be the same as the maximum thickness as the compression ramp, or 6.35 mm.

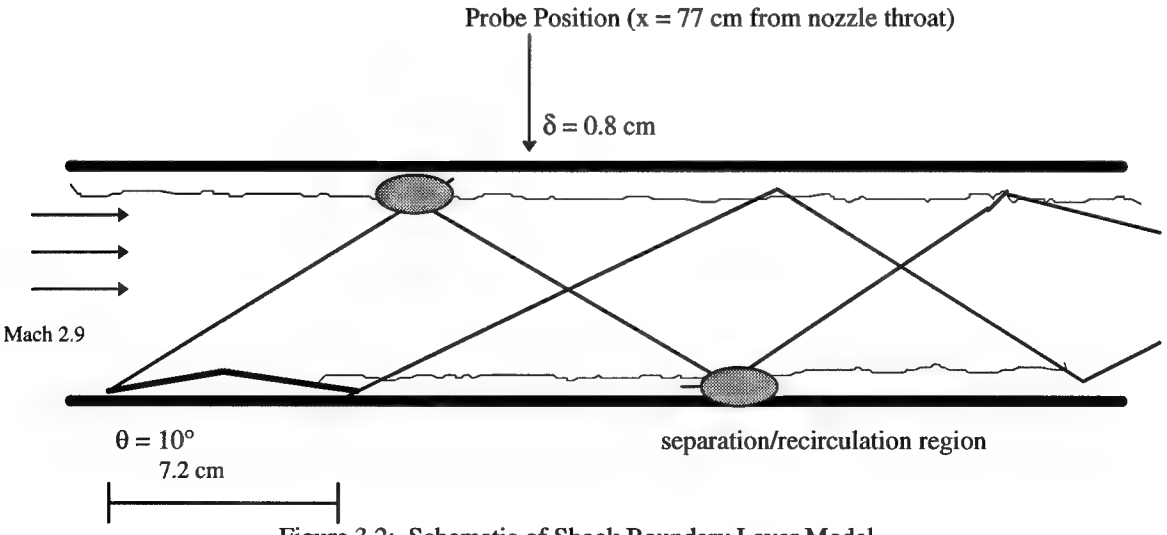

Figure 3.2: Schematic of Shock Boundary Layer Model

3.3 Mean Flow Instrumentation

The supersonic wind tunnel was manually operated. First, the valve between the tunnel and the sixteen vacuum tanks was opened, and then the 0.69 MPa air valve was opened. The tunnel configuration allowed for approximately 20-25 second run times. When turning the tunnel off, the air was turned off, then the vacuum valve was closed. Two computers were used: a Compaq 386 for data acquisition, and Zenith 286 to operate the traversing system.

3.3.1 Settling Chamber

The total pressure in the settling chamber was monitored by an Endevco 0-100 psig pressure transducer. The total pressure was roughly 2 atm for all runs and was recorded by the data acquisition system. For all runs, the upstream total pressure was used to trigger the data acquisition system (DAS) to acquire data on all channels. The total pressure was monitored and controlled with a feedback system consisting of a Fairchild pneumatic pressure regulator and a Leslie pressure reducing valve.

The total temperature in the settling chamber was monitored with an Omega Engineering, Inc., Type K thermocouple. The signal was not recorded by the DAS because the total temperature did not vary appreciably during runs (maximum variation in Tt_∞ was +/- 1 K).

3.3.2 Traverse and LVDT System

The traverse consisted of an Arrick Robotics MD-2 dual stepper motor driver package and a Size 23 Stepper Motor. The maximum speed of the stepper motor was 0.254 cm/sec. The position of the traverse was monitored by a Trans•Tek Incorp. Model 0217 linear voltage displacement transducer (LVDT). The range of the LVDT was +/- 2.54 cm from zero, with a maximum usable range of +/- 3.68 inches. The signal was recorded by the DAS.

3.3.3 Data Acquisition System

The mean flow data were recorded by the Nicolet MultiPro 120 Digitizer [22]. The Nicolet system, coupled with a personal computer, allowed four channels of data to be recorded simultaneously. For mean flow data, the sampling rate was set to 200 Hz.

3.3.4 Filters and Signal Conditioners

Before any mean flow signal was acquired by the DAS, it was conditioned, filtered, and amplified. All signals from the pressure transducers were sent through Endevco Model 4423 Signal Conditioners that filtered high-frequency noise, amplified the signal to the ranges of the Nicolet, and supplied the excitation voltage to the transducers. The signal to the LVDT passed through a Trans•Tek Model 1000-0012 oscillator/demodulator that provided excitation voltage, filtered any high-frequency noise, and converted the output to DC volts.

3.3.5 Downstream Pressure Probes

A conventional Pitot probe and a 10° cone-static probe were used in the present study. The Pitot probe was constructed from stainless steel tubing. The outer diameter of the tube was 1.59 mm. The Pitot tube was inserted in a 6.35 mm stainless steel tube for reinforcement. However, preliminary mean flow results for the wedge model indicated that the 6.35 mm thick outer casing was large enough to unstart wind tunnel. The outer casing was reduced to 3.175 mm, and no unstarting was observed. An Endevco 0-15 psig transducer was used to record the downstream Pitot pressure, and the signal was conditioned by the same Endevco signal conditioner as the upstream total pressure.

The cone-static probe consisted of a small 10° semivertex angle axisymmetric cone. The cone tip was machined from stainless steel and has four 0.34 mm pressure taps located 4.3 mm from the tip at 90° intervals around the circumference. The four pressure taps led to a common chamber where any errors, due to misalignment (up to 7°), were averaged out [23]. The cone-static probe was connected to similar 1.59 mm tubing, and was housed in 3.175 mm outer diameter tubing. The pressure was monitored by the same

pressure transducer as the downstream Pitot pressure, and the signal conditioned by the same Endevco signal conditioner.

3.4 Hot-Wire Instrumentation

The data acquisition was almost identical for the hot-wire data as with the mean flow. The total pressure, total temperature, and traverse locations were monitored and/or recorded in the manner discussed for the mean flow. The cross-wires and multiple overheat scanning circuitry, however, increased the complexity of the data acquisition process.

3.4.1 Nicolet Configuration

Four channels were used to acquire upstream total pressure, traverse/LVDT location, and cross-wire voltage data. For total pressure and cross-wire voltages, a sampling rate of 10 kHz was chosen. For the LVDT, the sampling rate was left at 200 Hz to save hard disk space.

3.4.2 Cross-Wire Probes

For the present study, TSI Incorporated, Model 1243-20, platinum hot film probes were used [24]. The length of each wire was 1 mm and the diameter 51 μm, and the temperature coefficient of resistance 0.24%/°C at 20° C (assumed constant for the temperature ranges encountered in this study). Model 1243-20 probes were used to acquire uv turbulence data, and Model 1243AN-20 probes were used to acquire uw turbulence data. The two different models of probes were identical, except in wire orientation.

3.4.3 Anemometer

The TSI Incorporated IFA 100 System Intelligent Flow Analyzer, constant temperature anemometer was used for the present study [25]. The IFA 100 consisted of the Model 150 anemometer, Model 157 Signal Conditioner, and transducers. The Model 158 master cabinet housed and provided power to the four channels of transducers and signal conditioners. The IFA 100 system symmetrical bridge had a top resistance of 50 Ω (R_s) and allowed an external bridge arm to fix the overheat ratio. The overheat

resistor was externally supplied, either by a 10 Ω resistor (plus 0.4 Ω cable resistance) or the overheat scanning circuit, described next.

3.4.4 Overheat Scanning Circuit

A minimum of three wire temperatures are required to obtain accurate results in supersonic flows. The overheat ratio can either be changed manually or electronically through a scanning circuit. In order to conserve time and reduce the risk of cross-wires breaking, the scanning circuit method was used. Circuitry similar to that used by Bowersox [18] was also used in this study.

The scanning circuit is presented in much greater detail in [26]. For this study, eight overheat ratios were used in the data acquisition process. However, only the six highest overheat ratios were used in the data reduction process (see Chapter 5). Data were acquired at each overheat for 0.3 seconds. The scanning circuit was triggered to scan through the eight overheats by a signal from the stepper motor driver package. When the stepper motor stopped, a signal was sent to the scanning circuit to rapidly scan through the number of overheat resistors. Data were acquired for five y/δ locations in the flowfield. The overheat operating resistances used for this study are given below:

Table 3.1 Multiple Overheat Operating Resistances

Overheat Number	Resistance (Ω)
1	10.40
2	9.92
3	9.49
4	9.05
5	8.75
6	8.58
7	7.90
8	7.54

3.5 Computational Facilities

Data reduction was accomplished with various personal computers and AFIT's Sun Sparc 20 work stations. All plots were generated using PLOTTER [27].

IV. Data Reduction Techniques

This chapter presents the data reduction techniques used in this study. The mean flow data reduction process is described first. The cross-wire data reduction process, for both single and multiple overheat ratios, is then presented.

4.1 Mean Flow

Mean flow data were recorded for the upstream Pitot pressure (P_{t1}) and total temperature (T_{t1}), as well as the downstream Pitot pressure (P_{t2}) and cone-static (p_c) profiles for the wedge and compression ramp test sections. The Mach number was calculated using the ratio of cone-static to downstream Pitot pressure, p_c/P_{t2}. This ratio is a function of Mach number and can be obtained from the exact solution of the asymmetric flow over a cone. For the 10° cone-static probe used in this study, the following least-squares curve fit of the Mach number vs. pressure ratio was used [18]

$$\frac{1}{M} = -0.052976 + 4.6840x - 18.6786x^2 + 50.7006x^3 - 54.1577x^4 \qquad (4.1)$$

where $x = p_c/P_{t2}$. Equation (4.1) is valid for Mach numbers between 1.5 and 4.4, and the standard deviation for this curve fit is 0.06%. For all locations and test sections, the geometry of the traverse Pitot probe allowed measurements to be obtained closer to the wall than the cone-static probe. In order to calculate the Mach number for these traverse Pitot pressure points, the static pressure was assumed to be constant and equal to the freestream static pressure. The Rayleigh-Pitot formula was then used to solve for the Mach number for the last two or three data points closest to the wall [21]. The remaining mean flow quantities were calculated using the normal perfect gas relations, including a few subsonic points in the shock boundary interaction [21].

4.2 Turbulent Flow

The data reduction methods for the fluctuating component of the flowfield is considerably more difficult than the mean flow component. This section presents the methods used for the cross-wire anemometry in this study, including both single and multiple overheat ratios.

4.2.1 General Theory

For turbulent compressible flow, the Nusselt number of a cylinder (hot-film probe) has the following functional relationship [28]

$$Nu = Nu\ (L/d, M, Pr, Re_e, \tau) \tag{4.2}$$

where L/d is the wire aspect ratio, M is the Mach number, Pr is the Prandtl number, Re_e is the effective Reynolds number based on wire diameter, and τ is the temperature loading factor [$\tau = (T_w\text{-}T_e)/T_t$]. T_w is the wire temperature, and T_e is the equilibrium temperature the wire would obtain if placed unheated in the flow. If the flow to be studied satisfies a number of conditions, (4.2) reduces to the following

$$Nu = Nu\ (Re_e, \tau). \tag{4.3}$$

Eqn (4.3) is restricted to high Reynolds number (Re > 20), constant Prandtl number flows where the Mach number normal to the wire is greater than approximately 1.2, and where the wire aspect ratio is large (L/d >> 1) [28]. For wires normal to the flow, hot-wire data has been found to collapse onto the following curve

$$Nu = a\sqrt{Re} + b \tag{4.4}$$

When using (4.4), the hot-wire must be calibrated at each wire temperature.

The Nusselt number is also proportional to the power supplied to the wire (q_w)

$$Nu = \frac{q_w}{\pi\, k_t\, L\, (T_w - T_e)} \tag{4.5}$$

where $i_w = V_w / (R_w + R_s + R_L)$. The Nusselt number can then be expressed as the following, if T_e is assumed to be T_t in both the calibration and data reduction process

$$\frac{V_w^2\, R_w}{\left(R_w + R_s + R_L\right)^2}\ \frac{1}{\pi\, k_t\, L\left(T_w - T_t\right)} \tag{4.6}$$

To arrive at the appropriate mean and fluctuating equations, the voltage, Reynolds number, and total temperature are replaced by their mean and fluctuating components, apply the binomial theorem, and noting that

$$\frac{\overline{V_w}^2}{C_o} = \left(\frac{\overline{T_t}}{T_o}\right)^{n_k} \left[a\sqrt{\overline{\mathrm{Re}_e}} + b\right]\left(T_w - \overline{T_t}\right) \tag{4.7}$$

where

$$\mathrm{C_o} = \frac{\left(R_w + R_s + R_L\right)^2}{R_w}\,\pi\, L\, k_o \tag{4.8}$$

and $n_k = 0.89$. The detailed procedure to derive (4.7) is presented in Ref. [29]. Solving for $v_w' / \overline{V_w}$ yields

$$\frac{v_w'}{\overline{V_w}} = f\left(\frac{\mathrm{Re}\,o_e'}{\overline{\mathrm{Re}\,o_e}}\right) + g\left(\frac{T_t'}{\overline{T_t}}\right) \tag{4.9}$$

where the hot-wire sensitivities (f and g) are given as the following

$$f = \frac{1}{4}\left(1 + \frac{b}{a\sqrt{\overline{\mathrm{Re}_e}}}\right)^{-1} \quad \text{and} \quad g = \frac{-\overline{T_t'}}{2\left(T_w - \overline{T_t}\right)} + \frac{n_k}{2} - f n_\mu \tag{4.10}$$

From (4.10), it is clear that $\sqrt{\overline{\mathrm{Re}_e}}$ and $\overline{T_t}$ must be known in order to evaluate the hot-wire sensitivities. Eqn (4.7) can be rewritten as

$$\sqrt{\overline{\mathrm{Re}_e}} + x_i\,\overline{T_t}\sqrt{\overline{\mathrm{Re}_e}} + y_i\,\overline{T_t} = z_i \tag{4.11}$$

where $x_i = -1/T_{wi}$, $y_i = -b_i/(a_i T_{wi})$, and $z_i = \overline{V}^2_{wi}/(C_i a_i T_{wi}) - b_i/a_i$. Within (4.11), i is the overheat number, and $C = C_o$. As a minimum, two overheat ratios are necessary to determine the two unknowns $\sqrt{\overline{\mathrm{Re}_e}}$ and $\overline{T_t}$. If more than three overheat ratios are used, then a least squares analysis can be used to obtain $\sqrt{\overline{\mathrm{Re}_e}}$ and $\overline{T_t}$.

Squaring Eqn. (4.9) yields the following hot-wire fluctuation equation

$$f_i^2\overline{\left(\frac{\mathrm{Re}\,o_e'}{\overline{\mathrm{Re}\,o_e}}\right)^2} + 2 f_i g_i \overline{\left(\frac{\mathrm{Re}\,o_e'}{\overline{\mathrm{Re}\,o_e}}\,\frac{T_t'}{\overline{T_t}}\right)} + g_i^2\overline{\left(\frac{T_t'}{\overline{T_t}}\right)^2} = \overline{\left(\frac{v_w'}{\overline{V_w}}\right)_i^2} \tag{4.12}$$

The general least squares (GLS) method yields the following 3 x 3 system, where i again denotes the overheat number and N the number of overheat ratios used

$$\begin{bmatrix} \Sigma f_i^4 & 2\Sigma f_i^3 g_i & \Sigma f_i^2 g_i^2 \\ \Sigma f_i^3 g_i & 2\Sigma f_i^2 g_i^2 & \Sigma f_i g_i^3 \\ \Sigma f_i^2 g_i^2 & 2\Sigma f_i g_i^3 & \Sigma g_i^4 \end{bmatrix} \begin{pmatrix} \overline{\left(\frac{Reo_e'}{Reo_e}\right)^2} \\ \overline{\left(\frac{Reo_e'}{Reo_e}\frac{T_t'}{T_t}\right)} \\ \overline{\left(\frac{T_t'}{T_t}\right)^2} \end{pmatrix} = \begin{pmatrix} \Sigma f_i^2 \overline{\left(\frac{v_w'}{V_w}\right)_i^2} \\ \Sigma f_i g_i \overline{\left(\frac{v_w'}{V_w}\right)_i^2} \\ \Sigma g_i^2 \overline{\left(\frac{v_w'}{V_w}\right)_i^2} \end{pmatrix} \tag{4.13}$$

It is important to note that, for the GLS method, any errors introduced in the experiment through scatter, are amplified by a combined power of four. This inherent disadvantage of the GLS approach led to the development of a new method, the quadratic least squares (QLS) method [26].

The QLS method begins by assuming that the error in the measured hot-wire voltages are purely random and that all bias errors are contained in f and g [29]. Defining τ^* as

$$\tau^* = \frac{\left(T_w - \overline{T_t}\right)}{\overline{T_t}}, \tag{4.14}$$

and rewriting the hot-wire sensitivities as

$$\begin{aligned} f &= f_o + m_f \frac{1}{\tau^*} \\ g &= g_o + m_g \frac{1}{\tau^*} \end{aligned} \tag{4.15}$$

(4.12) can be rewritten as

$$\overline{\left(\frac{V_w'}{V_w}\right)^2} = a_o + a_1\left(\frac{1}{\tau^*}\right) + a_2\left(\frac{1}{\tau^*}\right)^2 \tag{4.16}$$

where

$$\begin{bmatrix} f_o^2 & 2f_o g_o & g_o^2 \\ 2f_o m_f & 2\left(f_o m_g + g_o m_f\right) & 2g_o m_g \\ m_f^2 & 2m_f m_g & m_g^2 \end{bmatrix} \begin{pmatrix} \overline{\left(\frac{\mathrm{Re}o_e'}{\mathrm{Re}o_e}\right)^2} \\ \overline{\left(\frac{\mathrm{Re}o_e'}{\mathrm{Re}o_e}\frac{T_t'}{T_t}\right)} \\ \overline{\left(\frac{T_t'}{T_t}\right)^2} \end{pmatrix} = \begin{pmatrix} a_o \\ a_1 \\ a_2 \end{pmatrix} \tag{4.17}$$

A minimum of three overheat ratios are necessary to solve for the unknowns in (4.16). If more than three are used, then the QLS method can be used to evaluate the right-hand side of (4.16). The turbulence results can then be obtained by solving (4.17).

It is important to note that any error due to experimental scatter is amplified by a combined power of two. The GLS method and the QLS method yield identical results if (4.15) is valid and if the experimental scatter in the hot-wire sensitivities is purely random; the QLS method only reduces the effects of bias error in f and g [29].

The next step is to specify Re_e for the cross-wire probe.

4.2.2 Cross Wire

To obtain cross-wire turbulence results, Re_e must be related to the x and y tunnel coordinates. The following analysis is presented in full in Ref. [29].

It can be shown that

$$\mathrm{Re}^2 = \mathrm{Re}_n^2 + k_c^2\ \mathrm{Re}_t^2 = A_1\,\mathrm{Re}_x^2 + 2A_2\,\mathrm{Re}_x\,\mathrm{Re}_y + A_3\,\mathrm{Re}_y^2 \tag{4.18}$$

where A_i are given by the following

$$\begin{aligned} A_1 &= \cos^2(\phi) + k_c^2 \sin^2(\phi) \\ A_2 &= \left(1 - k_c^2\right)\cos(\phi)\sin(\phi) \\ A_3 &= k_c^2 \cos^2(\phi) + \sin^2(\phi) \end{aligned} \tag{4.19}$$

and ϕ is the hot-wire incidence angle.

Replacing Re_e, Re_x, and Re_y by their mean and fluctuating components, it can be shown that

$$\overline{Re o_{ej}} = \overline{Re o_x}\sqrt{B_{3j}}$$

$$\left(\frac{\overline{Re o_e}'}{\overline{Re o_e}}\right)_j = B_{1j}\left(\frac{\overline{Re o_x}'}{\overline{Re o_x}}\right) + B_{2j}\left(\frac{\overline{Re o_y}'}{\overline{Re o_x}}\right) \tag{4.20}$$

where $R_o = \overline{\rho v} / \overline{\rho u}$, $B_1 = A_1/B_3$, $B_2 = A_2/B_3$, $B_3 = A_1 + 2A_2R_o$, and j is the wire number on the cross-wire probe. Equation (4.20) assumes $R_o^2 << 1$.

4.2.3 Separation of Turbulence Variables

The information provided by multiple overheat cross-wire anemometry in supersonic flow includes the following "conservative" variable turbulence data

$$\overline{(\rho u_i)'(\rho u_j)'} \qquad \overline{T_t'^2} \qquad \overline{(\rho u_i)' T_t'} \,. \tag{4.21}$$

In order to separate the "conserved" turbulence data into "nonconservative" variables, two assumptions were made.

The first assumption, that the pressure fluctuations are small compared to the density and temperature fluctuations, is still controversial. Kistler [30] has suggested that p' is proportional to u'^2, which is second order and neglected. The validity of the p' ~ O(2) (or p' ≈ 0) assumption has been experimentally verified for a Mach 4.0 free mixing layer [18]. The second assumption is the thermally perfect gas assumption (p = ρRT). With first-order assumptions, the following "separated" results can be obtained [18], which include the p' information for completeness

$$\frac{u'}{u} = \frac{(\rho u)'}{\rho u} - \frac{\rho'}{\rho} \tag{4.22}$$

$$\frac{v'}{u} = \frac{(\rho v)'}{\rho u} - R_o\frac{\rho'}{\rho} \tag{4.23}$$

$$\frac{\rho'}{\rho} = \frac{1}{\alpha+\beta}\left[\beta\left(\frac{(\rho u)'}{\rho u} + R_o\frac{(\rho v)'}{\rho u}\right) - \frac{T_t'}{T_t} + \alpha\frac{p'}{p}\right] \tag{4.24}$$

where $\alpha = 1.0 / [1 + .5(\gamma - 1)M^2]$ and $\beta = (\gamma - 1)\alpha M^2$. With Eqns (4.22) - (4.24) and the p' = 0 assumption, all the turbulent shear terms in the RANS can be obtained. The following 6 x 6 matrix is generated [29] by performing all the possible products within (4.22) - (4.24)

$$\begin{bmatrix} 1 & 0 & 1 & 2 & \bar{\Pi} & 0 \\ 0 & 1 & R_o^2 & 0 & 2R_o & 0 \\ \beta^2 & \beta^2 R_o^2 & \alpha^2 & -2\alpha\beta & -2\alpha\beta R_o & 2\beta^2 R_o \\ 0 & 0 & R_o & R_o & 1 & 1 \\ \beta & 0 & -\alpha & \beta - \alpha & \beta R_o & \beta R_o \\ 0 & \beta R_o & -\alpha R_o & \beta R_o & \beta R_o^2 - \alpha & \beta \end{bmatrix} \begin{pmatrix} \overline{\left(\frac{u'}{u}\right)^2} \\ \overline{\left(\frac{v'}{u}\right)^2} \\ \overline{\left(\frac{\rho'}{\rho}\right)^2} \\ \frac{\rho' u'}{\rho u} \\ \frac{\rho' v'}{\rho u} \\ \frac{u' v'}{u u} \end{pmatrix} = \begin{pmatrix} \overline{\left(\frac{(\rho u)'}{\rho u}\right)^2} \\ \overline{\left(\frac{(\rho v)'}{\rho u}\right)^2} \\ \overline{\left(\frac{T_t'}{T_t}\right)^2} \\ \frac{(\rho u)'(\rho v)'}{\rho u \rho u} \\ \frac{(\rho u)' T_t'}{\rho u T_t} \\ \frac{(\rho v)' T_t'}{\rho u T_t} \end{pmatrix} \tag{4.25}$$

Solving for the separated turbulence quantities involves the inversion of the above 6 x 6 system.

4.2.5 Separation of Variables (Single Overheat Ratio)

For many compressible flows, the total temperature fluctuations are small; T_t is essentially constant and $d(T_t) = 0$ (adiabatic flow). For adiabatic flow with Pr = 1, provided $T_t' = 0$, the following results

$$\frac{T'}{\bar{T}} = -(\gamma - 1)M^2\left(\frac{u'}{\bar{u}} + R_o\frac{v'}{\bar{u}}\right) \tag{4.26}$$

But for air, $Pr \neq 1$, and $T_t' \neq 0$, even for flows that are adiabatic in the mean. Therefore, a correction factor can be added to account for $Pr \neq 1$ and $T_t' \neq 0$

$$\frac{T'}{\bar{T}} = -\kappa(\gamma - 1)M^2\left(\frac{u'}{\bar{u}} + R_o\frac{v'}{\bar{u}}\right) \tag{4.27}$$

Typically, $\kappa \in [0.3, 0.5]$, and $\kappa = 0.4$ was used in this study based on previous work [18]. Defining $\theta \equiv -\kappa(\gamma-1)M^2$ and assuming $R_o^2\theta << 1$ and $R_o^2\theta << 1-\theta$, then it can be shown that

$$\frac{u'}{\bar{u}} = \frac{1}{1-\theta}\left[\frac{(\rho u)'}{\overline{\rho u}} + R_o\theta\frac{(\rho v)'}{\overline{\rho u}}\right] \tag{4.28}$$

and

$$\frac{v'}{\bar{u}} = \frac{R_o\theta}{1-\theta}\frac{(\rho u)'}{\overline{\rho u}} + \frac{(\rho v)'}{\overline{\rho u}} \tag{4.29}$$

The total temperature fluctuation equation (4.27) now becomes

$$\frac{T_t'}{\bar{T}_t} = \frac{\beta+\alpha\theta}{1-\theta}\left[\frac{(\rho u)'}{\overline{\rho u}} + R_o\frac{(\rho v)'}{\overline{\rho u}}\right] \tag{4.30}$$

With the above equations (4.27) - (4.30), the single overheat cross-wire response can be approximated as

$$\left[S_{ij}\right] = \begin{pmatrix} \overline{\left(\frac{Reo_x'}{\overline{Reo_x}}\right)^2} \\ \hline \frac{\overline{Reo_x'\,Reo_y'}}{\overline{Reo_x}\;\overline{Reo_x}} \\ \overline{\left(\frac{Reo_y'}{\overline{Reo_x}}\right)^2} \end{pmatrix} = \begin{pmatrix} \overline{\left(\frac{v_w'}{\overline{V_w}}\right)^2}_1 \\ \hline \overline{\left(\frac{v_w'}{\overline{V_w}}\right)^2}_2 \\ \hline \left(\frac{v_w'}{\overline{V_w}}\right)\left(\frac{v_w'}{\overline{V_w}}\right)_2 \end{pmatrix} \tag{4.31}$$

where **S** is the single overheat matrix whose coefficients are given below

$$
\begin{aligned}
S_{11} &= f_1^2 B_{11}^2 + 2 f_1 g_1 R_{mT} B_{11} + g_1^2 R_{mT}^2 \\
S_{12} &= 2\left[f_1^2 B_{11} B_{21} + f_1 g_1 R_{mT} \left(R_{uT} R_o + R_{vT} B_{21} B_{11} \right) + g_1^2 R_{mT}^2 R_o \right] \\
S_{13} &= f_1^2 B_{21}^2 + 2 f_1 g_1 R_{mT} R_{vT} R_o B_{21} \\
S_{21} &= f_2^2 B_{12}^2 + 2 f_2 g_2 R_{mT} R_{uT} B_{12} + g_2^2 R_{mT}^2 \\
S_{22} &= 2\left[f_2^2 B_{12} B_{22} + f_2 g_2 R_{mT} \left(R_{uT} R_o B_{12} + R_{vT} B_{22} \right) + g_2^2 R_{mT}^2 R_o \right] \\
S_{23} &= f_2^2 B_{22}^2 + 2 f_2 g_2 R_{mT} R_{vT} R_o B_{22} \\
S_{31} &= f_1 f_2 B_{11} B_{12} + f_1 g_2 R_{mT} R_{uT} B_{11} + f_2 g_1 R_{mT} R_{ut} B_{12} + g_1 g_2 R_{mT}^2 \\
S_{32} &= f_1 f_2 \left(B_{11} B_{22} + B_{12} B_{21} \right) + f_1 g_2 R_{mT} \left(R_{uT} R_o B_{11} + R_{vT} B_{21} \right) \\
&\quad + f_2 g_1 R_{mT} \left(R_{uT} R_o B_{12} + R_{vT} B_{22} \right) + 2 g_1 g_2 R_{mT}^2 R_o \\
S_{33} &= f_1 f_2 B_{21} + f_1 g_2 R_{mT} R_{vT} R_o B_{21} + f_2 g_1 R_{mT} R_{vT} R_o B_{22}
\end{aligned}
\tag{4.32}
$$

where

$$
\begin{aligned}
R_{mT} &= \frac{\beta + \alpha\,\theta}{1 - \theta} \\
R_{uT} &= \frac{\overline{(\rho u)' T_t'}}{\sqrt{\overline{(\rho u)'^2}}\sqrt{\overline{T_t'^2}}} \\
R_{vT} &= \frac{\overline{(\rho v)' T_t'}}{\sqrt{\overline{(\rho v)'^2}}\sqrt{\overline{T_t'^2}}} \\
R_{wT} &= \frac{\overline{(\rho w)' T_t'}}{\sqrt{\overline{(\rho w)'^2}}\sqrt{\overline{T_t'^2}}}
\end{aligned}
\tag{4.33}
$$

Past work has shown that $R_{uT} \in [0.6, 0.9]$. There is little data, however, concerning R_{vT} and R_{wT}. Ref. [18] concluded that $R_{vT} \approx 0$ for a mixing layer. The present study found that $R_{uT} \approx 0.6$ and that $R_{vT} \approx -0.5$ and $R_{wT} \approx 0.15$ (see Chapter 5).

All of the single and multiple overheat ratio data reduction techniques have been coded in the FORTRAN program MSHeAR [31].

V. Results

This chapter presents the results of the compressible turbulence measurements. The (nominal) freestream tunnel conditions were measured as $M_\infty = 2.9$, $P_{t\infty} = 2.0$ atm, and $T_{t\infty} = 295$ K. Composite shadowgraphs and schlierens were taken of both the compression ramp and shock boundary layer wedge model. Conventional mean flow and hot-wire probe data were acquired in the vicinity of these two geometries as well as at a common upstream location.

5.1 Shadowgraph and Schlieren Analysis

Composite 600-μsec shadowgraphs and schlierens were taken of the flowfield above both configurations. Since the duration of the light source was relatively long, the flow is not "frozen" and eddies appear smeared. Despite this, the shadowgraphs and schlierens contain important qualitative features of each flow.

The compression ramp shadowgraph and schlieren are shown in Fig. 5.1. The flow is from right to left. A weak shock, formed from the coalescing of the compression waves, can be seen. The reflection of the shock off the bottom plate, as well as the expansion waves, are visible in the aft portion of the test section. The weak shocks observed at the front of the test section are most likely created by a lip resulting from the slight misalignment of the compression ramp and upstream test sections. The boundary layer thickness was estimated to be $\delta = 1.0$ cm (see Fig. 5.1). It should be noted that, because of the long duration of the light source, the boundary layer thickness estimate is a rough approximation.

The shock boundary layer wedge model shadowgraph and schlieren are shown in Fig. 5.2, where the flow is from right to left. From the shadowgraph, the freestream Mach number can be estimated based on the shock wave angle β. From the shadowgraph, β was measured as approximately 30°. From the θ-β-Mach relations [21], for $\beta \approx 30°$ and $\theta = 10°$, the Mach number is about 2.7. The lambda shock, common in shock boundary interactions, can be seen, as well as the expansion fan between the separation

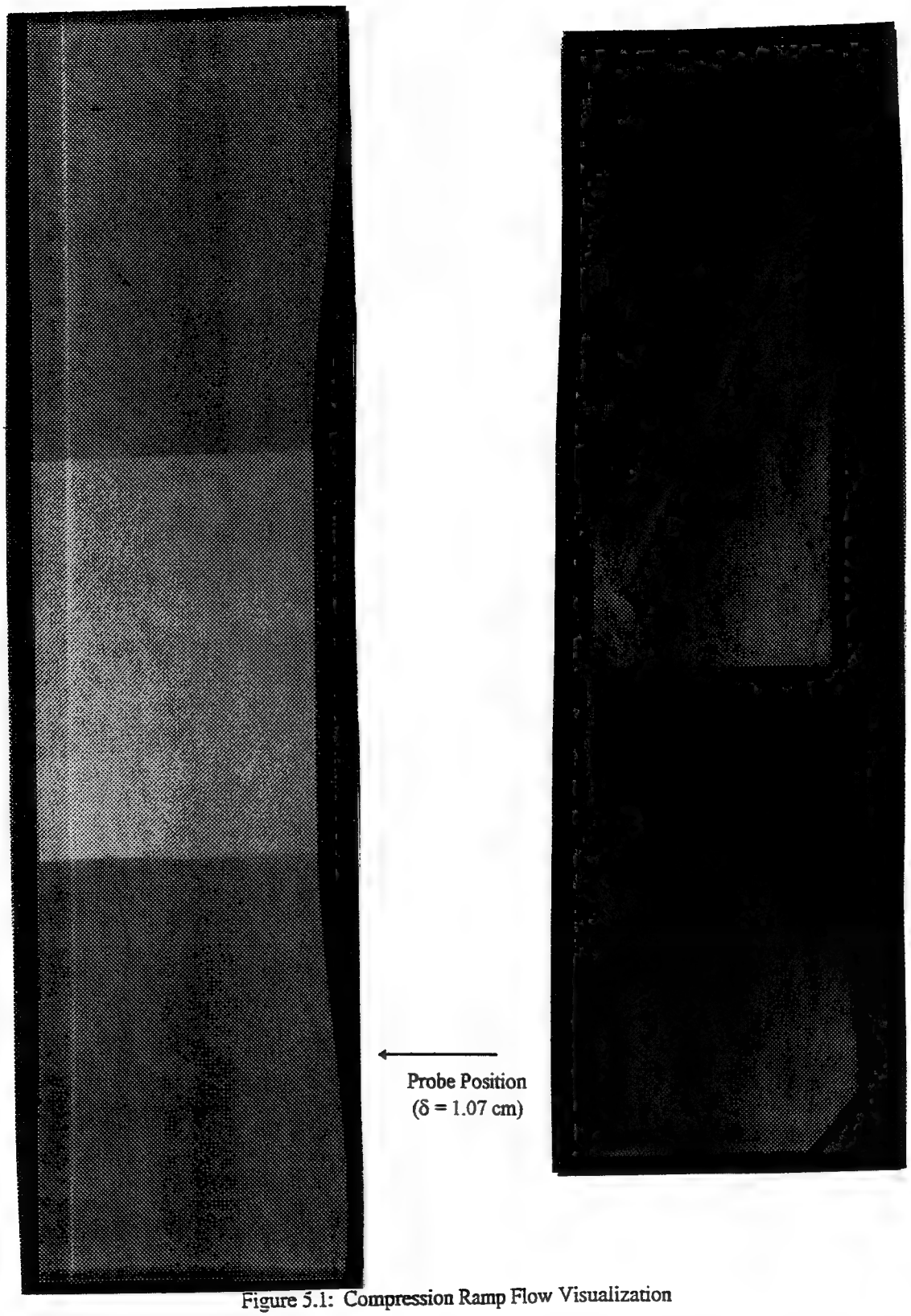

Figure 5.1: Compression Ramp Flow Visualization

Figure 5.2: Shock Boundary Layer Flow Visualization

shock and the reattachment shock aft of the recirculation "bubble". Again, although the flow is not "frozen", the turbulent boundary layer can clearly be seen. The boundary layer thickness was estimated to be 1.25 cm (see Fig. 5.2). Mean flow and cross-wire measurements were taken approximately 77 cm downstream of the nozzle throat (see Fig. 5.2 for probe location).

5.2 Conventional Probes

The conventional probe data consisted of Pitot and cone-static profiles at one common upstream location and one downstream location for each test section model. From these two profiles, the Mach number can be calculated. For reasons to be discussed in a later section, only mean flow data were acquired for the shock boundary layer model. For all mean flow data, every 100 raw data points were averaged into a single data point. The sampling rate was set at 200 Hz for all mean flow data.

5.2.1 Upstream

The upstream mean flow results (x = 44 cm) are presented in Figs. 5.3-5.5. Figure 5.3a gives the Pitot pressure normalized by the freestream total pressure (at the same instant in time). This nondimensionalization eliminates any error introduced by small fluctuations in Pt_∞. The pneumatic pressure valve control kept Pt_∞ essentially constant with only slight variations (+/- .1 atm). The Pitot probe allowed measurements as close as 0.074 cm ($y/\delta = 0.08$) to the wall. The upstream cone-static results are presented in Fig. 5.3b. The cone-static pressure remained essentially constant within the boundary layer and in the freestream. The cone-static probe allowed measurements near the wall as close as 0.11 cm.

The Mach number was computed by the p_c/Pt_2 ratio (see Chapter 4). The freestream Mach number was determined to be 2.9, and the lowest Mach number measured within the boundary layer 1.46 (Fig. 5.4a). The entire upstream flowfield measured in this study was above the minimum Mach requirement for cross-wire anemometry ($M_\infty \geq 1.4$) [19]. For the few data points where the Pitot probe could traverse closer to the wall than the cone-static probe, the Rayleigh-Pitot formula [21] was used to calculate the Mach number, assuming constant static pressure throughout the boundary layer. The Rayleigh-Pitot formula was also used to calculate the static pressure profile, presented in Fig. 5.4b.

The boundary layer thickness was calculated from the mean flow data. A boundary layer thickness $\delta = 0.86$ cm was calculated based on $y = \delta$ where $u = 0.995U_e$. For the upstream station, $U_e \approx 607$ m/s.

5.2.2 Compression Ramp

The compression ramp ($x = 71$ cm) mean flow results are shown in Figs. 5.6-5.8. The pressure profiles are similar to the upstream profiles. The Mach number profile (Fig. 5.7a) indicates that $M_\infty \approx 2.6$ for the compression ramp. The lowest Mach number measured was about 1.7, which is above the cross-wire anemometry limit of 1.4. An effect of the adverse pressure gradient can also be seen in the static pressure profile, Fig. 5.7b, near the wall. It is interesting to note the slight expansion beginning near $y/\delta \approx 1.6$ from the Mach and static pressure profiles. This is even more pronounced in the density, velocity, and axial mass flux profiles (Fig. 5.8).

The boundary layer thickness of the compression ramp is approximately $\delta = 1.1$ cm. This is based on $u = 0.995U_e$, where U_e is 585 m/s.

5.2.3 Shock Boundary Layer

The shock boundary layer results were obtained at $x = 77$ cm downstream of the nozzle throat. The pressure and Mach profiles are presented in Figs. 5.9-5.10. The freestream Mach number is about 1.7, which is considerably lower than the compression ramp test section. The Mach number remained above the cross-wire anemometry limit of about 1.4 for only the outer half of the boundary layer. For this reason, only conventional probe mean flow data were acquired for the shock boundary test section. It is expected that the existence of two downstream shocks caused the freestream Mach number to be lower than the predicted malue of $M_\infty = 2.0$ (i.e. oblique shock wave theory does not account for two downstream shocks).

The density, velocity, and axial mass flux profiles are shown in Fig. 5.11. They are very similar to those of the compression ramp, blending smoothly with the freestream as $y/\delta = 1.0$ is approached.

The boundary layer thickness of the wedge model is approximately $\delta = 0.8$ cm. This is based on $0.995U_e$, where U_e is 470 m/s.

5.3 *Cross-Wire Probes*

Cross-wire data were obtained at the same locations as the mean flow data, with an additional upstream, zero-pressure-gradient station (see Appendix B). Both single and multiple overheat data were acquired for the upstream and compression ramp (downstream) stations.

5.3.1 Filtering of Data

The Prandtl mixing length data (see Fig. 5.26) was filtered using a recursive filter [34]. The filter smoothed the inherent experimental scatter associated with the hot-wire turbulence data and did not "taint" the data in any way. The following equation, from Ref. [34], was used to filter the cross-wire data (where x is the data point, and f_c/f_s is the ratio of the time between samples and the filter time constant)

$$A = e^{(f_c/f_s)} = e^{-.2\pi}, B = 1 - A = 1 - e^{-.2\pi}$$
$$x_i = Ax_{i-1} + Bx_i \tag{5.1}$$

See Ref. [34] for a more complete discussion of the recursive filter.

5.3.2 Calibration Techniques

The cross-wires were calibrated, with respect to Reynolds number, in the freestream flow ($y/\delta \approx 1.4$). The Reynolds number was varied by changing the stagnation pressure. The lowest stagnation pressure obtained before the tunnel unstarted was approximately 1.57 atm, and the highest was roughly 2.86 atm (the stagnation pressure for all data collection runs was nominally 2.0 atm). After the anemometer was tuned , the cross-wire probe was calibrated during two runs (a high and low stagnation pressure run). For each wire, three to five data points were used in the determination of a and b in Eqn. (4.10). For the multiple overheat data, the same calibration process was followed, except that the scanning circuitry scanned through the eight overheat ratios at each pressure.

5.3.3 Multiple Overheat Data

For all of the multiple overheat data, eight overheat ratios of data were acquired, but only the highest six overheats were used. The minimum overheat ratio used in this study was approximately 1.25,

and the maximum was 2.20. The turbulence results obtained when the lowest two overheat ratios were included in the data reduction process exhibited wide experimental scatter. Multiple overheat data were acquired at five y/δ locations for the upstream and compression ramp downstream locations for both uv and uw probes. For most of the multiple overheat data, the lowest y/δ ≈ 0.1 location was discarded due to extreme experimental scatter.

Following is a table of the cross-wire probes used and the corresponding overheat ratios, where AN designates a uw probe, R denotes a repaired probe, and the overheat ratio is in parentheses.

Table 5.1 Cross-Wire Probe Operating Resistances and Overheat Ratios

Probe	Serial Number	Wire 1, Ω (OHR)	Wire 2, Ω (OHR)
1243 AN	944012	4.80 (2.17)	4.78 (2.18)
1243 AN	944010	4.80 (2.17)	4.73 (2.20)
12432 AN (R)	944012	5.61 (1.85)	5.03 (2.07)
1243	943011	5.19 (2.00)	5.21 (2.00)
1243	943009	6.48 (1.60)	6.25 (1.66)
1243	943008	6.44 (1.61)	6.34 (1.64)

Table 5.1 shows that, for the uw probes, high overheat ratios were used. For high overheat ratios, any errors due to total temperature variations are very small. That is, κ in Eqn. (4.27) has a small effect on the turbulence results. For low overheat ratios, the turbulence results are more sensitive to total temperature fluctuations and hence κ, especially the axial mass flux turbulence intensity. As mentioned in Chapter 4, the specification of $\kappa = 0.4$ was based on previous work [18]. However, because the overheat ratios for the uv probes were very low, $\kappa = 1.0$ was used for all single overheat data.

5.3.4 Upstream

The zero pressure gradient turbulence intensities are presented in Figs. 5.12-5.13. The axial mass flux turbulence intensity reached a maximum of about 10% at y/δ ≈ 0.4. The transverse mass flux turbulence intensity did not reach a maximum through the lowest y/δ measured in this study, but was approximately half as large as the axial mass flux turbulence intensity. Both decrease to approximately 2% in the freestream. The axial mass flux turbulence intensities from both wires agree very well. The total

temperature turbulence intensity remained essentially constant at 1-2% within the boundary layer and 0.5% in the freestream. The multiple overheat data agrees very well with the single overheat data for the uv probe, and fairly well for the uw probe.

The separated turbulence intensities show that the density fluctuations, for both probes, reach a maximum of 7% at $y/\delta \approx 0.4$. None of the velocity fluctuations reached a maximum for the y/δ reange considered in this study. But it is important to note that the density fluctuations are about 2-3 times larger than the velocity fluctuations (except below $y/\delta \approx 0.3$ where the density fluctuations begin to decrease).

The cross-wire shear data are presented in Figs. 5.14-5.15, along with an estimate (assuming $p' \approx 0$) of the second term in Eqn. (2.20). As can be seen in Figs. 5.14b and 5.15b, the first term is the only significant term for thin layer type flows where $\bar{v}$ is small. Thus, the cross-wire shear can be taken as a very accurate estimate of the total shear stress (see Eqn. (2.20)). The separated Reynolds shear data were obtained by invoking the $p' \approx 0$ assumption and are presented in Fig. 5.16. For the uv probe (xy plane), the second term in Eqn. (2.13) accounts for as much as 75% of the total Reynolds shear stress. This is important, since this term is neglected by most compressible turbulence models. Similarly, the second term in Eqn. (2.13) accounts for about 50% of the total Reynolds shear stress in the xz-plane.

The mass flux-total temperature correlations (measured with the multiple overheat method) and turbulent heat flux data are presented in Fig. 5.17. The axial and spanwise correlations are of the same magnitude, but opposite in sign. The transverse correlation is essentially zero. Two data points are presented for the axial mass flux-total temperature correlation for each y/δ location: one from the uv probe, and one from the uw probe. For the specific turbulent heat flux, both the axial and transverse components are of the same magnitude; both are important in thin layer type flows. The axial specific turbulent heat flux is essentially zero.

The velocity-velocity and density-velocity correlations are presented in Fig. 5.18. The $\overline{u'v'}$ correlation is always negative, and tends toward zero in the freestream. The $\overline{u'w'}$ correlation has a similar profile as the $\overline{u'v'}$ correlation, except that it is slightly positive for $y/\delta \in [0.4,0.8]$. The density-velocity correlations are given in Fig. 5.18b. The strongest correlation is $\overline{\rho'u'}$, and is always positive. The $\overline{\rho'v'}$

correlation is always negative, and the $\overline{\rho' w'}$ correlation changes sign at about the same y/δ location as the $\overline{u' w'}$ correlation.

The final upstream cross-wire data presented is the mean total temperature profile from the multiple overheat data. Figure 5.19a presents the upstream total temperature profile, and Fig. 5.19b give the total temperature profile for the compression ramp. From both profiles, it is clear that the total temperature remains essentially constant within the boundary layer and in the freestream.

5.3.5 Compression Ramp

The downstream turbulence intensities are presented in Figs. 5.20-5.21. The axial mass flux turbulence intensity reaches a maximum of 17% at about $y/\delta = 0.4$. Compared to the upstream station, the magnitude of the axial mass flux turbulence intensity is about one and a half times larger. The transverse mass flux turbulence intensity has the same profile, but the magnitude is about double the upstream value. The axial mass flux turbulence intensity obtained from the uw probe is about 80% of the value measured by the uv probe. This difference is most likely due to the choice of $\kappa = 1.0$ for all the single overheat data, as previously noted in Section 5.3.3. The separated turbulence intensities show that the density fluctuations downstream are double the upstream values. The axial velocity fluctuations downstream are slightly larger than the upstream values, but not significantly. The downstream transverse velocity fluctuations are about double the upstream values. The profiles of all three fluctuations (ρ', u', and v') are similar to those upstream; the magnitudes increase significantly downstream for ρ' and v'.

The cross-wire shear data are presented in Figs. 5.22-5.23, along with the estimate of the second term in Eqn. (2.20). For the downstream uv probe, the cross-wire shear is approximately five times as large as the zero pressure gradient case. For the downstream uw probe (Fig. 5.23a), the cross-wire shear is about one and a half times larger than the zero pressure gradient case. Note in Figs. 5.22b and 5.23b that the second term in Eqn. (2.20) is still very small, relative to the total shear, for both probes; but that it becomes slightly more significant below $y/\delta \approx 0.6$. The separated Reynolds shear data are presented in Fig. 5.24. Again, the magnitude of each of the terms of the xy-plane Reynolds shear (as well as the total Reynolds

shear) has increased roughly five-fold. Note that the second term in Eqn. (2.13) accounts for approximately 50% of the total Reynolds shear stress. For the xz-plane, the Reynolds shear stress is about one and a half times larger downstream than upstream. As with the xy-plane Reynolds shear, the second term in Eqn. (2.13) is important, accounting for half of the total Reynolds shear. It is also important to note that the shear stress reaches a maximum around $y/\delta \approx 0.3$ in the adverse pressure gradient region (no maxima were observed for the upstream, zero pressure gradient case).

The downstream velocity-velocity and density-velocity correlations are given in Fig. 5.25. The downstream velocity-velocity profiles are very similar to the upstream profiles, except that downstream the $\overline{u'w'}$ correlation remains negative throughout the measured portion of the boundary layer. The downstream velocity-velocity correlations are approximately three to four times larger in magnitude than their upstream counterparts. The downstream density-velocity correlations exhibit similar profiles as the zero pressure gradient station, though the profile shapes are better defined with sharper maxima. This was also observed in the Reynolds shear profiles. The downstream $\overline{\rho'v'}$ and $\overline{\rho'w'}$ correlations are approximately five times larger than the zero pressure gradient case. The downstream $\overline{\rho'u'}$ correlations are roughly four times larger than the upstream $\overline{\rho'u'}$ correlation values.

5.4 Simple Turbulence Model Analysis

It was mentioned previously that, in general, extensions to incompressible turbulence models exhibit poor performance for compressible flows with adverse pressure gradients. Prandtl's mixing length concept is a simple and popular approach to relating the turbulent fluctuations to a length scale and a mean flow velocity gradient [34]

$$-\tau_{xy}^{T} = \overline{\rho}\, l_m^2 \left|\frac{\partial \bar{u}}{\partial y}\right| \frac{\partial \bar{u}}{\partial y}\gamma \tag{5.2}$$

where l_m is the mixing length and is constant ($l_m = 0.09\delta$) in the outer layer region ($y/\delta \geq 0.22$), lm = 0.4y for $y/\delta \leq 0.22$, and γ is the Klebanoff intermittency factor. If y/δ becomes very small (smaller than the y/δ range investigated in this study), the the van Driest dampling factor would have to be included. Klebanoff

(1955) measured the intermittency (percentage of time that the flow is turbulent) in a turbulent boundary layer, with zero pressure gradient, and produced the following curve fit [35]

$$\gamma = \left[1 + 5.5\left(\frac{y}{\delta}\right)^6\right]^{-1} \tag{5.3}$$

Using the mean flow results, the turbulent shear stresses (xy plane) were calculated using Prandtl's mixing length concept. A simple first-order finite-difference approximation was used to determine $\partial \bar{u} / \partial y$. The results are presented in Fig. 5.26. The zero pressure gradient case is shown in Fig. 5.26a, where it can be seen that Prandtl's mixing length model generally predicts a turbulent shear stress that is roughly in the middle between the incompressible term and the total Reynolds shear stress. For the adverse pressure gradient flow (Fig. 5.26b), the model performs even more poorly, predicting a turbulent Reynolds shear below the "incompressible" term.

In addition to Prandtl's mixing length model, the velocity profile for the upstream location was compared to the common power-law approximations used as a basis for the integral analysis of turbulent boundary layers for flat plates. Prandtl first introduced the power-law velocity profile concept [34], shown below

$$\frac{\bar{u}}{U_e} \approx \left(\frac{y}{\delta}\right)^{1/n} \tag{5.3}$$

where n is typically 6, 7, or 8. Velocity profiles for n = 6, 7, and 8 were computed and compared to the upstream mean flow velocity profile. The results, shown in Fig. 5.27, show that all three power-law relations underpredict the actual velocity profile.

5.5 Favre Data

In addition to the above RANS turbulence data, the present cross-wire anemometry techniques yield a limited amount of Favre (mass-weighted time-averaged) data. Although the primary emphasis of this study was placed on RANS data, Favre data is important because practically all modern turbulence models are based on the Favre-averaged Navier-Stokes equations. Figure 5.28a presents the Favre terms

for the zero pressure gradient case from the multiple overheat data. Two sets of u"/U data were acquired: one set from probe type (uv and uw). In addition to the above Favre terms, the Favre shear stresses are presented in Fig. 5.28b. The single overheat Favre shear stress is simply the incompressible term of the Reynolds shear stress (where third-order and higher terms are neglected).

5.6 Error Analysis

Scatter (error) is an inherent facet of any experimental research. This section attempts to identify sources and estimate the magnitude of these errors. The present analysis uses the L_2 (or Euclidean) norm as the measure of the error. The L_2 norm is given by

$$e_x = \left[\sum_{i=1}^{n} e_i^2 \right]^{1/2} \tag{5.4}$$

where i indexes the various errors associated with the measurement of x.

5.6.1 Conventional Probes

Volluz [23] reports that turbulence induces about ± 0.0068 atm error for both probe types , Pitot and cone-static. The calibration error is approximately 0.005 atm for both probes. The settling chamber pressure has an error of about 0.017 atm. The temperature error is 1 K.

The probe location error is estimated to be ± 0.5% (the probe was observed to flex about 0.25 cm when the wind tunnel was turned on). Therefore, the error in the Mach number is appromimately ± 0.2, or ± 6%. The error in the local mass flux, based on previous work [18], is ± 2.0%.

5.6.2 Cross-Wire Probes

Because 1,024 data points were acquired at each overheat ratio, the statistical error estimates are very small. The largest error is expected to be asssociated with the probe calibration. Following the error analysis of Ref. [18], the errors associated with the conventional probe data above can be carried over to the cross-wire analysis. The calibration errors can be estimated through a perturbation analysis. This perturbation analysis has shown [18] that any error associated with the probe location is small, primarily due to the calibration of the probes at each station, thereby minimizing the effects of misalignment. In

additon, the error analysis of Ref. [18] has shown the error associated with the linearization of the hot-wire response equation, through the binomial theorem (see Chapter 4), is very small. Ref. [26] presents the following hot-wire errors associated with similar turbulence measurements (under similar flow conditions) made in the present study:

Table 5.2 Cross-wire Errors

e_T	7 K	7.6%
e_ρ	0.015 kg/m^3	3.6%
eu	10 m/s	1.5%
$e_{\rho u}$	5.75 kg/m^{2}s	2.1%
e_f	0.0025	1.0%
e_g	0.005	1.0%
$e_{()'()'}$	0.0053	8.4%

The above cross-wire errors, combined with the conventional probes errors, result in a total estimated error of approximately 8.5%

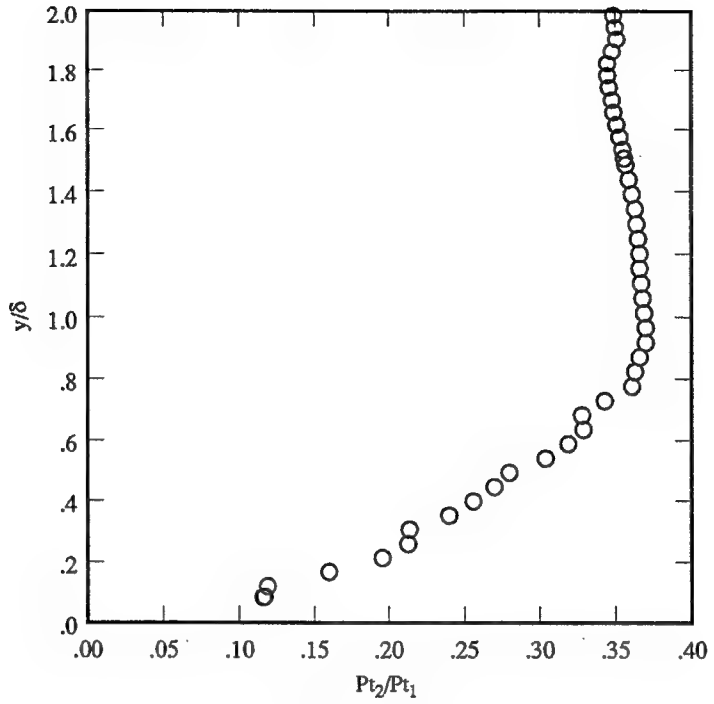

(a) Pitot pressure

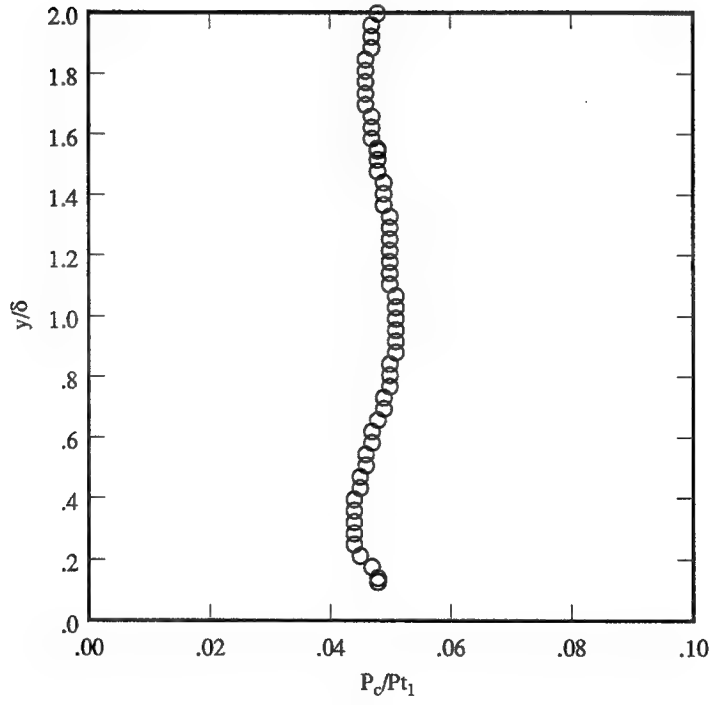

(b) Cone-static pressure

FIGURE 5.3: Conventional mean flow Pitot and cone-static pressure data (x = 44 cm).

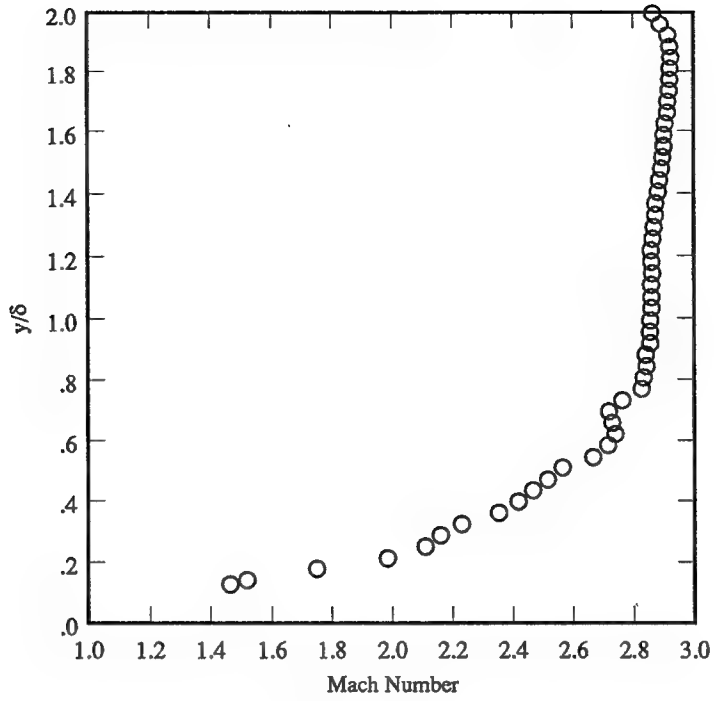

(a) Mach number

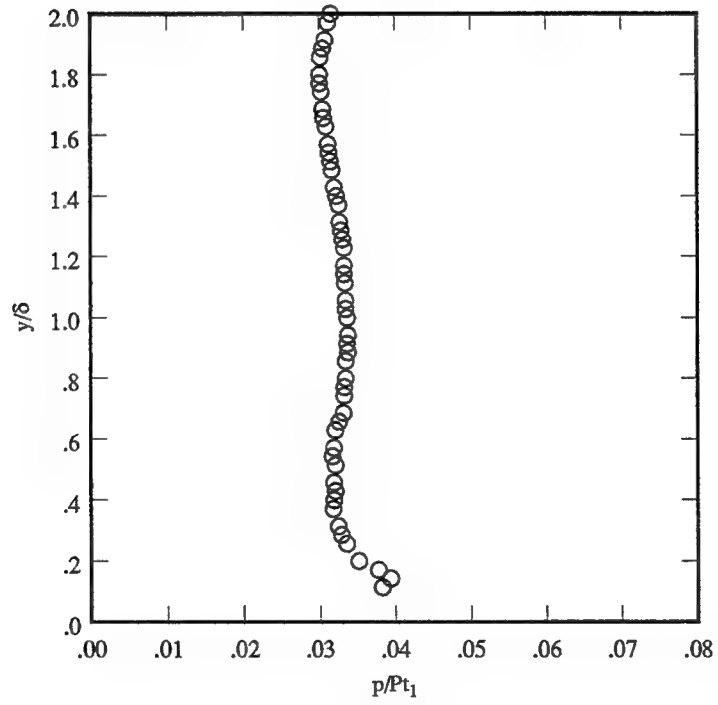

(b) Static pressure

FIGURE 5.4: Conventional mean flow Mach number and static pressure data (x = 44 cm).

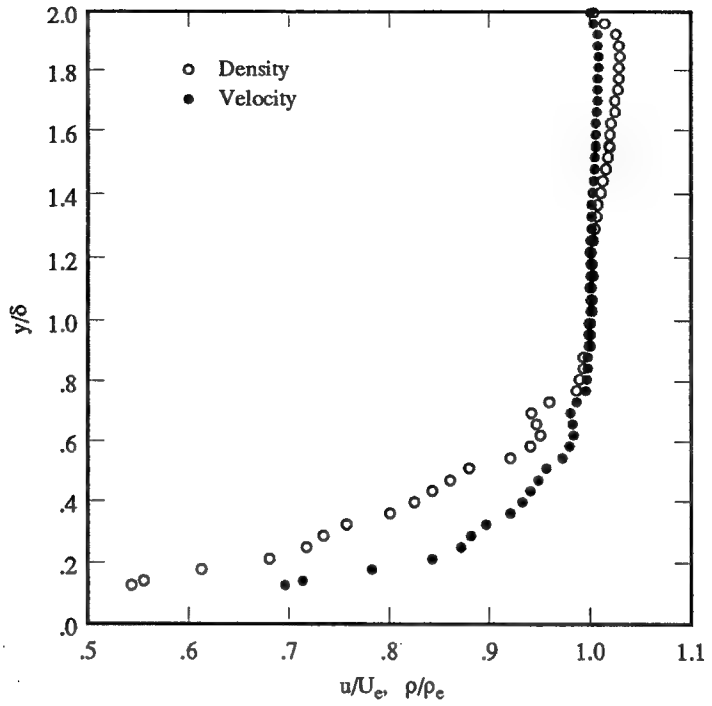

(a) Density and velocity

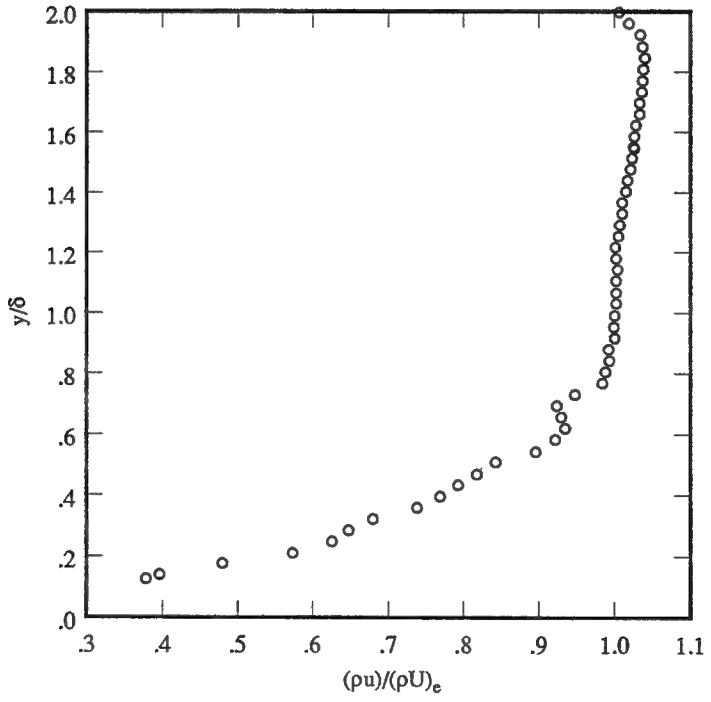

(b) Mass flux

FIGURE 5.5: Conventional mean flow density, velocity, and mass flux data (x = 44 cm).

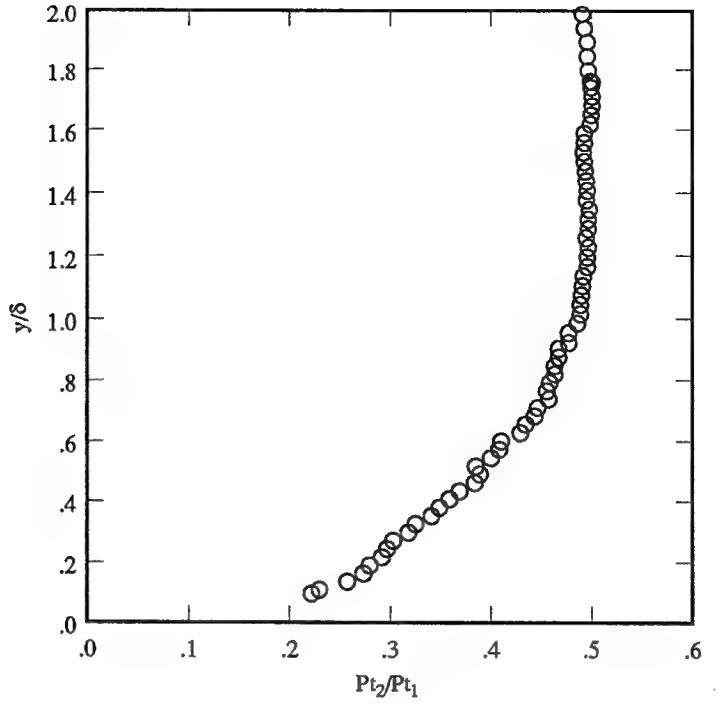

(a) Pitot pressure

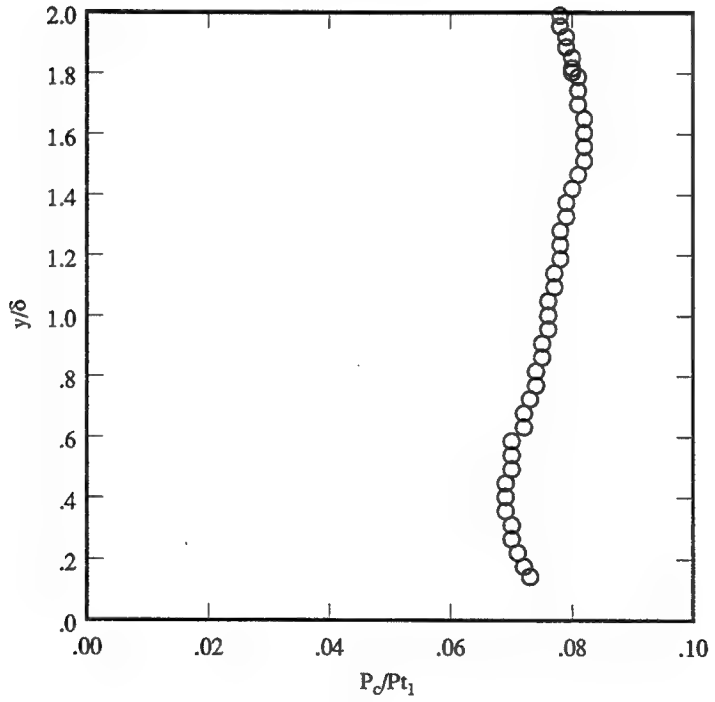

(b) Cone-static pressure

FIGURE 5.6: Conventional mean flow Pitot and cone-static pressure data (x = 71 cm).

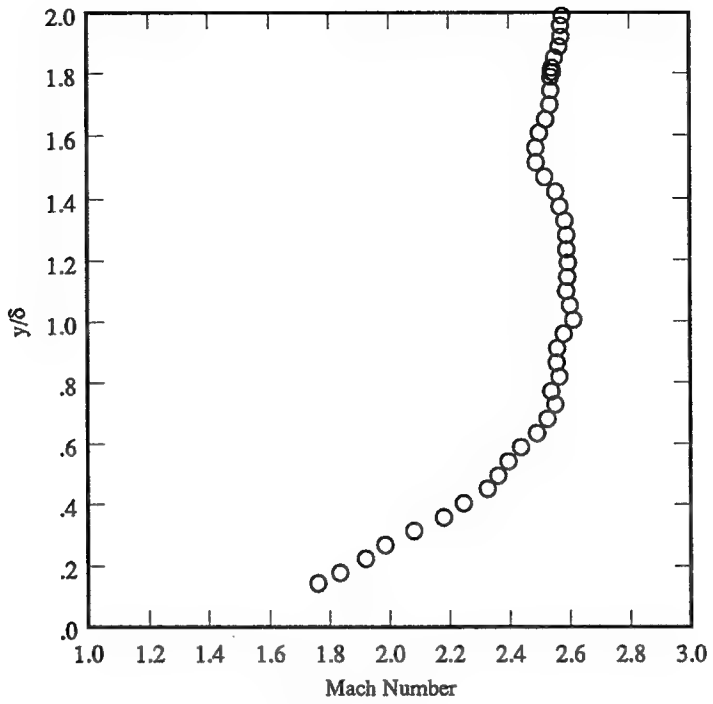

(a) Mach number

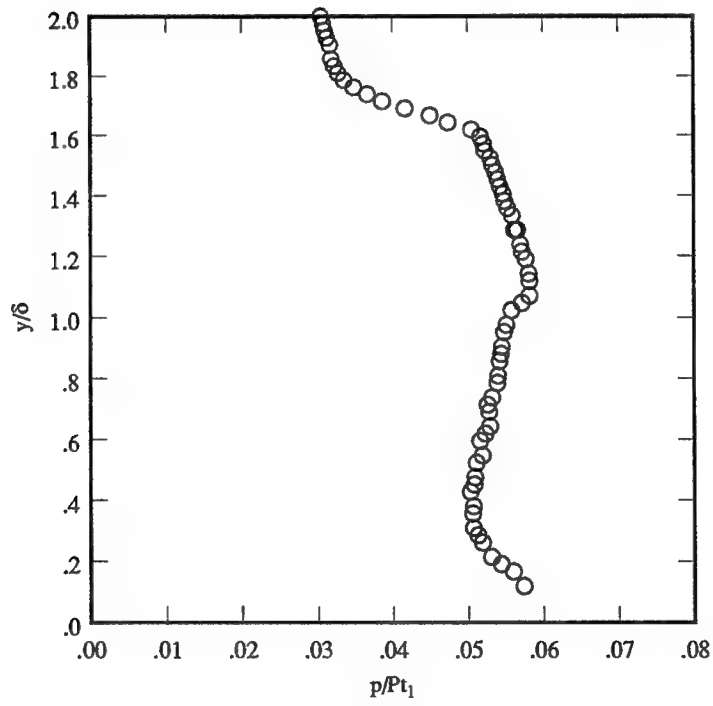

(b) Static pressure

FIGURE 5.7: Conventional mean flow Mach number and static pressure data (x = 71 cm).

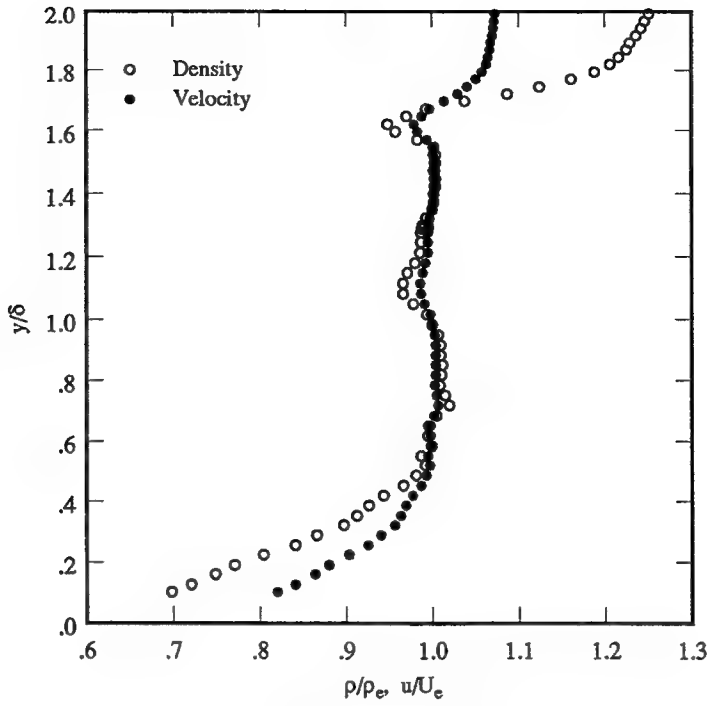

(a) Density and velocity

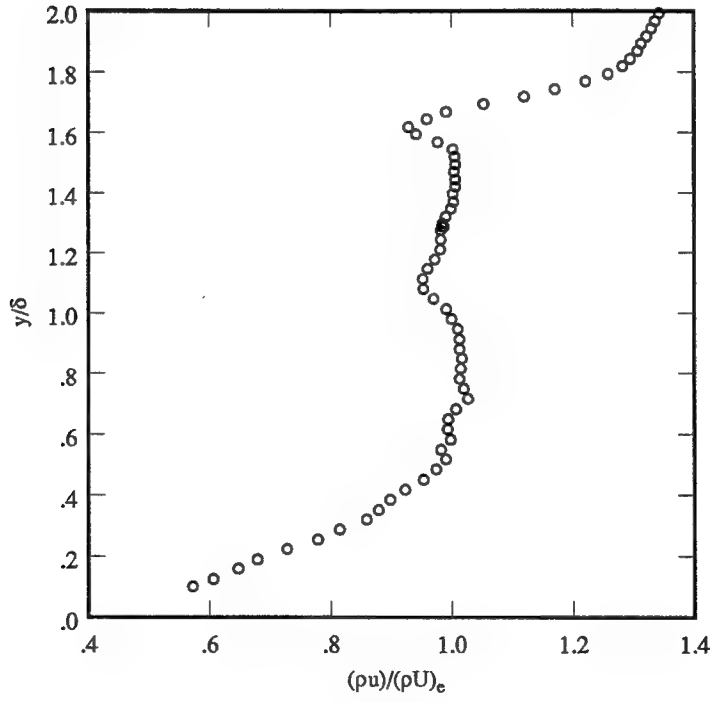

(b) Mass flux

FIGURE 5.8: Conventional mean flow density, velocity, and mass flux data (x = 71 cm).

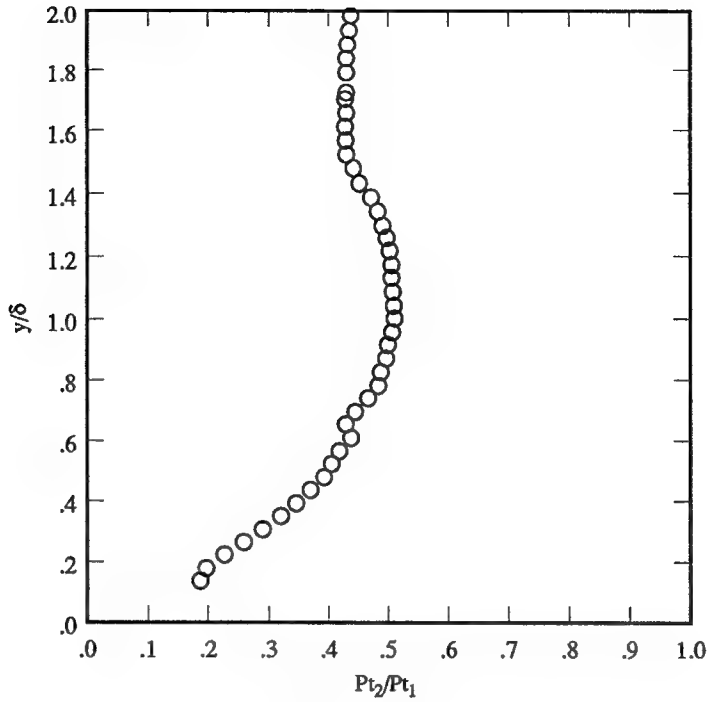

(a) Pitot pressure

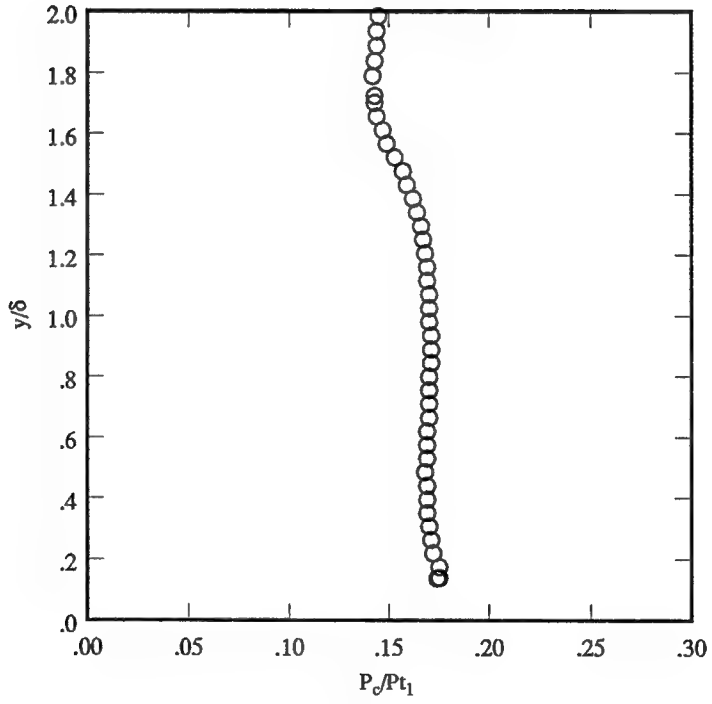

(b) Cone-static pressure

FIGURE 5.9: Conventional mean flow Pitot and cone-static pressure data (x = 77 cm).

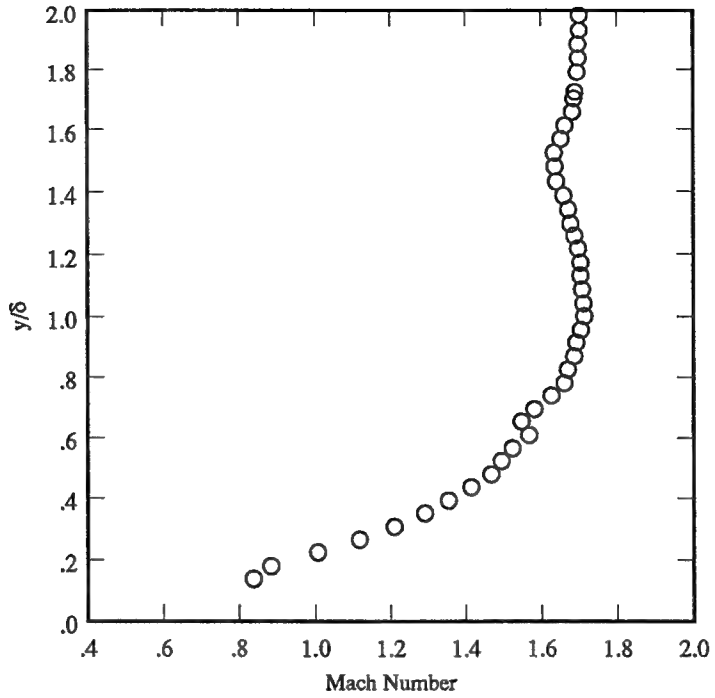

(a) Mach number

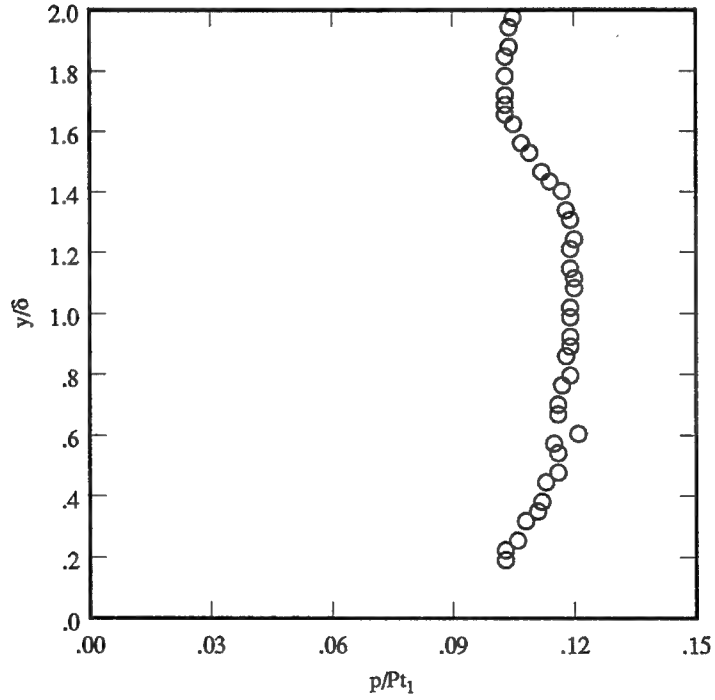

(b) Static pressure

FIGURE 5.10: Conventional mean flow Mach number and static pressure data (x = 77 cm).

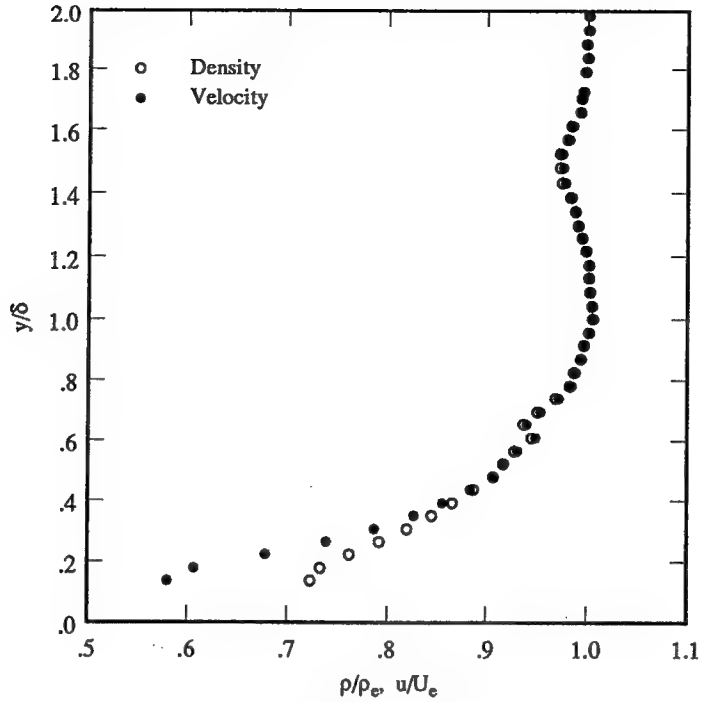

(a) Density and velocity

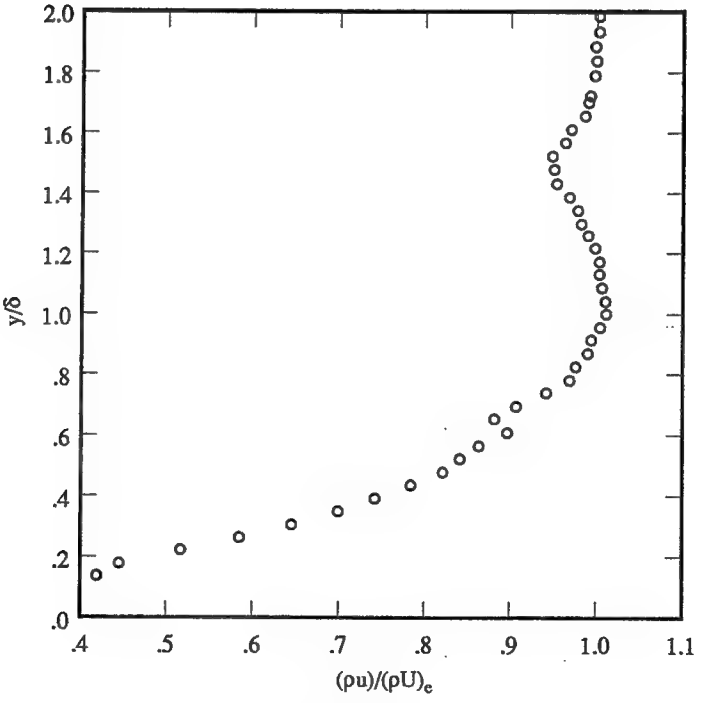

(b) Mass flux

FIGURE 5.11: Conventional mean flow density, velocity, and mass flux data (x = 77 cm).

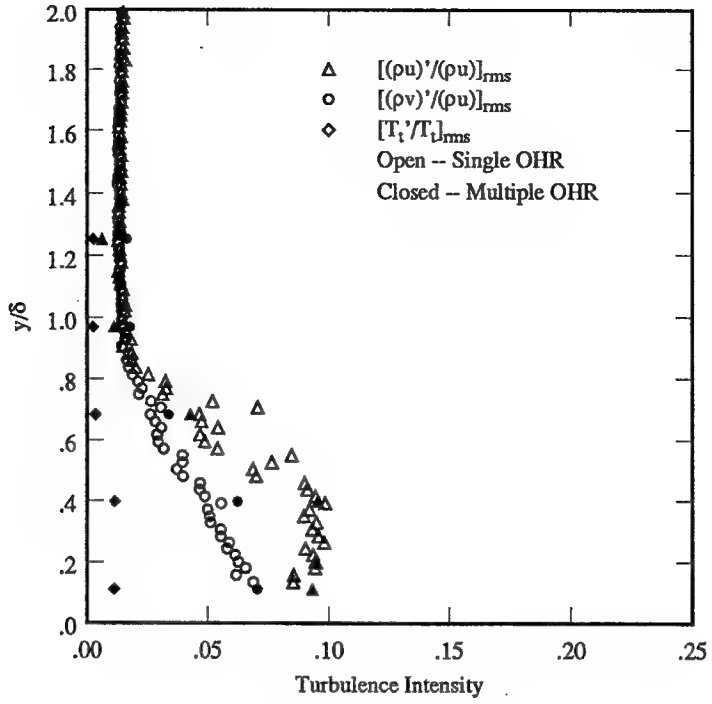

(a) Turbulence intensities

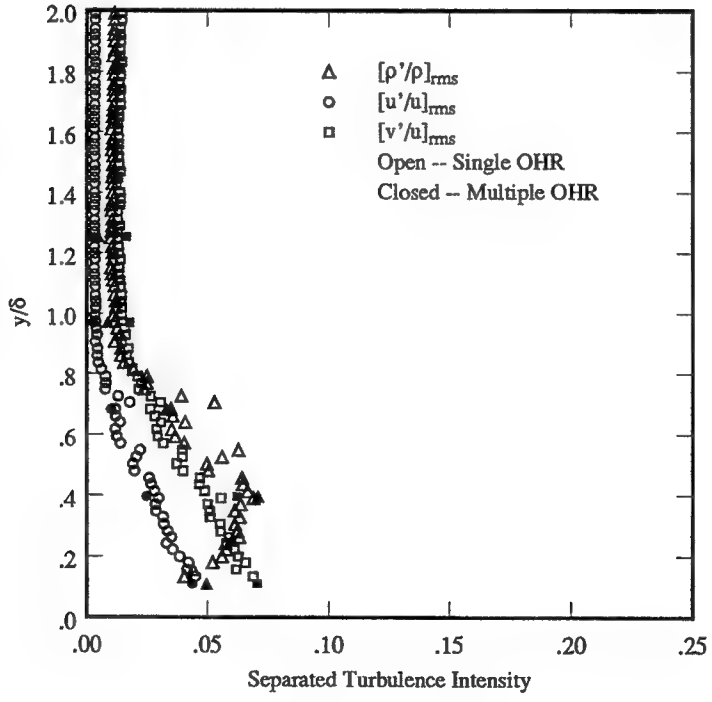

(b) Separated turbulence intensities

FIGURE 5.12: Turbulence intensities, uv probe (x = 44 cm).

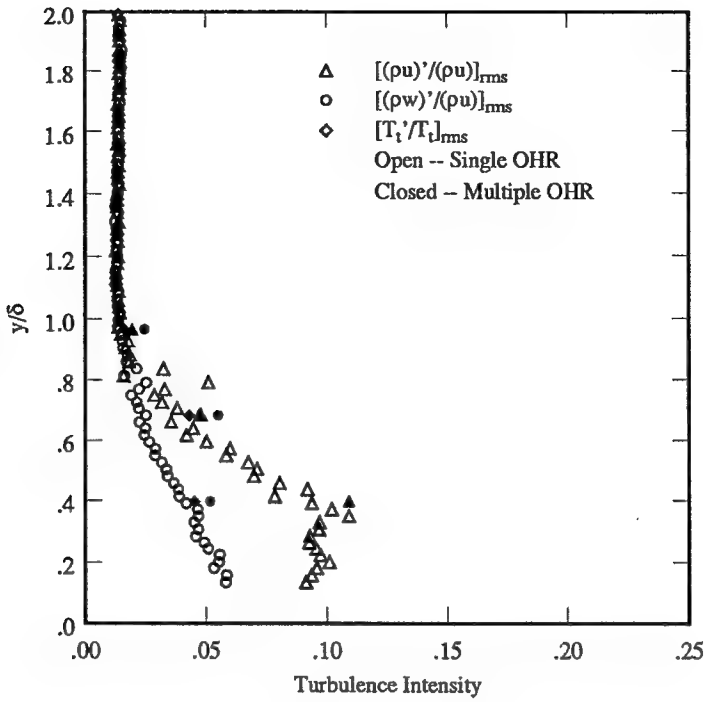

(a) Turbulence intensities

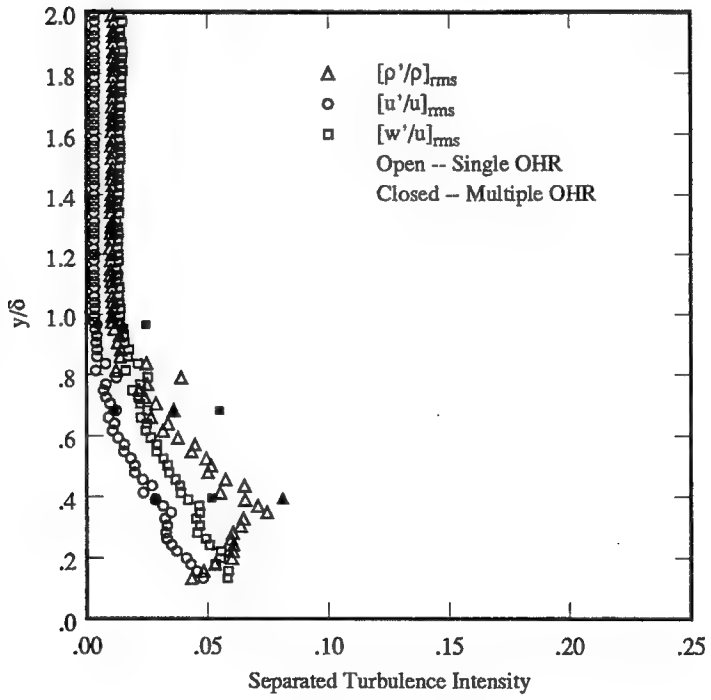

(b) Separated turbulence intensities

FIGURE 5.13: Turbulence intensities, uw probe (x = 44 cm).

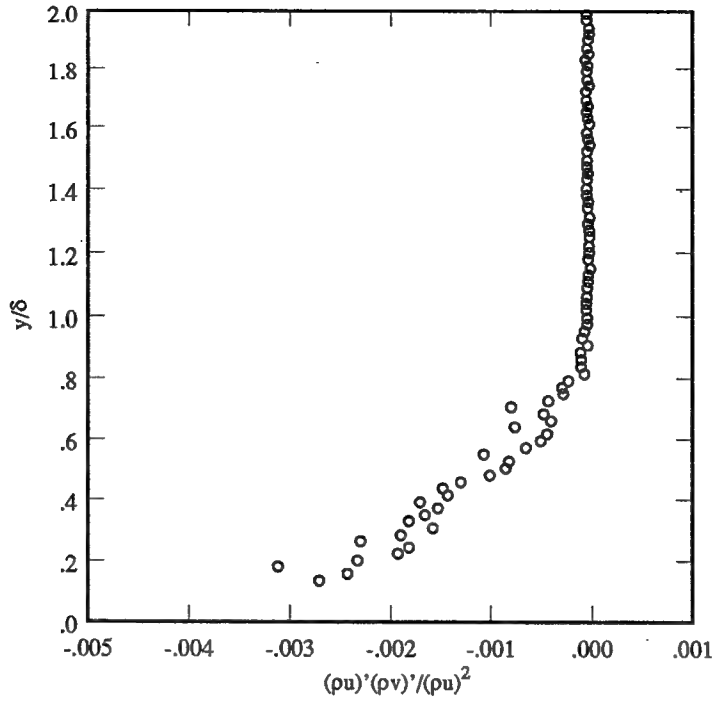

(a) Shear

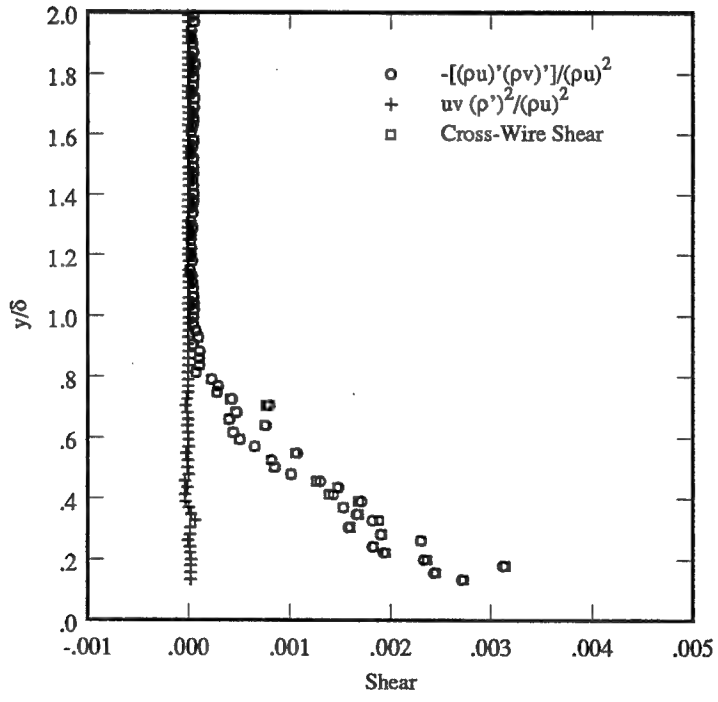

(b) Transformed shear

FIGURE 5.14: Cross-wire transformed turbulent x-y shear data (x = 44 cm).

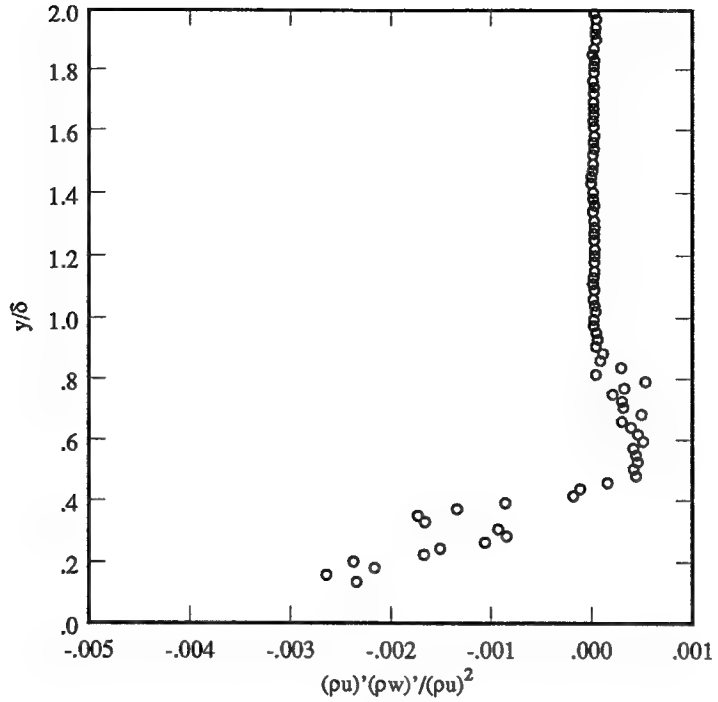

(a) Shear

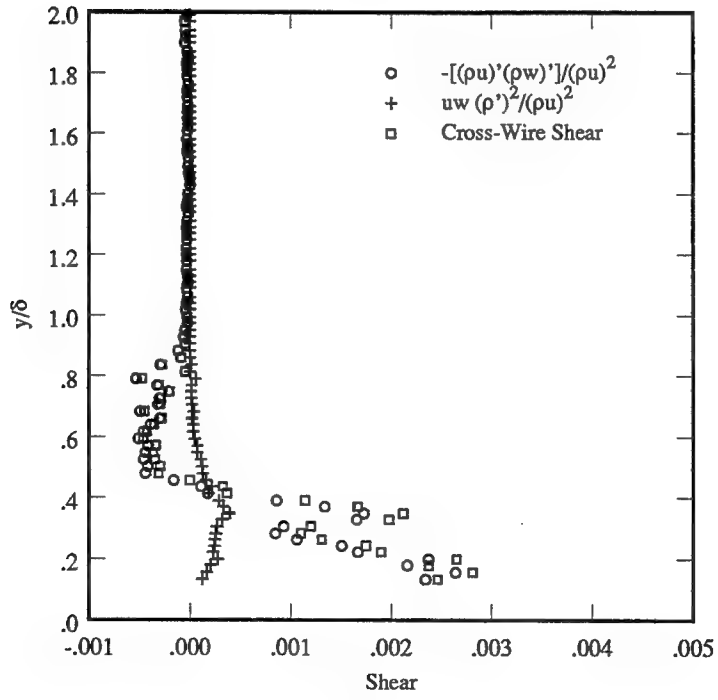

(b) Transformed shear

FIGURE 5.15: Cross-wire transformed turbulent x-z shear data (x = 44 cm).

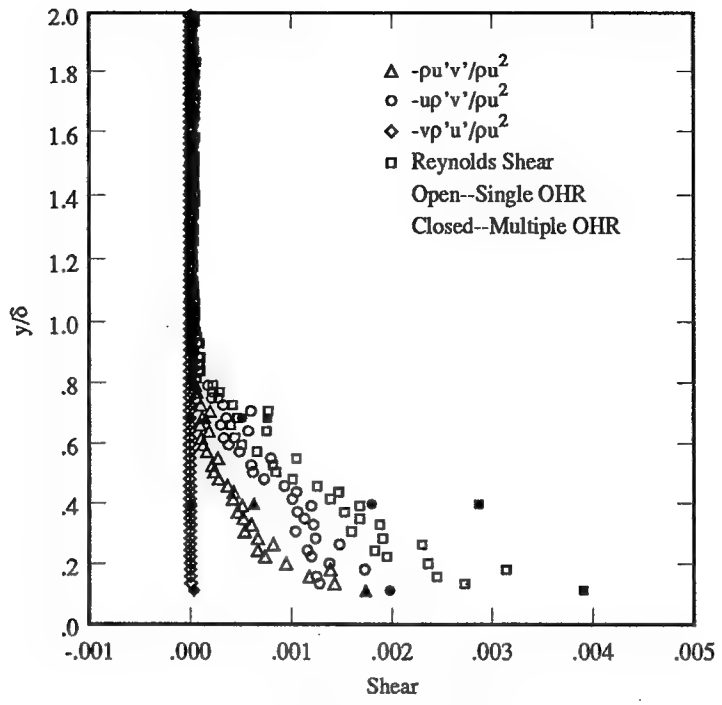

(a) Reynolds shear stress

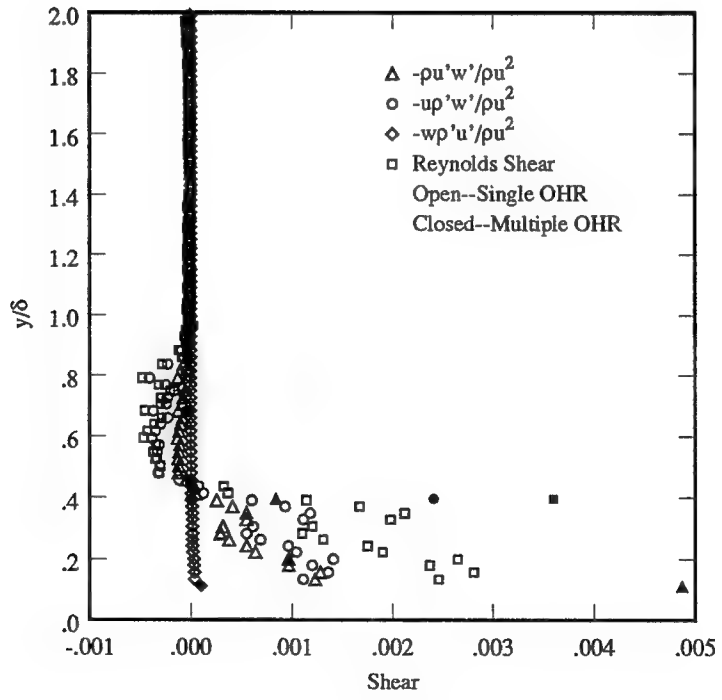

(b) Reynolds shear stress

FIGURE 5.16: Cross-wire x-y and x-z plane Reynolds shear stress data (x = 44 cm).

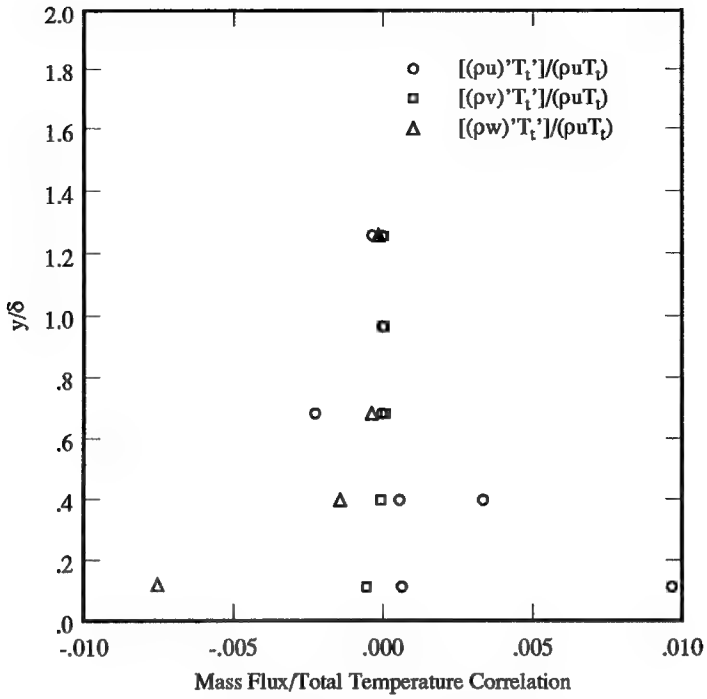

(a) Mass flux/total temperature correlation

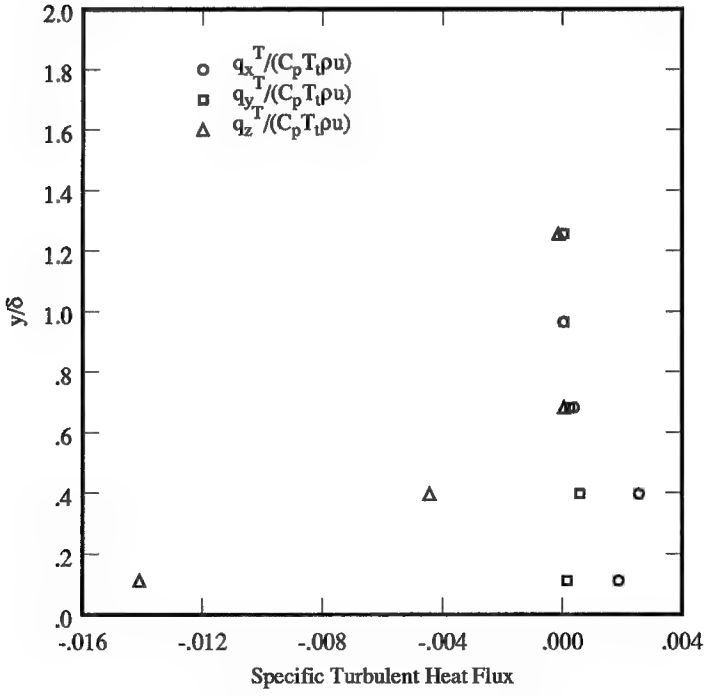

(b) Specific turbulent heat flux

FIGURE 5.17: Mass flux/total temperature and specific turbulent heat flux data (x = 44 cm).

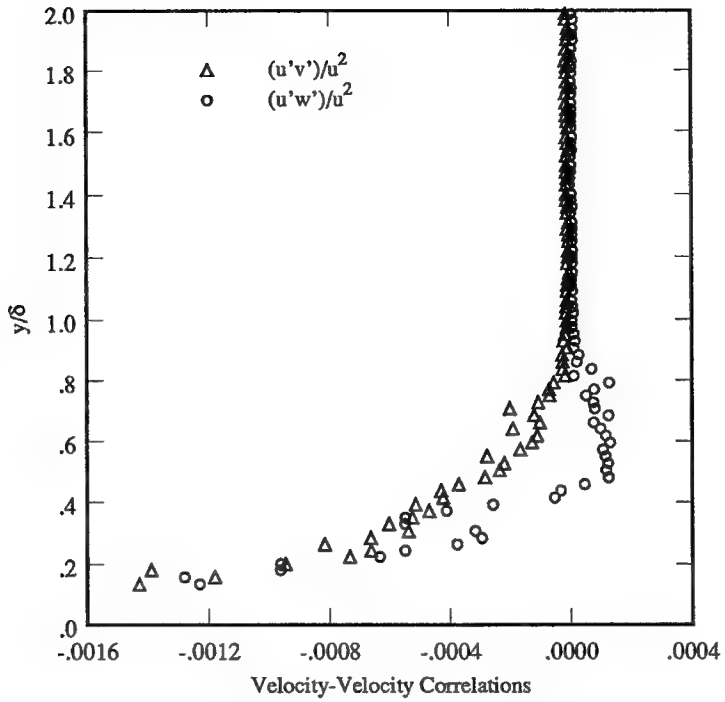

(a) Velocity-velocity correlations

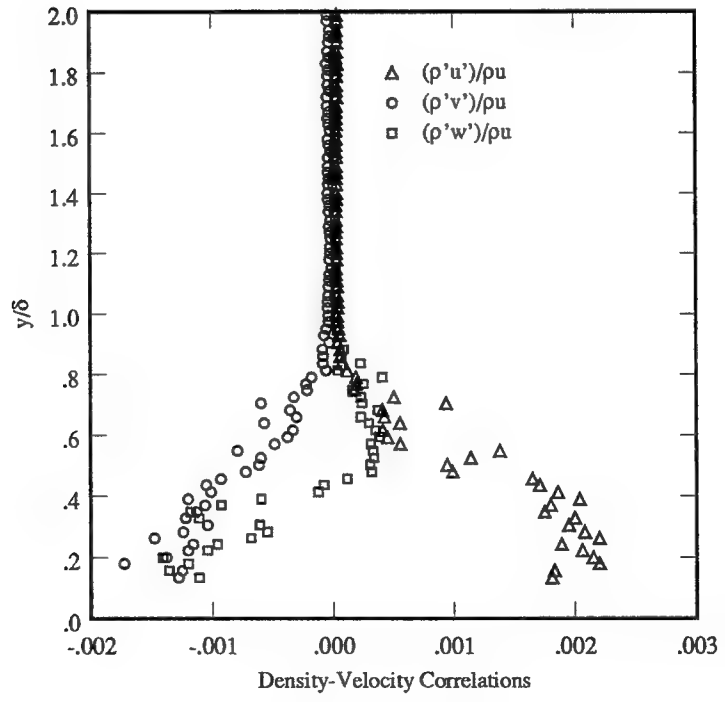

(b) Density-velocity correlations

FIGURE 5.18: Velocity-velocity and density-velocity correlations (x = 44 cm).

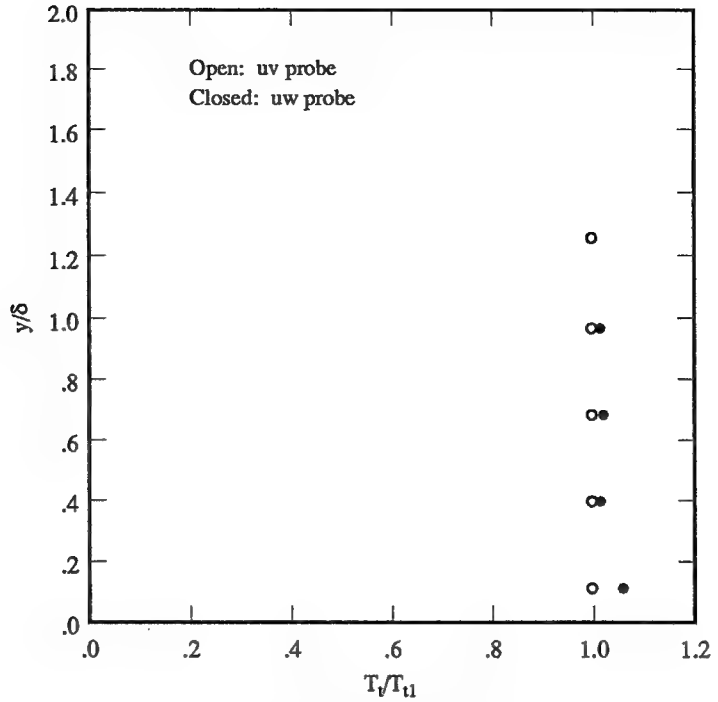

(a) Upstream total temperature

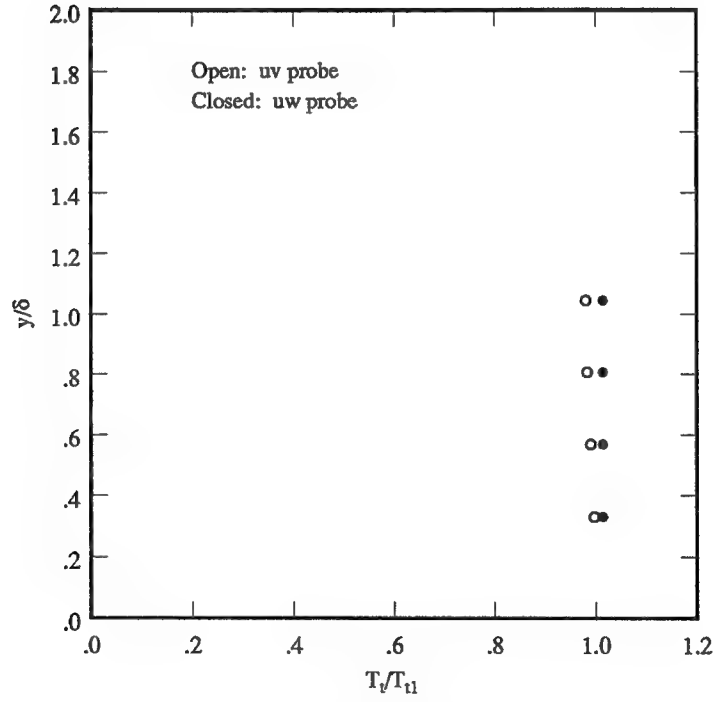

(b) Downstream total temperature

FIGURE 5.19: Total temperature profiles (x = 44 cm, x = 71 cm).

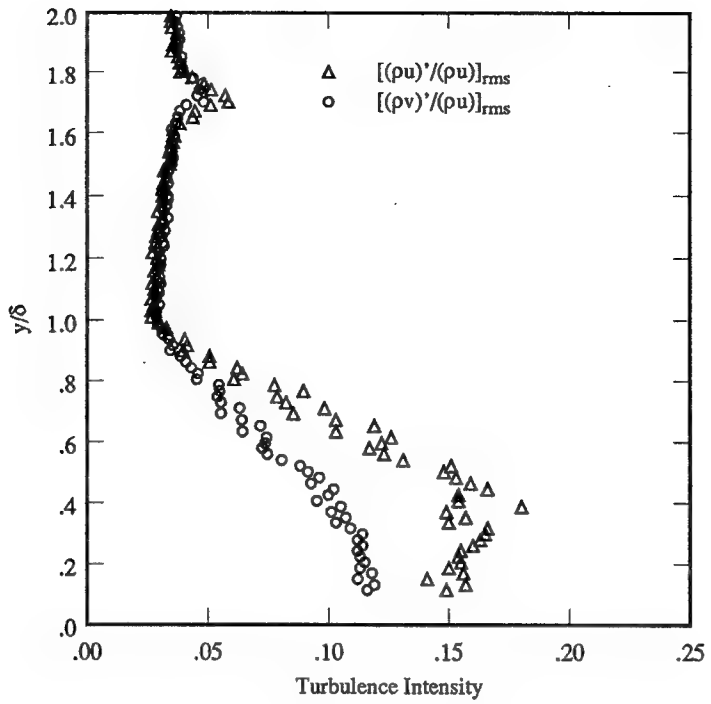

(a) Turbulence intensities

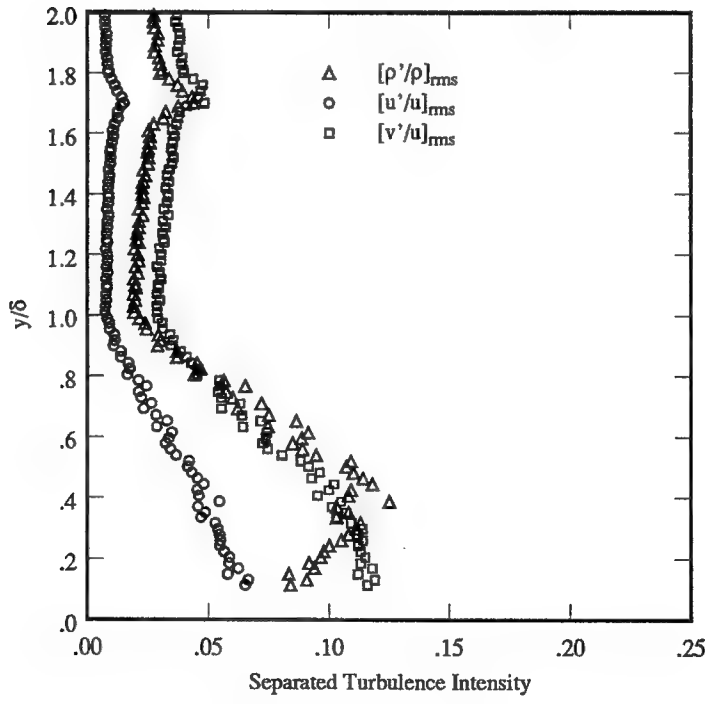

(b) Separated turbulence intensities

FIGURE 5.20: Turbulence intensities, uv probe (x = 71 cm).

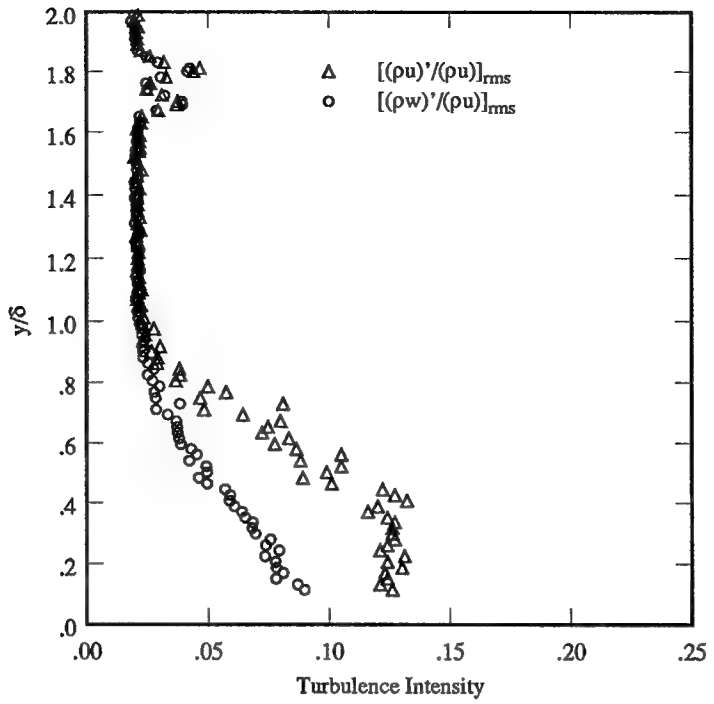

(a) Turbulence intensities

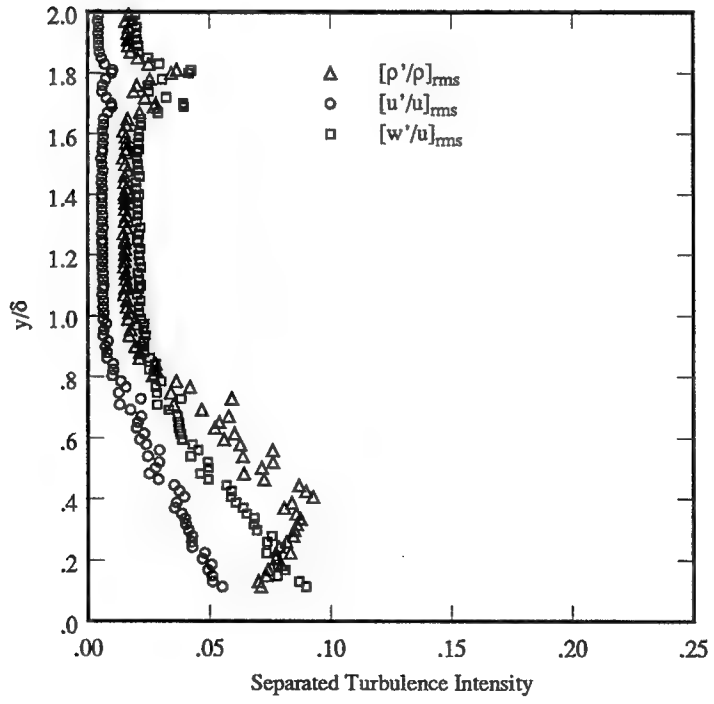

(b) Separated turbulence intensities

FIGURE 5.21: Turbulence intensities, uw probe (x = 71 cm).

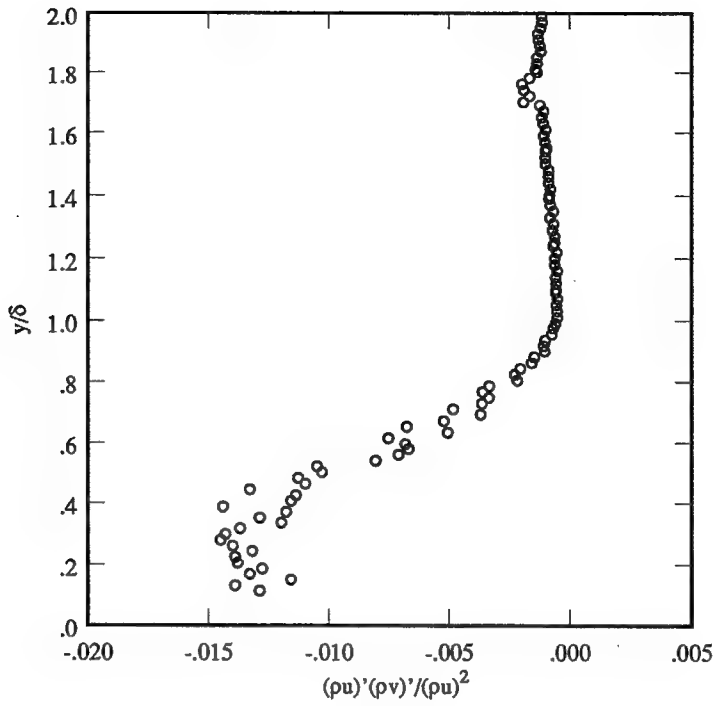

(a) Shear

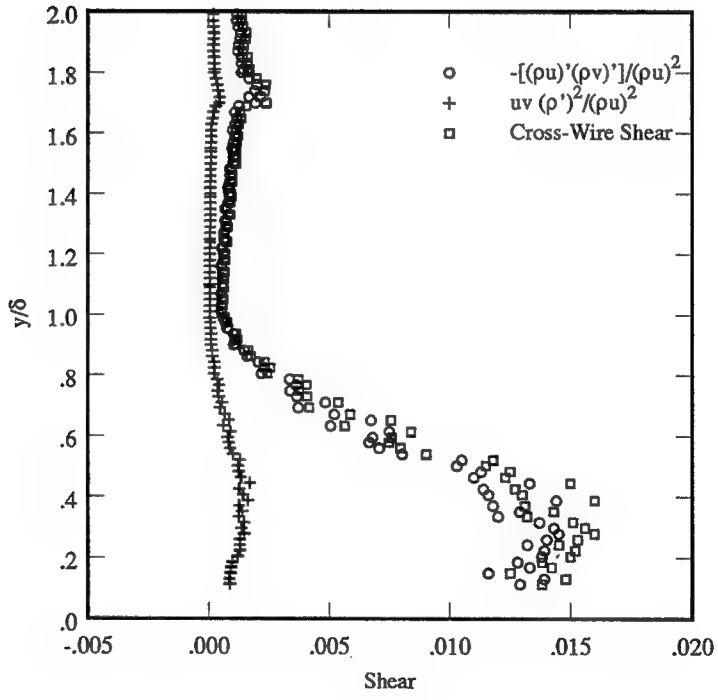

(b) Transformed shear

FIGURE 5.22: Cross-wire transformed turbulent x-y shear data (x = 71 cm).

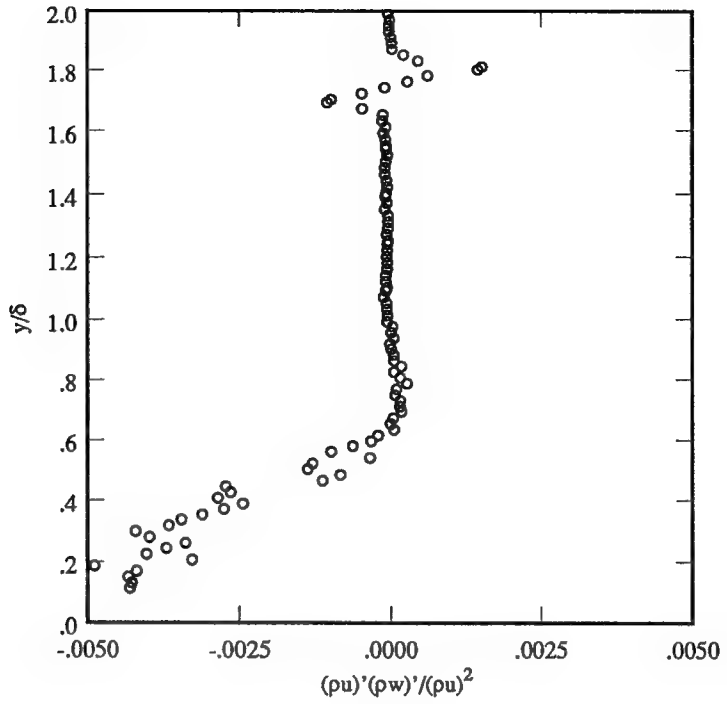

(a) Shear

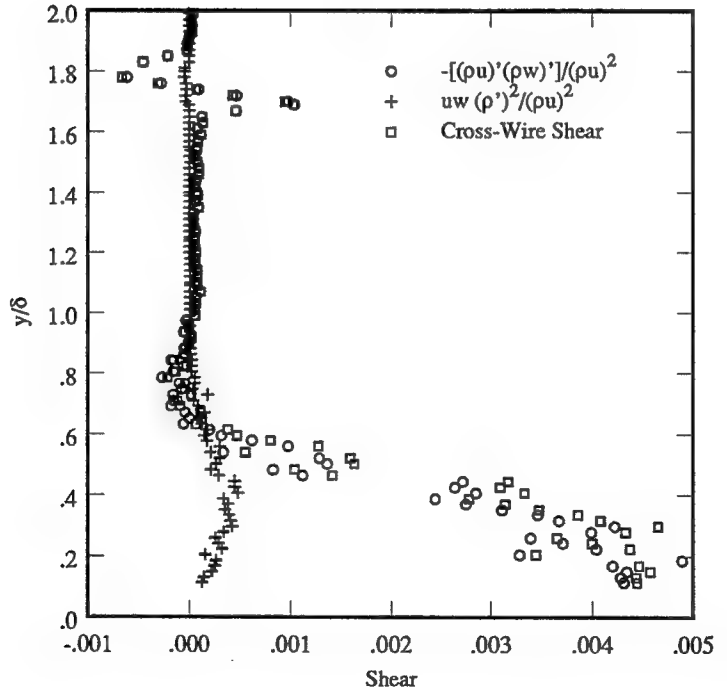

(b) Transformed shear

FIGURE 5.23: Cross-wire transformed turbulent x-z shear data (x = 71 cm).

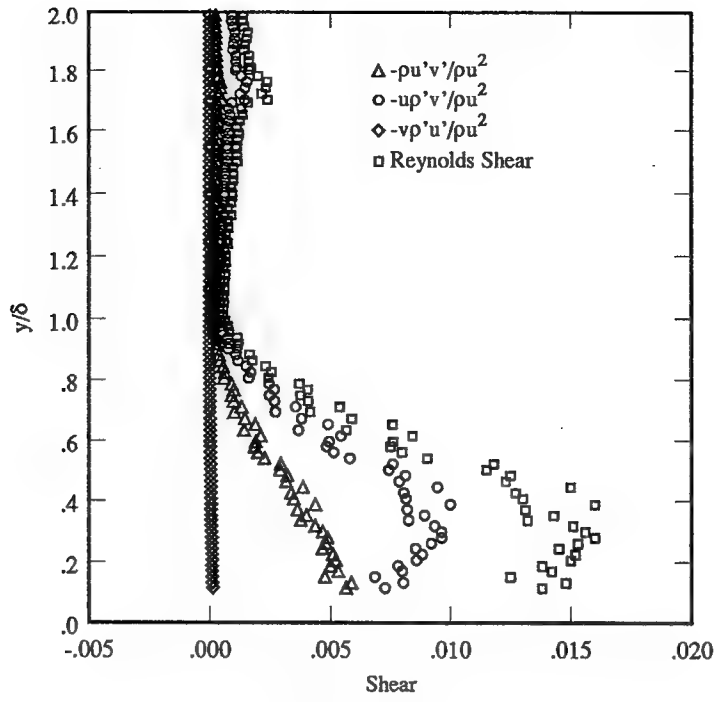

(a) Reynolds shear stress

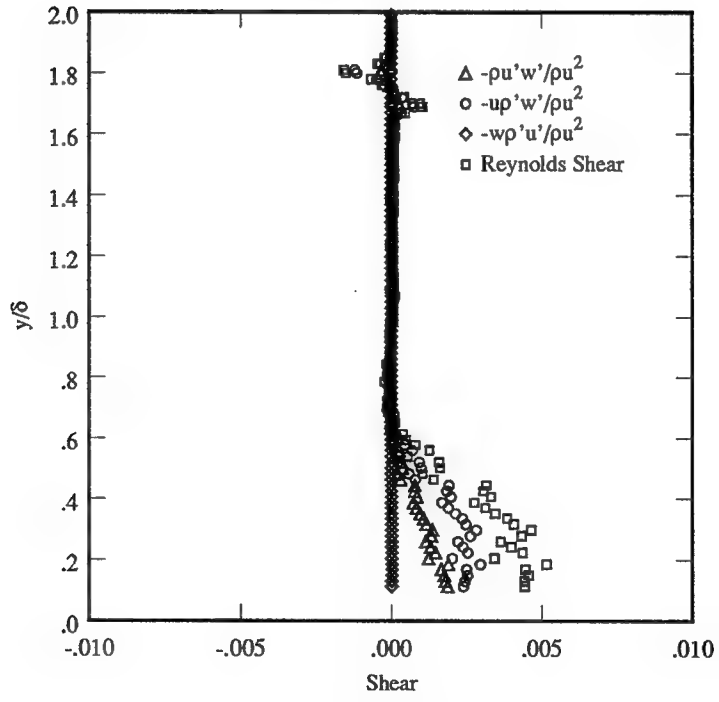

(b) Reynolds shear stress

FIGURE 5.24: Cross-wire x-y and x-z plane Reynolds shear stress (x = 71 cm).

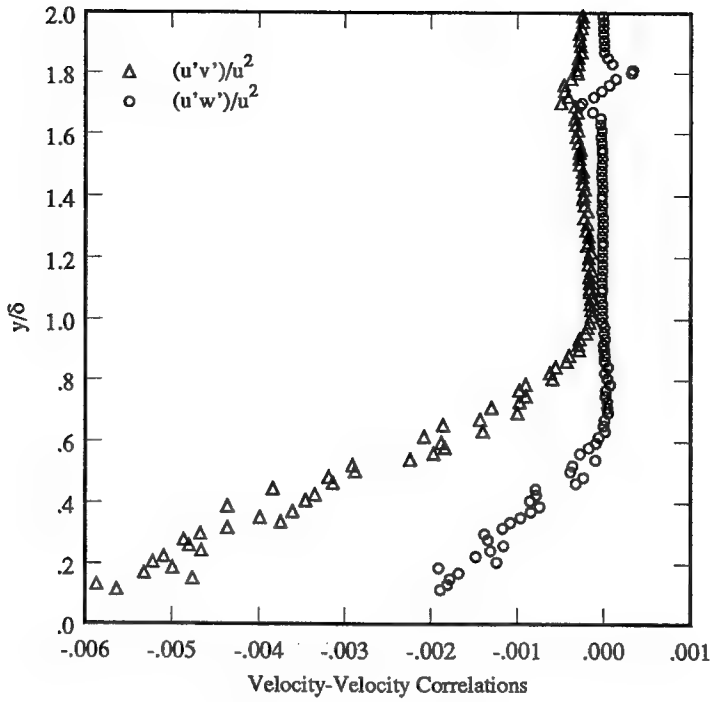

(a) Velocity-velocity correlations

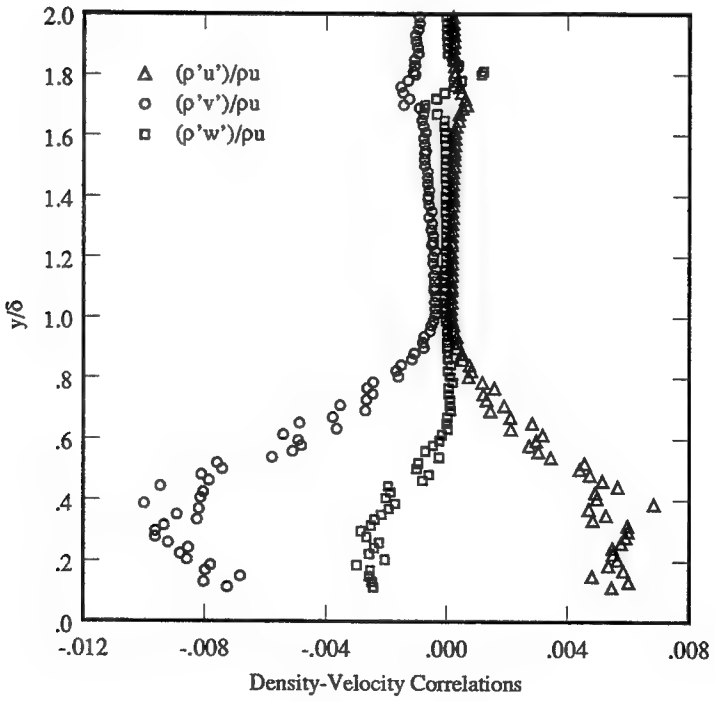

(b) Density-velocity correlations

FIGURE 5.25: Velcity-velocity and density-velocity correlations (x = 71 cm).

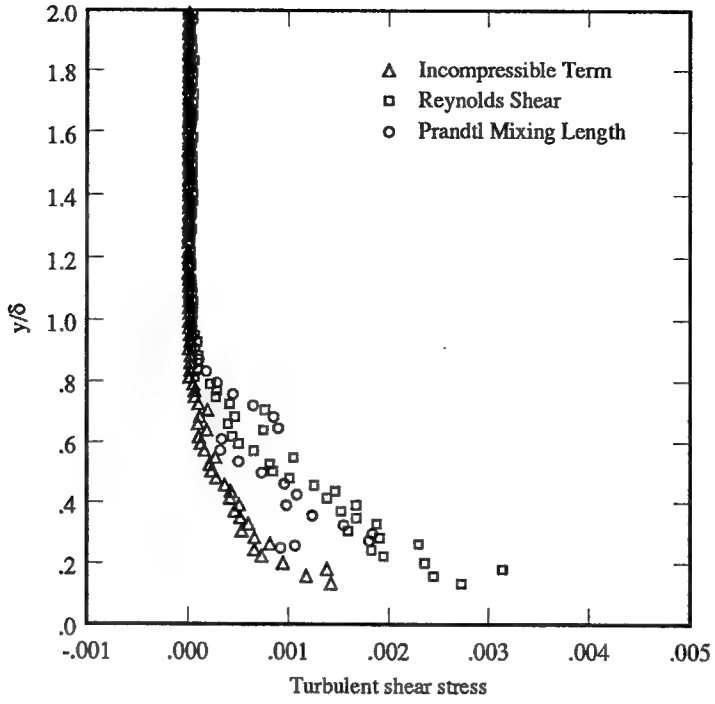

(a) Upstream

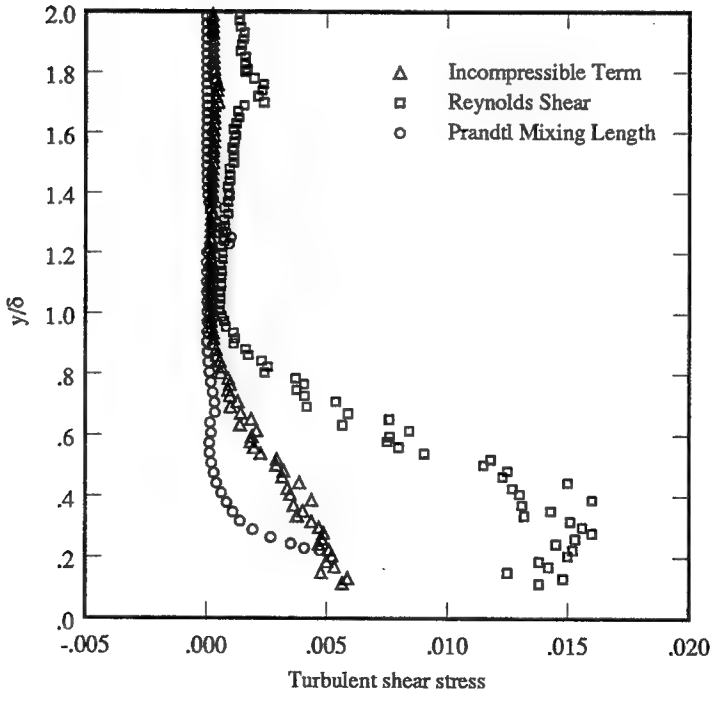

(b) Downstream (compression ramp)

FIGURE 5.26: Prandtl mixing length model evaluations (x = 44 cm, x = 71 cm).

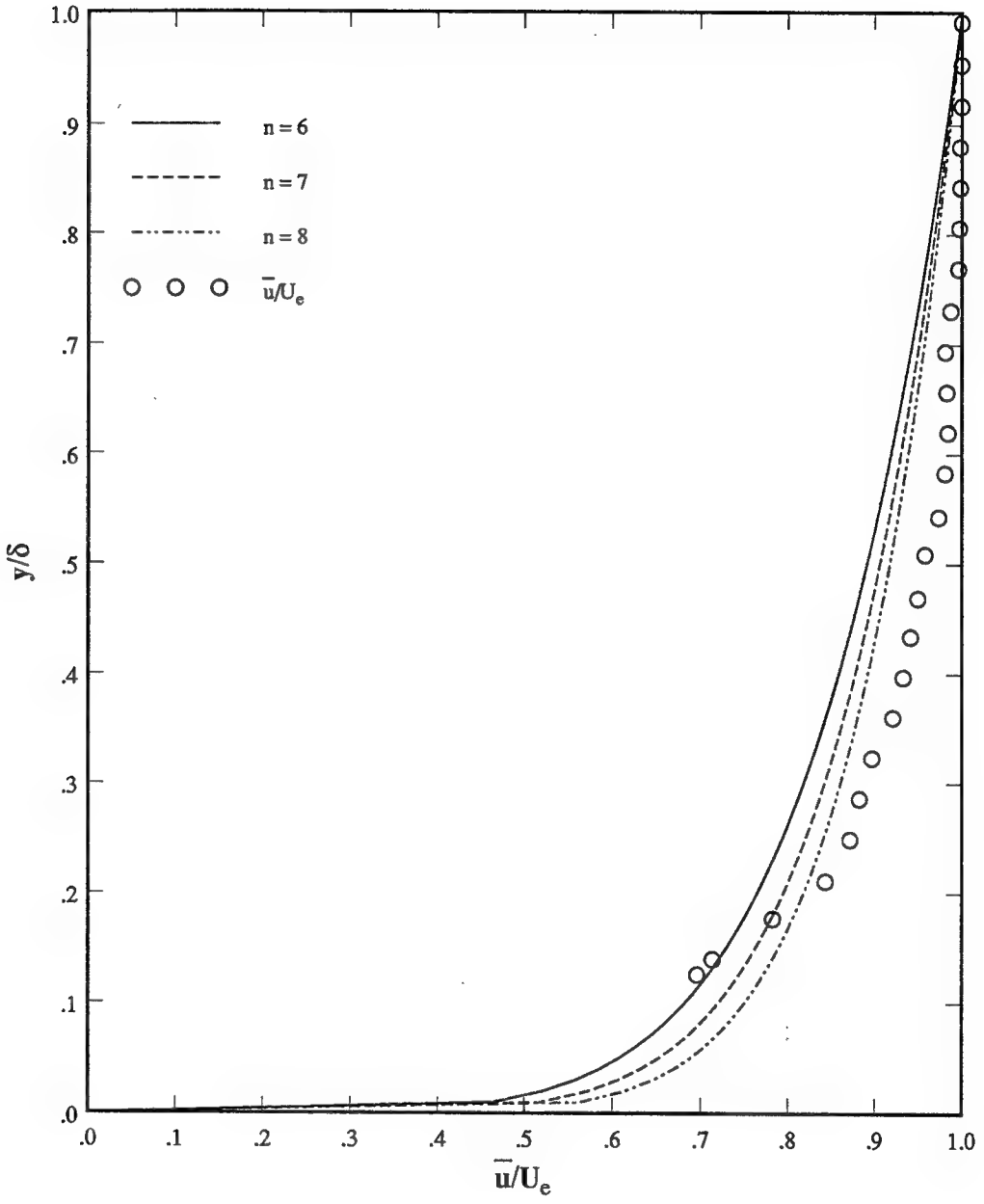

FIGURE 5.27: Power law relations (x = 44 cm).

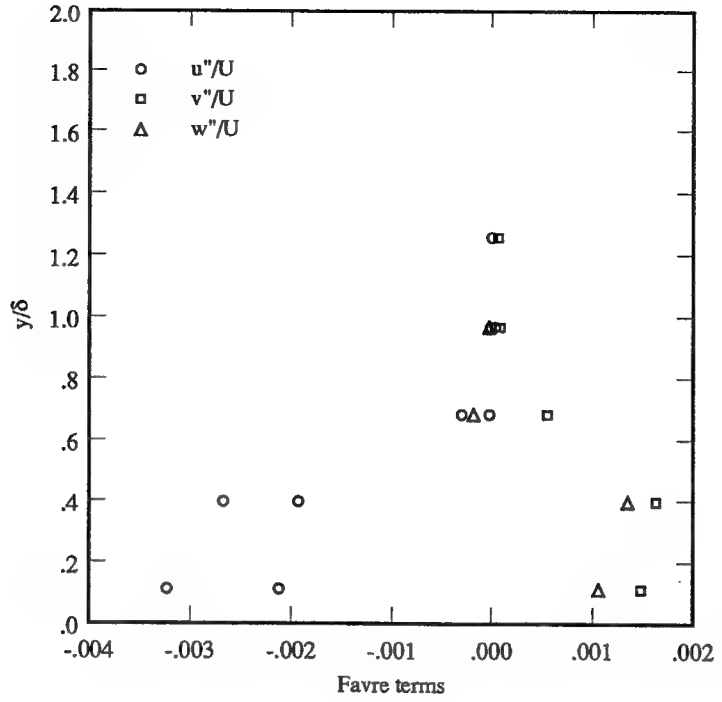

(a) Favre terms

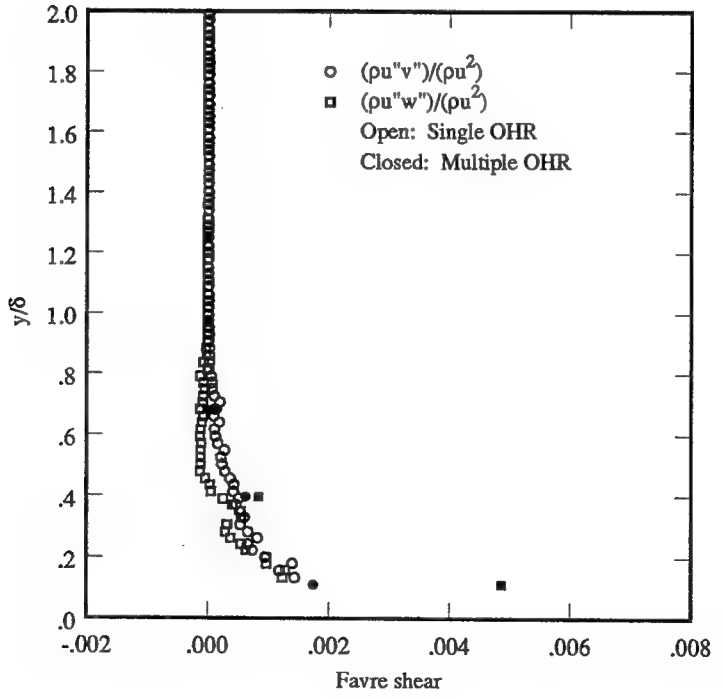

(b) Favre shear

FIGURE 5.28: Upstream Favre data (x = 44 cm).

VI. Conclusions and Recommendations

The chapter presents the main conclusions from the study and identifies some areas for further research.

6.1 Conclusions

Mean flow measurements were obtained for two flows with adverse pressure gradients: a compression ramp and a shock boundary layer interaction, as well as a common upstream location. Compressible turbulence measurements were obtained for the upstream, zero-pressure-gradient flow and the compression ramp using single and multiple overheat cross-wire anemometry.

Results indicate that compressibility effects are important not only for supersonic turbulent boundary layers with adverse pressure gradient, but also for the zero pressure gradient flow studied in this invesitigation. In particular, the density fluctuations are large, compared to the velocity fluctuations at all stations surveyed.

The results also indicate that compressibility manifests itself in the total Reynolds shear stress. The last two terms in Eqn. (2.13), repeated here, are not significant. But the first two terms are significant, especially the second term, which is frequently neglected in current turbulence models

$$-\tau_{ij}^{T} = \overline{\rho u_i'' u_j''} + \overline{u_i} \overline{\rho'' u_j''} + \overline{u_j} \overline{\rho'' u_i''} + \overline{\rho'' u_i'' u_j''} \tag{6.1}$$

In fact, for the conditions investigated, compressibility accounted for more than half of the total Reynolds shear stress, suggesting that turbulence models should account for this effect.

6.2 Recommendations For Further Study

As mentioned in Chapter 3, in order to obtain compressible turbulence measurements in a shock boundary interaction with hot wires, the Mach number must be greater than approximately 1.4. Several options are available with the existing wedge model, or with minor modifications to the wedge model.

One option is to measure turbulence quantities after the flow has passed through the initial oblique shock wave instead of both the initial and reflected oblique shock waves. From normal/oblique shock relations for a Mach 2.9 flow, the freestream Mach number would be approximately 2.42 for a 10° wedge model after passing through the initial oblique shock. Measurements could be obtained using existing probes, instrumentation, and data reduction techniques by drilling a 10° probe whole in the wedge model bottom plate. Another option is to decrease the flow turning angle below 10°.

This study measured most of the terms in the turbulent shear stress tensor, shown below, in Cartesian coordinates

$$\tau^{T} = \begin{bmatrix} \tau_{xx}^{T} & \tau_{xy}^{T} & \tau_{xz}^{T} \\ \tau_{yx}^{T} & \tau_{yy}^{T} & \tau_{yz}^{T} \\ \tau_{zx}^{T} & \tau_{zy}^{T} & \tau_{zz}^{T} \end{bmatrix}. \tag{6.1}$$

Assuming symmetry, the only remaining unknown term is τ_{yz}^{T}. A three-component cross wire could be used to obtain the complete turbulent stress tensor.

Finally, in order to better isolate the pressure gradient effects from any effects resulting from the natural growth of the boundary layer with axial distance, a measurement of a zero pressure gradient boundary layer at the same location (71 cm) as the compression ramp should be conducted.

Appendix A: Data

The raw data from all of the figures presented in Chapter 5 are included in the following pages. The data are presented by figure number, and the first column is assumed to be the x-axis values, and the second column the y-axis values.

Fig 5.3a

0.116	0.083
0.117	0.085
0.119	0.119
0.160	0.166
0.196	0.212
0.213	0.258
0.214	0.305
0.240	0.351
0.256	0.398
0.270	0.445
0.280	0.492
0.304	0.539
0.319	0.587
0.329	0.634
0.328	0.681
0.343	0.728
0.361	0.775
0.363	0.823
0.366	0.870
0.370	0.917
0.370	0.965
0.369	1.012
0.368	1.059
0.367	1.107
0.366	1.154
0.366	1.201
0.365	1.248
0.364	1.295
0.363	1.343
0.361	1.390
0.359	1.437
0.357	1.484
0.356	1.505
0.356	1.505
0.356	1.505
0.356	1.506
0.355	1.534
0.353	1.575
0.351	1.616
0.349	1.657
0.348	1.698
0.346	1.740
0.345	1.781
0.345	1.822
0.348	1.863
0.351	1.905
0.350	1.946
0.349	1.987
0.348	2.028

Fig 5.3b

0.048	0.127
0.048	0.140
0.047	0.176
0.045	0.212
0.044	0.249
0.044	0.285
0.044	0.322
0.044	0.359
0.044	0.396
0.045	0.433
0.045	0.470
0.046	0.507
0.046	0.544
0.047	0.582
0.047	0.619
0.048	0.657
0.049	0.694
0.049	0.731
0.050	0.768
0.050	0.806
0.050	0.843
0.051	0.881
0.051	0.918
0.051	0.955
0.051	0.993
0.051	1.030
0.051	1.067
0.050	1.105
0.050	1.142
0.050	1.179
0.050	1.216
0.050	1.253
0.050	1.291
0.050	1.328
0.049	1.366
0.049	1.403
0.049	1.440
0.048	1.477
0.048	1.515
0.048	1.545
0.048	1.553
0.047	1.585
0.047	1.622
0.047	1.659
0.046	1.697
0.046	1.734
0.046	1.772
0.046	1.809
0.046	1.846
0.047	1.884
0.047	1.921
0.047	1.959
0.048	1.997
0.048	2.034

Fig 5.4a

1.464	0.126
1.519	0.140
1.750	0.177
1.985	0.211
2.110	0.249
2.160	0.286
2.230	0.323
2.354	0.360
2.419	0.397
2.467	0.434
2.516	0.469
2.565	0.509
2.667	0.543
2.716	0.583
2.740	0.620
2.730	0.657
2.719	0.694
2.763	0.731
2.827	0.769
2.834	0.806
2.843	0.843
2.841	0.880
2.856	0.917
2.855	0.954
2.856	0.991
2.860	1.031
2.860	1.066
2.859	1.106
2.863	1.143
2.860	1.180
2.858	1.217
2.864	1.254
2.868	1.291
2.873	1.329
2.874	1.366
2.882	1.403
2.886	1.440
2.893	1.477
2.897	1.514
2.902	1.546
2.900	1.551
2.901	1.586
2.905	1.623
2.913	1.660
2.914	1.697
2.919	1.734
2.921	1.771
2.922	1.809
2.925	1.846
2.921	1.883
2.915	1.923
2.890	1.960
2.866	1.997

Fig 5.4b

0.0383	0.114
0.0394	0.143
0.0378	0.171
0.0352	0.200
0.0336	0.257
0.0329	0.286
0.0325	0.314
0.0318	0.371
0.0319	0.400
0.0321	0.429
0.0319	0.457
0.0321	0.514
0.0317	0.543
0.0319	0.571
0.0321	0.629
0.0326	0.657
0.0332	0.686
0.0333	0.743
0.0333	0.771
0.0335	0.800
0.0335	0.857
0.0338	0.886
0.0337	0.914
0.0338	0.943
0.0337	1.000
0.0335	1.029
0.0335	1.057
0.0334	1.114
0.0333	1.143
0.0333	1.171
0.0333	1.229
0.0331	1.257
0.0329	1.286
0.0327	1.314
0.0326	1.371
0.0323	1.400
0.032	1.429
0.0317	1.486
0.0315	1.514
0.0313	1.543
0.0313	1.543
0.0312	1.571
0.0309	1.629
0.0306	1.657
0.0305	1.686
0.0303	1.743
0.0301	1.771
0.0301	1.800
0.0302	1.857
0.0305	1.886
0.0308	1.914
0.0312	1.971
0.0316	2.000

Fig 5.5a

velocity

0.696	0.126
0.714	0.140
0.783	0.177
0.843	0.211
0.872	0.249
0.882	0.286
0.897	0.323
0.921	0.360
0.933	0.397
0.941	0.434
0.949	0.469
0.957	0.509
0.973	0.543
0.980	0.583
0.984	0.620
0.983	0.657
0.981	0.694
0.987	0.731
0.996	0.769
0.997	0.806
0.998	0.843
0.998	0.880
1.000	0.917
1.000	0.954
1.000	0.991
1.001	1.031
1.001	1.066
1.000	1.106
1.001	1.143
1.001	1.180
1.000	1.217
1.001	1.254
1.002	1.291
1.002	1.329
1.002	1.366
1.003	1.403
1.004	1.440
1.005	1.477
1.005	1.514

1.006	1.546
1.006	1.551
1.006	1.586
1.006	1.623
1.007	1.660
1.008	1.697
1.008	1.734
1.008	1.771
1.009	1.809
1.009	1.846
1.008	1.883
1.008	1.923
1.004	1.960
1.001	1.997
0.999	2.034

Density

0.543	0.126
0.555	0.140
0.613	0.177
0.680	0.211
0.718	0.249
0.735	0.286
0.758	0.323
0.801	0.360
0.825	0.397
0.843	0.434
0.861	0.469
0.880	0.509
0.921	0.543
0.941	0.583
0.951	0.620
0.947	0.657
0.942	0.694
0.960	0.731
0.987	0.769
0.990	0.806
0.994	0.843
0.994	0.880
1.000	0.917
1.000	0.954
1.000	0.991
1.002	1.031
1.002	1.066
1.001	1.106
1.003	1.143
1.002	1.180
1.001	1.217
1.003	1.254
1.005	1.291
1.007	1.329
1.008	1.366
1.011	1.403
1.013	1.440
1.016	1.477
1.018	1.514
1.020	1.546
1.019	1.551
1.020	1.586
1.021	1.623
1.025	1.660
1.025	1.697
1.028	1.734
1.029	1.771
1.029	1.809
1.030	1.846
1.029	1.883
1.026	1.923
1.015	1.960
1.004	1.997
0.997	2.034

Mass Flux

0.378	0.126
0.396	0.140
0.480	0.177
0.573	0.211
0.626	0.249
0.648	0.286
0.680	0.323
0.738	0.360
0.769	0.397
0.793	0.434
0.818	0.469
0.843	0.509
0.896	0.543
0.922	0.583
0.935	0.620
0.930	0.657
0.924	0.694
0.948	0.731
0.984	0.769
0.988	0.806
0.993	0.843
0.992	0.880
1.000	0.917
0.999	0.954
1.000	0.991
1.002	1.031
1.002	1.066
1.002	1.106
1.004	1.143
1.002	1.180
1.001	1.217
1.005	1.254
1.007	1.291
1.010	1.329
1.010	1.366
1.015	1.403
1.017	1.440
1.021	1.477
1.023	1.514
1.026	1.546
1.025	1.551
1.026	1.586
1.028	1.623
1.033	1.660
1.033	1.697
1.036	1.734
1.037	1.771
1.038	1.809
1.040	1.846
1.037	1.883
1.034	1.923
1.019	1.960
1.006	1.997
0.997	2.034

Fig. 5.6a

0.222	0.095
0.230	0.108
0.258	0.135
0.274	0.162
0.280	0.189
0.292	0.216
0.297	0.243
0.303	0.270
0.318	0.297
0.325	0.325
0.341	0.351
0.349	0.379
0.359	0.407
0.369	0.433
0.384	0.461
0.389	0.489
0.385	0.515
0.400	0.543
0.408	0.571
0.410	0.598
0.429	0.626
0.434	0.654
0.443	0.681
0.446	0.709
0.457	0.737
0.455	0.764
0.458	0.791
0.463	0.819
0.463	0.846
0.467	0.874
0.467	0.902
0.477	0.921
0.477	0.953
0.486	0.984
0.489	1.014
0.489	1.044
0.490	1.074
0.491	1.104
0.492	1.135
0.496	1.165
0.496	1.195
0.497	1.226
0.495	1.256
0.497	1.285
0.497	1.315
0.498	1.346
0.495	1.376
0.496	1.406
0.495	1.436
0.494	1.467
0.493	1.497
0.492	1.527
0.493	1.558
0.493	1.588
0.499	1.618
0.500	1.648
0.501	1.678
0.501	1.709
0.500	1.739
0.501	1.757
0.501	1.757
0.499	1.760
0.497	1.796
0.496	1.844
0.496	1.893
0.493	1.940
0.491	1.989
0.486	2.037

Fig 5.6b

0.073	0.144
0.072	0.177
0.071	0.222
0.070	0.267
0.070	0.312
0.069	0.358
0.069	0.404
0.069	0.449
0.070	0.495
0.070	0.541
0.070	0.587
0.072	0.633
0.072	0.679
0.073	0.726
0.074	0.771
0.074	0.818
0.075	0.864
0.075	0.910
0.076	0.957
0.076	1.003
0.076	1.050
0.077	1.096
0.077	1.142
0.078	1.189
0.078	1.235
0.078	1.281
0.079	1.328
0.079	1.374
0.080	1.420
0.081	1.467
0.082	1.512
0.082	1.559
0.082	1.605
0.082	1.651
0.081	1.697
0.081	1.743
0.081	1.788
0.080	1.803
0.080	1.804
0.080	1.817
0.080	1.851
0.079	1.886
0.079	1.920
0.078	1.955
0.078	1.990
0.077	2.024

Fig 5.7a

1.760	0.143
1.834	0.177
1.920	0.223
1.985	0.267
2.081	0.313
2.180	0.357
2.246	0.403
2.326	0.450
2.362	0.493
2.396	0.540
2.438	0.587
2.491	0.633
2.526	0.680

2.552 0.727
2.539 0.770
2.566 0.817
2.557 0.863
2.559 0.910
2.581 0.957
2.613 1.003
2.602 1.050
2.590 1.097
2.594 1.143
2.596 1.190
2.591 1.233
2.591 1.280
2.585 1.327
2.569 1.373
2.555 1.420
2.519 1.467
2.491 1.513
2.490 1.560
2.502 1.607
2.523 1.650
2.537 1.697
2.540 1.743
2.540 1.787
2.547 1.803
2.542 1.803
2.544 1.817
2.553 1.850
2.568 1.887
2.574 1.920
2.573 1.957
2.578 1.990
2.578 2.023

Fig 5.7b

0.0574 0.119048
0.056 0.166667
0.0544 0.190476
0.0531 0.214286
0.0519 0.261905
0.0513 0.285714
0.0507 0.309524
0.0506 0.357143
0.0507 0.380952
0.0503 0.428571
0.0508 0.452381
0.0509 0.47619
0.0511 0.52381
0.0519 0.547619
0.0516 0.595238
0.0523 0.619048
0.0529 0.642857
0.0528 0.690476
0.0526 0.714286
0.0532 0.738095
0.0539 0.785714
0.054 0.809524
0.0542 0.857143
0.0544 0.880952
0.0545 0.904762
0.0548 0.952381
0.0551 0.97619
0.0558 1.02381
0.0572 1.047619
0.0582 1.071429
0.0582 1.119048
0.0581 1.142857
0.0577 1.190476
0.0572 1.214286
0.057 1.238095
0.0566 1.285714
0.0562 1.285714
0.0564 1.285714
0.0563 1.285714
0.0559 1.333333
0.0553 1.357143
0.0549 1.380952
0.0547 1.404762
0.0543 1.428571
0.054 1.452381
0.0537 1.47619
0.0533 1.5
0.053 1.52381
0.0523 1.547619
0.0521 1.571429
0.0517 1.595238
0.0505 1.619048
0.0474 1.642857
0.045 1.666667
0.0417 1.690476
0.0387 1.714286
0.0367 1.738095
0.0349 1.761905
0.0336 1.785714
0.0328 1.809524
0.0323 1.833333
0.0319 1.857143
0.0317 1.904762
0.0313 1.928571
0.031 1.952381
0.0308 1.97619
0.0305 2

Fig. 5.8a

Density

0.698 0.102
0.721 0.126
0.749 0.160
0.771 0.190
0.804 0.224
0.841 0.255
0.866 0.288
0.897 0.321
0.912 0.352
0.926 0.386
0.943 0.419
0.966 0.452
0.981 0.486
0.992 0.519
0.987 0.550
0.999 0.583
0.995 0.617
0.996 0.650
1.005 0.683
1.020 0.717
1.015 0.750
1.009 0.783
1.011 0.817
1.012 0.850
1.010 0.881
1.010 0.914
1.007 0.948
1.000 0.981
0.994 1.014
0.978 1.048
0.966 1.081
0.966 1.114
0.971 1.148
0.980 1.179
0.986 1.212
0.987 1.245
0.987 1.276
0.990 1.288
0.988 1.288
0.989 1.298
0.993 1.321
1.000 1.348
1.002 1.371
1.002 1.398
1.004 1.421
1.004 1.445
1.003 1.471
1.004 1.495
1.004 1.521
1.002 1.545
0.983 1.569
0.957 1.595
0.948 1.619
0.970 1.645
0.993 1.669
1.038 1.695
1.087 1.719
1.124 1.743
1.161 1.769
1.188 1.793
1.206 1.819
1.216 1.843
1.225 1.869
1.229 1.893
1.236 1.917
1.242 1.943
1.246 1.967
1.251 1.993
1.253 2.017

Velocity

0.820 0.102
0.841 0.126
0.864 0.160
0.880 0.190
0.903 0.224
0.925 0.255
0.940 0.288
0.956 0.321
0.963 0.352
0.969 0.386
0.977 0.419
0.987 0.452
0.993 0.486
0.997 0.519
0.995 0.550
0.999 0.583
0.998 0.617
0.998 0.650
1.002 0.683
1.007 0.717
1.005 0.750
1.003 0.783
1.004 0.817
1.004 0.850
1.004 0.881
1.004 0.914
1.003 0.948
1.000 0.981
0.998 1.014
0.991 1.048
0.987 1.081
0.986 1.114
0.989 1.148
0.992 1.179
0.995 1.212
0.995 1.245
0.995 1.276
0.996 1.288
0.995 1.288
0.996 1.298
0.997 1.321
1.000 1.348
1.001 1.371
1.001 1.398
1.002 1.421
1.002 1.445
1.001 1.471
1.002 1.495
1.001 1.521
1.001 1.545
0.994 1.569
0.983 1.595
0.979 1.619
0.988 1.645
0.997 1.669
1.014 1.695
1.030 1.719
1.041 1.743
1.051 1.769
1.058 1.793
1.063 1.819
1.065 1.843
1.067 1.869
1.068 1.893
1.070 1.917
1.071 1.943
1.072 1.967
1.073 1.993
1.074 2.017

Fig 5.8b

0.572 0.102
0.606 0.126
0.647 0.160
0.678 0.190
0.727 0.224
0.778 0.255
0.814 0.288
0.858 0.321
0.878 0.352
0.897 0.386
0.922 0.419
0.953 0.452

0.974 0.486
0.990 0.519
0.982 0.550
0.998 0.583
0.993 0.617
0.994 0.650
1.007 0.683
1.027 0.717
1.020 0.750
1.013 0.783
1.015 0.817
1.017 0.850
1.013 0.881
1.013 0.914
1.010 0.948
1.000 0.981
0.991 1.014
0.970 1.048
0.953 1.081
0.952 1.114
0.960 1.148
0.972 1.179
0.981 1.212
0.982 1.245
0.982 1.276
0.987 1.288
0.984 1.288
0.985 1.298
0.990 1.321
0.999 1.348
1.003 1.371
1.002 1.398
1.006 1.421
1.006 1.445
1.004 1.471
1.006 1.495
1.005 1.521
1.002 1.545
0.977 1.569
0.941 1.595
0.928 1.619
0.959 1.645
0.991 1.669
1.053 1.695
1.119 1.719
1.170 1.743
1.221 1.769
1.258 1.793
1.282 1.819
1.295 1.843
1.307 1.869
1.313 1.893
1.322 1.917
1.330 1.943
1.336 1.967
1.343 1.993
1.346 2.017

Fig. 5.9a

0.187 0.137
0.197 0.178
0.227 0.223
0.259 0.264
0.290 0.306
0.320 0.350
0.345 0.392
0.369 0.436
0.392 0.478
0.405 0.522
0.418 0.564
0.438 0.608
0.429 0.653
0.445 0.694
0.467 0.739
0.484 0.780
0.488 0.825
0.497 0.869
0.500 0.914
0.507 0.955
0.511 1.000
0.510 1.041
0.508 1.086
0.506 1.131
0.506 1.172
0.503 1.217
0.498 1.258
0.491 1.296
0.483 1.341
0.472 1.385
0.452 1.430
0.442 1.478
0.430 1.522
0.429 1.567
0.428 1.611
0.430 1.656
0.428 1.701
0.430 1.723
0.430 1.790
0.430 1.838
0.432 1.885
0.435 1.933
0.438 1.984
0.441 2.032
0.443 2.080

Fig 5.9b

0.174 0.138
0.175 0.140
0.175 0.175
0.172 0.220
0.171 0.264
0.170 0.308
0.169 0.352
0.169 0.396
0.169 0.441
0.168 0.486
0.169 0.531
0.169 0.575
0.169 0.620
0.170 0.665
0.170 0.711
0.170 0.756
0.170 0.800
0.171 0.846
0.171 0.890
0.171 0.936
0.170 0.981
0.170 1.026
0.170 1.071
0.169 1.116
0.169 1.161
0.168 1.206
0.167 1.252
0.166 1.296
0.164 1.341
0.162 1.386
0.159 1.431
0.157 1.476
0.153 1.521
0.149 1.566
0.147 1.611
0.144 1.656
0.143 1.701
0.143 1.724
0.142 1.789
0.143 1.838
0.144 1.887
0.144 1.935
0.145 1.984
0.146 2.032
0.147 2.081

Fig. 5.10a

0.838 0.137
0.884 0.178
1.007 0.223
1.118 0.264
1.211 0.306
1.292 0.350
1.355 0.392
1.415 0.436
1.468 0.478
1.495 0.522
1.524 0.564
1.568 0.608
1.548 0.653
1.582 0.694
1.627 0.739
1.661 0.780
1.67 0.825
1.687 0.869
1.693 0.914
1.705 0.955
1.714 1.000
1.712 1.041
1.708 1.086
1.704 1.131
1.704 1.172
1.698 1.217
1.688 1.258
1.678 1.296
1.672 1.341
1.66 1.385
1.641 1.430
1.637 1.478
1.635 1.522
1.653 1.567
1.663 1.611
1.683 1.656
1.687 1.701
1.69 1.723
1.696 1.790
1.699 1.838
1.698 1.885
1.702 1.933
1.702 1.984
1.699 2.032
1.699 2.080

Fig. 5.10b

0.103 0.191083
0.103 0.22293
0.106 0.254777
0.108 0.318471
0.111 0.350318
0.112 0.382166
0.113 0.44586
0.116 0.477707
0.116 0.541401
0.115 0.573248
0.121 0.605096
0.116 0.66879
0.116 0.700637
0.117 0.764331
0.119 0.796178
0.118 0.859873
0.119 0.89172
0.119 0.923567
0.119 0.987261
0.119 1.019108
0.12 1.082803
0.12 1.11465
0.119 1.146497
0.119 1.210191
0.12 1.242038
0.119 1.305732
0.118 1.33758
0.117 1.401274
0.114 1.433121
0.112 1.464968
0.109 1.528662
0.107 1.56051
0.105 1.624204
0.103 1.656051
0.103 1.687898
0.103 1.719745
0.103 1.783439
0.103 1.847134
0.104 1.878981
0.104 1.942675
0.105 1.974522
0.105 2.038217

Fig. 5.11a

density

0.723 0.137
0.733 0.178
0.762 0.223
0.792 0.264
0.820 0.306
0.845 0.350
0.866 0.392
0.887 0.436
0.907 0.478
0.917 0.522
0.928 0.564
0.945 0.608
0.937 0.653

0.951	0.694
0.969	0.739
0.983	0.780
0.987	0.825
0.994	0.869
0.997	0.914
1.002	0.955
1.006	1.000
1.005	1.041
1.003	1.086
1.002	1.131
1.002	1.172
0.999	1.217
0.995	1.258
0.991	1.296
0.988	1.341
0.983	1.385
0.975	1.430
0.973	1.478
0.973	1.522
0.980	1.567
0.984	1.611
0.993	1.656
0.994	1.701
0.996	1.723
0.998	1.790
1.000	1.838
0.999	1.885
1.001	1.933
1.001	1.984
1.000	2.032
1.000	2.080

Velocity

0.580	0.137
0.607	0.178
0.678	0.223
0.739	0.264
0.787	0.306
0.827	0.350
0.856	0.392
0.884	0.436
0.907	0.478
0.918	0.522
0.931	0.564
0.949	0.608
0.940	0.653
0.954	0.694
0.972	0.739
0.985	0.780
0.989	0.825
0.995	0.869
0.997	0.914
1.002	0.955
1.005	1.000
1.004	1.041
1.003	1.086
1.001	1.131
1.001	1.172
0.999	1.217
0.996	1.258
0.992	1.296
0.989	1.341
0.985	1.385
0.978	1.430
0.976	1.478
0.975	1.522
0.982	1.567
0.986	1.611
0.994	1.656
0.995	1.701
0.996	1.723
0.999	1.790
1.000	1.838
0.999	1.885
1.001	1.933
1.001	1.984
1.000	2.032
1.000	2.080

Fig. 5.11b

0.419	0.137
0.445	0.178
0.517	0.223
0.585	0.264
0.645	0.306
0.699	0.350
0.742	0.392
0.784	0.436
0.822	0.478
0.842	0.522
0.864	0.564
0.897	0.608
0.882	0.653
0.907	0.694
0.942	0.739
0.969	0.780
0.976	0.825
0.990	0.869
0.994	0.914
1.004	0.955
1.011	1.000
1.010	1.041
1.006	1.086
1.003	1.131
1.003	1.172
0.998	1.217
0.990	1.258
0.982	1.296
0.978	1.341
0.968	1.385
0.953	1.430
0.950	1.478
0.948	1.522
0.963	1.567
0.970	1.611
0.986	1.656
0.990	1.701
0.992	1.723
0.997	1.790
0.999	1.838
0.998	1.885
1.002	1.933
1.002	1.984
0.999	2.032
0.999	2.080

Fig. 5.12a

$[(\rho u)'/(\rho u)]_{rms}$

0.853E-01	0.134E+00
0.855E-01	0.157E+00
0.943E-01	0.180E+00
0.944E-01	0.200E+00
0.935E-01	0.223E+00
0.904E-01	0.243E+00
0.981E-01	0.263E+00
0.957E-01	0.283E+00
0.932E-01	0.306E+00
0.949E-01	0.329E+00
0.898E-01	0.349E+00
0.920E-01	0.371E+00
0.985E-01	0.391E+00
0.945E-01	0.414E+00
0.912E-01	0.437E+00
0.900E-01	0.457E+00
0.700E-01	0.480E+00
0.687E-01	0.503E+00
0.764E-01	0.526E+00
0.847E-01	0.549E+00
0.541E-01	0.571E+00
0.488E-01	0.594E+00
0.468E-01	0.617E+00
0.543E-01	0.640E+00
0.475E-01	0.660E+00
0.465E-01	0.683E+00
0.706E-01	0.706E+00
0.520E-01	0.726E+00
0.312E-01	0.749E+00
0.326E-01	0.769E+00
0.324E-01	0.791E+00
0.253E-01	0.814E+00
0.201E-01	0.837E+00
0.183E-01	0.860E+00
0.184E-01	0.883E+00
0.149E-01	0.906E+00
0.180E-01	0.929E+00
0.163E-01	0.951E+00
0.150E-01	0.974E+00
0.142E-01	0.994E+00
0.155E-01	0.102E+01
0.156E-01	0.104E+01
0.146E-01	0.106E+01
0.148E-01	0.109E+01
0.138E-01	0.111E+01
0.133E-01	0.113E+01
0.128E-01	0.115E+01
0.140E-01	0.118E+01
0.137E-01	0.120E+01
0.134E-01	0.122E+01
0.128E-01	0.125E+01
0.131E-01	0.127E+01
0.135E-01	0.129E+01
0.134E-01	0.131E+01
0.131E-01	0.134E+01
0.130E-01	0.136E+01
0.143E-01	0.138E+01
0.138E-01	0.140E+01
0.138E-01	0.143E+01
0.135E-01	0.145E+01
0.140E-01	0.147E+01
0.137E-01	0.149E+01
0.140E-01	0.152E+01
0.132E-01	0.154E+01
0.134E-01	0.156E+01
0.139E-01	0.158E+01
0.130E-01	0.161E+01
0.136E-01	0.163E+01
0.137E-01	0.165E+01
0.137E-01	0.167E+01
0.142E-01	0.169E+01
0.144E-01	0.172E+01
0.142E-01	0.174E+01
0.144E-01	0.176E+01
0.144E-01	0.179E+01
0.142E-01	0.181E+01
0.156E-01	0.183E+01
0.138E-01	0.185E+01
0.149E-01	0.187E+01
0.147E-01	0.190E+01
0.143E-01	0.192E+01
0.146E-01	0.194E+01
0.150E-01	0.197E+01
0.149E-01	0.199E+01

$[(\rho v)'/(\rho u)]_{rms}$

0.688E-01	0.134E+00
0.618E-01	0.157E+00
0.657E-01	0.180E+00
0.627E-01	0.200E+00
0.613E-01	0.223E+00
0.580E-01	0.243E+00
0.589E-01	0.263E+00
0.555E-01	0.283E+00
0.554E-01	0.306E+00
0.512E-01	0.329E+00
0.508E-01	0.349E+00
0.500E-01	0.371E+00
0.556E-01	0.391E+00
0.488E-01	0.414E+00
0.466E-01	0.437E+00
0.468E-01	0.457E+00
0.397E-01	0.480E+00
0.371E-01	0.503E+00
0.395E-01	0.526E+00
0.395E-01	0.549E+00
0.316E-01	0.571E+00
0.293E-01	0.594E+00
0.289E-01	0.617E+00
0.306E-01	0.640E+00
0.281E-01	0.660E+00
0.262E-01	0.683E+00
0.305E-01	0.706E+00
0.264E-01	0.726E+00
0.214E-01	0.749E+00
0.226E-01	0.769E+00
0.210E-01	0.791E+00
0.187E-01	0.814E+00
0.172E-01	0.837E+00
0.165E-01	0.860E+00
0.171E-01	0.883E+00
0.144E-01	0.906E+00
0.159E-01	0.929E+00
0.157E-01	0.951E+00
0.146E-01	0.974E+00
0.144E-01	0.994E+00
0.144E-01	0.102E+01
0.141E-01	0.104E+01
0.143E-01	0.106E+01

0.140E-01 0.109E+01
0.137E-01 0.111E+01
0.132E-01 0.113E+01
0.133E-01 0.115E+01
0.138E-01 0.118E+01
0.133E-01 0.120E+01
0.131E-01 0.122E+01
0.127E-01 0.125E+01
0.127E-01 0.127E+01
0.135E-01 0.129E+01
0.128E-01 0.131E+01
0.129E-01 0.134E+01
0.135E-01 0.136E+01
0.138E-01 0.138E+01
0.135E-01 0.140E+01
0.124E-01 0.143E+01
0.127E-01 0.145E+01
0.138E-01 0.147E+01
0.134E-01 0.149E+01
0.131E-01 0.152E+01
0.126E-01 0.154E+01
0.130E-01 0.156E+01
0.131E-01 0.158E+01
0.128E-01 0.161E+01
0.129E-01 0.163E+01
0.132E-01 0.165E+01
0.131E-01 0.167E+01
0.139E-01 0.169E+01
0.135E-01 0.172E+01
0.138E-01 0.174E+01
0.134E-01 0.176E+01
0.139E-01 0.179E+01
0.133E-01 0.181E+01
0.144E-01 0.183E+01
0.137E-01 0.185E+01
0.136E-01 0.187E+01
0.139E-01 0.190E+01
0.139E-01 0.192E+01
0.138E-01 0.194E+01
0.145E-01 0.197E+01
0.144E-01 0.199E+01

$[(\rho u)'/(\rho u)]_{rms}$ mohr

.0932 .111
.0954 .397
.0427 .683
.0111 .969
.0061 1.254

$[(\rho v)'/(\rho u)]_{rms}$ mohr

.0704 .111
.0623 .397
.0337 .683
.0176 .969
.0163 1.254

$[Tt'/Tt]_{srm}$

.0111 .111
.0114 .397
.00332 .683
.00239 .969
.0025 1.254

Fig. 5.12b

ρ' intensity

0.404E-01 0.134E+00
0.440E-01 0.157E+00
0.522E-01 0.180E+00
0.560E-01 0.200E+00
0.580E-01 0.223E+00
0.575E-01 0.243E+00
0.632E-01 0.263E+00
0.623E-01 0.283E+00
0.614E-01 0.306E+00
0.634E-01 0.329E+00
0.613E-01 0.349E+00
0.637E-01 0.371E+00
0.689E-01 0.391E+00
0.666E-01 0.414E+00
0.647E-01 0.437E+00
0.643E-01 0.457E+00
0.504E-01 0.480E+00
0.497E-01 0.503E+00
0.560E-01 0.526E+00
0.628E-01 0.549E+00
0.403E-01 0.571E+00
0.365E-01 0.594E+00
0.351E-01 0.617E+00
0.407E-01 0.640E+00
0.356E-01 0.660E+00
0.348E-01 0.683E+00
0.529E-01 0.706E+00
0.391E-01 0.726E+00
0.236E-01 0.749E+00
0.248E-01 0.769E+00
0.247E-01 0.791E+00
0.193E-01 0.814E+00
0.153E-01 0.837E+00
0.140E-01 0.860E+00
0.141E-01 0.883E+00
0.114E-01 0.906E+00
0.138E-01 0.929E+00
0.125E-01 0.951E+00
0.115E-01 0.974E+00
0.109E-01 0.994E+00
0.119E-01 0.102E+01
0.119E-01 0.104E+01
0.112E-01 0.106E+01
0.113E-01 0.109E+01
0.106E-01 0.111E+01
0.102E-01 0.113E+01
0.981E-02 0.115E+01
0.107E-01 0.118E+01
0.105E-01 0.120E+01
0.103E-01 0.122E+01
0.981E-02 0.125E+01
0.100E-01 0.127E+01
0.104E-01 0.129E+01
0.103E-01 0.131E+01
0.101E-01 0.134E+01
0.998E-02 0.136E+01
0.110E-01 0.138E+01
0.106E-01 0.140E+01
0.106E-01 0.143E+01
0.104E-01 0.145E+01
0.108E-01 0.147E+01
0.106E-01 0.149E+01
0.108E-01 0.152E+01
0.102E-01 0.154E+01
0.103E-01 0.156E+01
0.107E-01 0.158E+01
0.100E-01 0.161E+01
0.105E-01 0.163E+01
0.106E-01 0.165E+01
0.106E-01 0.167E+01
0.110E-01 0.169E+01
0.111E-01 0.172E+01
0.110E-01 0.174E+01
0.111E-01 0.176E+01
0.111E-01 0.179E+01
0.110E-01 0.181E+01
0.121E-01 0.183E+01
0.107E-01 0.185E+01
0.115E-01 0.187E+01
0.114E-01 0.190E+01
0.111E-01 0.192E+01
0.113E-01 0.194E+01
0.115E-01 0.197E+01
0.114E-01 0.199E+01

u' intensity

0.449E-01 0.134E+00
0.415E-01 0.157E+00
0.421E-01 0.180E+00
0.384E-01 0.200E+00
0.355E-01 0.223E+00
0.329E-01 0.243E+00
0.349E-01 0.263E+00
0.334E-01 0.283E+00
0.318E-01 0.306E+00
0.315E-01 0.329E+00
0.285E-01 0.349E+00
0.283E-01 0.371E+00
0.296E-01 0.391E+00
0.279E-01 0.414E+00
0.265E-01 0.437E+00
0.257E-01 0.457E+00
0.196E-01 0.480E+00
0.190E-01 0.503E+00
0.204E-01 0.526E+00
0.219E-01 0.549E+00
0.138E-01 0.571E+00
0.123E-01 0.594E+00
0.117E-01 0.617E+00
0.136E-01 0.640E+00
0.119E-01 0.660E+00
0.117E-01 0.683E+00
0.177E-01 0.706E+00
0.129E-01 0.726E+00
0.758E-02 0.749E+00
0.777E-02 0.769E+00
0.770E-02 0.791E+00
0.600E-02 0.814E+00
0.475E-02 0.837E+00
0.433E-02 0.860E+00
0.435E-02 0.883E+00
0.350E-02 0.906E+00
0.422E-02 0.929E+00
0.383E-02 0.951E+00
0.352E-02 0.974E+00
0.333E-02 0.994E+00
0.363E-02 0.102E+01
0.365E-02 0.104E+01
0.342E-02 0.106E+01
0.347E-02 0.109E+01
0.323E-02 0.111E+01
0.311E-02 0.113E+01
0.299E-02 0.115E+01
0.328E-02 0.118E+01
0.321E-02 0.120E+01
0.314E-02 0.122E+01
0.299E-02 0.125E+01
0.306E-02 0.127E+01
0.315E-02 0.129E+01
0.312E-02 0.131E+01
0.305E-02 0.134E+01
0.302E-02 0.136E+01
0.332E-02 0.138E+01
0.319E-02 0.140E+01
0.319E-02 0.143E+01
0.311E-02 0.145E+01
0.322E-02 0.147E+01
0.315E-02 0.149E+01
0.321E-02 0.152E+01
0.302E-02 0.154E+01
0.307E-02 0.156E+01
0.318E-02 0.158E+01
0.297E-02 0.161E+01
0.311E-02 0.163E+01
0.312E-02 0.165E+01
0.312E-02 0.167E+01
0.323E-02 0.169E+01
0.327E-02 0.172E+01
0.322E-02 0.174E+01
0.326E-02 0.176E+01
0.326E-02 0.179E+01
0.322E-02 0.181E+01
0.353E-02 0.183E+01
0.312E-02 0.185E+01
0.337E-02 0.187E+01
0.333E-02 0.190E+01
0.325E-02 0.192E+01
0.334E-02 0.194E+01
0.346E-02 0.197E+01
0.347E-02 0.199E+01

v' intensity

0.688E-01 0.134E+00
0.618E-01 0.157E+00
0.657E-01 0.180E+00
0.627E-01 0.200E+00
0.613E-01 0.223E+00
0.580E-01 0.243E+00
0.589E-01 0.263E+00
0.555E-01 0.283E+00
0.554E-01 0.306E+00
0.512E-01 0.329E+00
0.508E-01 0.349E+00
0.500E-01 0.371E+00
0.556E-01 0.391E+00
0.488E-01 0.414E+00
0.466E-01 0.437E+00
0.468E-01 0.457E+00
0.397E-01 0.480E+00
0.371E-01 0.503E+00
0.395E-01 0.526E+00
0.395E-01 0.549E+00

0.316E-01 0.571E+00
0.293E-01 0.594E+00
0.289E-01 0.617E+00
0.306E-01 0.640E+00
0.281E-01 0.660E+00
0.262E-01 0.683E+00
0.305E-01 0.706E+00
0.264E-01 0.726E+00
0.214E-01 0.749E+00
0.226E-01 0.769E+00
0.210E-01 0.791E+00
0.187E-01 0.814E+00
0.172E-01 0.837E+00
0.165E-01 0.860E+00
0.171E-01 0.883E+00
0.144E-01 0.906E+00
0.159E-01 0.929E+00
0.157E-01 0.951E+00
0.146E-01 0.974E+00
0.144E-01 0.994E+00
0.144E-01 0.102E+01
0.141E-01 0.104E+01
0.143E-01 0.106E+01
0.140E-01 0.109E+01
0.137E-01 0.111E+01
0.132E-01 0.113E+01
0.133E-01 0.115E+01
0.138E-01 0.118E+01
0.133E-01 0.120E+01
0.131E-01 0.122E+01
0.127E-01 0.125E+01
0.127E-01 0.127E+01
0.135E-01 0.129E+01
0.128E-01 0.131E+01
0.129E-01 0.134E+01
0.135E-01 0.136E+01
0.138E-01 0.138E+01
0.135E-01 0.140E+01
0.124E-01 0.143E+01
0.127E-01 0.145E+01
0.138E-01 0.147E+01
0.134E-01 0.149E+01
0.131E-01 0.152E+01
0.126E-01 0.154E+01
0.130E-01 0.156E+01
0.131E-01 0.158E+01
0.128E-01 0.161E+01
0.129E-01 0.163E+01
0.132E-01 0.165E+01
0.131E-01 0.167E+01
0.139E-01 0.169E+01
0.135E-01 0.172E+01
0.138E-01 0.174E+01
0.134E-01 0.176E+01
0.139E-01 0.179E+01
0.133E-01 0.181E+01
0.144E-01 0.183E+01
0.137E-01 0.185E+01
0.136E-01 0.187E+01
0.139E-01 0.190E+01
0.139E-01 0.192E+01
0.138E-01 0.194E+01
0.145E-01 0.197E+01
0.144E-01 0.199E+01

ρ' mohr

0.496E-01 .111
0.708E-01 .397
0.328E-01 .683
0.854E-02 .969
0.473E-02 1.254

u' mohr

0.436E-01 .111
0.246E-01 .397
0.992E-02 .683
0.256E-02 .969
0.137E-02 1.254

v' mohr

0.704E-01 .111
0.623E-01 .397
0.337E-01 .683
0.176E-01 .969
0.163E-01 1.254

Fig. 5.13a

axial mass flux t.i.

0.913E-01 0.134E+00
0.936E-01 0.157E+00
0.958E-01 0.180E+00
0.101E+00
0.200E+00
0.973E-01 0.223E+00
0.955E-01 0.243E+00
0.926E-01 0.263E+00
0.929E-01 0.283E+00
0.967E-01 0.306E+00
0.969E-01 0.329E+00
0.109E+00
0.349E+00
0.102E+00
0.371E+00
0.937E-01 0.391E+00
0.783E-01 0.414E+00
0.919E-01 0.437E+00
0.803E-01 0.457E+00
0.697E-01 0.480E+00
0.710E-01 0.503E+00
0.674E-01 0.526E+00
0.583E-01 0.549E+00
0.599E-01 0.571E+00
0.502E-01 0.594E+00
0.418E-01 0.617E+00
0.446E-01 0.640E+00
0.353E-01 0.660E+00
0.477E-01 0.683E+00
0.379E-01 0.706E+00
0.315E-01 0.726E+00
0.284E-01 0.749E+00
0.326E-01 0.769E+00
0.510E-01 0.791E+00
0.156E-01 0.814E+00
0.321E-01 0.837E+00
0.179E-01 0.860E+00
0.182E-01 0.883E+00
0.165E-01 0.906E+00

0.175E-01 0.929E+00
0.147E-01 0.951E+00
0.136E-01 0.974E+00
0.136E-01 0.994E+00
0.142E-01 0.102E+01
0.138E-01 0.104E+01
0.135E-01 0.106E+01
0.136E-01 0.109E+01
0.131E-01 0.111E+01
0.126E-01 0.113E+01
0.127E-01 0.115E+01
0.129E-01 0.118E+01
0.134E-01 0.120E+01
0.124E-01 0.122E+01
0.132E-01 0.125E+01
0.129E-01 0.127E+01
0.131E-01 0.129E+01
0.137E-01 0.131E+01
0.130E-01 0.134E+01
0.130E-01 0.136E+01
0.130E-01 0.138E+01
0.131E-01 0.140E+01
0.139E-01 0.143E+01
0.134E-01 0.145E+01
0.134E-01 0.147E+01
0.137E-01 0.149E+01
0.134E-01 0.152E+01
0.139E-01 0.154E+01
0.131E-01 0.156E+01
0.137E-01 0.158E+01
0.134E-01 0.161E+01
0.136E-01 0.163E+01
0.137E-01 0.165E+01
0.138E-01 0.167E+01
0.134E-01 0.169E+01
0.138E-01 0.172E+01
0.142E-01 0.174E+01
0.141E-01 0.176E+01
0.138E-01 0.179E+01
0.141E-01 0.181E+01
0.144E-01 0.183E+01
0.140E-01 0.185E+01
0.140E-01 0.187E+01
0.141E-01 0.190E+01
0.141E-01 0.192E+01
0.142E-01 0.194E+01
0.144E-01 0.197E+01
0.137E-01 0.199E+01

spanwise mass flux t.i.

0.581E-01 0.134E+00
0.585E-01 0.157E+00
0.532E-01 0.180E+00
0.553E-01 0.200E+00
0.556E-01 0.223E+00
0.508E-01 0.243E+00
0.492E-01 0.263E+00
0.456E-01 0.283E+00
0.467E-01 0.306E+00
0.450E-01 0.329E+00
0.467E-01 0.349E+00
0.464E-01 0.371E+00
0.417E-01 0.391E+00
0.387E-01 0.414E+00
0.383E-01 0.437E+00

0.364E-01 0.457E+00
0.338E-01 0.480E+00
0.332E-01 0.503E+00
0.314E-01 0.526E+00
0.286E-01 0.549E+00
0.287E-01 0.571E+00
0.262E-01 0.594E+00
0.242E-01 0.617E+00
0.246E-01 0.640E+00
0.222E-01 0.660E+00
0.249E-01 0.683E+00
0.219E-01 0.706E+00
0.211E-01 0.726E+00
0.188E-01 0.749E+00
0.220E-01 0.769E+00
0.250E-01 0.791E+00
0.159E-01 0.814E+00
0.210E-01 0.837E+00
0.168E-01 0.860E+00
0.172E-01 0.883E+00
0.155E-01 0.906E+00
0.152E-01 0.929E+00
0.148E-01 0.951E+00
0.134E-01 0.974E+00
0.136E-01 0.994E+00
0.139E-01 0.102E+01
0.133E-01 0.104E+01
0.131E-01 0.106E+01
0.134E-01 0.109E+01
0.124E-01 0.111E+01
0.127E-01 0.113E+01
0.123E-01 0.115E+01
0.130E-01 0.118E+01
0.131E-01 0.120E+01
0.128E-01 0.122E+01
0.128E-01 0.125E+01
0.131E-01 0.127E+01
0.128E-01 0.129E+01
0.122E-01 0.131E+01
0.134E-01 0.134E+01
0.123E-01 0.136E+01
0.127E-01 0.138E+01
0.133E-01 0.140E+01
0.133E-01 0.143E+01
0.131E-01 0.145E+01
0.130E-01 0.147E+01
0.134E-01 0.149E+01
0.140E-01 0.152E+01
0.140E-01 0.154E+01
0.140E-01 0.156E+01
0.136E-01 0.158E+01
0.134E-01 0.161E+01
0.138E-01 0.163E+01
0.134E-01 0.165E+01
0.135E-01 0.167E+01
0.141E-01 0.169E+01
0.136E-01 0.172E+01
0.145E-01 0.174E+01
0.144E-01 0.176E+01
0.145E-01 0.179E+01
0.148E-01 0.181E+01
0.141E-01 0.183E+01
0.147E-01 0.185E+01
0.150E-01 0.187E+01
0.143E-01 0.190E+01
0.138E-01 0.192E+01

0.139E-01 0.194E+01
0.146E-01 0.197E+01
0.136E-01 0.199E+01

axial mass flux t.i.
(mohr)

0.109E+00 .397
0.469E-01 .682
0.192E-01 .966

spanwise mass flux t.i.
(mohr)

0.516E-01 .397
0.550E-01 .682
0.243E-01 .966

total temperature t.i.
(mohr)

.0451 .397
.0429 .682
.0159 .966

Fig. 5.13b

density t.i.

0.433E-01 0.134E+00
0.482E-01 0.157E+00
0.530E-01 0.180E+00
0.600E-01 0.200E+00
0.604E-01 0.223E+00
0.607E-01 0.243E+00
0.597E-01 0.263E+00
0.604E-01 0.283E+00
0.637E-01 0.306E+00
0.648E-01 0.329E+00
0.744E-01 0.349E+00
0.707E-01 0.371E+00
0.655E-01 0.391E+00
0.552E-01 0.414E+00
0.652E-01 0.437E+00
0.574E-01 0.457E+00
0.501E-01 0.480E+00
0.514E-01 0.503E+00
0.494E-01 0.526E+00
0.432E-01 0.549E+00
0.446E-01 0.571E+00
0.375E-01 0.594E+00
0.313E-01 0.617E+00
0.334E-01 0.640E+00
0.264E-01 0.660E+00
0.357E-01 0.683E+00
0.284E-01 0.706E+00
0.237E-01 0.726E+00
0.215E-01 0.749E+00
0.248E-01 0.769E+00
0.389E-01 0.791E+00
0.119E-01 0.814E+00
0.245E-01 0.837E+00
0.137E-01 0.860E+00
0.139E-01 0.883E+00
0.126E-01 0.906E+00
0.134E-01 0.929E+00
0.112E-01 0.951E+00
0.104E-01 0.974E+00
0.104E-01 0.994E+00
0.109E-01 0.102E+01
0.106E-01 0.104E+01
0.103E-01 0.106E+01
0.104E-01 0.109E+01
0.100E-01 0.111E+01
0.965E-02 0.113E+01
0.973E-02 0.115E+01
0.988E-02 0.118E+01
0.103E-01 0.120E+01
0.950E-02 0.122E+01
0.101E-01 0.125E+01
0.989E-02 0.127E+01
0.100E-01 0.129E+01
0.105E-01 0.131E+01
0.998E-02 0.134E+01
0.998E-02 0.136E+01
0.998E-02 0.138E+01
0.101E-01 0.140E+01
0.107E-01 0.143E+01
0.103E-01 0.145E+01
0.103E-01 0.147E+01
0.106E-01 0.149E+01
0.103E-01 0.152E+01
0.107E-01 0.154E+01
0.101E-01 0.156E+01
0.106E-01 0.158E+01
0.103E-01 0.161E+01
0.105E-01 0.163E+01
0.106E-01 0.165E+01
0.107E-01 0.167E+01
0.104E-01 0.169E+01
0.107E-01 0.172E+01
0.110E-01 0.174E+01
0.109E-01 0.176E+01
0.107E-01 0.179E+01
0.109E-01 0.181E+01
0.111E-01 0.183E+01
0.108E-01 0.185E+01
0.108E-01 0.187E+01
0.109E-01 0.190E+01
0.109E-01 0.192E+01
0.109E-01 0.194E+01
0.111E-01 0.197E+01
0.105E-01 0.199E+01

u' t.i.

0.480E-01 0.134E+00
0.454E-01 0.157E+00
0.428E-01 0.180E+00
0.410E-01 0.200E+00
0.369E-01 0.223E+00
0.348E-01 0.243E+00
0.329E-01 0.263E+00
0.325E-01 0.283E+00
0.330E-01 0.306E+00
0.321E-01 0.329E+00
0.346E-01 0.349E+00
0.313E-01 0.371E+00
0.282E-01 0.391E+00
0.231E-01 0.414E+00
0.267E-01 0.437E+00
0.229E-01 0.457E+00
0.196E-01 0.480E+00
0.196E-01 0.503E+00
0.180E-01 0.526E+00
0.151E-01 0.549E+00
0.153E-01 0.571E+00
0.127E-01 0.594E+00
0.105E-01 0.617E+00
0.112E-01 0.640E+00
0.887E-02 0.660E+00
0.120E-01 0.683E+00
0.951E-02 0.706E+00
0.780E-02 0.726E+00
0.690E-02 0.749E+00
0.777E-02 0.769E+00
0.121E-01 0.791E+00
0.370E-02 0.814E+00
0.759E-02 0.837E+00
0.423E-02 0.860E+00
0.430E-02 0.883E+00
0.388E-02 0.906E+00
0.411E-02 0.929E+00
0.345E-02 0.951E+00
0.319E-02 0.974E+00
0.319E-02 0.994E+00
0.333E-02 0.102E+01
0.323E-02 0.104E+01
0.316E-02 0.106E+01
0.319E-02 0.109E+01
0.307E-02 0.111E+01
0.295E-02 0.113E+01
0.297E-02 0.115E+01
0.302E-02 0.118E+01
0.314E-02 0.120E+01
0.290E-02 0.122E+01
0.309E-02 0.125E+01
0.301E-02 0.127E+01
0.305E-02 0.129E+01
0.319E-02 0.131E+01
0.302E-02 0.134E+01
0.302E-02 0.136E+01
0.302E-02 0.138E+01
0.303E-02 0.140E+01
0.321E-02 0.143E+01
0.309E-02 0.145E+01
0.308E-02 0.147E+01
0.315E-02 0.149E+01
0.308E-02 0.152E+01
0.318E-02 0.154E+01
0.300E-02 0.156E+01
0.314E-02 0.158E+01
0.307E-02 0.161E+01
0.311E-02 0.163E+01
0.312E-02 0.165E+01
0.314E-02 0.167E+01
0.305E-02 0.169E+01
0.313E-02 0.172E+01
0.322E-02 0.174E+01
0.320E-02 0.176E+01
0.313E-02 0.179E+01
0.319E-02 0.181E+01
0.326E-02 0.183E+01
0.317E-02 0.185E+01
0.317E-02 0.187E+01
0.320E-02 0.190E+01
0.320E-02 0.192E+01
0.325E-02 0.194E+01
0.332E-02 0.197E+01
0.319E-02 0.199E+01

w' t.i.

0.581E-01 0.134E+00
0.585E-01 0.157E+00
0.532E-01 0.180E+00
0.553E-01 0.200E+00
0.556E-01 0.223E+00
0.508E-01 0.243E+00
0.492E-01 0.263E+00
0.456E-01 0.283E+00
0.467E-01 0.306E+00
0.450E-01 0.329E+00
0.467E-01 0.349E+00
0.464E-01 0.371E+00
0.417E-01 0.391E+00
0.387E-01 0.414E+00
0.383E-01 0.437E+00
0.364E-01 0.457E+00
0.338E-01 0.480E+00
0.332E-01 0.503E+00
0.314E-01 0.526E+00
0.286E-01 0.549E+00
0.287E-01 0.571E+00
0.262E-01 0.594E+00
0.242E-01 0.617E+00
0.246E-01 0.640E+00
0.222E-01 0.660E+00
0.249E-01 0.683E+00
0.219E-01 0.706E+00
0.211E-01 0.726E+00
0.188E-01 0.749E+00
0.220E-01 0.769E+00
0.250E-01 0.791E+00
0.159E-01 0.814E+00
0.210E-01 0.837E+00
0.168E-01 0.860E+00
0.172E-01 0.883E+00
0.155E-01 0.906E+00
0.152E-01 0.929E+00
0.148E-01 0.951E+00
0.134E-01 0.974E+00
0.136E-01 0.994E+00
0.139E-01 0.102E+01
0.133E-01 0.104E+01
0.131E-01 0.106E+01
0.134E-01 0.109E+01
0.124E-01 0.111E+01
0.127E-01 0.113E+01
0.123E-01 0.115E+01
0.130E-01 0.118E+01
0.131E-01 0.120E+01
0.128E-01 0.122E+01
0.128E-01 0.125E+01
0.131E-01 0.127E+01
0.128E-01 0.129E+01
0.122E-01 0.131E+01
0.134E-01 0.134E+01
0.123E-01 0.136E+01
0.127E-01 0.138E+01
0.133E-01 0.140E+01
0.133E-01 0.143E+01
0.131E-01 0.145E+01
0.130E-01 0.147E+01

0.134E-01	0.149E+01
0.140E-01	0.152E+01
0.140E-01	0.154E+01
0.140E-01	0.156E+01
0.136E-01	0.158E+01
0.134E-01	0.161E+01
0.138E-01	0.163E+01
0.134E-01	0.165E+01
0.135E-01	0.167E+01
0.141E-01	0.169E+01
0.136E-01	0.172E+01
0.145E-01	0.174E+01
0.144E-01	0.176E+01
0.145E-01	0.179E+01
0.148E-01	0.181E+01
0.141E-01	0.183E+01
0.147E-01	0.185E+01
0.150E-01	0.187E+01
0.143E-01	0.190E+01
0.138E-01	0.192E+01
0.139E-01	0.194E+01
0.146E-01	0.197E+01
0.136E-01	0.199E+01

density t.i. (mohr)

0.809E-01	.397
0.360E-01	.682
0.148E-01	.966

u' t.i. (mohr)

0.281E-01	.397
0.109E-01	.682
0.442E-02	.966

w' t.i. (mohr)

0.516E-01	.397
0.550E-01	.682
0.243E-01	.966

Fig. 5.14a

-0.271E-02	0.134E+00
-0.243E-02	0.157E+00
-0.312E-02	0.180E+00
-0.233E-02	0.200E+00
-0.193E-02	0.223E+00
-0.182E-02	0.243E+00
-0.230E-02	0.263E+00
-0.190E-02	0.283E+00
-0.158E-02	0.306E+00
-0.182E-02	0.329E+00
-0.166E-02	0.349E+00
-0.153E-02	0.371E+00
-0.171E-02	0.391E+00
-0.143E-02	0.414E+00
-0.148E-02	0.437E+00
-0.130E-02	0.457E+00
-0.101E-02	0.480E+00
-0.853E-03	0.503E+00
-0.821E-03	0.526E+00
-0.107E-02	0.549E+00
-0.654E-03	0.571E+00
-0.508E-03	0.594E+00
-0.445E-03	0.617E+00
-0.763E-03	0.640E+00
-0.407E-03	0.660E+00
-0.479E-03	0.683E+00
-0.799E-03	0.706E+00
-0.433E-03	0.726E+00
-0.285E-03	0.749E+00
-0.296E-03	0.769E+00
-0.233E-03	0.791E+00
-0.743E-04	0.814E+00
-0.108E-03	0.837E+00
-0.106E-03	0.860E+00
-0.112E-03	0.883E+00
-0.417E-04	0.906E+00
-0.951E-04	0.929E+00
-0.722E-04	0.951E+00
-0.459E-04	0.974E+00
-0.468E-04	0.994E+00
-0.553E-04	0.102E+01
-0.540E-04	0.104E+01
-0.496E-04	0.106E+01
-0.458E-04	0.109E+01
-0.385E-04	0.111E+01
-0.360E-04	0.113E+01
-0.145E-04	0.115E+01
-0.368E-04	0.118E+01
-0.268E-04	0.120E+01
-0.289E-04	0.122E+01
-0.230E-04	0.125E+01
-0.263E-04	0.127E+01
-0.394E-04	0.129E+01
-0.223E-04	0.131E+01
-0.421E-04	0.134E+01
-0.353E-04	0.136E+01
-0.503E-04	0.138E+01
-0.522E-04	0.140E+01
-0.470E-04	0.143E+01
-0.384E-04	0.145E+01
-0.490E-04	0.147E+01
-0.472E-04	0.149E+01
-0.467E-04	0.152E+01
-0.210E-04	0.154E+01
-0.383E-04	0.156E+01
-0.498E-04	0.158E+01
-0.247E-04	0.161E+01
-0.420E-04	0.163E+01
-0.522E-04	0.165E+01
-0.385E-04	0.167E+01
-0.552E-04	0.169E+01
-0.583E-04	0.172E+01
-0.278E-04	0.174E+01
-0.457E-04	0.176E+01
-0.508E-04	0.179E+01
-0.428E-04	0.181E+01
-0.638E-04	0.183E+01
-0.307E-04	0.185E+01
-0.485E-04	0.187E+01
-0.384E-04	0.190E+01
-0.264E-04	0.192E+01
-0.288E-04	0.194E+01
-0.541E-04	0.197E+01
-0.527E-04	0.199E+01

Fig. 5.14b

C_{xy} term

0.271E-02	0.134E+00
0.243E-02	0.157E+00
0.312E-02	0.180E+00
0.233E-02	0.200E+00
0.193E-02	0.223E+00
0.182E-02	0.243E+00
0.230E-02	0.263E+00
0.190E-02	0.283E+00
0.158E-02	0.306E+00
0.182E-02	0.329E+00
0.166E-02	0.349E+00
0.153E-02	0.371E+00
0.171E-02	0.391E+00
0.143E-02	0.414E+00
0.148E-02	0.437E+00
0.130E-02	0.457E+00
0.101E-02	0.480E+00
0.853E-03	0.503E+00
0.821E-03	0.526E+00
0.107E-02	0.549E+00
0.654E-03	0.571E+00
0.508E-03	0.594E+00
0.445E-03	0.617E+00
0.763E-03	0.640E+00
0.407E-03	0.660E+00
0.479E-03	0.683E+00
0.799E-03	0.706E+00
0.433E-03	0.726E+00
0.285E-03	0.749E+00
0.296E-03	0.769E+00
0.233E-03	0.791E+00
0.743E-04	0.814E+00
0.108E-03	0.837E+00
0.106E-03	0.860E+00
0.112E-03	0.883E+00
0.417E-04	0.906E+00
0.951E-04	0.929E+00
0.722E-04	0.951E+00
0.459E-04	0.974E+00
0.468E-04	0.994E+00
0.553E-04	0.102E+01
0.540E-04	0.104E+01
0.496E-04	0.106E+01
0.458E-04	0.109E+01
0.385E-04	0.111E+01
0.360E-04	0.113E+01
0.145E-04	0.115E+01
0.368E-04	0.118E+01
0.268E-04	0.120E+01
0.289E-04	0.122E+01
0.230E-04	0.125E+01
0.263E-04	0.127E+01
0.394E-04	0.129E+01
0.223E-04	0.131E+01
0.421E-04	0.134E+01
0.353E-04	0.136E+01
0.503E-04	0.138E+01
0.522E-04	0.140E+01
0.470E-04	0.143E+01
0.384E-04	0.145E+01
0.490E-04	0.147E+01
0.472E-04	0.149E+01
0.467E-04	0.152E+01
0.210E-04	0.154E+01
0.383E-04	0.156E+01
0.498E-04	0.158E+01
0.247E-04	0.161E+01
0.420E-04	0.163E+01
0.522E-04	0.165E+01
0.385E-04	0.167E+01
0.552E-04	0.169E+01
0.583E-04	0.172E+01
0.278E-04	0.174E+01
0.457E-04	0.176E+01
0.508E-04	0.179E+01
0.428E-04	0.181E+01
0.638E-04	0.183E+01
0.307E-04	0.185E+01
0.485E-04	0.187E+01
0.384E-04	0.190E+01
0.264E-04	0.192E+01
0.288E-04	0.194E+01
0.541E-04	0.197E+01
0.527E-04	0.199E+01

small term

0.218E-04	0.134E+00
0.192E-04	0.157E+00
0.218E-04	0.180E+00
0.267E-04	0.200E+00
0.171E-04	0.223E+00
0.131E-04	0.243E+00
-0.425E-05	0.263E+00
0.143E-04	0.283E+00
0.167E-04	0.306E+00
0.630E-04	0.329E+00
0.236E-04	0.349E+00
0.316E-05	0.371E+00
-0.308E-04	0.391E+00
-0.367E-04	0.414E+00
-0.964E-05	0.437E+00
-0.384E-04	0.457E+00
-0.317E-06	0.480E+00
-0.101E-04	0.503E+00
-0.623E-05	0.526E+00
-0.243E-04	0.549E+00
0.884E-06	0.571E+00
-0.174E-05	0.594E+00
-0.256E-05	0.617E+00
-0.117E-04	0.640E+00
-0.563E-05	0.660E+00
-0.895E-05	0.683E+00
-0.307E-04	0.706E+00
-0.143E-04	0.726E+00
-0.462E-05	0.749E+00
-0.561E-05	0.769E+00
-0.579E-05	0.791E+00
-0.262E-05	0.814E+00
-0.227E-05	0.837E+00
-0.190E-05	0.860E+00
-0.230E-05	0.883E+00
-0.148E-05	0.906E+00
-0.278E-05	0.929E+00
-0.229E-05	0.951E+00
-0.197E-05	0.974E+00
-0.188E-05	0.994E+00
-0.248E-05	0.102E+01
-0.252E-05	0.104E+01
-0.231E-05	0.106E+01
-0.240E-05	0.109E+01

-0.224E-05	0.111E+01
-0.210E-05	0.113E+01
-0.210E-05	0.115E+01
-0.251E-05	0.118E+01
-0.259E-05	0.120E+01
-0.248E-05	0.122E+01
-0.237E-05	0.125E+01
-0.252E-05	0.127E+01
-0.281E-05	0.129E+01
-0.271E-05	0.131E+01
-0.261E-05	0.134E+01
-0.266E-05	0.136E+01
-0.297E-05	0.138E+01
-0.263E-05	0.140E+01
-0.216E-05	0.143E+01
-0.205E-05	0.145E+01
-0.221E-05	0.147E+01
-0.224E-05	0.149E+01
-0.248E-05	0.152E+01
-0.224E-05	0.154E+01
-0.231E-05	0.156E+01
-0.255E-05	0.158E+01
-0.230E-05	0.161E+01
-0.252E-05	0.163E+01
-0.236E-05	0.165E+01
-0.231E-05	0.167E+01
-0.256E-05	0.169E+01
-0.266E-05	0.172E+01
-0.269E-05	0.174E+01
-0.268E-05	0.176E+01
-0.279E-05	0.179E+01
-0.284E-05	0.181E+01
-0.354E-05	0.183E+01
-0.295E-05	0.185E+01
-0.364E-05	0.187E+01
-0.365E-05	0.190E+01
-0.367E-05	0.192E+01
-0.341E-05	0.194E+01
-0.356E-05	0.197E+01
-0.322E-05	0.199E+01

cross-wire shear

0.273E-02	0.134E+00
0.245E-02	0.157E+00
0.314E-02	0.180E+00
0.236E-02	0.200E+00
0.195E-02	0.223E+00
0.183E-02	0.243E+00
0.230E-02	0.263E+00
0.191E-02	0.283E+00
0.160E-02	0.306E+00
0.188E-02	0.329E+00
0.168E-02	0.349E+00
0.153E-02	0.371E+00
0.168E-02	0.391E+00
0.139E-02	0.414E+00
0.147E-02	0.437E+00
0.126E-02	0.457E+00
0.101E-02	0.480E+00
0.843E-03	0.503E+00
0.815E-03	0.526E+00
0.105E-02	0.549E+00
0.655E-03	0.571E+00
0.506E-03	0.594E+00
0.442E-03	0.617E+00
0.751E-03	0.640E+00
0.401E-03	0.660E+00
0.470E-03	0.683E+00
0.768E-03	0.706E+00
0.419E-03	0.726E+00
0.280E-03	0.749E+00
0.290E-03	0.769E+00
0.227E-03	0.791E+00
0.717E-04	0.814E+00
0.106E-03	0.837E+00
0.104E-03	0.860E+00
0.110E-03	0.883E+00
0.402E-04	0.906E+00
0.923E-04	0.929E+00
0.699E-04	0.951E+00
0.439E-04	0.974E+00
0.449E-04	0.994E+00
0.528E-04	0.102E+01
0.515E-04	0.104E+01
0.473E-04	0.106E+01
0.434E-04	0.109E+01
0.363E-04	0.111E+01
0.339E-04	0.113E+01
0.124E-04	0.115E+01
0.343E-04	0.118E+01
0.242E-04	0.120E+01
0.264E-04	0.122E+01
0.206E-04	0.125E+01
0.238E-04	0.127E+01
0.366E-04	0.129E+01
0.196E-04	0.131E+01
0.395E-04	0.134E+01
0.326E-04	0.136E+01
0.473E-04	0.138E+01
0.496E-04	0.140E+01
0.448E-04	0.143E+01
0.363E-04	0.145E+01
0.468E-04	0.147E+01
0.450E-04	0.149E+01
0.442E-04	0.152E+01
0.188E-04	0.154E+01
0.360E-04	0.156E+01
0.473E-04	0.158E+01
0.224E-04	0.161E+01
0.395E-04	0.163E+01
0.498E-04	0.165E+01
0.362E-04	0.167E+01
0.526E-04	0.169E+01
0.556E-04	0.172E+01
0.251E-04	0.174E+01
0.430E-04	0.176E+01
0.480E-04	0.179E+01
0.400E-04	0.181E+01
0.603E-04	0.183E+01
0.278E-04	0.185E+01
0.449E-04	0.187E+01
0.347E-04	0.190E+01
0.227E-04	0.192E+01
0.254E-04	0.194E+01
0.505E-04	0.197E+01
0.495E-04	0.199E+01

Fig. 5.15a

-0.234E-02	0.134E+00
-0.264E-02	0.157E+00
-0.216E-02	0.180E+00
-0.237E-02	0.200E+00
-0.167E-02	0.223E+00
-0.151E-02	0.243E+00
-0.106E-02	0.263E+00
-0.845E-03	0.283E+00
-0.928E-03	0.306E+00
-0.166E-02	0.329E+00
-0.173E-02	0.349E+00
-0.134E-02	0.371E+00
-0.857E-03	0.391E+00
-0.179E-03	0.414E+00
-0.110E-03	0.437E+00
0.162E-03	0.457E+00
0.445E-03	0.480E+00
0.422E-03	0.503E+00
0.460E-03	0.526E+00
0.444E-03	0.549E+00
0.419E-03	0.571E+00
0.514E-03	0.594E+00
0.464E-03	0.617E+00
0.394E-03	0.640E+00
0.304E-03	0.660E+00
0.497E-03	0.683E+00
0.320E-03	0.706E+00
0.306E-03	0.726E+00
0.213E-03	0.749E+00
0.329E-03	0.769E+00
0.537E-03	0.791E+00
0.480E-04	0.814E+00
0.298E-03	0.837E+00
0.914E-04	0.860E+00
0.118E-03	0.883E+00
0.477E-04	0.906E+00
0.647E-04	0.929E+00
0.514E-04	0.951E+00
0.249E-04	0.974E+00
0.276E-04	0.994E+00
0.443E-04	0.102E+01
0.351E-04	0.104E+01
0.224E-04	0.106E+01
0.327E-04	0.109E+01
0.188E-04	0.111E+01
0.239E-04	0.113E+01
0.344E-04	0.115E+01
0.320E-04	0.118E+01
0.343E-04	0.120E+01
0.363E-04	0.122E+01
0.305E-04	0.125E+01
0.298E-04	0.127E+01
0.348E-04	0.129E+01
0.305E-04	0.131E+01
0.168E-04	0.134E+01
0.340E-04	0.136E+01
0.198E-04	0.138E+01
0.196E-04	0.140E+01
-0.423E-06	0.143E+01
0.143E-05	0.145E+01
0.142E-04	0.147E+01
0.185E-04	0.149E+01
0.164E-04	0.152E+01
0.292E-04	0.154E+01
0.220E-04	0.156E+01
0.330E-04	0.158E+01
0.254E-04	0.161E+01
0.182E-04	0.163E+01
0.251E-04	0.165E+01
0.244E-04	0.167E+01
0.222E-04	0.169E+01
0.254E-04	0.172E+01
0.298E-04	0.174E+01
0.177E-04	0.176E+01
0.277E-04	0.179E+01
0.280E-04	0.181E+01
0.336E-04	0.183E+01
0.130E-04	0.185E+01
0.287E-04	0.187E+01
0.509E-04	0.190E+01
0.402E-04	0.192E+01
0.457E-04	0.194E+01
0.510E-04	0.197E+01
0.299E-04	0.199E+01

Fig. 5.15b

$-C_{xy}$ term

0.234E-02	0.134E+00
0.264E-02	0.157E+00
0.216E-02	0.180E+00
0.237E-02	0.200E+00
0.167E-02	0.223E+00
0.151E-02	0.243E+00
0.106E-02	0.263E+00
0.845E-03	0.283E+00
0.928E-03	0.306E+00
0.166E-02	0.329E+00
0.173E-02	0.349E+00
0.134E-02	0.371E+00
0.857E-03	0.391E+00
0.179E-03	0.414E+00
0.110E-03	0.437E+00
-0.162E-03	0.457E+00
-0.445E-03	0.480E+00
-0.422E-03	0.503E+00
-0.460E-03	0.526E+00
-0.444E-03	0.549E+00
-0.419E-03	0.571E+00
-0.514E-03	0.594E+00
-0.464E-03	0.617E+00
-0.394E-03	0.640E+00
-0.304E-03	0.660E+00
-0.497E-03	0.683E+00
-0.320E-03	0.706E+00
-0.306E-03	0.726E+00
-0.213E-03	0.749E+00
-0.329E-03	0.769E+00
-0.537E-03	0.791E+00
-0.480E-04	0.814E+00
-0.298E-03	0.837E+00
-0.914E-04	0.860E+00
-0.118E-03	0.883E+00
-0.477E-04	0.906E+00
-0.647E-04	0.929E+00
-0.514E-04	0.951E+00
-0.249E-04	0.974E+00
-0.276E-04	0.994E+00
-0.443E-04	0.102E+01
-0.351E-04	0.104E+01
-0.224E-04	0.106E+01
-0.327E-04	0.109E+01
-0.188E-04	0.111E+01

-0.239E-04	0.113E+01
-0.344E-04	0.115E+01
-0.320E-04	0.118E+01
-0.343E-04	0.120E+01
-0.363E-04	0.122E+01
-0.305E-04	0.125E+01
-0.298E-04	0.127E+01
-0.348E-04	0.129E+01
-0.305E-04	0.131E+01
-0.168E-04	0.134E+01
-0.340E-04	0.136E+01
-0.198E-04	0.138E+01
-0.196E-04	0.140E+01
0.423E-06	0.143E+01
-0.143E-05	0.145E+01
-0.142E-04	0.147E+01
-0.185E-04	0.149E+01
-0.164E-04	0.152E+01
-0.292E-04	0.154E+01
-0.220E-04	0.156E+01
-0.330E-04	0.158E+01
-0.254E-04	0.161E+01
-0.182E-04	0.163E+01
-0.251E-04	0.165E+01
-0.244E-04	0.167E+01
-0.222E-04	0.169E+01
-0.254E-04	0.172E+01
-0.298E-04	0.174E+01
-0.177E-04	0.176E+01
-0.277E-04	0.179E+01
-0.280E-04	0.181E+01
-0.336E-04	0.183E+01
-0.130E-04	0.185E+01
-0.287E-04	0.187E+01
-0.509E-04	0.190E+01
-0.402E-04	0.192E+01
-0.457E-04	0.194E+01
-0.510E-04	0.197E+01
-0.299E-04	0.199E+01

small term

0.122E-03	0.134E+00
0.167E-03	0.157E+00
0.206E-03	0.180E+00
0.277E-03	0.200E+00
0.230E-03	0.223E+00
0.243E-03	0.243E+00
0.250E-03	0.263E+00
0.257E-03	0.283E+00
0.270E-03	0.306E+00
0.321E-03	0.329E+00
0.393E-03	0.349E+00
0.332E-03	0.371E+00
0.287E-03	0.391E+00
0.188E-03	0.414E+00
0.216E-03	0.437E+00
0.161E-03	0.457E+00
0.128E-03	0.480E+00
0.121E-03	0.503E+00
0.108E-03	0.526E+00
0.740E-04	0.549E+00
0.740E-04	0.571E+00
0.468E-04	0.594E+00
0.328E-04	0.617E+00
0.332E-04	0.640E+00
0.189E-04	0.660E+00
0.415E-04	0.683E+00
0.219E-04	0.706E+00
0.137E-04	0.726E+00
0.119E-04	0.749E+00
0.168E-04	0.769E+00
0.559E-04	0.791E+00
0.272E-05	0.814E+00
0.162E-04	0.837E+00
0.369E-05	0.860E+00
0.347E-05	0.883E+00
0.222E-05	0.906E+00
0.268E-05	0.929E+00
0.189E-05	0.951E+00
0.127E-05	0.974E+00
0.116E-05	0.994E+00
0.101E-05	0.102E+01
0.116E-05	0.104E+01
0.112E-05	0.106E+01
0.115E-05	0.109E+01
0.100E-05	0.111E+01
0.807E-06	0.113E+01
0.811E-06	0.115E+01
0.935E-06	0.118E+01
0.739E-06	0.120E+01
0.592E-06	0.122E+01
0.666E-06	0.125E+01
0.637E-06	0.127E+01
0.560E-06	0.129E+01
0.656E-06	0.131E+01
0.561E-06	0.134E+01
0.598E-06	0.136E+01
0.708E-06	0.138E+01
0.683E-06	0.140E+01
0.140E-05	0.143E+01
0.154E-05	0.145E+01
0.182E-05	0.147E+01
0.196E-05	0.149E+01
0.207E-05	0.152E+01
0.195E-05	0.154E+01
0.167E-05	0.156E+01
0.176E-05	0.158E+01
0.143E-05	0.161E+01
0.137E-05	0.163E+01
0.136E-05	0.165E+01
0.131E-05	0.167E+01
0.122E-05	0.169E+01
0.137E-05	0.172E+01
0.152E-05	0.174E+01
0.149E-05	0.176E+01
0.138E-05	0.179E+01
0.187E-05	0.181E+01
0.190E-05	0.183E+01
0.142E-05	0.185E+01
0.974E-06	0.187E+01
0.572E-06	0.190E+01
0.506E-06	0.192E+01
0.224E-06	0.194E+01
0.428E-06	0.197E+01
0.662E-06	0.199E+01

cross-wire shear

0.246E-02	0.134E+00
0.281E-02	0.157E+00
0.237E-02	0.180E+00
0.265E-02	0.200E+00
0.190E-02	0.223E+00
0.175E-02	0.243E+00
0.131E-02	0.263E+00
0.110E-02	0.283E+00
0.120E-02	0.306E+00
0.198E-02	0.329E+00
0.212E-02	0.349E+00
0.167E-02	0.371E+00
0.114E-02	0.391E+00
0.367E-03	0.414E+00
0.326E-03	0.437E+00
-0.103E-05	0.457E+00
-0.317E-03	0.480E+00
-0.301E-03	0.503E+00
-0.352E-03	0.526E+00
-0.370E-03	0.549E+00
-0.345E-03	0.571E+00
-0.467E-03	0.594E+00
-0.431E-03	0.617E+00
-0.361E-03	0.640E+00
-0.285E-03	0.660E+00
-0.455E-03	0.683E+00
-0.298E-03	0.706E+00
-0.292E-03	0.726E+00
-0.201E-03	0.749E+00
-0.312E-03	0.769E+00
-0.481E-03	0.791E+00
-0.453E-04	0.814E+00
-0.282E-03	0.837E+00
-0.877E-04	0.860E+00
-0.115E-03	0.883E+00
-0.455E-04	0.906E+00
-0.620E-04	0.929E+00
-0.495E-04	0.951E+00
-0.236E-04	0.974E+00
-0.264E-04	0.994E+00
-0.433E-04	0.102E+01
-0.339E-04	0.104E+01
-0.213E-04	0.106E+01
-0.316E-04	0.109E+01
-0.178E-04	0.111E+01
-0.231E-04	0.113E+01
-0.336E-04	0.115E+01
-0.311E-04	0.118E+01
-0.336E-04	0.120E+01
-0.357E-04	0.122E+01
-0.298E-04	0.125E+01
-0.292E-04	0.127E+01
-0.342E-04	0.129E+01
-0.298E-04	0.131E+01
-0.162E-04	0.134E+01
-0.334E-04	0.136E+01
-0.191E-04	0.138E+01
-0.189E-04	0.140E+01
0.182E-05	0.143E+01
0.106E-06	0.145E+01
-0.124E-04	0.147E+01
-0.165E-04	0.149E+01
-0.143E-04	0.152E+01
-0.273E-04	0.154E+01
-0.203E-04	0.156E+01
-0.312E-04	0.158E+01
-0.240E-04	0.161E+01
-0.168E-04	0.163E+01
-0.237E-04	0.165E+01
-0.231E-04	0.167E+01
-0.210E-04	0.169E+01
-0.240E-04	0.172E+01
-0.283E-04	0.174E+01
-0.162E-04	0.176E+01
-0.263E-04	0.179E+01
-0.261E-04	0.181E+01
-0.317E-04	0.183E+01
-0.116E-04	0.185E+01
-0.277E-04	0.187E+01
-0.503E-04	0.190E+01
-0.397E-04	0.192E+01
-0.455E-04	0.194E+01
-0.506E-04	0.197E+01
-0.292E-04	0.199E+01

Fig. 5.16a

term 1

0.143E-02	0.134E+00
0.118E-02	0.157E+00
0.139E-02	0.180E+00
0.947E-03	0.200E+00
0.733E-03	0.223E+00
0.663E-03	0.243E+00
0.817E-03	0.263E+00
0.664E-03	0.283E+00
0.539E-03	0.306E+00
0.603E-03	0.329E+00
0.526E-03	0.349E+00
0.470E-03	0.371E+00
0.515E-03	0.391E+00
0.423E-03	0.414E+00
0.430E-03	0.437E+00
0.371E-03	0.457E+00
0.284E-03	0.480E+00
0.236E-03	0.503E+00
0.220E-03	0.526E+00
0.277E-03	0.549E+00
0.167E-03	0.571E+00
0.128E-03	0.594E+00
0.111E-03	0.617E+00
0.191E-03	0.640E+00
0.102E-03	0.660E+00
0.121E-03	0.683E+00
0.201E-03	0.706E+00
0.107E-03	0.726E+00
0.693E-04	0.749E+00
0.705E-04	0.769E+00
0.554E-04	0.791E+00
0.176E-04	0.814E+00
0.255E-04	0.837E+00
0.251E-04	0.860E+00
0.265E-04	0.883E+00
0.981E-05	0.906E+00
0.223E-04	0.929E+00
0.169E-04	0.951E+00
0.108E-04	0.974E+00
0.110E-04	0.994E+00
0.130E-04	0.102E+01
0.126E-04	0.104E+01
0.116E-04	0.106E+01
0.107E-04	0.109E+01
0.902E-05	0.111E+01
0.842E-05	0.113E+01

0.339E-05	0.115E+01
0.861E-05	0.118E+01
0.628E-05	0.120E+01
0.677E-05	0.122E+01
0.538E-05	0.125E+01
0.614E-05	0.127E+01
0.918E-05	0.129E+01
0.519E-05	0.131E+01
0.979E-05	0.134E+01
0.820E-05	0.136E+01
0.117E-04	0.138E+01
0.121E-04	0.140E+01
0.109E-04	0.143E+01
0.886E-05	0.145E+01
0.113E-04	0.147E+01
0.108E-04	0.149E+01
0.107E-04	0.152E+01
0.481E-05	0.154E+01
0.878E-05	0.156E+01
0.114E-04	0.158E+01
0.565E-05	0.161E+01
0.959E-05	0.163E+01
0.119E-04	0.165E+01
0.876E-05	0.167E+01
0.126E-04	0.169E+01
0.132E-04	0.172E+01
0.631E-05	0.174E+01
0.104E-04	0.176E+01
0.115E-04	0.179E+01
0.969E-05	0.181E+01
0.144E-04	0.183E+01
0.695E-05	0.185E+01
0.110E-04	0.187E+01
0.871E-05	0.190E+01
0.600E-05	0.192E+01
0.659E-05	0.194E+01
0.125E-04	0.197E+01
0.123E-04	0.199E+01

term 2

0.128E-02	0.134E+00
0.125E-02	0.157E+00
0.173E-02	0.180E+00
0.138E-02	0.200E+00
0.120E-02	0.223E+00
0.116E-02	0.243E+00
0.148E-02	0.263E+00
0.124E-02	0.283E+00
0.104E-02	0.306E+00
0.122E-02	0.329E+00
0.113E-02	0.349E+00
0.106E-02	0.371E+00
0.120E-02	0.391E+00
0.101E-02	0.414E+00
0.105E-02	0.437E+00
0.929E-03	0.457E+00
0.726E-03	0.480E+00
0.617E-03	0.503E+00
0.601E-03	0.526E+00
0.793E-03	0.549E+00
0.487E-03	0.571E+00
0.380E-03	0.594E+00
0.334E-03	0.617E+00
0.572E-03	0.640E+00
0.305E-03	0.660E+00
0.358E-03	0.683E+00
0.598E-03	0.706E+00
0.326E-03	0.726E+00
0.216E-03	0.749E+00
0.225E-03	0.769E+00
0.178E-03	0.791E+00
0.567E-04	0.814E+00
0.825E-04	0.837E+00
0.809E-04	0.860E+00
0.855E-04	0.883E+00
0.319E-04	0.906E+00
0.728E-04	0.929E+00
0.553E-04	0.951E+00
0.351E-04	0.974E+00
0.358E-04	0.994E+00
0.423E-04	0.102E+01
0.414E-04	0.104E+01
0.380E-04	0.106E+01
0.351E-04	0.109E+01
0.295E-04	0.111E+01
0.276E-04	0.113E+01
0.111E-04	0.115E+01
0.282E-04	0.118E+01
0.205E-04	0.120E+01
0.221E-04	0.122E+01
0.176E-04	0.125E+01
0.202E-04	0.127E+01
0.302E-04	0.129E+01
0.171E-04	0.131E+01
0.323E-04	0.134E+01
0.271E-04	0.136E+01
0.386E-04	0.138E+01
0.401E-04	0.140E+01
0.361E-04	0.143E+01
0.295E-04	0.145E+01
0.377E-04	0.147E+01
0.364E-04	0.149E+01
0.360E-04	0.152E+01
0.162E-04	0.154E+01
0.295E-04	0.156E+01
0.384E-04	0.158E+01
0.190E-04	0.161E+01
0.324E-04	0.163E+01
0.403E-04	0.165E+01
0.297E-04	0.167E+01
0.426E-04	0.169E+01
0.451E-04	0.172E+01
0.215E-04	0.174E+01
0.353E-04	0.176E+01
0.393E-04	0.179E+01
0.331E-04	0.181E+01
0.494E-04	0.183E+01
0.238E-04	0.185E+01
0.375E-04	0.187E+01
0.297E-04	0.190E+01
0.204E-04	0.192E+01
0.222E-04	0.194E+01
0.416E-04	0.197E+01
0.404E-04	0.199E+01

term 3

0.668E-05	0.134E+00
0.427E-05	0.157E+00
0.351E-05	0.180E+00
0.302E-05	0.200E+00
0.151E-05	0.223E+00
0.100E-05	0.243E+00
-0.296E-06	0.263E+00
0.940E-06	0.283E+00
0.101E-05	0.306E+00
0.344E-05	0.329E+00
0.110E-05	0.349E+00
0.132E-06	0.371E+00
-0.120E-05	0.391E+00
-0.134E-05	0.414E+00
-0.334E-06	0.437E+00
-0.125E-05	0.457E+00
-0.976E-08	0.480E+00
-0.295E-06	0.503E+00
-0.163E-06	0.526E+00
-0.569E-06	0.549E+00
0.197E-07	0.571E+00
-0.372E-07	0.594E+00
-0.534E-07	0.617E+00
-0.245E-06	0.640E+00
-0.119E-06	0.660E+00
-0.192E-06	0.683E+00
-0.648E-06	0.706E+00
-0.290E-06	0.726E+00
-0.878E-07	0.749E+00
-0.996E-07	0.769E+00
-0.102E-06	0.791E+00
-0.458E-07	0.814E+00
-0.393E-07	0.837E+00
-0.328E-07	0.860E+00
-0.398E-07	0.883E+00
-0.253E-07	0.906E+00
-0.468E-07	0.929E+00
-0.388E-07	0.951E+00
-0.333E-07	0.974E+00
-0.316E-07	0.994E+00
-0.417E-07	0.102E+01
-0.422E-07	0.104E+01
-0.387E-07	0.106E+01
-0.403E-07	0.109E+01
-0.376E-07	0.111E+01
-0.351E-07	0.113E+01
-0.350E-07	0.115E+01
-0.420E-07	0.118E+01
-0.435E-07	0.120E+01
-0.416E-07	0.122E+01
-0.395E-07	0.125E+01
-0.418E-07	0.127E+01
-0.464E-07	0.129E+01
-0.446E-07	0.131E+01
-0.428E-07	0.134E+01
-0.435E-07	0.136E+01
-0.483E-07	0.138E+01
-0.424E-07	0.140E+01
-0.347E-07	0.143E+01
-0.328E-07	0.145E+01
-0.350E-07	0.147E+01
-0.352E-07	0.149E+01
-0.389E-07	0.152E+01
-0.349E-07	0.154E+01
-0.360E-07	0.156E+01
-0.397E-07	0.158E+01
-0.357E-07	0.161E+01
-0.389E-07	0.163E+01
-0.362E-07	0.165E+01
-0.352E-07	0.167E+01
-0.390E-07	0.169E+01
-0.403E-07	0.172E+01
-0.407E-07	0.174E+01
-0.404E-07	0.176E+01
-0.420E-07	0.179E+01
-0.427E-07	0.181E+01
-0.529E-07	0.183E+01
-0.441E-07	0.185E+01
-0.547E-07	0.187E+01
-0.552E-07	0.190E+01
-0.557E-07	0.192E+01
-0.530E-07	0.194E+01
-0.569E-07	0.197E+01
-0.528E-07	0.199E+01

Reynolds shear

0.273E-02	0.134E+00
0.245E-02	0.157E+00
0.314E-02	0.180E+00
0.236E-02	0.200E+00
0.195E-02	0.223E+00
0.183E-02	0.243E+00
0.230E-02	0.263E+00
0.191E-02	0.283E+00
0.160E-02	0.306E+00
0.188E-02	0.329E+00
0.168E-02	0.349E+00
0.153E-02	0.371E+00
0.168E-02	0.391E+00
0.139E-02	0.414E+00
0.147E-02	0.437E+00
0.126E-02	0.457E+00
0.101E-02	0.480E+00
0.843E-03	0.503E+00
0.815E-03	0.526E+00
0.105E-02	0.549E+00
0.655E-03	0.571E+00
0.506E-03	0.594E+00
0.442E-03	0.617E+00
0.751E-03	0.640E+00
0.401E-03	0.660E+00
0.470E-03	0.683E+00
0.768E-03	0.706E+00
0.419E-03	0.726E+00
0.280E-03	0.749E+00
0.290E-03	0.769E+00
0.227E-03	0.791E+00
0.717E-04	0.814E+00
0.106E-03	0.837E+00
0.104E-03	0.860E+00
0.110E-03	0.883E+00
0.402E-04	0.906E+00
0.923E-04	0.929E+00
0.699E-04	0.951E+00
0.439E-04	0.974E+00
0.449E-04	0.994E+00
0.528E-04	0.102E+01
0.515E-04	0.104E+01
0.473E-04	0.106E+01
0.434E-04	0.109E+01
0.363E-04	0.111E+01
0.339E-04	0.113E+01
0.124E-04	0.115E+01
0.343E-04	0.118E+01
0.242E-04	0.120E+01

0.264E-04 0.122E+01
0.206E-04 0.125E+01
0.238E-04 0.127E+01
0.366E-04 0.129E+01
0.196E-04 0.131E+01
0.395E-04 0.134E+01
0.326E-04 0.136E+01
0.473E-04 0.138E+01
0.496E-04 0.140E+01
0.448E-04 0.143E+01
0.363E-04 0.145E+01
0.468E-04 0.147E+01
0.450E-04 0.149E+01
0.442E-04 0.152E+01
0.188E-04 0.154E+01
0.360E-04 0.156E+01
0.473E-04 0.158E+01
0.224E-04 0.161E+01
0.395E-04 0.163E+01
0.498E-04 0.165E+01
0.362E-04 0.167E+01
0.526E-04 0.169E+01
0.556E-04 0.172E+01
0.251E-04 0.174E+01
0.430E-04 0.176E+01
0.480E-04 0.179E+01
0.400E-04 0.181E+01
0.603E-04 0.183E+01
0.278E-04 0.185E+01
0.449E-04 0.187E+01
0.347E-04 0.190E+01
0.227E-04 0.192E+01
0.254E-04 0.194E+01
0.505E-04 0.197E+01
0.495E-04 0.199E+01

term 1 (mohr)

0.174E-02 .111
0.626E-03 .397
0.155E-03 .683
0.133E-04 .969
0.956E-05 1.254

term 2 (mohr)

0.198E-02 .111
0.180E-02 .397
0.513E-03 .683
0.444E-04 .969
0.330E-04 1.254

term 3 (mohr)

0.358E-04 .111
0.100E-04 .397
0.153E-05 .683
0.874E-07 .969
0.191E-07 1.254

Re shear (mohr)

0.391E-02 .111
0.287E-02 .397
0.761E-03 .683
0.632E-04 .969
0.439E-04 1.254

Fig. 5.16b

term 1

0.123E-02 0.134E+00
0.128E-02 0.157E+00
0.964E-03 0.180E+00
0.963E-03 0.200E+00
0.634E-03 0.223E+00
0.550E-03 0.243E+00
0.377E-03 0.263E+00
0.295E-03 0.283E+00
0.317E-03 0.306E+00
0.550E-03 0.329E+00
0.549E-03 0.349E+00
0.412E-03 0.371E+00
0.258E-03 0.391E+00
0.529E-04 0.414E+00
0.320E-04 0.437E+00
-0.463E-04 0.457E+00
-0.125E-03 0.480E+00
-0.117E-03 0.503E+00
-0.123E-03 0.526E+00
-0.115E-03 0.549E+00
-0.107E-03 0.571E+00
-0.130E-03 0.594E+00
-0.116E-03 0.617E+00
-0.987E-04 0.640E+00
-0.764E-04 0.660E+00
-0.125E-03 0.683E+00
-0.803E-04 0.706E+00
-0.758E-04 0.726E+00
-0.518E-04 0.749E+00
-0.784E-04 0.769E+00
-0.128E-03 0.791E+00
-0.114E-04 0.814E+00
-0.704E-04 0.837E+00
-0.216E-04 0.860E+00
-0.279E-04 0.883E+00
-0.112E-04 0.906E+00
-0.152E-04 0.929E+00
-0.121E-04 0.951E+00
-0.584E-05 0.974E+00
-0.647E-05 0.994E+00
-0.104E-04 0.102E+01
-0.822E-05 0.104E+01
-0.524E-05 0.106E+01
-0.766E-05 0.109E+01
-0.440E-05 0.111E+01
-0.559E-05 0.113E+01
-0.804E-05 0.115E+01
-0.749E-05 0.118E+01
-0.803E-05 0.120E+01
-0.850E-05 0.122E+01
-0.713E-05 0.125E+01
-0.696E-05 0.127E+01
-0.811E-05 0.129E+01
-0.710E-05 0.131E+01
-0.391E-05 0.134E+01
-0.790E-05 0.136E+01
-0.459E-05 0.138E+01
-0.453E-05 0.140E+01
0.978E-07 0.143E+01
-0.330E-06 0.145E+01
-0.327E-05 0.147E+01
-0.425E-05 0.149E+01
-0.376E-05 0.152E+01
-0.669E-05 0.154E+01
-0.504E-05 0.156E+01
-0.756E-05 0.158E+01
-0.581E-05 0.161E+01
-0.416E-05 0.163E+01
-0.572E-05 0.165E+01
-0.555E-05 0.167E+01
-0.505E-05 0.169E+01
-0.577E-05 0.172E+01
-0.676E-05 0.174E+01
-0.401E-05 0.176E+01
-0.628E-05 0.179E+01
-0.634E-05 0.181E+01
-0.760E-05 0.183E+01
-0.294E-05 0.185E+01
-0.650E-05 0.187E+01
-0.115E-04 0.190E+01
-0.913E-05 0.192E+01
-0.105E-04 0.194E+01
-0.118E-04 0.197E+01
-0.695E-05 0.199E+01

term 2

0.111E-02 0.134E+00
0.136E-02 0.157E+00
0.120E-02 0.180E+00
0.141E-02 0.200E+00
0.104E-02 0.223E+00
0.960E-03 0.243E+00
0.683E-03 0.263E+00
0.550E-03 0.283E+00
0.611E-03 0.306E+00
0.111E-02 0.329E+00
0.118E-02 0.349E+00
0.928E-03 0.371E+00
0.599E-03 0.391E+00
0.126E-03 0.414E+00
0.780E-04 0.437E+00
-0.116E-03 0.457E+00
-0.320E-03 0.480E+00
-0.305E-03 0.503E+00
-0.337E-03 0.526E+00
-0.329E-03 0.549E+00
-0.312E-03 0.571E+00
-0.384E-03 0.594E+00
-0.348E-03 0.617E+00
-0.295E-03 0.640E+00
-0.228E-03 0.660E+00
-0.372E-03 0.683E+00
-0.240E-03 0.706E+00
-0.230E-03 0.726E+00
-0.161E-03 0.749E+00
-0.251E-03 0.769E+00
-0.409E-03 0.791E+00
-0.366E-04 0.814E+00
-0.228E-03 0.837E+00
-0.698E-04 0.860E+00
-0.901E-04 0.883E+00
-0.365E-04 0.906E+00
-0.495E-04 0.929E+00
-0.393E-04 0.951E+00
-0.191E-04 0.974E+00
-0.211E-04 0.994E+00
-0.339E-04 0.102E+01
-0.269E-04 0.104E+01
-0.172E-04 0.106E+01
-0.250E-04 0.109E+01
-0.144E-04 0.111E+01
-0.183E-04 0.113E+01
-0.264E-04 0.115E+01
-0.245E-04 0.118E+01
-0.263E-04 0.120E+01
-0.278E-04 0.122E+01
-0.234E-04 0.125E+01
-0.228E-04 0.127E+01
-0.267E-04 0.129E+01
-0.234E-04 0.131E+01
-0.129E-04 0.134E+01
-0.261E-04 0.136E+01
-0.152E-04 0.138E+01
-0.151E-04 0.140E+01
0.325E-06 0.143E+01
-0.110E-05 0.145E+01
-0.109E-04 0.147E+01
-0.142E-04 0.149E+01
-0.126E-04 0.152E+01
-0.225E-04 0.154E+01
-0.170E-04 0.156E+01
-0.254E-04 0.158E+01
-0.196E-04 0.161E+01
-0.140E-04 0.163E+01
-0.194E-04 0.165E+01
-0.188E-04 0.167E+01
-0.172E-04 0.169E+01
-0.196E-04 0.172E+01
-0.230E-04 0.174E+01
-0.137E-04 0.176E+01
-0.214E-04 0.179E+01
-0.217E-04 0.181E+01
-0.260E-04 0.183E+01
-0.101E-04 0.185E+01
-0.222E-04 0.187E+01
-0.394E-04 0.190E+01
-0.311E-04 0.192E+01
-0.352E-04 0.194E+01
-0.392E-04 0.197E+01
-0.229E-04 0.199E+01

term 3

0.376E-04 0.134E+00
0.370E-04 0.157E+00
0.331E-04 0.180E+00
0.313E-04 0.200E+00
0.203E-04 0.223E+00
0.185E-04 0.243E+00
0.174E-04 0.263E+00
0.169E-04 0.283E+00
0.163E-04 0.306E+00
0.175E-04 0.329E+00
0.184E-04 0.349E+00
0.139E-04 0.371E+00
0.112E-04 0.391E+00
0.688E-05 0.414E+00
0.748E-05 0.437E+00
0.525E-05 0.457E+00
0.394E-05 0.480E+00
0.354E-05 0.503E+00

0.281E-05 0.526E+00
0.174E-05 0.549E+00
0.165E-05 0.571E+00
0.100E-05 0.594E+00
0.683E-06 0.617E+00
0.695E-06 0.640E+00
0.401E-06 0.660E+00
0.891E-06 0.683E+00
0.464E-06 0.706E+00
0.277E-06 0.726E+00
0.227E-06 0.749E+00
0.298E-06 0.769E+00
0.986E-06 0.791E+00
0.475E-07 0.814E+00
0.279E-06 0.837E+00
0.637E-07 0.860E+00
0.601E-07 0.883E+00
0.377E-07 0.906E+00
0.452E-07 0.929E+00
0.320E-07 0.951E+00
0.215E-07 0.974E+00
0.195E-07 0.994E+00
0.170E-07 0.102E+01
0.194E-07 0.104E+01
0.187E-07 0.106E+01
0.193E-07 0.109E+01
0.168E-07 0.111E+01
0.135E-07 0.113E+01
0.135E-07 0.115E+01
0.157E-07 0.118E+01
0.124E-07 0.120E+01
0.993E-08 0.122E+01
0.111E-07 0.125E+01
0.106E-07 0.127E+01
0.925E-08 0.129E+01
0.108E-07 0.131E+01
0.919E-08 0.134E+01
0.977E-08 0.136E+01
0.115E-07 0.138E+01
0.110E-07 0.140E+01
0.224E-07 0.143E+01
0.245E-07 0.145E+01
0.288E-07 0.147E+01
0.309E-07 0.149E+01
0.324E-07 0.152E+01
0.303E-07 0.154E+01
0.260E-07 0.156E+01
0.275E-07 0.158E+01
0.222E-07 0.161E+01
0.211E-07 0.163E+01
0.208E-07 0.165E+01
0.200E-07 0.167E+01
0.185E-07 0.169E+01
0.207E-07 0.172E+01
0.229E-07 0.174E+01
0.224E-07 0.176E+01
0.207E-07 0.179E+01
0.281E-07 0.181E+01
0.284E-07 0.183E+01
0.213E-07 0.185E+01
0.146E-07 0.187E+01
0.864E-08 0.190E+01
0.767E-08 0.192E+01
0.348E-08 0.194E+01
0.685E-08 0.197E+01
0.109E-07 0.199E+01

Re shear

0.246E-02 0.134E+00
0.281E-02 0.157E+00
0.237E-02 0.180E+00
0.265E-02 0.200E+00
0.190E-02 0.223E+00
0.175E-02 0.243E+00
0.131E-02 0.263E+00
0.110E-02 0.283E+00
0.120E-02 0.306E+00
0.198E-02 0.329E+00
0.212E-02 0.349E+00
0.167E-02 0.371E+00
0.114E-02 0.391E+00
0.367E-03 0.414E+00
0.326E-03 0.437E+00
-0.103E-05 0.457E+00
-0.317E-03 0.480E+00
-0.301E-03 0.503E+00
-0.352E-03 0.526E+00
-0.370E-03 0.549E+00
-0.345E-03 0.571E+00
-0.467E-03 0.594E+00
-0.431E-03 0.617E+00
-0.361E-03 0.640E+00
-0.285E-03 0.660E+00
-0.455E-03 0.683E+00
-0.298E-03 0.706E+00
-0.292E-03 0.726E+00
-0.201E-03 0.749E+00
-0.312E-03 0.769E+00
-0.481E-03 0.791E+00
-0.453E-04 0.814E+00
-0.282E-03 0.837E+00
-0.877E-04 0.860E+00
-0.115E-03 0.883E+00
-0.455E-04 0.906E+00
-0.620E-04 0.929E+00
-0.495E-04 0.951E+00
-0.236E-04 0.974E+00
-0.264E-04 0.994E+00
-0.433E-04 0.102E+01
-0.339E-04 0.104E+01
-0.213E-04 0.106E+01
-0.316E-04 0.109E+01
-0.178E-04 0.111E+01
-0.231E-04 0.113E+01
-0.336E-04 0.115E+01
-0.311E-04 0.118E+01
-0.336E-04 0.120E+01
-0.357E-04 0.122E+01
-0.298E-04 0.125E+01
-0.292E-04 0.127E+01
-0.342E-04 0.129E+01
-0.298E-04 0.131E+01
-0.162E-04 0.134E+01
-0.334E-04 0.136E+01
-0.191E-04 0.138E+01
-0.189E-04 0.140E+01
0.182E-05 0.143E+01
0.106E-06 0.145E+01
-0.124E-04 0.147E+01
-0.165E-04 0.149E+01
-0.143E-04 0.152E+01
-0.273E-04 0.154E+01
-0.203E-04 0.156E+01
-0.312E-04 0.158E+01
-0.240E-04 0.161E+01
-0.168E-04 0.163E+01
-0.237E-04 0.165E+01
-0.231E-04 0.167E+01
-0.210E-04 0.169E+01
-0.240E-04 0.172E+01
-0.283E-04 0.174E+01
-0.162E-04 0.176E+01
-0.263E-04 0.179E+01
-0.261E-04 0.181E+01
-0.317E-04 0.183E+01
-0.116E-04 0.185E+01
-0.277E-04 0.187E+01
-0.503E-04 0.190E+01
-0.397E-04 0.192E+01
-0.455E-04 0.194E+01
-0.506E-04 0.197E+01
-0.292E-04 0.199E+01

term 1 (mohr)

0.837E-03 .397
-0.164E-04 .682
0.670E-05 .966

term 2 (mohr)

0.241E-02 .397
-0.543E-04 .682
0.224E-04 .966

term 3 (mohr)

0.797E-05 .397
0.573E-06 .682
0.240E-07 .966

Re shear (mohr)

0.360E-02 .397
-0.356E-04 .682
0.306E-04 .966

Fig. 5.17a

axial

0.627E-03 .112
0.546E-03 .397
-0.316E-04 .682
-0.149E-04 .965
-0.135E-04 1.256
.966E-02 .112
.333E-02 .397
-.227E-02 .682
-.358E-03 1.258

transverse

-0.547E-03 .112
-0.720E-04 .397
0.829E-04 .682
0.394E-04 .965
0.300E-04 1.256

spanwise

-.753E-02 .119
-.143E-02 .397
-.373E-03 .682
-.150E-03 1.258

Fig. 5.17b

axial

6.628E-05 .112
5.56E-04 .397
-3.007E-05 .682
-1.48126E-05 .965
-1.34809E-05 1.256

transverse

1.433E-03 .112
1.7828E-03 .397
5.959E-04 .682
8.38E-05 .965
6.4E-05 1.256

spanwise

-1.306E-02 .112
-3.84E-03 .397
-3.187E-04 .682
-1.724E-04 1.256

Fig. 5.18a

u'v'

-0.143E-02 0.134E+00
-0.118E-02 0.157E+00
-0.139E-02 0.180E+00
-0.947E-03 0.200E+00
-0.733E-03 0.223E+00
-0.663E-03 0.243E+00
-0.817E-03 0.263E+00
-0.664E-03 0.283E+00
-0.539E-03 0.306E+00
-0.603E-03 0.329E+00
-0.526E-03 0.349E+00
-0.470E-03 0.371E+00
-0.515E-03 0.391E+00
-0.423E-03 0.414E+00
-0.430E-03 0.437E+00
-0.371E-03 0.457E+00
-0.284E-03 0.480E+00
-0.236E-03 0.503E+00
-0.220E-03 0.526E+00
-0.277E-03 0.549E+00
-0.167E-03 0.571E+00
-0.128E-03 0.594E+00
-0.111E-03 0.617E+00
-0.191E-03 0.640E+00
-0.102E-03 0.660E+00
-0.121E-03 0.683E+00
-0.201E-03 0.706E+00
-0.107E-03 0.726E+00

-0.693E-04	0.749E+00
-0.705E-04	0.769E+00
-0.554E-04	0.791E+00
-0.176E-04	0.814E+00
-0.255E-04	0.837E+00
-0.251E-04	0.860E+00
-0.265E-04	0.883E+00
-0.981E-05	0.906E+00
-0.223E-04	0.929E+00
-0.169E-04	0.951E+00
-0.108E-04	0.974E+00
-0.110E-04	0.994E+00
-0.130E-04	0.102E+01
-0.126E-04	0.104E+01
-0.116E-04	0.106E+01
-0.107E-04	0.109E+01
-0.902E-05	0.111E+01
-0.842E-05	0.113E+01
-0.339E-05	0.115E+01
-0.861E-05	0.118E+01
-0.628E-05	0.120E+01
-0.677E-05	0.122E+01
-0.538E-05	0.125E+01
-0.614E-05	0.127E+01
-0.918E-05	0.129E+01
-0.519E-05	0.131E+01
-0.979E-05	0.134E+01
-0.820E-05	0.136E+01
-0.117E-04	0.138E+01
-0.121E-04	0.140E+01
-0.109E-04	0.143E+01
-0.886E-05	0.145E+01
-0.113E-04	0.147E+01
-0.108E-04	0.149E+01
-0.107E-04	0.152E+01
-0.481E-05	0.154E+01
-0.878E-05	0.156E+01
-0.114E-04	0.158E+01
-0.565E-05	0.161E+01
-0.959E-05	0.163E+01
-0.119E-04	0.165E+01
-0.876E-05	0.167E+01
-0.126E-04	0.169E+01
-0.132E-04	0.172E+01
-0.631E-05	0.174E+01
-0.104E-04	0.176E+01
-0.115E-04	0.179E+01
-0.969E-05	0.181E+01
-0.144E-04	0.183E+01
-0.695E-05	0.185E+01
-0.110E-04	0.187E+01
-0.871E-05	0.190E+01
-0.600E-05	0.192E+01
-0.659E-05	0.194E+01
-0.125E-04	0.197E+01
-0.123E-04	0.199E+01

u'w'

-0.123E-02	0.134E+00
-0.128E-02	0.157E+00
-0.964E-03	0.180E+00
-0.963E-03	0.200E+00
-0.634E-03	0.223E+00
-0.550E-03	0.243E+00
-0.377E-03	0.263E+00
-0.295E-03	0.283E+00
-0.317E-03	0.306E+00
-0.550E-03	0.329E+00
-0.549E-03	0.349E+00
-0.412E-03	0.371E+00
-0.258E-03	0.391E+00
-0.529E-04	0.414E+00
-0.320E-04	0.437E+00
0.463E-04	0.457E+00
0.125E-03	0.480E+00
0.117E-03	0.503E+00
0.123E-03	0.526E+00
0.115E-03	0.549E+00
0.107E-03	0.571E+00
0.130E-03	0.594E+00
0.116E-03	0.617E+00
0.987E-04	0.640E+00
0.764E-04	0.660E+00
0.125E-03	0.683E+00
0.803E-04	0.706E+00
0.758E-04	0.726E+00
0.518E-04	0.749E+00
0.784E-04	0.769E+00
0.128E-03	0.791E+00
0.114E-04	0.814E+00
0.704E-04	0.837E+00
0.216E-04	0.860E+00
0.279E-04	0.883E+00
0.112E-04	0.906E+00
0.152E-04	0.929E+00
0.121E-04	0.951E+00
0.584E-05	0.974E+00
0.647E-05	0.994E+00
0.104E-04	0.102E+01
0.822E-05	0.104E+01
0.524E-05	0.106E+01
0.766E-05	0.109E+01
0.440E-05	0.111E+01
0.559E-05	0.113E+01
0.804E-05	0.115E+01
0.749E-05	0.118E+01
0.803E-05	0.120E+01
0.850E-05	0.122E+01
0.713E-05	0.125E+01
0.696E-05	0.127E+01
0.811E-05	0.129E+01
0.710E-05	0.131E+01
0.391E-05	0.134E+01
0.790E-05	0.136E+01
0.459E-05	0.138E+01
0.453E-05	0.140E+01
-0.978E-07	0.143E+01
0.330E-06	0.145E+01
0.327E-05	0.147E+01
0.425E-05	0.149E+01
0.376E-05	0.152E+01
0.669E-05	0.154E+01
0.504E-05	0.156E+01
0.756E-05	0.158E+01
0.581E-05	0.161E+01
0.416E-05	0.163E+01
0.572E-05	0.165E+01
0.555E-05	0.167E+01
0.505E-05	0.169E+01
0.577E-05	0.172E+01
0.676E-05	0.174E+01
0.401E-05	0.176E+01
0.628E-05	0.179E+01
0.634E-05	0.181E+01
0.760E-05	0.183E+01
0.294E-05	0.185E+01
0.650E-05	0.187E+01
0.115E-04	0.190E+01
0.913E-05	0.192E+01
0.105E-04	0.194E+01
0.118E-04	0.197E+01
0.695E-05	0.199E+01

Fig. 5.18b

ρ'u'

0.181E-02	0.134E+00
0.183E-02	0.157E+00
0.220E-02	0.180E+00
0.215E-02	0.200E+00
0.206E-02	0.223E+00
0.189E-02	0.243E+00
0.220E-02	0.263E+00
0.208E-02	0.283E+00
0.195E-02	0.306E+00
0.200E-02	0.329E+00
0.175E-02	0.349E+00
0.180E-02	0.371E+00
0.204E-02	0.391E+00
0.186E-02	0.414E+00
0.171E-02	0.437E+00
0.165E-02	0.457E+00
0.989E-03	0.480E+00
0.944E-03	0.503E+00
0.114E-02	0.526E+00
0.138E-02	0.549E+00
0.556E-03	0.571E+00
0.449E-03	0.594E+00
0.411E-03	0.617E+00
0.554E-03	0.640E+00
0.425E-03	0.660E+00
0.408E-03	0.683E+00
0.937E-03	0.706E+00
0.504E-03	0.726E+00
0.179E-03	0.749E+00
0.193E-03	0.769E+00
0.190E-03	0.791E+00
0.116E-03	0.814E+00
0.729E-04	0.837E+00
0.604E-04	0.860E+00
0.611E-04	0.883E+00
0.399E-04	0.906E+00
0.582E-04	0.929E+00
0.477E-04	0.951E+00
0.404E-04	0.974E+00
0.362E-04	0.994E+00
0.431E-04	0.102E+01
0.436E-04	0.104E+01
0.382E-04	0.106E+01
0.393E-04	0.109E+01
0.342E-04	0.111E+01
0.317E-04	0.113E+01
0.294E-04	0.115E+01
0.351E-04	0.118E+01
0.337E-04	0.120E+01
0.322E-04	0.122E+01
0.293E-04	0.125E+01
0.307E-04	0.127E+01
0.326E-04	0.129E+01
0.321E-04	0.131E+01
0.306E-04	0.134E+01
0.301E-04	0.136E+01
0.364E-04	0.138E+01
0.339E-04	0.140E+01
0.338E-04	0.143E+01
0.323E-04	0.145E+01
0.347E-04	0.147E+01
0.332E-04	0.149E+01
0.347E-04	0.152E+01
0.308E-04	0.154E+01
0.317E-04	0.156E+01
0.341E-04	0.158E+01
0.298E-04	0.161E+01
0.326E-04	0.163E+01
0.330E-04	0.165E+01
0.330E-04	0.167E+01
0.354E-04	0.169E+01
0.364E-04	0.172E+01
0.354E-04	0.174E+01
0.363E-04	0.176E+01
0.363E-04	0.179E+01
0.353E-04	0.181E+01
0.426E-04	0.183E+01
0.333E-04	0.185E+01
0.389E-04	0.187E+01
0.379E-04	0.190E+01
0.359E-04	0.192E+01
0.376E-04	0.194E+01
0.400E-04	0.197E+01
0.396E-04	0.199E+01

ρ'v'

-0.128E-02	0.134E+00
-0.125E-02	0.157E+00
-0.173E-02	0.180E+00
-0.138E-02	0.200E+00
-0.120E-02	0.223E+00
-0.116E-02	0.243E+00
-0.148E-02	0.263E+00
-0.124E-02	0.283E+00
-0.104E-02	0.306E+00
-0.122E-02	0.329E+00
-0.113E-02	0.349E+00
-0.106E-02	0.371E+00
-0.120E-02	0.391E+00
-0.101E-02	0.414E+00
-0.105E-02	0.437E+00
-0.929E-03	0.457E+00
-0.726E-03	0.480E+00
-0.617E-03	0.503E+00
-0.601E-03	0.526E+00
-0.793E-03	0.549E+00
-0.487E-03	0.571E+00
-0.380E-03	0.594E+00
-0.334E-03	0.617E+00
-0.572E-03	0.640E+00
-0.305E-03	0.660E+00
-0.358E-03	0.683E+00
-0.598E-03	0.706E+00
-0.326E-03	0.726E+00
-0.216E-03	0.749E+00

-0.225E-03 0.769E+00
-0.178E-03 0.791E+00
-0.567E-04 0.814E+00
-0.825E-04 0.837E+00
-0.809E-04 0.860E+00
-0.855E-04 0.883E+00
-0.319E-04 0.906E+00
-0.728E-04 0.929E+00
-0.553E-04 0.951E+00
-0.351E-04 0.974E+00
-0.358E-04 0.994E+00
-0.423E-04 0.102E+01
-0.414E-04 0.104E+01
-0.380E-04 0.106E+01
-0.351E-04 0.109E+01
-0.295E-04 0.111E+01
-0.276E-04 0.113E+01
-0.111E-04 0.115E+01
-0.282E-04 0.118E+01
-0.205E-04 0.120E+01
-0.221E-04 0.122E+01
-0.176E-04 0.125E+01
-0.202E-04 0.127E+01
-0.302E-04 0.129E+01
-0.171E-04 0.131E+01
-0.323E-04 0.134E+01
-0.271E-04 0.136E+01
-0.386E-04 0.138E+01
-0.401E-04 0.140E+01
-0.361E-04 0.143E+01
-0.295E-04 0.145E+01
-0.377E-04 0.147E+01
-0.364E-04 0.149E+01
-0.360E-04 0.152E+01
-0.162E-04 0.154E+01
-0.295E-04 0.156E+01
-0.384E-04 0.158E+01
-0.190E-04 0.161E+01
-0.324E-04 0.163E+01
-0.403E-04 0.165E+01
-0.297E-04 0.167E+01
-0.426E-04 0.169E+01
-0.451E-04 0.172E+01
-0.215E-04 0.174E+01
-0.353E-04 0.176E+01
-0.393E-04 0.179E+01
-0.331E-04 0.181E+01
-0.494E-04 0.183E+01
-0.238E-04 0.185E+01
-0.375E-04 0.187E+01
-0.297E-04 0.190E+01
-0.204E-04 0.192E+01
-0.222E-04 0.194E+01
-0.416E-04 0.197E+01
-0.404E-04 0.199E+01

ρ'w'

-0.111E-02 0.134E+00
-0.136E-02 0.157E+00
-0.120E-02 0.180E+00
-0.141E-02 0.200E+00
-0.104E-02 0.223E+00
-0.960E-03 0.243E+00
-0.683E-03 0.263E+00
-0.550E-03 0.283E+00
-0.611E-03 0.306E+00
-0.111E-02 0.329E+00
-0.118E-02 0.349E+00
-0.928E-03 0.371E+00
-0.599E-03 0.391E+00
-0.126E-03 0.414E+00
-0.780E-04 0.437E+00
0.116E-03 0.457E+00
0.320E-03 0.480E+00
0.305E-03 0.503E+00
0.337E-03 0.526E+00
0.329E-03 0.549E+00
0.312E-03 0.571E+00
0.384E-03 0.594E+00
0.348E-03 0.617E+00
0.295E-03 0.640E+00
0.228E-03 0.660E+00
0.372E-03 0.683E+00
0.240E-03 0.706E+00
0.230E-03 0.726E+00
0.161E-03 0.749E+00
0.251E-03 0.769E+00
0.409E-03 0.791E+00
0.366E-04 0.814E+00
0.228E-03 0.837E+00
0.698E-04 0.860E+00
0.901E-04 0.883E+00
0.365E-04 0.906E+00
0.495E-04 0.929E+00
0.393E-04 0.951E+00
0.191E-04 0.974E+00
0.211E-04 0.994E+00
0.339E-04 0.102E+01
0.269E-04 0.104E+01
0.172E-04 0.106E+01
0.250E-04 0.109E+01
0.144E-04 0.111E+01
0.183E-04 0.113E+01
0.264E-04 0.115E+01
0.245E-04 0.118E+01
0.263E-04 0.120E+01
0.278E-04 0.122E+01
0.234E-04 0.125E+01
0.228E-04 0.127E+01
0.267E-04 0.129E+01
0.234E-04 0.131E+01
0.129E-04 0.134E+01
0.261E-04 0.136E+01
0.152E-04 0.138E+01
0.151E-04 0.140E+01
-0.325E-06 0.143E+01
0.110E-05 0.145E+01
0.109E-04 0.147E+01
0.142E-04 0.149E+01
0.126E-04 0.152E+01
0.225E-04 0.154E+01
0.170E-04 0.156E+01
0.254E-04 0.158E+01
0.196E-04 0.161E+01
0.140E-04 0.163E+01
0.194E-04 0.165E+01
0.188E-04 0.167E+01
0.172E-04 0.169E+01
0.196E-04 0.172E+01
0.230E-04 0.174E+01
0.137E-04 0.176E+01
0.214E-04 0.179E+01
0.217E-04 0.181E+01
0.260E-04 0.183E+01
0.101E-04 0.185E+01
0.222E-04 0.187E+01
0.394E-04 0.190E+01
0.311E-04 0.192E+01
0.352E-04 0.194E+01
0.392E-04 0.197E+01
0.229E-04 0.199E+01

Fig. 5.19a

uv probe

0.997 .112
0.997 .397
0.997 .682
0.997 .966
0.997 1.256

uw probe

1.058 .112
1.014 .397
1.02 .682
1.014 .966

Fig. 5.19b

uv probe

0.997 0.331
0.990 0.569
0.983 0.807
0.980 1.045

uw probe

1.014 0.331
1.014 0.569
1.014 0.807
1.014 1.045

Fig. 5.20a

axial t.i.

0.149E+00
0.114E+00
0.157E+00
0.131E+00
0.141E+00
0.150E+00
0.156E+00
0.169E+00
0.150E+00
0.186E+00
0.155E+00
0.205E+00
0.154E+00
0.224E+00
0.155E+00
0.243E+00
0.160E+00
0.260E+00
0.163E+00
0.279E+00
0.165E+00
0.298E+00
0.166E+00
0.317E+00
0.150E+00
0.336E+00
0.157E+00
0.352E+00
0.149E+00
0.371E+00
0.180E+00
0.388E+00
0.154E+00
0.407E+00
0.154E+00
0.426E+00
0.166E+00
0.445E+00
0.159E+00
0.464E+00
0.153E+00
0.483E+00
0.148E+00
0.502E+00
0.151E+00
0.521E+00
0.131E+00
0.540E+00
0.123E+00
0.560E+00
0.117E+00
0.579E+00
0.122E+00
0.595E+00
0.126E+00
0.614E+00
0.103E+00
0.633E+00
0.119E+00
0.652E+00
0.103E+00
0.671E+00
0.852E-01 0.693E+00
0.982E-01 0.710E+00
0.821E-01 0.729E+00
0.784E-01 0.748E+00
0.894E-01 0.767E+00
0.773E-01 0.786E+00
0.606E-01 0.805E+00
0.641E-01 0.824E+00
0.620E-01 0.843E+00
0.506E-01 0.862E+00
0.506E-01 0.881E+00
0.396E-01 0.900E+00
0.413E-01 0.917E+00
0.403E-01 0.936E+00
0.334E-01 0.955E+00
0.327E-01 0.974E+00
0.294E-01 0.990E+00
0.265E-01 0.101E+01
0.265E-01 0.103E+01
0.274E-01 0.105E+01
0.266E-01 0.107E+01
0.279E-01 0.109E+01

0.276E-01	0.110E+01
0.268E-01	0.112E+01
0.289E-01	0.114E+01
0.276E-01	0.116E+01
0.293E-01	0.118E+01
0.288E-01	0.120E+01
0.269E-01	0.122E+01
0.293E-01	0.124E+01
0.280E-01	0.125E+01
0.283E-01	0.127E+01
0.292E-01	0.129E+01
0.295E-01	0.131E+01
0.312E-01	0.133E+01
0.291E-01	0.135E+01
0.311E-01	0.137E+01
0.317E-01	0.139E+01
0.311E-01	0.140E+01
0.309E-01	0.142E+01
0.315E-01	0.144E+01
0.327E-01	0.146E+01
0.317E-01	0.148E+01
0.341E-01	0.150E+01
0.345E-01	0.152E+01
0.340E-01	0.154E+01
0.344E-01	0.155E+01
0.356E-01	0.157E+01
0.362E-01	0.159E+01
0.356E-01	0.161E+01
0.383E-01	0.163E+01
0.436E-01	0.165E+01
0.446E-01	0.167E+01
0.511E-01	0.169E+01
0.584E-01	0.170E+01
0.571E-01	0.172E+01
0.513E-01	0.174E+01
0.484E-01	0.176E+01
0.435E-01	0.178E+01
0.385E-01	0.180E+01
0.392E-01	0.181E+01
0.383E-01	0.183E+01
0.375E-01	0.185E+01
0.351E-01	0.187E+01
0.355E-01	0.189E+01
0.366E-01	0.191E+01
0.370E-01	0.193E+01
0.349E-01	0.195E+01
0.345E-01	0.197E+01
0.346E-01	0.199E+01

transverse t.i.

0.116E+00
0.114E+00
0.119E+00
0.131E+00
0.112E+00
0.150E+00
0.118E+00
0.169E+00
0.113E+00
0.186E+00
0.115E+00
0.205E+00
0.113E+00
0.224E+00

0.112E+00
0.243E+00
0.114E+00
0.260E+00
0.112E+00
0.279E+00
0.114E+00
0.298E+00
0.109E+00
0.317E+00
0.103E+00
0.336E+00
0.107E+00
0.352E+00
0.101E+00
0.371E+00
0.105E+00
0.388E+00

0.950E-01	0.407E+00
0.998E-01	0.426E+00
0.102E+00	
0.445E+00	
0.926E-01	0.464E+00
0.960E-01	0.483E+00
0.913E-01	0.502E+00
0.880E-01	0.521E+00
0.803E-01	0.540E+00
0.743E-01	0.560E+00
0.723E-01	0.579E+00
0.735E-01	0.595E+00
0.740E-01	0.614E+00
0.642E-01	0.633E+00
0.715E-01	0.652E+00
0.639E-01	0.671E+00
0.553E-01	0.693E+00
0.630E-01	0.710E+00
0.553E-01	0.729E+00
0.539E-01	0.748E+00
0.547E-01	0.767E+00
0.545E-01	0.786E+00
0.453E-01	0.805E+00
0.458E-01	0.824E+00
0.430E-01	0.843E+00
0.408E-01	0.862E+00
0.385E-01	0.881E+00
0.343E-01	0.900E+00
0.353E-01	0.917E+00
0.339E-01	0.936E+00
0.311E-01	0.955E+00
0.307E-01	0.974E+00
0.290E-01	0.990E+00
0.286E-01	0.101E+01
0.285E-01	0.103E+01
0.297E-01	0.105E+01
0.285E-01	0.107E+01
0.296E-01	0.109E+01
0.292E-01	0.110E+01
0.303E-01	0.112E+01
0.298E-01	0.114E+01
0.287E-01	0.116E+01
0.302E-01	0.118E+01
0.303E-01	0.120E+01
0.296E-01	0.122E+01
0.316E-01	0.124E+01
0.313E-01	0.125E+01
0.309E-01	0.127E+01

0.320E-01	0.129E+01
0.312E-01	0.131E+01
0.332E-01	0.133E+01
0.315E-01	0.135E+01
0.327E-01	0.137E+01
0.333E-01	0.139E+01
0.332E-01	0.140E+01
0.322E-01	0.142E+01
0.334E-01	0.144E+01
0.328E-01	0.146E+01
0.336E-01	0.148E+01
0.348E-01	0.150E+01
0.353E-01	0.152E+01
0.349E-01	0.154E+01
0.344E-01	0.155E+01
0.350E-01	0.157E+01
0.357E-01	0.159E+01
0.350E-01	0.161E+01
0.366E-01	0.163E+01
0.375E-01	0.165E+01
0.383E-01	0.167E+01
0.410E-01	0.169E+01
0.482E-01	0.170E+01
0.456E-01	0.172E+01
0.466E-01	0.174E+01
0.475E-01	0.176E+01
0.436E-01	0.178E+01
0.397E-01	0.180E+01
0.395E-01	0.181E+01
0.387E-01	0.183E+01
0.391E-01	0.185E+01
0.371E-01	0.187E+01
0.375E-01	0.189E+01
0.381E-01	0.191E+01
0.381E-01	0.193E+01
0.373E-01	0.195E+01
0.363E-01	0.197E+01
0.368E-01	0.199E+01

Fig. 5.20b

density t.i.

0.838E-01	0.114E+00
0.906E-01	0.131E+00
0.831E-01	0.150E+00
0.937E-01	0.169E+00
0.915E-01	0.186E+00
0.964E-01	0.205E+00
0.976E-01	0.224E+00
0.100E+00	0.243E+00
0.105E+00	0.260E+00
0.108E+00	0.279E+00
0.111E+00	0.298E+00
0.113E+00	0.317E+00
0.103E+00	0.336E+00
0.108E+00	0.352E+00
0.103E+00	0.371E+00
0.125E+00	0.388E+00
0.108E+00	0.407E+00
0.109E+00	0.426E+00
0.118E+00	0.445E+00
0.114E+00	0.464E+00
0.110E+00	0.483E+00
0.107E+00	0.502E+00
0.109E+00	0.521E+00

0.945E-01	0.540E+00
0.888E-01	0.560E+00
0.847E-01	0.579E+00
0.884E-01	0.595E+00
0.912E-01	0.614E+00
0.745E-01	0.633E+00
0.862E-01	0.652E+00
0.748E-01	0.671E+00
0.621E-01	0.693E+00
0.718E-01	0.710E+00
0.600E-01	0.729E+00
0.573E-01	0.748E+00
0.652E-01	0.767E+00
0.563E-01	0.786E+00
0.442E-01	0.805E+00
0.467E-01	0.824E+00
0.452E-01	0.843E+00
0.369E-01	0.862E+00
0.369E-01	0.881E+00
0.289E-01	0.900E+00
0.301E-01	0.917E+00
0.293E-01	0.936E+00
0.243E-01	0.955E+00
0.237E-01	0.974E+00
0.213E-01	0.990E+00
0.192E-01	0.101E+01
0.191E-01	0.103E+01
0.197E-01	0.105E+01
0.190E-01	0.107E+01
0.199E-01	0.109E+01
0.197E-01	0.110E+01
0.191E-01	0.112E+01
0.206E-01	0.114E+01
0.198E-01	0.116E+01
0.210E-01	0.118E+01
0.207E-01	0.120E+01
0.194E-01	0.122E+01
0.211E-01	0.124E+01
0.202E-01	0.125E+01
0.204E-01	0.127E+01
0.211E-01	0.129E+01
0.213E-01	0.131E+01
0.226E-01	0.133E+01
0.211E-01	0.135E+01
0.226E-01	0.137E+01
0.230E-01	0.139E+01
0.226E-01	0.140E+01
0.225E-01	0.142E+01
0.229E-01	0.144E+01
0.238E-01	0.146E+01
0.230E-01	0.148E+01
0.248E-01	0.150E+01
0.251E-01	0.152E+01
0.247E-01	0.154E+01
0.249E-01	0.155E+01
0.256E-01	0.157E+01
0.257E-01	0.159E+01
0.252E-01	0.161E+01
0.272E-01	0.163E+01
0.312E-01	0.165E+01
0.322E-01	0.167E+01
0.374E-01	0.169E+01
0.435E-01	0.170E+01
0.431E-01	0.172E+01
0.391E-01	0.174E+01
0.372E-01	0.176E+01

0.337E-01	0.178E+01
0.300E-01	0.180E+01
0.306E-01	0.181E+01
0.300E-01	0.183E+01
0.294E-01	0.185E+01
0.276E-01	0.187E+01
0.279E-01	0.189E+01
0.289E-01	0.191E+01
0.292E-01	0.193E+01
0.276E-01	0.195E+01
0.273E-01	0.197E+01
0.274E-01	0.199E+01

u' t.i.

0.652E-01	0.114E+00
0.664E-01	0.131E+00
0.579E-01	0.150E+00
0.623E-01	0.169E+00
0.585E-01	0.186E+00
0.586E-01	0.205E+00
0.564E-01	0.224E+00
0.547E-01	0.243E+00
0.549E-01	0.260E+00
0.546E-01	0.279E+00
0.539E-01	0.298E+00
0.528E-01	0.317E+00
0.469E-01	0.336E+00
0.486E-01	0.352E+00
0.456E-01	0.371E+00
0.545E-01	0.388E+00
0.460E-01	0.407E+00
0.453E-01	0.426E+00
0.480E-01	0.445E+00
0.454E-01	0.464E+00
0.431E-01	0.483E+00
0.414E-01	0.502E+00
0.419E-01	0.521E+00
0.365E-01	0.540E+00
0.342E-01	0.560E+00
0.323E-01	0.579E+00
0.336E-01	0.595E+00
0.348E-01	0.614E+00
0.285E-01	0.633E+00
0.328E-01	0.652E+00
0.282E-01	0.671E+00
0.231E-01	0.693E+00
0.264E-01	0.710E+00
0.221E-01	0.729E+00
0.211E-01	0.748E+00
0.242E-01	0.767E+00
0.210E-01	0.786E+00
0.164E-01	0.805E+00
0.174E-01	0.824E+00
0.168E-01	0.843E+00
0.137E-01	0.862E+00
0.137E-01	0.881E+00
0.107E-01	0.900E+00
0.112E-01	0.917E+00
0.110E-01	0.936E+00
0.911E-02	0.955E+00
0.897E-02	0.974E+00
0.810E-02	0.990E+00
0.733E-02	0.101E+01
0.740E-02	0.103E+01
0.774E-02	0.105E+01
0.759E-02	0.107E+01
0.801E-02	0.109E+01
0.793E-02	0.110E+01
0.769E-02	0.112E+01
0.826E-02	0.114E+01
0.783E-02	0.116E+01
0.826E-02	0.118E+01
0.808E-02	0.120E+01
0.752E-02	0.122E+01
0.819E-02	0.124E+01
0.782E-02	0.125E+01
0.790E-02	0.127E+01
0.814E-02	0.129E+01
0.820E-02	0.131E+01
0.863E-02	0.133E+01
0.799E-02	0.135E+01
0.852E-02	0.137E+01
0.869E-02	0.139E+01
0.852E-02	0.140E+01
0.845E-02	0.142E+01
0.861E-02	0.144E+01
0.894E-02	0.146E+01
0.867E-02	0.148E+01
0.932E-02	0.150E+01
0.944E-02	0.152E+01
0.931E-02	0.154E+01
0.950E-02	0.155E+01
0.100E-01	0.157E+01
0.105E-01	0.159E+01
0.104E-01	0.161E+01
0.111E-01	0.163E+01
0.124E-01	0.165E+01
0.124E-01	0.167E+01
0.137E-01	0.169E+01
0.149E-01	0.170E+01
0.140E-01	0.172E+01
0.122E-01	0.174E+01
0.112E-01	0.176E+01
0.983E-02	0.178E+01
0.852E-02	0.180E+01
0.855E-02	0.181E+01
0.828E-02	0.183E+01
0.806E-02	0.185E+01
0.749E-02	0.187E+01
0.755E-02	0.189E+01
0.775E-02	0.191E+01
0.780E-02	0.193E+01
0.732E-02	0.195E+01
0.721E-02	0.197E+01
0.721E-02	0.199E+01

v' t.i.

0.116E+00	0.114E+00
0.119E+00	0.131E+00
0.112E+00	0.150E+00
0.118E+00	0.169E+00
0.113E+00	0.186E+00
0.115E+00	0.205E+00
0.113E+00	0.224E+00
0.112E+00	0.243E+00
0.114E+00	0.260E+00
0.112E+00	0.279E+00
0.114E+00	0.298E+00
0.109E+00	0.317E+00
0.103E+00	0.336E+00
0.107E+00	0.352E+00
0.101E+00	0.371E+00
0.105E+00	0.388E+00
0.950E-01	0.407E+00
0.998E-01	0.426E+00
0.102E+00	0.445E+00
0.926E-01	0.464E+00
0.960E-01	0.483E+00
0.913E-01	0.502E+00
0.880E-01	0.521E+00
0.803E-01	0.540E+00
0.743E-01	0.560E+00
0.723E-01	0.579E+00
0.735E-01	0.595E+00
0.740E-01	0.614E+00
0.642E-01	0.633E+00
0.715E-01	0.652E+00
0.639E-01	0.671E+00
0.553E-01	0.693E+00
0.630E-01	0.710E+00
0.553E-01	0.729E+00
0.539E-01	0.748E+00
0.547E-01	0.767E+00
0.545E-01	0.786E+00
0.453E-01	0.805E+00
0.458E-01	0.824E+00
0.430E-01	0.843E+00
0.408E-01	0.862E+00
0.385E-01	0.881E+00
0.343E-01	0.900E+00
0.353E-01	0.917E+00
0.339E-01	0.936E+00
0.311E-01	0.955E+00
0.307E-01	0.974E+00
0.290E-01	0.990E+00
0.286E-01	0.101E+01
0.285E-01	0.103E+01
0.297E-01	0.105E+01
0.285E-01	0.107E+01
0.296E-01	0.109E+01
0.292E-01	0.110E+01
0.303E-01	0.112E+01
0.298E-01	0.114E+01
0.287E-01	0.116E+01
0.302E-01	0.118E+01
0.303E-01	0.120E+01
0.296E-01	0.122E+01
0.316E-01	0.124E+01
0.313E-01	0.125E+01
0.309E-01	0.127E+01
0.320E-01	0.129E+01
0.312E-01	0.131E+01
0.332E-01	0.133E+01
0.315E-01	0.135E+01
0.327E-01	0.137E+01
0.333E-01	0.139E+01
0.332E-01	0.140E+01
0.322E-01	0.142E+01
0.334E-01	0.144E+01
0.328E-01	0.146E+01
0.336E-01	0.148E+01
0.348E-01	0.150E+01
0.353E-01	0.152E+01
0.349E-01	0.154E+01
0.344E-01	0.155E+01
0.350E-01	0.157E+01
0.357E-01	0.159E+01
0.350E-01	0.161E+01
0.366E-01	0.163E+01
0.375E-01	0.165E+01
0.383E-01	0.167E+01
0.410E-01	0.169E+01
0.482E-01	0.170E+01
0.456E-01	0.172E+01
0.466E-01	0.174E+01
0.475E-01	0.176E+01
0.436E-01	0.178E+01
0.397E-01	0.180E+01
0.395E-01	0.181E+01
0.387E-01	0.183E+01
0.391E-01	0.185E+01
0.371E-01	0.187E+01
0.375E-01	0.189E+01
0.381E-01	0.191E+01
0.381E-01	0.193E+01
0.373E-01	0.195E+01
0.363E-01	0.197E+01
0.368E-01	0.199E+01

Fig. 5.21a

axial

0.126E+00	0.114E+00
0.121E+00	0.131E+00
0.124E+00	0.150E+00
0.123E+00	0.169E+00
0.130E+00	0.186E+00
0.124E+00	0.205E+00
0.131E+00	0.224E+00
0.121E+00	0.243E+00
0.124E+00	0.260E+00
0.127E+00	0.279E+00
0.126E+00	0.298E+00
0.126E+00	0.317E+00
0.127E+00	0.336E+00
0.124E+00	0.352E+00
0.116E+00	0.371E+00
0.120E+00	0.388E+00
0.132E+00	0.407E+00
0.127E+00	0.426E+00
0.122E+00	0.445E+00
0.101E+00	0.464E+00
0.890E-01	0.483E+00
0.989E-01	0.502E+00
0.105E+00	0.521E+00
0.880E-01	0.540E+00
0.105E+00	0.560E+00
0.862E-01	0.579E+00
0.772E-01	0.595E+00
0.831E-01	0.614E+00
0.720E-01	0.633E+00
0.744E-01	0.652E+00
0.796E-01	0.671E+00
0.641E-01	0.693E+00
0.482E-01	0.710E+00
0.807E-01	0.729E+00
0.466E-01	0.748E+00
0.573E-01	0.767E+00
0.497E-01	0.786E+00
0.365E-01	0.805E+00
0.384E-01	0.824E+00

0.380E-01 0.843E+00
0.289E-01 0.862E+00
0.291E-01 0.881E+00
0.266E-01 0.900E+00
0.301E-01 0.917E+00
0.232E-01 0.936E+00
0.240E-01 0.955E+00
0.275E-01 0.974E+00
0.228E-01 0.990E+00
0.233E-01 0.101E+01
0.222E-01 0.103E+01
0.223E-01 0.105E+01
0.207E-01 0.107E+01
0.214E-01 0.109E+01
0.225E-01 0.110E+01
0.218E-01 0.112E+01
0.216E-01 0.114E+01
0.206E-01 0.116E+01
0.210E-01 0.118E+01
0.210E-01 0.120E+01
0.213E-01 0.122E+01
0.211E-01 0.124E+01
0.211E-01 0.125E+01
0.203E-01 0.127E+01
0.221E-01 0.129E+01
0.209E-01 0.131E+01
0.218E-01 0.133E+01
0.210E-01 0.135E+01
0.211E-01 0.137E+01
0.209E-01 0.139E+01
0.208E-01 0.140E+01
0.217E-01 0.142E+01
0.206E-01 0.144E+01
0.208E-01 0.146E+01
0.225E-01 0.148E+01
0.210E-01 0.150E+01
0.197E-01 0.152E+01
0.216E-01 0.154E+01
0.218E-01 0.155E+01
0.218E-01 0.157E+01
0.218E-01 0.159E+01
0.206E-01 0.161E+01
0.223E-01 0.163E+01
0.228E-01 0.165E+01
0.294E-01 0.167E+01
0.370E-01 0.169E+01
0.374E-01 0.170E+01
0.310E-01 0.172E+01
0.247E-01 0.174E+01
0.262E-01 0.176E+01
0.328E-01 0.178E+01
0.439E-01 0.180E+01
0.466E-01 0.181E+01
0.318E-01 0.183E+01
0.260E-01 0.185E+01
0.224E-01 0.187E+01
0.209E-01 0.189E+01
0.209E-01 0.191E+01
0.204E-01 0.193E+01
0.213E-01 0.195E+01
0.195E-01 0.197E+01
0.212E-01 0.199E+01

spanwise

0.896E-01 0.114E+00
0.867E-01 0.131E+00
0.777E-01 0.150E+00
0.807E-01 0.169E+00
0.779E-01 0.186E+00
0.775E-01 0.205E+00
0.732E-01 0.224E+00
0.790E-01 0.243E+00
0.735E-01 0.260E+00
0.754E-01 0.279E+00
0.692E-01 0.298E+00
0.679E-01 0.317E+00
0.680E-01 0.336E+00
0.650E-01 0.352E+00
0.636E-01 0.371E+00
0.606E-01 0.388E+00
0.587E-01 0.407E+00
0.588E-01 0.426E+00
0.568E-01 0.445E+00
0.494E-01 0.464E+00
0.460E-01 0.483E+00
0.494E-01 0.502E+00
0.491E-01 0.521E+00
0.421E-01 0.540E+00
0.452E-01 0.560E+00
0.428E-01 0.579E+00
0.386E-01 0.595E+00
0.379E-01 0.614E+00
0.373E-01 0.633E+00
0.371E-01 0.652E+00
0.367E-01 0.671E+00
0.332E-01 0.693E+00
0.284E-01 0.710E+00
0.382E-01 0.729E+00
0.282E-01 0.748E+00
0.277E-01 0.767E+00
0.299E-01 0.786E+00
0.270E-01 0.805E+00
0.251E-01 0.824E+00
0.275E-01 0.843E+00
0.252E-01 0.862E+00
0.232E-01 0.881E+00
0.231E-01 0.900E+00
0.228E-01 0.917E+00
0.236E-01 0.936E+00
0.227E-01 0.955E+00
0.230E-01 0.974E+00
0.218E-01 0.990E+00
0.211E-01 0.101E+01
0.208E-01 0.103E+01
0.216E-01 0.105E+01
0.201E-01 0.107E+01
0.209E-01 0.109E+01
0.219E-01 0.110E+01
0.209E-01 0.112E+01
0.205E-01 0.114E+01
0.219E-01 0.116E+01
0.213E-01 0.118E+01
0.210E-01 0.120E+01
0.215E-01 0.122E+01
0.207E-01 0.124E+01
0.202E-01 0.125E+01
0.210E-01 0.127E+01
0.215E-01 0.129E+01
0.199E-01 0.131E+01
0.206E-01 0.133E+01
0.204E-01 0.135E+01
0.205E-01 0.137E+01
0.198E-01 0.139E+01
0.210E-01 0.140E+01
0.200E-01 0.142E+01
0.197E-01 0.144E+01
0.212E-01 0.146E+01
0.207E-01 0.148E+01
0.205E-01 0.150E+01
0.200E-01 0.152E+01
0.202E-01 0.154E+01
0.210E-01 0.155E+01
0.207E-01 0.157E+01
0.210E-01 0.159E+01
0.211E-01 0.161E+01
0.219E-01 0.163E+01
0.218E-01 0.165E+01
0.287E-01 0.167E+01
0.393E-01 0.169E+01
0.391E-01 0.170E+01
0.321E-01 0.172E+01
0.250E-01 0.174E+01
0.245E-01 0.176E+01
0.305E-01 0.178E+01
0.414E-01 0.180E+01
0.424E-01 0.181E+01
0.292E-01 0.183E+01
0.246E-01 0.185E+01
0.210E-01 0.187E+01
0.207E-01 0.189E+01
0.201E-01 0.191E+01
0.200E-01 0.193E+01
0.201E-01 0.195E+01
0.185E-01 0.197E+01
0.195E-01 0.199E+01

Fig. 5.21b

density t.i.

0.709E-01 0.114E+00
0.699E-01 0.131E+00
0.731E-01 0.150E+00
0.738E-01 0.169E+00
0.793E-01 0.186E+00
0.771E-01 0.205E+00
0.831E-01 0.224E+00
0.783E-01 0.243E+00
0.815E-01 0.260E+00
0.844E-01 0.279E+00
0.848E-01 0.298E+00
0.859E-01 0.317E+00
0.873E-01 0.336E+00
0.856E-01 0.352E+00
0.805E-01 0.371E+00
0.837E-01 0.388E+00
0.926E-01 0.407E+00
0.896E-01 0.426E+00
0.867E-01 0.445E+00
0.722E-01 0.464E+00
0.639E-01 0.483E+00
0.713E-01 0.502E+00
0.759E-01 0.521E+00
0.635E-01 0.540E+00
0.758E-01 0.560E+00
0.624E-01 0.579E+00
0.559E-01 0.595E+00
0.601E-01 0.614E+00
0.521E-01 0.633E+00
0.539E-01 0.652E+00
0.578E-01 0.671E+00
0.467E-01 0.693E+00
0.352E-01 0.710E+00
0.590E-01 0.729E+00
0.340E-01 0.748E+00
0.418E-01 0.767E+00
0.362E-01 0.786E+00
0.266E-01 0.805E+00
0.280E-01 0.824E+00
0.277E-01 0.843E+00
0.211E-01 0.862E+00
0.212E-01 0.881E+00
0.194E-01 0.900E+00
0.219E-01 0.917E+00
0.169E-01 0.936E+00
0.175E-01 0.955E+00
0.200E-01 0.974E+00
0.165E-01 0.990E+00
0.169E-01 0.101E+01
0.160E-01 0.103E+01
0.160E-01 0.105E+01
0.148E-01 0.107E+01
0.153E-01 0.109E+01
0.160E-01 0.110E+01
0.155E-01 0.112E+01
0.154E-01 0.114E+01
0.148E-01 0.116E+01
0.151E-01 0.118E+01
0.151E-01 0.120E+01
0.153E-01 0.122E+01
0.152E-01 0.124E+01
0.152E-01 0.125E+01
0.146E-01 0.127E+01
0.159E-01 0.129E+01
0.151E-01 0.131E+01
0.158E-01 0.133E+01
0.152E-01 0.135E+01
0.153E-01 0.137E+01
0.152E-01 0.139E+01
0.151E-01 0.140E+01
0.158E-01 0.142E+01
0.150E-01 0.144E+01
0.151E-01 0.146E+01
0.163E-01 0.148E+01
0.153E-01 0.150E+01
0.143E-01 0.152E+01
0.157E-01 0.154E+01
0.158E-01 0.155E+01
0.157E-01 0.157E+01
0.155E-01 0.159E+01
0.146E-01 0.161E+01
0.158E-01 0.163E+01
0.163E-01 0.165E+01
0.212E-01 0.167E+01
0.271E-01 0.169E+01
0.278E-01 0.170E+01
0.234E-01 0.172E+01
0.188E-01 0.174E+01
0.201E-01 0.176E+01
0.254E-01 0.178E+01
0.342E-01 0.180E+01
0.364E-01 0.181E+01
0.249E-01 0.183E+01

0.204E-01	0.185E+01
0.176E-01	0.187E+01
0.165E-01	0.189E+01
0.165E-01	0.191E+01
0.161E-01	0.193E+01
0.168E-01	0.195E+01
0.154E-01	0.197E+01
0.168E-01	0.199E+01

u' t.i.

0.551E-01	0.114E+00
0.511E-01	0.131E+00
0.509E-01	0.150E+00
0.492E-01	0.169E+00
0.507E-01	0.186E+00
0.469E-01	0.205E+00
0.479E-01	0.224E+00
0.427E-01	0.243E+00
0.425E-01	0.260E+00
0.426E-01	0.279E+00
0.412E-01	0.298E+00
0.401E-01	0.317E+00
0.397E-01	0.336E+00
0.384E-01	0.352E+00
0.355E-01	0.371E+00
0.363E-01	0.388E+00
0.394E-01	0.407E+00
0.374E-01	0.426E+00
0.353E-01	0.445E+00
0.288E-01	0.464E+00
0.251E-01	0.483E+00
0.276E-01	0.502E+00
0.291E-01	0.521E+00
0.245E-01	0.540E+00
0.292E-01	0.560E+00
0.238E-01	0.579E+00
0.213E-01	0.595E+00
0.230E-01	0.614E+00
0.199E-01	0.633E+00
0.205E-01	0.652E+00
0.218E-01	0.671E+00
0.174E-01	0.693E+00
0.130E-01	0.710E+00
0.217E-01	0.729E+00
0.126E-01	0.748E+00
0.155E-01	0.767E+00
0.135E-01	0.786E+00
0.989E-02	0.805E+00
0.104E-01	0.824E+00
0.103E-01	0.843E+00
0.783E-02	0.862E+00
0.790E-02	0.881E+00
0.722E-02	0.900E+00
0.817E-02	0.917E+00
0.631E-02	0.936E+00
0.655E-02	0.955E+00
0.754E-02	0.974E+00
0.628E-02	0.990E+00
0.644E-02	0.101E+01
0.620E-02	0.103E+01
0.630E-02	0.105E+01
0.590E-02	0.107E+01
0.615E-02	0.109E+01
0.647E-02	0.110E+01
0.625E-02	0.112E+01
0.617E-02	0.114E+01
0.585E-02	0.116E+01
0.592E-02	0.118E+01
0.589E-02	0.120E+01
0.596E-02	0.122E+01
0.590E-02	0.124E+01
0.589E-02	0.125E+01
0.567E-02	0.127E+01
0.616E-02	0.129E+01
0.581E-02	0.131E+01
0.603E-02	0.133E+01
0.577E-02	0.135E+01
0.578E-02	0.137E+01
0.573E-02	0.139E+01
0.570E-02	0.140E+01
0.593E-02	0.142E+01
0.563E-02	0.144E+01
0.569E-02	0.146E+01
0.615E-02	0.148E+01
0.574E-02	0.150E+01
0.539E-02	0.152E+01
0.591E-02	0.154E+01
0.602E-02	0.155E+01
0.614E-02	0.157E+01
0.631E-02	0.159E+01
0.603E-02	0.161E+01
0.649E-02	0.163E+01
0.649E-02	0.165E+01
0.817E-02	0.167E+01
0.989E-02	0.169E+01
0.957E-02	0.170E+01
0.761E-02	0.172E+01
0.586E-02	0.174E+01
0.606E-02	0.176E+01
0.741E-02	0.178E+01
0.971E-02	0.180E+01
0.102E-01	0.181E+01
0.688E-02	0.183E+01
0.558E-02	0.185E+01
0.478E-02	0.187E+01
0.445E-02	0.189E+01
0.442E-02	0.191E+01
0.430E-02	0.193E+01
0.447E-02	0.195E+01
0.408E-02	0.197E+01
0.442E-02	0.199E+01

w' t.i.

0.896E-01	0.114E+00
0.867E-01	0.131E+00
0.777E-01	0.150E+00
0.807E-01	0.169E+00
0.779E-01	0.186E+00
0.775E-01	0.205E+00
0.732E-01	0.224E+00
0.790E-01	0.243E+00
0.735E-01	0.260E+00
0.754E-01	0.279E+00
0.692E-01	0.298E+00
0.679E-01	0.317E+00
0.680E-01	0.336E+00
0.650E-01	0.352E+00
0.636E-01	0.371E+00
0.606E-01	0.388E+00
0.587E-01	0.407E+00
0.588E-01	0.426E+00
0.568E-01	0.445E+00
0.494E-01	0.464E+00
0.460E-01	0.483E+00
0.494E-01	0.502E+00
0.491E-01	0.521E+00
0.421E-01	0.540E+00
0.452E-01	0.560E+00
0.428E-01	0.579E+00
0.386E-01	0.595E+00
0.379E-01	0.614E+00
0.373E-01	0.633E+00
0.371E-01	0.652E+00
0.367E-01	0.671E+00
0.332E-01	0.693E+00
0.284E-01	0.710E+00
0.382E-01	0.729E+00
0.282E-01	0.748E+00
0.277E-01	0.767E+00
0.299E-01	0.786E+00
0.270E-01	0.805E+00
0.251E-01	0.824E+00
0.275E-01	0.843E+00
0.252E-01	0.862E+00
0.232E-01	0.881E+00
0.231E-01	0.900E+00
0.228E-01	0.917E+00
0.236E-01	0.936E+00
0.227E-01	0.955E+00
0.230E-01	0.974E+00
0.218E-01	0.990E+00
0.211E-01	0.101E+01
0.208E-01	0.103E+01
0.216E-01	0.105E+01
0.201E-01	0.107E+01
0.209E-01	0.109E+01
0.219E-01	0.110E+01
0.209E-01	0.112E+01
0.205E-01	0.114E+01
0.219E-01	0.116E+01
0.213E-01	0.118E+01
0.210E-01	0.120E+01
0.215E-01	0.122E+01
0.207E-01	0.124E+01
0.202E-01	0.125E+01
0.210E-01	0.127E+01
0.215E-01	0.129E+01
0.199E-01	0.131E+01
0.206E-01	0.133E+01
0.204E-01	0.135E+01
0.205E-01	0.137E+01
0.198E-01	0.139E+01
0.210E-01	0.140E+01
0.200E-01	0.142E+01
0.197E-01	0.144E+01
0.212E-01	0.146E+01
0.207E-01	0.148E+01
0.205E-01	0.150E+01
0.200E-01	0.152E+01
0.202E-01	0.154E+01
0.210E-01	0.155E+01
0.207E-01	0.157E+01
0.210E-01	0.159E+01
0.211E-01	0.161E+01
0.219E-01	0.163E+01
0.218E-01	0.165E+01
0.287E-01	0.167E+01
0.393E-01	0.169E+01
0.391E-01	0.170E+01
0.321E-01	0.172E+01
0.250E-01	0.174E+01
0.245E-01	0.176E+01
0.305E-01	0.178E+01
0.414E-01	0.180E+01
0.424E-01	0.181E+01
0.292E-01	0.183E+01
0.246E-01	0.185E+01
0.210E-01	0.187E+01
0.207E-01	0.189E+01
0.201E-01	0.191E+01
0.200E-01	0.193E+01
0.201E-01	0.195E+01
0.185E-01	0.197E+01
0.195E-01	0.199E+01

Fig. 5.22a

-0.129E-01	0.114E+00
-0.139E-01	0.131E+00
-0.116E-01	0.150E+00
-0.133E-01	0.169E+00
-0.128E-01	0.186E+00
-0.138E-01	0.205E+00
-0.139E-01	0.224E+00
-0.132E-01	0.243E+00
-0.140E-01	0.260E+00
-0.145E-01	0.279E+00
-0.143E-01	0.298E+00
-0.137E-01	0.317E+00
-0.120E-01	0.336E+00
-0.129E-01	0.352E+00
-0.118E-01	0.371E+00
-0.144E-01	0.388E+00
-0.116E-01	0.407E+00
-0.114E-01	0.426E+00
-0.133E-01	0.445E+00
-0.110E-01	0.464E+00
-0.113E-01	0.483E+00
-0.103E-01	0.502E+00
-0.105E-01	0.521E+00
-0.804E-02	0.540E+00
-0.709E-02	0.560E+00
-0.667E-02	0.579E+00
-0.681E-02	0.595E+00
-0.751E-02	0.614E+00
-0.505E-02	0.633E+00
-0.675E-02	0.652E+00
-0.521E-02	0.671E+00
-0.369E-02	0.693E+00
-0.483E-02	0.710E+00
-0.363E-02	0.729E+00
-0.335E-02	0.748E+00
-0.361E-02	0.767E+00
-0.333E-02	0.786E+00
-0.218E-02	0.805E+00
-0.228E-02	0.824E+00
-0.205E-02	0.843E+00
-0.158E-02	0.862E+00
-0.147E-02	0.881E+00
-0.104E-02	0.900E+00
-0.108E-02	0.917E+00
-0.102E-02	0.936E+00

-0.751E-03	0.955E+00
-0.689E-03	0.974E+00
-0.593E-03	0.990E+00
-0.515E-03	0.101E+01
-0.526E-03	0.103E+01
-0.555E-03	0.105E+01
-0.511E-03	0.107E+01
-0.579E-03	0.109E+01
-0.570E-03	0.110E+01
-0.567E-03	0.112E+01
-0.589E-03	0.114E+01
-0.520E-03	0.116E+01
-0.623E-03	0.118E+01
-0.625E-03	0.120E+01
-0.542E-03	0.122E+01
-0.691E-03	0.124E+01
-0.631E-03	0.125E+01
-0.627E-03	0.127E+01
-0.715E-03	0.129E+01
-0.678E-03	0.131E+01
-0.817E-03	0.133E+01
-0.682E-03	0.135E+01
-0.811E-03	0.137E+01
-0.861E-03	0.139E+01
-0.844E-03	0.140E+01
-0.803E-03	0.142E+01
-0.880E-03	0.144E+01
-0.882E-03	0.146E+01
-0.877E-03	0.148E+01
-0.101E-02	0.150E+01
-0.102E-02	0.152E+01
-0.101E-02	0.154E+01
-0.964E-03	0.155E+01
-0.103E-02	0.157E+01
-0.108E-02	0.159E+01
-0.998E-03	0.161E+01
-0.110E-02	0.163E+01
-0.116E-02	0.165E+01
-0.109E-02	0.167E+01
-0.124E-02	0.169E+01
-0.192E-02	0.170E+01
-0.166E-02	0.172E+01
-0.190E-02	0.174E+01
-0.198E-02	0.176E+01
-0.167E-02	0.178E+01
-0.136E-02	0.180E+01
-0.142E-02	0.181E+01
-0.136E-02	0.183E+01
-0.136E-02	0.185E+01
-0.121E-02	0.187E+01
-0.124E-02	0.189E+01
-0.130E-02	0.191E+01
-0.132E-02	0.193E+01
-0.121E-02	0.195E+01
-0.115E-02	0.197E+01
-0.117E-02	0.199E+01

Fig. 5.22b

$-C_{xy}$ term

0.129E-01	0.114E+00
0.139E-01	0.131E+00
0.116E-01	0.150E+00
0.133E-01	0.169E+00
0.128E-01	0.186E+00
0.138E-01	0.205E+00
0.139E-01	0.224E+00
0.132E-01	0.243E+00
0.140E-01	0.260E+00
0.145E-01	0.279E+00
0.143E-01	0.298E+00
0.137E-01	0.317E+00
0.120E-01	0.336E+00
0.129E-01	0.352E+00
0.118E-01	0.371E+00
0.144E-01	0.388E+00
0.116E-01	0.407E+00
0.114E-01	0.426E+00
0.133E-01	0.445E+00
0.110E-01	0.464E+00
0.113E-01	0.483E+00
0.103E-01	0.502E+00
0.105E-01	0.521E+00
0.804E-02	0.540E+00
0.709E-02	0.560E+00
0.667E-02	0.579E+00
0.681E-02	0.595E+00
0.751E-02	0.614E+00
0.505E-02	0.633E+00
0.675E-02	0.652E+00
0.521E-02	0.671E+00
0.369E-02	0.693E+00
0.483E-02	0.710E+00
0.363E-02	0.729E+00
0.335E-02	0.748E+00
0.361E-02	0.767E+00
0.333E-02	0.786E+00
0.218E-02	0.805E+00
0.228E-02	0.824E+00
0.205E-02	0.843E+00
0.158E-02	0.862E+00
0.147E-02	0.881E+00
0.104E-02	0.900E+00
0.108E-02	0.917E+00
0.102E-02	0.936E+00
0.751E-03	0.955E+00
0.689E-03	0.974E+00
0.593E-03	0.990E+00
0.515E-03	0.101E+01
0.526E-03	0.103E+01
0.555E-03	0.105E+01
0.511E-03	0.107E+01
0.579E-03	0.109E+01
0.570E-03	0.110E+01
0.567E-03	0.112E+01
0.589E-03	0.114E+01
0.520E-03	0.116E+01
0.623E-03	0.118E+01
0.625E-03	0.120E+01
0.542E-03	0.122E+01
0.691E-03	0.124E+01
0.631E-03	0.125E+01
0.627E-03	0.127E+01
0.715E-03	0.129E+01
0.678E-03	0.131E+01
0.817E-03	0.133E+01
0.682E-03	0.135E+01
0.811E-03	0.137E+01
0.861E-03	0.139E+01
0.844E-03	0.140E+01
0.803E-03	0.142E+01
0.880E-03	0.144E+01
0.882E-03	0.146E+01
0.877E-03	0.148E+01
0.101E-02	0.150E+01
0.102E-02	0.152E+01
0.101E-02	0.154E+01
0.964E-03	0.155E+01
0.103E-02	0.157E+01
0.108E-02	0.159E+01
0.998E-03	0.161E+01
0.110E-02	0.163E+01
0.116E-02	0.165E+01
0.109E-02	0.167E+01
0.124E-02	0.169E+01
0.192E-02	0.170E+01
0.166E-02	0.172E+01
0.190E-02	0.174E+01
0.198E-02	0.176E+01
0.167E-02	0.178E+01
0.136E-02	0.180E+01
0.142E-02	0.181E+01
0.136E-02	0.183E+01
0.136E-02	0.185E+01
0.121E-02	0.187E+01
0.124E-02	0.189E+01
0.130E-02	0.191E+01
0.132E-02	0.193E+01
0.121E-02	0.195E+01
0.115E-02	0.197E+01
0.117E-02	0.199E+01

small term

0.864E-03	0.114E+00
0.852E-03	0.131E+00
0.902E-03	0.150E+00
0.911E-03	0.169E+00
0.968E-03	0.186E+00
0.118E-02	0.205E+00
0.128E-02	0.224E+00
0.128E-02	0.243E+00
0.128E-02	0.260E+00
0.145E-02	0.279E+00
0.134E-02	0.298E+00
0.144E-02	0.317E+00
0.124E-02	0.336E+00
0.137E-02	0.352E+00
0.125E-02	0.371E+00
0.161E-02	0.388E+00
0.141E-02	0.407E+00
0.125E-02	0.426E+00
0.169E-02	0.445E+00
0.133E-02	0.464E+00
0.124E-02	0.483E+00
0.122E-02	0.502E+00
0.128E-02	0.521E+00
0.990E-03	0.540E+00
0.879E-03	0.560E+00
0.827E-03	0.579E+00
0.786E-03	0.595E+00
0.899E-03	0.614E+00
0.602E-03	0.633E+00
0.830E-03	0.652E+00
0.666E-03	0.671E+00
0.459E-03	0.693E+00
0.541E-03	0.710E+00
0.418E-03	0.729E+00
0.368E-03	0.748E+00
0.433E-03	0.767E+00
0.357E-03	0.786E+00
0.220E-03	0.805E+00
0.238E-03	0.824E+00
0.230E-03	0.843E+00
0.149E-03	0.862E+00
0.153E-03	0.881E+00
0.940E-04	0.900E+00
0.990E-04	0.917E+00
0.972E-04	0.936E+00
0.666E-04	0.955E+00
0.617E-04	0.974E+00
0.512E-04	0.990E+00
0.415E-04	0.101E+01
0.399E-04	0.103E+01
0.423E-04	0.105E+01
0.396E-04	0.107E+01
0.446E-04	0.109E+01
0.437E-04	0.110E+01
0.413E-04	0.112E+01
0.496E-04	0.114E+01
0.455E-04	0.116E+01
0.545E-04	0.118E+01
0.529E-04	0.120E+01
0.488E-04	0.122E+01
0.593E-04	0.124E+01
0.542E-04	0.125E+01
0.581E-04	0.127E+01
0.619E-04	0.129E+01
0.634E-04	0.131E+01
0.745E-04	0.133E+01
0.651E-04	0.135E+01
0.763E-04	0.137E+01
0.809E-04	0.139E+01
0.796E-04	0.140E+01
0.787E-04	0.142E+01
0.818E-04	0.144E+01
0.881E-04	0.146E+01
0.828E-04	0.148E+01
0.979E-04	0.150E+01
0.102E-03	0.152E+01
0.972E-04	0.154E+01
0.103E-03	0.155E+01
0.111E-03	0.157E+01
0.112E-03	0.159E+01
0.109E-03	0.161E+01
0.131E-03	0.163E+01
0.180E-03	0.165E+01
0.202E-03	0.167E+01
0.306E-03	0.169E+01
0.439E-03	0.170E+01
0.456E-03	0.172E+01
0.402E-03	0.174E+01
0.371E-03	0.176E+01
0.304E-03	0.178E+01
0.241E-03	0.180E+01
0.252E-03	0.181E+01
0.241E-03	0.183E+01
0.232E-03	0.185E+01
0.203E-03	0.187E+01
0.208E-03	0.189E+01
0.221E-03	0.191E+01
0.227E-03	0.193E+01
0.200E-03	0.195E+01

0.195E-03	0.197E+01
0.195E-03	0.199E+01

cross-wire shear

0.138E-01	0.114E+00
0.148E-01	0.131E+00
0.125E-01	0.150E+00
0.142E-01	0.169E+00
0.138E-01	0.186E+00
0.150E-01	0.205E+00
0.152E-01	0.224E+00
0.145E-01	0.243E+00
0.153E-01	0.260E+00
0.160E-01	0.279E+00
0.156E-01	0.298E+00
0.151E-01	0.317E+00
0.132E-01	0.336E+00
0.143E-01	0.352E+00
0.131E-01	0.371E+00
0.160E-01	0.388E+00
0.130E-01	0.407E+00
0.127E-01	0.426E+00
0.150E-01	0.445E+00
0.123E-01	0.464E+00
0.125E-01	0.483E+00
0.115E-01	0.502E+00
0.118E-01	0.521E+00
0.903E-02	0.540E+00
0.797E-02	0.560E+00
0.750E-02	0.579E+00
0.760E-02	0.595E+00
0.841E-02	0.614E+00
0.565E-02	0.633E+00
0.758E-02	0.652E+00
0.588E-02	0.671E+00
0.415E-02	0.693E+00
0.537E-02	0.710E+00
0.405E-02	0.729E+00
0.372E-02	0.748E+00
0.404E-02	0.767E+00
0.369E-02	0.786E+00
0.240E-02	0.805E+00
0.252E-02	0.824E+00
0.228E-02	0.843E+00
0.173E-02	0.862E+00
0.162E-02	0.881E+00
0.113E-02	0.900E+00
0.118E-02	0.917E+00
0.112E-02	0.936E+00
0.818E-03	0.955E+00
0.751E-03	0.974E+00
0.644E-03	0.990E+00
0.556E-03	0.101E+01
0.566E-03	0.103E+01
0.597E-03	0.105E+01
0.551E-03	0.107E+01
0.624E-03	0.109E+01
0.614E-03	0.110E+01
0.608E-03	0.112E+01
0.639E-03	0.114E+01
0.565E-03	0.116E+01
0.678E-03	0.118E+01
0.678E-03	0.120E+01
0.591E-03	0.122E+01
0.750E-03	0.124E+01
0.685E-03	0.125E+01
0.685E-03	0.127E+01
0.777E-03	0.129E+01
0.741E-03	0.131E+01
0.892E-03	0.133E+01
0.747E-03	0.135E+01
0.887E-03	0.137E+01
0.942E-03	0.139E+01
0.924E-03	0.140E+01
0.882E-03	0.142E+01
0.962E-03	0.144E+01
0.970E-03	0.146E+01
0.960E-03	0.148E+01
0.111E-02	0.150E+01
0.112E-02	0.152E+01
0.111E-02	0.154E+01
0.107E-02	0.155E+01
0.114E-02	0.157E+01
0.119E-02	0.159E+01
0.111E-02	0.161E+01
0.123E-02	0.163E+01
0.134E-02	0.165E+01
0.129E-02	0.167E+01
0.155E-02	0.169E+01
0.236E-02	0.170E+01
0.212E-02	0.172E+01
0.230E-02	0.174E+01
0.235E-02	0.176E+01
0.197E-02	0.178E+01
0.160E-02	0.180E+01
0.167E-02	0.181E+01
0.160E-02	0.183E+01
0.159E-02	0.185E+01
0.141E-02	0.187E+01
0.145E-02	0.189E+01
0.152E-02	0.191E+01
0.155E-02	0.193E+01
0.141E-02	0.195E+01
0.135E-02	0.197E+01
0.137E-02	0.199E+01

Fig. 5.23a

-0.431E-02	0.114E+00
-0.428E-02	0.131E+00
-0.434E-02	0.150E+00
-0.420E-02	0.169E+00
-0.489E-02	0.186E+00
-0.328E-02	0.205E+00
-0.404E-02	0.224E+00
-0.371E-02	0.243E+00
-0.339E-02	0.260E+00
-0.399E-02	0.279E+00
-0.422E-02	0.298E+00
-0.367E-02	0.317E+00
-0.346E-02	0.336E+00
-0.311E-02	0.352E+00
-0.275E-02	0.371E+00
-0.244E-02	0.388E+00
-0.285E-02	0.407E+00
-0.264E-02	0.426E+00
-0.272E-02	0.445E+00
-0.112E-02	0.464E+00
-0.825E-03	0.483E+00
-0.137E-02	0.502E+00
-0.129E-02	0.521E+00
-0.341E-03	0.540E+00
-0.975E-03	0.560E+00
-0.621E-03	0.579E+00
-0.323E-03	0.595E+00
-0.206E-03	0.614E+00
0.561E-04	0.633E+00
-0.125E-05	0.652E+00
0.414E-04	0.671E+00
0.181E-03	0.693E+00
0.156E-03	0.710E+00
0.161E-03	0.729E+00
0.761E-04	0.748E+00
0.976E-04	0.767E+00
0.272E-03	0.786E+00
0.160E-03	0.805E+00
0.560E-04	0.824E+00
0.180E-03	0.843E+00
0.546E-04	0.862E+00
0.524E-04	0.881E+00
0.108E-04	0.900E+00
-0.112E-04	0.917E+00
0.527E-04	0.936E+00
0.826E-05	0.955E+00
0.316E-04	0.974E+00
-0.550E-04	0.990E+00
-0.510E-04	0.101E+01
-0.610E-04	0.103E+01
-0.659E-04	0.105E+01
-0.111E-03	0.107E+01
-0.786E-04	0.109E+01
-0.568E-04	0.110E+01
-0.782E-04	0.112E+01
-0.777E-04	0.114E+01
-0.583E-04	0.116E+01
-0.548E-04	0.118E+01
-0.638E-04	0.120E+01
-0.553E-04	0.122E+01
-0.520E-04	0.124E+01
-0.422E-04	0.125E+01
-0.641E-04	0.127E+01
-0.440E-04	0.129E+01
-0.419E-04	0.131E+01
-0.417E-04	0.133E+01
-0.929E-04	0.135E+01
-0.610E-04	0.137E+01
-0.855E-04	0.139E+01
-0.754E-04	0.140E+01
-0.535E-04	0.142E+01
-0.674E-04	0.144E+01
-0.935E-04	0.146E+01
-0.944E-04	0.148E+01
-0.800E-04	0.150E+01
-0.536E-04	0.152E+01
-0.745E-04	0.154E+01
-0.762E-04	0.155E+01
-0.855E-04	0.157E+01
-0.117E-03	0.159E+01
-0.814E-04	0.161E+01
-0.134E-03	0.163E+01
-0.127E-03	0.165E+01
-0.465E-03	0.167E+01
-0.104E-02	0.169E+01
-0.975E-03	0.170E+01
-0.471E-03	0.172E+01
-0.974E-04	0.174E+01
0.282E-03	0.176E+01
0.618E-03	0.178E+01
0.146E-02	0.180E+01
0.153E-02	0.181E+01
0.459E-03	0.183E+01
0.215E-03	0.185E+01
0.241E-04	0.187E+01
0.187E-04	0.189E+01
0.325E-05	0.191E+01
-0.262E-04	0.193E+01
-0.287E-04	0.195E+01
-0.174E-04	0.197E+01
-0.401E-04	0.199E+01

Fig. 5.23b

$-C_{xy}$ term

0.431E-02	0.114E+00
0.428E-02	0.131E+00
0.434E-02	0.150E+00
0.420E-02	0.169E+00
0.489E-02	0.186E+00
0.328E-02	0.205E+00
0.404E-02	0.224E+00
0.371E-02	0.243E+00
0.339E-02	0.260E+00
0.399E-02	0.279E+00
0.422E-02	0.298E+00
0.367E-02	0.317E+00
0.346E-02	0.336E+00
0.311E-02	0.352E+00
0.275E-02	0.371E+00
0.244E-02	0.388E+00
0.285E-02	0.407E+00
0.264E-02	0.426E+00
0.272E-02	0.445E+00
0.112E-02	0.464E+00
0.825E-03	0.483E+00
0.137E-02	0.502E+00
0.129E-02	0.521E+00
0.341E-03	0.540E+00
0.975E-03	0.560E+00
0.621E-03	0.579E+00
0.323E-03	0.595E+00
0.206E-03	0.614E+00
-0.561E-04	0.633E+00
0.125E-05	0.652E+00
-0.414E-04	0.671E+00
-0.181E-03	0.693E+00
-0.156E-03	0.710E+00
-0.161E-03	0.729E+00
-0.761E-04	0.748E+00
-0.976E-04	0.767E+00
-0.272E-03	0.786E+00
-0.160E-03	0.805E+00
-0.560E-04	0.824E+00
-0.180E-03	0.843E+00
-0.546E-04	0.862E+00
-0.524E-04	0.881E+00
-0.108E-04	0.900E+00
0.112E-04	0.917E+00
-0.527E-04	0.936E+00
-0.826E-05	0.955E+00
-0.316E-04	0.974E+00
0.550E-04	0.990E+00
0.510E-04	0.101E+01

0.610E-04 0.103E+01
0.659E-04 0.105E+01
0.111E-03 0.107E+01
0.786E-04 0.109E+01
0.568E-04 0.110E+01
0.782E-04 0.112E+01
0.777E-04 0.114E+01
0.583E-04 0.116E+01
0.548E-04 0.118E+01
0.638E-04 0.120E+01
0.553E-04 0.122E+01
0.520E-04 0.124E+01
0.422E-04 0.125E+01
0.641E-04 0.127E+01
0.440E-04 0.129E+01
0.419E-04 0.131E+01
0.417E-04 0.133E+01
0.929E-04 0.135E+01
0.610E-04 0.137E+01
0.855E-04 0.139E+01
0.754E-04 0.140E+01
0.535E-04 0.142E+01
0.674E-04 0.144E+01
0.935E-04 0.146E+01
0.944E-04 0.148E+01
0.800E-04 0.150E+01
0.536E-04 0.152E+01
0.745E-04 0.154E+01
0.762E-04 0.155E+01
0.855E-04 0.157E+01
0.117E-03 0.159E+01
0.814E-04 0.161E+01
0.134E-03 0.163E+01
0.127E-03 0.165E+01
0.465E-03 0.167E+01
0.104E-02 0.169E+01
0.975E-03 0.170E+01
0.471E-03 0.172E+01
0.974E-04 0.174E+01
-0.282E-03 0.176E+01
-0.618E-03 0.178E+01
-0.146E-02 0.180E+01
-0.153E-02 0.181E+01
-0.459E-03 0.183E+01
-0.215E-03 0.185E+01
-0.241E-04 0.187E+01
-0.187E-04 0.189E+01
-0.325E-05 0.191E+01
0.262E-04 0.193E+01
0.287E-04 0.195E+01
0.174E-04 0.197E+01
0.401E-04 0.199E+01

small term

0.129E-03 0.114E+00
0.147E-03 0.131E+00
0.227E-03 0.150E+00
0.255E-03 0.169E+00
0.270E-03 0.186E+00
0.161E-03 0.205E+00
0.328E-03 0.224E+00
0.293E-03 0.243E+00
0.264E-03 0.260E+00
0.342E-03 0.279E+00
0.429E-03 0.298E+00
0.413E-03 0.317E+00
0.398E-03 0.336E+00
0.356E-03 0.352E+00
0.390E-03 0.371E+00
0.342E-03 0.388E+00
0.484E-03 0.407E+00
0.453E-03 0.426E+00
0.454E-03 0.445E+00
0.296E-03 0.464E+00
0.218E-03 0.483E+00
0.271E-03 0.502E+00
0.307E-03 0.521E+00
0.215E-03 0.540E+00
0.306E-03 0.560E+00
0.180E-03 0.579E+00
0.156E-03 0.595E+00
0.180E-03 0.614E+00
0.126E-03 0.633E+00
0.124E-03 0.652E+00
0.155E-03 0.671E+00
0.933E-04 0.693E+00
0.442E-04 0.710E+00
0.186E-03 0.729E+00
0.372E-04 0.748E+00
0.561E-04 0.767E+00
0.561E-04 0.786E+00
0.253E-04 0.805E+00
0.281E-04 0.824E+00
0.247E-04 0.843E+00
0.127E-04 0.862E+00
0.129E-04 0.881E+00
0.108E-04 0.900E+00
0.138E-04 0.917E+00
0.717E-05 0.936E+00
0.766E-05 0.955E+00
0.114E-04 0.974E+00
0.686E-05 0.990E+00
0.615E-05 0.101E+01
0.554E-05 0.103E+01
0.643E-05 0.105E+01
0.554E-05 0.107E+01
0.589E-05 0.109E+01
0.651E-05 0.110E+01
0.700E-05 0.112E+01
0.690E-05 0.114E+01
0.395E-05 0.116E+01
0.417E-05 0.118E+01
0.335E-05 0.120E+01
0.262E-05 0.122E+01
0.173E-05 0.124E+01
0.888E-06 0.125E+01
0.158E-05 0.127E+01
0.944E-06 0.129E+01
0.823E-06 0.131E+01
0.899E-06 0.133E+01
0.166E-05 0.135E+01
0.819E-06 0.137E+01
0.162E-05 0.139E+01
0.158E-05 0.140E+01
0.264E-05 0.142E+01
0.235E-05 0.144E+01
0.321E-05 0.146E+01
0.376E-05 0.148E+01
0.411E-05 0.150E+01
0.361E-05 0.152E+01
0.434E-05 0.154E+01
0.345E-05 0.155E+01
0.343E-05 0.157E+01
0.332E-05 0.159E+01
0.294E-05 0.161E+01
0.344E-05 0.163E+01
0.268E-05 0.165E+01
0.120E-05 0.167E+01
-0.638E-05 0.169E+01
-0.331E-04 0.170E+01
-0.359E-04 0.172E+01
-0.261E-04 0.174E+01
-0.300E-04 0.176E+01
-0.479E-04 0.178E+01
-0.447E-04 0.180E+01
-0.410E-04 0.181E+01
-0.689E-06 0.183E+01
0.104E-05 0.185E+01
0.312E-05 0.187E+01
0.272E-05 0.189E+01
0.269E-05 0.191E+01
0.257E-05 0.193E+01
0.280E-05 0.195E+01
0.232E-05 0.197E+01
0.275E-05 0.199E+01

cross-wire shear

0.444E-02 0.114E+00
0.443E-02 0.131E+00
0.457E-02 0.150E+00
0.446E-02 0.169E+00
0.516E-02 0.186E+00
0.344E-02 0.205E+00
0.437E-02 0.224E+00
0.400E-02 0.243E+00
0.365E-02 0.260E+00
0.433E-02 0.279E+00
0.465E-02 0.298E+00
0.408E-02 0.317E+00
0.386E-02 0.336E+00
0.347E-02 0.352E+00
0.314E-02 0.371E+00
0.278E-02 0.388E+00
0.333E-02 0.407E+00
0.309E-02 0.426E+00
0.317E-02 0.445E+00
0.142E-02 0.464E+00
0.104E-02 0.483E+00
0.164E-02 0.502E+00
0.160E-02 0.521E+00
0.556E-03 0.540E+00
0.128E-02 0.560E+00
0.801E-03 0.579E+00
0.479E-03 0.595E+00
0.386E-03 0.614E+00
0.695E-04 0.633E+00
0.125E-03 0.652E+00
0.113E-03 0.671E+00
-0.877E-04 0.693E+00
-0.112E-03 0.710E+00
0.252E-04 0.729E+00
-0.389E-04 0.748E+00
-0.415E-04 0.767E+00
-0.216E-03 0.786E+00
-0.135E-03 0.805E+00
-0.279E-04 0.824E+00
-0.155E-03 0.843E+00
-0.419E-04 0.862E+00
-0.395E-04 0.881E+00
-0.442E-07 0.900E+00
0.250E-04 0.917E+00
-0.455E-04 0.936E+00
-0.601E-06 0.955E+00
-0.202E-04 0.974E+00
0.619E-04 0.990E+00
0.571E-04 0.101E+01
0.665E-04 0.103E+01
0.723E-04 0.105E+01
0.117E-03 0.107E+01
0.845E-04 0.109E+01
0.633E-04 0.110E+01
0.852E-04 0.112E+01
0.846E-04 0.114E+01
0.623E-04 0.116E+01
0.590E-04 0.118E+01
0.671E-04 0.120E+01
0.579E-04 0.122E+01
0.537E-04 0.124E+01
0.431E-04 0.125E+01
0.657E-04 0.127E+01
0.449E-04 0.129E+01
0.427E-04 0.131E+01
0.426E-04 0.133E+01
0.946E-04 0.135E+01
0.618E-04 0.137E+01
0.871E-04 0.139E+01
0.770E-04 0.140E+01
0.561E-04 0.142E+01
0.698E-04 0.144E+01
0.967E-04 0.146E+01
0.982E-04 0.148E+01
0.841E-04 0.150E+01
0.572E-04 0.152E+01
0.788E-04 0.154E+01
0.797E-04 0.155E+01
0.889E-04 0.157E+01
0.120E-03 0.159E+01
0.843E-04 0.161E+01
0.137E-03 0.163E+01
0.130E-03 0.165E+01
0.466E-03 0.167E+01
0.103E-02 0.169E+01
0.942E-03 0.170E+01
0.435E-03 0.172E+01
0.713E-04 0.174E+01
-0.312E-03 0.176E+01
-0.666E-03 0.178E+01
-0.150E-02 0.180E+01
-0.157E-02 0.181E+01
-0.460E-03 0.183E+01
-0.214E-03 0.185E+01
-0.210E-04 0.187E+01
-0.160E-04 0.189E+01
-0.564E-06 0.191E+01
0.288E-04 0.193E+01
0.315E-04 0.195E+01
0.197E-04 0.197E+01
0.428E-04 0.199E+01

Fig. 5.24a

term 1

0.564E-02	0.114E+00
0.587E-02	0.131E+00
0.476E-02	0.150E+00
0.532E-02	0.169E+00
0.499E-02	0.186E+00
0.522E-02	0.205E+00
0.509E-02	0.224E+00
0.466E-02	0.243E+00
0.480E-02	0.260E+00
0.486E-02	0.279E+00
0.467E-02	0.298E+00
0.436E-02	0.317E+00
0.375E-02	0.336E+00
0.399E-02	0.352E+00
0.361E-02	0.371E+00
0.436E-02	0.388E+00
0.346E-02	0.407E+00
0.335E-02	0.426E+00
0.384E-02	0.445E+00
0.314E-02	0.464E+00
0.319E-02	0.483E+00
0.288E-02	0.502E+00
0.291E-02	0.521E+00
0.224E-02	0.540E+00
0.197E-02	0.560E+00
0.184E-02	0.579E+00
0.188E-02	0.595E+00
0.208E-02	0.614E+00
0.140E-02	0.633E+00
0.186E-02	0.652E+00
0.143E-02	0.671E+00
0.100E-02	0.693E+00
0.130E-02	0.710E+00
0.975E-03	0.729E+00
0.903E-03	0.748E+00
0.977E-03	0.767E+00
0.904E-03	0.786E+00
0.591E-03	0.805E+00
0.618E-03	0.824E+00
0.555E-03	0.843E+00
0.428E-03	0.862E+00
0.399E-03	0.881E+00
0.282E-03	0.900E+00
0.293E-03	0.917E+00
0.277E-03	0.936E+00
0.205E-03	0.955E+00
0.189E-03	0.974E+00
0.163E-03	0.990E+00
0.142E-03	0.101E+01
0.147E-03	0.103E+01
0.157E-03	0.105E+01
0.146E-03	0.107E+01
0.166E-03	0.109E+01
0.164E-03	0.110E+01
0.163E-03	0.112E+01
0.168E-03	0.114E+01
0.148E-03	0.116E+01
0.176E-03	0.118E+01
0.175E-03	0.120E+01
0.152E-03	0.122E+01
0.193E-03	0.124E+01
0.176E-03	0.125E+01
0.175E-03	0.127E+01
0.199E-03	0.129E+01
0.188E-03	0.131E+01
0.226E-03	0.133E+01
0.187E-03	0.135E+01
0.222E-03	0.137E+01
0.236E-03	0.139E+01
0.231E-03	0.140E+01
0.219E-03	0.142E+01
0.241E-03	0.144E+01
0.241E-03	0.146E+01
0.240E-03	0.148E+01
0.276E-03	0.150E+01
0.279E-03	0.152E+01
0.277E-03	0.154E+01
0.266E-03	0.155E+01
0.290E-03	0.157E+01
0.313E-03	0.159E+01
0.292E-03	0.161E+01
0.320E-03	0.163E+01
0.330E-03	0.165E+01
0.303E-03	0.167E+01
0.331E-03	0.169E+01
0.491E-03	0.170E+01
0.407E-03	0.172E+01
0.451E-03	0.174E+01
0.458E-03	0.176E+01
0.377E-03	0.178E+01
0.301E-03	0.180E+01
0.310E-03	0.181E+01
0.294E-03	0.183E+01
0.292E-03	0.185E+01
0.258E-03	0.187E+01
0.264E-03	0.189E+01
0.275E-03	0.191E+01
0.278E-03	0.193E+01
0.254E-03	0.195E+01
0.240E-03	0.197E+01
0.244E-03	0.199E+01

term 2

0.726E-02	0.114E+00
0.803E-02	0.131E+00
0.684E-02	0.150E+00
0.798E-02	0.169E+00
0.781E-02	0.186E+00
0.858E-02	0.205E+00
0.881E-02	0.224E+00
0.854E-02	0.243E+00
0.920E-02	0.260E+00
0.964E-02	0.279E+00
0.963E-02	0.298E+00
0.934E-02	0.317E+00
0.825E-02	0.336E+00
0.891E-02	0.352E+00
0.819E-02	0.371E+00
0.100E-01	0.388E+00
0.814E-02	0.407E+00
0.805E-02	0.426E+00
0.946E-02	0.445E+00
0.786E-02	0.464E+00
0.811E-02	0.483E+00
0.742E-02	0.502E+00
0.759E-02	0.521E+00
0.580E-02	0.540E+00
0.512E-02	0.560E+00
0.483E-02	0.579E+00
0.493E-02	0.595E+00
0.543E-02	0.614E+00
0.365E-02	0.633E+00
0.489E-02	0.652E+00
0.378E-02	0.671E+00
0.269E-02	0.693E+00
0.353E-02	0.710E+00
0.265E-02	0.729E+00
0.245E-02	0.748E+00
0.263E-02	0.767E+00
0.243E-02	0.786E+00
0.159E-02	0.805E+00
0.166E-02	0.824E+00
0.150E-02	0.843E+00
0.115E-02	0.862E+00
0.107E-02	0.881E+00
0.758E-03	0.900E+00
0.787E-03	0.917E+00
0.743E-03	0.936E+00
0.546E-03	0.955E+00
0.500E-03	0.974E+00
0.430E-03	0.990E+00
0.373E-03	0.101E+01
0.379E-03	0.103E+01
0.398E-03	0.105E+01
0.365E-03	0.107E+01
0.413E-03	0.109E+01
0.406E-03	0.110E+01
0.404E-03	0.112E+01
0.421E-03	0.114E+01
0.372E-03	0.116E+01
0.447E-03	0.118E+01
0.450E-03	0.120E+01
0.390E-03	0.122E+01
0.498E-03	0.124E+01
0.455E-03	0.125E+01
0.452E-03	0.127E+01
0.516E-03	0.129E+01
0.490E-03	0.131E+01
0.591E-03	0.133E+01
0.495E-03	0.135E+01
0.589E-03	0.137E+01
0.625E-03	0.139E+01
0.613E-03	0.140E+01
0.584E-03	0.142E+01
0.639E-03	0.144E+01
0.641E-03	0.146E+01
0.637E-03	0.148E+01
0.734E-03	0.150E+01
0.741E-03	0.152E+01
0.733E-03	0.154E+01
0.698E-03	0.155E+01
0.740E-03	0.157E+01
0.767E-03	0.159E+01
0.706E-03	0.161E+01
0.780E-03	0.163E+01
0.830E-03	0.165E+01
0.787E-03	0.167E+01
0.909E-03	0.169E+01
0.143E-02	0.170E+01
0.125E-02	0.172E+01
0.145E-02	0.174E+01
0.152E-02	0.176E+01
0.129E-02	0.178E+01
0.106E-02	0.180E+01
0.111E-02	0.181E+01
0.107E-02	0.183E+01
0.107E-02	0.185E+01
0.952E-03	0.187E+01
0.976E-03	0.189E+01
0.102E-02	0.191E+01
0.104E-02	0.193E+01
0.956E-03	0.195E+01
0.910E-03	0.197E+01
0.926E-03	0.199E+01

term 3

0.129E-03	0.114E+00
0.111E-03	0.131E+00
0.106E-03	0.150E+00
0.969E-04	0.169E+00
0.943E-04	0.186E+00
0.103E-03	0.205E+00
0.993E-04	0.224E+00
0.869E-04	0.243E+00
0.788E-04	0.260E+00
0.824E-04	0.279E+00
0.695E-04	0.298E+00
0.682E-04	0.317E+00
0.554E-04	0.336E+00
0.590E-04	0.352E+00
0.518E-04	0.371E+00
0.639E-04	0.388E+00
0.536E-04	0.407E+00
0.453E-04	0.426E+00
0.573E-04	0.445E+00
0.430E-04	0.464E+00
0.388E-04	0.483E+00
0.368E-04	0.502E+00
0.378E-04	0.521E+00
0.298E-04	0.540E+00
0.262E-04	0.560E+00
0.240E-04	0.579E+00
0.227E-04	0.595E+00
0.262E-04	0.614E+00
0.176E-04	0.633E+00
0.241E-04	0.652E+00
0.189E-04	0.671E+00
0.126E-04	0.693E+00
0.144E-04	0.710E+00
0.111E-04	0.729E+00
0.988E-05	0.748E+00
0.118E-04	0.767E+00
0.980E-05	0.786E+00
0.601E-05	0.805E+00
0.650E-05	0.824E+00
0.626E-05	0.843E+00
0.406E-05	0.862E+00
0.420E-05	0.881E+00
0.258E-05	0.900E+00
0.272E-05	0.917E+00
0.268E-05	0.936E+00
0.186E-05	0.955E+00
0.175E-05	0.974E+00
0.148E-05	0.990E+00
0.121E-05	0.101E+01
0.121E-05	0.103E+01
0.133E-05	0.105E+01
0.129E-05	0.107E+01
0.148E-05	0.109E+01
0.146E-05	0.110E+01
0.137E-05	0.112E+01

0.162E-05 0.114E+01
0.145E-05 0.116E+01
0.170E-05 0.118E+01
0.162E-05 0.120E+01
0.148E-05 0.122E+01
0.180E-05 0.124E+01
0.164E-05 0.125E+01
0.176E-05 0.127E+01
0.186E-05 0.129E+01
0.188E-05 0.131E+01
0.218E-05 0.133E+01
0.186E-05 0.135E+01
0.216E-05 0.137E+01
0.230E-05 0.139E+01
0.225E-05 0.140E+01
0.221E-05 0.142E+01
0.230E-05 0.144E+01
0.248E-05 0.146E+01
0.233E-05 0.148E+01
0.275E-05 0.150E+01
0.288E-05 0.152E+01
0.275E-05 0.154E+01
0.299E-05 0.155E+01
0.344E-05 0.157E+01
0.383E-05 0.159E+01
0.387E-05 0.161E+01
0.457E-05 0.163E+01
0.582E-05 0.165E+01
0.599E-05 0.167E+01
0.796E-05 0.169E+01
0.990E-05 0.170E+01
0.893E-05 0.172E+01
0.703E-05 0.174E+01
0.597E-05 0.176E+01
0.453E-05 0.178E+01
0.335E-05 0.180E+01
0.334E-05 0.181E+01
0.312E-05 0.183E+01
0.293E-05 0.185E+01
0.251E-05 0.187E+01
0.254E-05 0.189E+01
0.267E-05 0.191E+01
0.269E-05 0.193E+01
0.233E-05 0.195E+01
0.226E-05 0.197E+01
0.223E-05 0.199E+01

Re shear

0.138E-01 0.114E+00
0.148E-01 0.131E+00
0.125E-01 0.150E+00
0.142E-01 0.169E+00
0.138E-01 0.186E+00
0.150E-01 0.205E+00
0.152E-01 0.224E+00
0.145E-01 0.243E+00
0.153E-01 0.260E+00
0.160E-01 0.279E+00
0.156E-01 0.298E+00
0.151E-01 0.317E+00
0.132E-01 0.336E+00
0.143E-01 0.352E+00
0.131E-01 0.371E+00
0.160E-01 0.388E+00
0.130E-01 0.407E+00
0.127E-01 0.426E+00
0.150E-01 0.445E+00
0.123E-01 0.464E+00
0.125E-01 0.483E+00
0.115E-01 0.502E+00
0.118E-01 0.521E+00
0.903E-02 0.540E+00
0.797E-02 0.560E+00
0.750E-02 0.579E+00
0.760E-02 0.595E+00
0.841E-02 0.614E+00
0.565E-02 0.633E+00
0.758E-02 0.652E+00
0.588E-02 0.671E+00
0.415E-02 0.693E+00
0.537E-02 0.710E+00
0.405E-02 0.729E+00
0.372E-02 0.748E+00
0.404E-02 0.767E+00
0.369E-02 0.786E+00
0.240E-02 0.805E+00
0.252E-02 0.824E+00
0.228E-02 0.843E+00
0.173E-02 0.862E+00
0.162E-02 0.881E+00
0.113E-02 0.900E+00
0.118E-02 0.917E+00
0.112E-02 0.936E+00
0.818E-03 0.955E+00
0.751E-03 0.974E+00
0.644E-03 0.990E+00
0.556E-03 0.101E+01
0.566E-03 0.103E+01
0.597E-03 0.105E+01
0.551E-03 0.107E+01
0.624E-03 0.109E+01
0.614E-03 0.110E+01
0.608E-03 0.112E+01
0.639E-03 0.114E+01
0.565E-03 0.116E+01
0.678E-03 0.118E+01
0.678E-03 0.120E+01
0.591E-03 0.122E+01
0.750E-03 0.124E+01
0.685E-03 0.125E+01
0.685E-03 0.127E+01
0.777E-03 0.129E+01
0.741E-03 0.131E+01
0.892E-03 0.133E+01
0.747E-03 0.135E+01
0.887E-03 0.137E+01
0.942E-03 0.139E+01
0.924E-03 0.140E+01
0.882E-03 0.142E+01
0.962E-03 0.144E+01
0.970E-03 0.146E+01
0.960E-03 0.148E+01
0.111E-02 0.150E+01
0.112E-02 0.152E+01
0.111E-02 0.154E+01
0.107E-02 0.155E+01
0.114E-02 0.157E+01
0.119E-02 0.159E+01
0.111E-02 0.161E+01
0.123E-02 0.163E+01
0.134E-02 0.165E+01
0.129E-02 0.167E+01
0.155E-02 0.169E+01
0.236E-02 0.170E+01
0.212E-02 0.172E+01
0.230E-02 0.174E+01
0.235E-02 0.176E+01
0.197E-02 0.178E+01
0.160E-02 0.180E+01
0.167E-02 0.181E+01
0.160E-02 0.183E+01
0.159E-02 0.185E+01
0.141E-02 0.187E+01
0.145E-02 0.189E+01
0.152E-02 0.191E+01
0.155E-02 0.193E+01
0.141E-02 0.195E+01
0.135E-02 0.197E+01
0.137E-02 0.199E+01

Fig. 5.24b

term 1

0.189E-02 0.114E+00
0.181E-02 0.131E+00
0.178E-02 0.150E+00
0.168E-02 0.169E+00
0.191E-02 0.186E+00
0.124E-02 0.205E+00
0.148E-02 0.224E+00
0.131E-02 0.243E+00
0.116E-02 0.260E+00
0.134E-02 0.279E+00
0.138E-02 0.298E+00
0.117E-02 0.317E+00
0.108E-02 0.336E+00
0.962E-03 0.352E+00
0.842E-03 0.371E+00
0.739E-03 0.388E+00
0.851E-03 0.407E+00
0.777E-03 0.426E+00
0.786E-03 0.445E+00
0.319E-03 0.464E+00
0.233E-03 0.483E+00
0.383E-03 0.502E+00
0.358E-03 0.521E+00
0.951E-04 0.540E+00
0.271E-03 0.560E+00
0.171E-03 0.579E+00
0.890E-04 0.595E+00
0.569E-04 0.614E+00
-0.155E-04 0.633E+00
0.345E-06 0.652E+00
-0.113E-04 0.671E+00
-0.491E-04 0.693E+00
-0.420E-04 0.710E+00
-0.432E-04 0.729E+00
-0.205E-04 0.748E+00
-0.264E-04 0.767E+00
-0.738E-04 0.786E+00
-0.434E-04 0.805E+00
-0.152E-04 0.824E+00
-0.487E-04 0.843E+00
-0.148E-04 0.862E+00
-0.142E-04 0.881E+00
-0.293E-05 0.900E+00
0.304E-05 0.917E+00
-0.143E-04 0.936E+00
-0.225E-05 0.955E+00
-0.867E-05 0.974E+00
0.151E-04 0.990E+00
0.141E-04 0.101E+01
0.170E-04 0.103E+01
0.186E-04 0.105E+01
0.317E-04 0.107E+01
0.226E-04 0.109E+01
0.163E-04 0.110E+01
0.224E-04 0.112E+01
0.222E-04 0.114E+01
0.165E-04 0.116E+01
0.154E-04 0.118E+01
0.179E-04 0.120E+01
0.155E-04 0.122E+01
0.145E-04 0.124E+01
0.118E-04 0.125E+01
0.179E-04 0.127E+01
0.123E-04 0.129E+01
0.116E-04 0.131E+01
0.115E-04 0.133E+01
0.255E-04 0.135E+01
0.167E-04 0.137E+01
0.234E-04 0.139E+01
0.207E-04 0.140E+01
0.146E-04 0.142E+01
0.184E-04 0.144E+01
0.256E-04 0.146E+01
0.258E-04 0.148E+01
0.219E-04 0.150E+01
0.147E-04 0.152E+01
0.204E-04 0.154E+01
0.210E-04 0.155E+01
0.241E-04 0.157E+01
0.339E-04 0.159E+01
0.238E-04 0.161E+01
0.390E-04 0.163E+01
0.362E-04 0.165E+01
0.129E-03 0.167E+01
0.278E-03 0.169E+01
0.250E-03 0.170E+01
0.116E-03 0.172E+01
0.231E-04 0.174E+01
-0.652E-04 0.176E+01
-0.140E-03 0.178E+01
-0.323E-03 0.180E+01
-0.334E-03 0.181E+01
-0.993E-04 0.183E+01
-0.462E-04 0.185E+01
-0.514E-05 0.187E+01
-0.398E-05 0.189E+01
-0.688E-06 0.191E+01
0.552E-05 0.193E+01
0.602E-05 0.195E+01
0.364E-05 0.197E+01
0.836E-05 0.199E+01

term 2

0.242E-02 0.114E+00
0.247E-02 0.131E+00
0.256E-02 0.150E+00
0.252E-02 0.169E+00
0.298E-02 0.186E+00

0.204E-02	0.205E+00
0.256E-02	0.224E+00
0.240E-02	0.243E+00
0.223E-02	0.260E+00
0.265E-02	0.279E+00
0.284E-02	0.298E+00
0.250E-02	0.317E+00
0.238E-02	0.336E+00
0.215E-02	0.352E+00
0.191E-02	0.371E+00
0.170E-02	0.388E+00
0.200E-02	0.407E+00
0.186E-02	0.426E+00
0.193E-02	0.445E+00
0.801E-03	0.464E+00
0.592E-03	0.483E+00
0.987E-03	0.502E+00
0.932E-03	0.521E+00
0.246E-03	0.540E+00
0.704E-03	0.560E+00
0.450E-03	0.579E+00
0.234E-03	0.595E+00
0.149E-03	0.614E+00
-0.406E-04	0.633E+00
0.905E-06	0.652E+00
-0.301E-04	0.671E+00
-0.132E-03	0.693E+00
-0.114E-03	0.710E+00
-0.118E-03	0.729E+00
-0.556E-04	0.748E+00
-0.712E-04	0.767E+00
-0.198E-03	0.786E+00
-0.117E-03	0.805E+00
-0.408E-04	0.824E+00
-0.131E-03	0.843E+00
-0.398E-04	0.862E+00
-0.382E-04	0.881E+00
-0.787E-05	0.900E+00
0.816E-05	0.917E+00
-0.384E-04	0.936E+00
-0.601E-05	0.955E+00
-0.229E-04	0.974E+00
0.399E-04	0.990E+00
0.369E-04	0.101E+01
0.440E-04	0.103E+01
0.473E-04	0.105E+01
0.793E-04	0.107E+01
0.560E-04	0.109E+01
0.405E-04	0.110E+01
0.558E-04	0.112E+01
0.555E-04	0.114E+01
0.418E-04	0.116E+01
0.394E-04	0.118E+01
0.459E-04	0.120E+01
0.398E-04	0.122E+01
0.375E-04	0.124E+01
0.304E-04	0.125E+01
0.462E-04	0.127E+01
0.317E-04	0.129E+01
0.303E-04	0.131E+01
0.302E-04	0.133E+01
0.674E-04	0.135E+01
0.443E-04	0.137E+01
0.621E-04	0.139E+01
0.547E-04	0.140E+01
0.389E-04	0.142E+01
0.490E-04	0.144E+01
0.679E-04	0.146E+01
0.686E-04	0.148E+01
0.581E-04	0.150E+01
0.389E-04	0.152E+01
0.541E-04	0.154E+01
0.552E-04	0.155E+01
0.614E-04	0.157E+01
0.831E-04	0.159E+01
0.576E-04	0.161E+01
0.950E-04	0.163E+01
0.908E-04	0.165E+01
0.336E-03	0.167E+01
0.762E-03	0.169E+01
0.725E-03	0.170E+01
0.355E-03	0.172E+01
0.743E-04	0.174E+01
-0.217E-03	0.176E+01
-0.478E-03	0.178E+01
-0.114E-02	0.180E+01
-0.120E-02	0.181E+01
-0.360E-03	0.183E+01
-0.169E-03	0.185E+01
-0.190E-04	0.187E+01
-0.147E-04	0.189E+01
-0.256E-05	0.191E+01
0.207E-04	0.193E+01
0.227E-04	0.195E+01
0.138E-04	0.197E+01
0.317E-04	0.199E+01

term 3

0.192E-04	0.114E+00
0.193E-04	0.131E+00
0.266E-04	0.150E+00
0.271E-04	0.169E+00
0.263E-04	0.186E+00
0.140E-04	0.205E+00
0.253E-04	0.224E+00
0.198E-04	0.243E+00
0.162E-04	0.260E+00
0.194E-04	0.279E+00
0.222E-04	0.298E+00
0.195E-04	0.317E+00
0.177E-04	0.336E+00
0.153E-04	0.352E+00
0.161E-04	0.371E+00
0.136E-04	0.388E+00
0.184E-04	0.407E+00
0.164E-04	0.426E+00
0.154E-04	0.445E+00
0.961E-05	0.464E+00
0.680E-05	0.483E+00
0.819E-05	0.502E+00
0.907E-05	0.521E+00
0.647E-05	0.540E+00
0.913E-05	0.560E+00
0.521E-05	0.579E+00
0.452E-05	0.595E+00
0.526E-05	0.614E+00
0.367E-05	0.633E+00
0.359E-05	0.652E+00
0.438E-05	0.671E+00
0.256E-05	0.693E+00
0.118E-05	0.710E+00
0.494E-05	0.729E+00
0.998E-06	0.748E+00
0.152E-05	0.767E+00
0.154E-05	0.786E+00
0.692E-06	0.805E+00
0.765E-06	0.824E+00
0.670E-06	0.843E+00
0.347E-06	0.862E+00
0.353E-06	0.881E+00
0.295E-06	0.900E+00
0.378E-06	0.917E+00
0.198E-06	0.936E+00
0.214E-06	0.955E+00
0.324E-06	0.974E+00
0.198E-06	0.990E+00
0.180E-06	0.101E+01
0.167E-06	0.103E+01
0.202E-06	0.105E+01
0.180E-06	0.107E+01
0.196E-06	0.109E+01
0.217E-06	0.110E+01
0.232E-06	0.112E+01
0.225E-06	0.114E+01
0.126E-06	0.116E+01
0.130E-06	0.118E+01
0.103E-06	0.120E+01
0.794E-07	0.122E+01
0.524E-07	0.124E+01
0.268E-07	0.125E+01
0.478E-07	0.127E+01
0.284E-07	0.129E+01
0.244E-07	0.131E+01
0.262E-07	0.133E+01
0.475E-07	0.135E+01
0.232E-07	0.137E+01
0.460E-07	0.139E+01
0.448E-07	0.140E+01
0.742E-07	0.142E+01
0.662E-07	0.144E+01
0.905E-07	0.146E+01
0.106E-06	0.148E+01
0.115E-06	0.150E+01
0.102E-06	0.152E+01
0.123E-06	0.154E+01
0.100E-06	0.155E+01
0.106E-06	0.157E+01
0.114E-06	0.159E+01
0.104E-06	0.161E+01
0.120E-06	0.163E+01
0.864E-07	0.165E+01
0.355E-07	0.167E+01
-0.166E-06	0.169E+01
-0.746E-06	0.170E+01
-0.702E-06	0.172E+01
-0.456E-06	0.174E+01
-0.483E-06	0.176E+01
-0.714E-06	0.178E+01
-0.621E-06	0.180E+01
-0.545E-06	0.181E+01
-0.890E-08	0.183E+01
0.131E-07	0.185E+01
0.385E-07	0.187E+01
0.333E-07	0.189E+01
0.323E-07	0.191E+01
0.304E-07	0.193E+01
0.327E-07	0.195E+01
0.268E-07	0.197E+01
0.314E-07	0.199E+01

Re shear

0.444E-02	0.114E+00
0.443E-02	0.131E+00
0.457E-02	0.150E+00
0.446E-02	0.169E+00
0.516E-02	0.186E+00
0.344E-02	0.205E+00
0.437E-02	0.224E+00
0.400E-02	0.243E+00
0.365E-02	0.260E+00
0.433E-02	0.279E+00
0.465E-02	0.298E+00
0.408E-02	0.317E+00
0.386E-02	0.336E+00
0.347E-02	0.352E+00
0.314E-02	0.371E+00
0.278E-02	0.388E+00
0.333E-02	0.407E+00
0.309E-02	0.426E+00
0.317E-02	0.445E+00
0.142E-02	0.464E+00
0.104E-02	0.483E+00
0.164E-02	0.502E+00
0.160E-02	0.521E+00
0.556E-03	0.540E+00
0.128E-02	0.560E+00
0.801E-03	0.579E+00
0.479E-03	0.595E+00
0.386E-03	0.614E+00
0.695E-04	0.633E+00
0.125E-03	0.652E+00
0.113E-03	0.671E+00
-0.877E-04	0.693E+00
-0.112E-03	0.710E+00
0.252E-04	0.729E+00
-0.389E-04	0.748E+00
-0.415E-04	0.767E+00
-0.216E-03	0.786E+00
-0.135E-03	0.805E+00
-0.279E-04	0.824E+00
-0.155E-03	0.843E+00
-0.419E-04	0.862E+00
-0.395E-04	0.881E+00
-0.442E-07	0.900E+00
0.250E-04	0.917E+00
-0.455E-04	0.936E+00
-0.601E-06	0.955E+00
-0.202E-04	0.974E+00
0.619E-04	0.990E+00
0.571E-04	0.101E+01
0.665E-04	0.103E+01
0.723E-04	0.105E+01
0.117E-03	0.107E+01
0.845E-04	0.109E+01
0.633E-04	0.110E+01
0.852E-04	0.112E+01
0.846E-04	0.114E+01
0.623E-04	0.116E+01
0.590E-04	0.118E+01
0.671E-04	0.120E+01
0.579E-04	0.122E+01
0.537E-04	0.124E+01

0.431E-04	0.125E+01
0.657E-04	0.127E+01
0.449E-04	0.129E+01
0.427E-04	0.131E+01
0.426E-04	0.133E+01
0.946E-04	0.135E+01
0.618E-04	0.137E+01
0.871E-04	0.139E+01
0.770E-04	0.140E+01
0.561E-04	0.142E+01
0.698E-04	0.144E+01
0.967E-04	0.146E+01
0.982E-04	0.148E+01
0.841E-04	0.150E+01
0.572E-04	0.152E+01
0.788E-04	0.154E+01
0.797E-04	0.155E+01
0.889E-04	0.157E+01
0.120E-03	0.159E+01
0.843E-04	0.161E+01
0.137E-03	0.163E+01
0.130E-03	0.165E+01
0.466E-03	0.167E+01
0.103E-02	0.169E+01
0.942E-03	0.170E+01
0.435E-03	0.172E+01
0.713E-04	0.174E+01
-0.312E-03	0.176E+01
-0.666E-03	0.178E+01
-0.150E-02	0.180E+01
-0.157E-02	0.181E+01
-0.460E-03	0.183E+01
-0.214E-03	0.185E+01
-0.210E-04	0.187E+01
-0.160E-04	0.189E+01
-0.564E-06	0.191E+01
0.288E-04	0.193E+01
0.315E-04	0.195E+01
0.197E-04	0.197E+01
0.428E-04	0.199E+01

Fig. 5.25a

u'v'

-0.564E-02	0.114E+00
-0.587E-02	0.131E+00
-0.476E-02	0.150E+00
-0.532E-02	0.169E+00
-0.499E-02	0.186E+00
-0.522E-02	0.205E+00
-0.509E-02	0.224E+00
-0.466E-02	0.243E+00
-0.480E-02	0.260E+00
-0.486E-02	0.279E+00
-0.467E-02	0.298E+00
-0.436E-02	0.317E+00
-0.375E-02	0.336E+00
-0.399E-02	0.352E+00
-0.361E-02	0.371E+00
-0.436E-02	0.388E+00
-0.346E-02	0.407E+00
-0.335E-02	0.426E+00
-0.384E-02	0.445E+00
-0.314E-02	0.464E+00
-0.319E-02	0.483E+00
-0.288E-02	0.502E+00
-0.291E-02	0.521E+00
-0.224E-02	0.540E+00
-0.197E-02	0.560E+00
-0.184E-02	0.579E+00
-0.188E-02	0.595E+00
-0.208E-02	0.614E+00
-0.140E-02	0.633E+00
-0.186E-02	0.652E+00
-0.143E-02	0.671E+00
-0.100E-02	0.693E+00
-0.130E-02	0.710E+00
-0.975E-03	0.729E+00
-0.903E-03	0.748E+00
-0.977E-03	0.767E+00
-0.904E-03	0.786E+00
-0.591E-03	0.805E+00
-0.618E-03	0.824E+00
-0.555E-03	0.843E+00
-0.428E-03	0.862E+00
-0.399E-03	0.881E+00
-0.282E-03	0.900E+00
-0.293E-03	0.917E+00
-0.277E-03	0.936E+00
-0.205E-03	0.955E+00
-0.189E-03	0.974E+00
-0.163E-03	0.990E+00
-0.142E-03	0.101E+01
-0.147E-03	0.103E+01
-0.157E-03	0.105E+01
-0.146E-03	0.107E+01
-0.166E-03	0.109E+01
-0.164E-03	0.110E+01
-0.163E-03	0.112E+01
-0.168E-03	0.114E+01
-0.148E-03	0.116E+01
-0.176E-03	0.118E+01
-0.175E-03	0.120E+01
-0.152E-03	0.122E+01
-0.193E-03	0.124E+01
-0.176E-03	0.125E+01
-0.175E-03	0.127E+01
-0.199E-03	0.129E+01
-0.188E-03	0.131E+01
-0.226E-03	0.133E+01
-0.187E-03	0.135E+01
-0.222E-03	0.137E+01
-0.236E-03	0.139E+01
-0.231E-03	0.140E+01
-0.219E-03	0.142E+01
-0.241E-03	0.144E+01
-0.241E-03	0.146E+01
-0.240E-03	0.148E+01
-0.276E-03	0.150E+01
-0.279E-03	0.152E+01
-0.277E-03	0.154E+01
-0.266E-03	0.155E+01
-0.290E-03	0.157E+01
-0.313E-03	0.159E+01
-0.292E-03	0.161E+01
-0.320E-03	0.163E+01
-0.330E-03	0.165E+01
-0.303E-03	0.167E+01
-0.331E-03	0.169E+01
-0.491E-03	0.170E+01
-0.407E-03	0.172E+01
-0.451E-03	0.174E+01
-0.458E-03	0.176E+01
-0.377E-03	0.178E+01
-0.301E-03	0.180E+01
-0.310E-03	0.181E+01
-0.294E-03	0.183E+01
-0.292E-03	0.185E+01
-0.258E-03	0.187E+01
-0.264E-03	0.189E+01
-0.275E-03	0.191E+01
-0.278E-03	0.193E+01
-0.254E-03	0.195E+01
-0.240E-03	0.197E+01
-0.244E-03	0.199E+01

u'w'

-0.189E-02	0.114E+00
-0.181E-02	0.131E+00
-0.178E-02	0.150E+00
-0.168E-02	0.169E+00
-0.191E-02	0.186E+00
-0.124E-02	0.205E+00
-0.148E-02	0.224E+00
-0.131E-02	0.243E+00
-0.116E-02	0.260E+00
-0.134E-02	0.279E+00
-0.138E-02	0.298E+00
-0.117E-02	0.317E+00
-0.108E-02	0.336E+00
-0.962E-03	0.352E+00
-0.842E-03	0.371E+00
-0.739E-03	0.388E+00
-0.851E-03	0.407E+00
-0.777E-03	0.426E+00
-0.786E-03	0.445E+00
-0.319E-03	0.464E+00
-0.233E-03	0.483E+00
-0.383E-03	0.502E+00
-0.358E-03	0.521E+00
-0.951E-04	0.540E+00
-0.271E-03	0.560E+00
-0.171E-03	0.579E+00
-0.890E-04	0.595E+00
-0.569E-04	0.614E+00
0.155E-04	0.633E+00
-0.345E-06	0.652E+00
0.113E-04	0.671E+00
0.491E-04	0.693E+00
0.420E-04	0.710E+00
0.432E-04	0.729E+00
0.205E-04	0.748E+00
0.264E-04	0.767E+00
0.738E-04	0.786E+00
0.434E-04	0.805E+00
0.152E-04	0.824E+00
0.487E-04	0.843E+00
0.148E-04	0.862E+00
0.142E-04	0.881E+00
0.293E-05	0.900E+00
-0.304E-05	0.917E+00
0.143E-04	0.936E+00
0.225E-05	0.955E+00
0.867E-05	0.974E+00
-0.151E-04	0.990E+00
-0.141E-04	0.101E+01
-0.170E-04	0.103E+01
-0.186E-04	0.105E+01
-0.317E-04	0.107E+01
-0.226E-04	0.109E+01
-0.163E-04	0.110E+01
-0.224E-04	0.112E+01
-0.222E-04	0.114E+01
-0.165E-04	0.116E+01
-0.154E-04	0.118E+01
-0.179E-04	0.120E+01
-0.155E-04	0.122E+01
-0.145E-04	0.124E+01
-0.118E-04	0.125E+01
-0.179E-04	0.127E+01
-0.123E-04	0.129E+01
-0.116E-04	0.131E+01
-0.115E-04	0.133E+01
-0.255E-04	0.135E+01
-0.167E-04	0.137E+01
-0.234E-04	0.139E+01
-0.207E-04	0.140E+01
-0.146E-04	0.142E+01
-0.184E-04	0.144E+01
-0.256E-04	0.146E+01
-0.258E-04	0.148E+01
-0.219E-04	0.150E+01
-0.147E-04	0.152E+01
-0.204E-04	0.154E+01
-0.210E-04	0.155E+01
-0.241E-04	0.157E+01
-0.339E-04	0.159E+01
-0.238E-04	0.161E+01
-0.390E-04	0.163E+01
-0.362E-04	0.165E+01
-0.129E-03	0.167E+01
-0.278E-03	0.169E+01
-0.250E-03	0.170E+01
-0.116E-03	0.172E+01
-0.231E-04	0.174E+01
0.652E-04	0.176E+01
0.140E-03	0.178E+01
0.323E-03	0.180E+01
0.334E-03	0.181E+01
0.993E-04	0.183E+01
0.462E-04	0.185E+01
0.514E-05	0.187E+01
0.398E-05	0.189E+01
0.688E-06	0.191E+01
-0.552E-05	0.193E+01
-0.602E-05	0.195E+01
-0.364E-05	0.197E+01
-0.836E-05	0.199E+01

Fig. 5.25b

ρ'u'

0.546E-02	0.114E+00
0.601E-02	0.131E+00
0.481E-02	0.150E+00
0.584E-02	0.169E+00
0.535E-02	0.186E+00
0.565E-02	0.205E+00
0.550E-02	0.224E+00
0.548E-02	0.243E+00
0.577E-02	0.260E+00

0.592E-02	0.279E+00
0.599E-02	0.298E+00
0.598E-02	0.317E+00
0.484E-02	0.336E+00
0.527E-02	0.352E+00
0.471E-02	0.371E+00
0.684E-02	0.388E+00
0.497E-02	0.407E+00
0.492E-02	0.426E+00
0.566E-02	0.445E+00
0.515E-02	0.464E+00
0.474E-02	0.483E+00
0.441E-02	0.502E+00
0.457E-02	0.521E+00
0.345E-02	0.540E+00
0.304E-02	0.560E+00
0.273E-02	0.579E+00
0.297E-02	0.595E+00
0.318E-02	0.614E+00
0.212E-02	0.633E+00
0.283E-02	0.652E+00
0.211E-02	0.671E+00
0.144E-02	0.693E+00
0.190E-02	0.710E+00
0.132E-02	0.729E+00
0.121E-02	0.748E+00
0.158E-02	0.767E+00
0.118E-02	0.786E+00
0.726E-03	0.805E+00
0.812E-03	0.824E+00
0.759E-03	0.843E+00
0.506E-03	0.862E+00
0.506E-03	0.881E+00
0.310E-03	0.900E+00
0.337E-03	0.917E+00
0.322E-03	0.936E+00
0.221E-03	0.955E+00
0.213E-03	0.974E+00
0.172E-03	0.990E+00
0.141E-03	0.101E+01
0.141E-03	0.103E+01
0.152E-03	0.105E+01
0.144E-03	0.107E+01
0.159E-03	0.109E+01
0.156E-03	0.110E+01
0.147E-03	0.112E+01
0.170E-03	0.114E+01
0.155E-03	0.116E+01
0.174E-03	0.118E+01
0.167E-03	0.120E+01
0.146E-03	0.122E+01
0.173E-03	0.124E+01
0.158E-03	0.125E+01
0.161E-03	0.127E+01
0.171E-03	0.129E+01
0.175E-03	0.131E+01
0.195E-03	0.133E+01
0.169E-03	0.135E+01
0.192E-03	0.137E+01
0.200E-03	0.139E+01
0.192E-03	0.140E+01
0.190E-03	0.142E+01
0.197E-03	0.144E+01
0.212E-03	0.146E+01
0.200E-03	0.148E+01
0.231E-03	0.150E+01
0.236E-03	0.152E+01
0.230E-03	0.154E+01
0.237E-03	0.155E+01
0.256E-03	0.157E+01
0.270E-03	0.159E+01
0.262E-03	0.161E+01
0.303E-03	0.163E+01
0.387E-03	0.165E+01
0.399E-03	0.167E+01
0.511E-03	0.169E+01
0.649E-03	0.170E+01
0.604E-03	0.172E+01
0.476E-03	0.174E+01
0.416E-03	0.176E+01
0.331E-03	0.178E+01
0.255E-03	0.180E+01
0.262E-03	0.181E+01
0.249E-03	0.183E+01
0.237E-03	0.185E+01
0.207E-03	0.187E+01
0.211E-03	0.189E+01
0.224E-03	0.191E+01
0.228E-03	0.193E+01
0.202E-03	0.195E+01
0.197E-03	0.197E+01
0.197E-03	0.199E+01

ρ'v'

-0.726E-02	0.114E+00
-0.803E-02	0.131E+00
-0.684E-02	0.150E+00
-0.798E-02	0.169E+00
-0.781E-02	0.186E+00
-0.858E-02	0.205E+00
-0.881E-02	0.224E+00
-0.854E-02	0.243E+00
-0.920E-02	0.260E+00
-0.964E-02	0.279E+00
-0.963E-02	0.298E+00
-0.934E-02	0.317E+00
-0.825E-02	0.336E+00
-0.891E-02	0.352E+00
-0.819E-02	0.371E+00
-0.100E-01	0.388E+00
-0.814E-02	0.407E+00
-0.805E-02	0.426E+00
-0.946E-02	0.445E+00
-0.786E-02	0.464E+00
-0.811E-02	0.483E+00
-0.742E-02	0.502E+00
-0.759E-02	0.521E+00
-0.580E-02	0.540E+00
-0.512E-02	0.560E+00
-0.483E-02	0.579E+00
-0.493E-02	0.595E+00
-0.543E-02	0.614E+00
-0.365E-02	0.633E+00
-0.489E-02	0.652E+00
-0.378E-02	0.671E+00
-0.269E-02	0.693E+00
-0.353E-02	0.710E+00
-0.265E-02	0.729E+00
-0.245E-02	0.748E+00
-0.263E-02	0.767E+00
-0.243E-02	0.786E+00
-0.159E-02	0.805E+00
-0.166E-02	0.824E+00
-0.150E-02	0.843E+00
-0.115E-02	0.862E+00
-0.107E-02	0.881E+00
-0.758E-03	0.900E+00
-0.787E-03	0.917E+00
-0.743E-03	0.936E+00
-0.546E-03	0.955E+00
-0.500E-03	0.974E+00
-0.430E-03	0.990E+00
-0.373E-03	0.101E+01
-0.379E-03	0.103E+01
-0.398E-03	0.105E+01
-0.365E-03	0.107E+01
-0.413E-03	0.109E+01
-0.406E-03	0.110E+01
-0.404E-03	0.112E+01
-0.421E-03	0.114E+01
-0.372E-03	0.116E+01
-0.447E-03	0.118E+01
-0.450E-03	0.120E+01
-0.390E-03	0.122E+01
-0.498E-03	0.124E+01
-0.455E-03	0.125E+01
-0.452E-03	0.127E+01
-0.516E-03	0.129E+01
-0.490E-03	0.131E+01
-0.591E-03	0.133E+01
-0.495E-03	0.135E+01
-0.589E-03	0.137E+01
-0.625E-03	0.139E+01
-0.613E-03	0.140E+01
-0.584E-03	0.142E+01
-0.639E-03	0.144E+01
-0.641E-03	0.146E+01
-0.637E-03	0.148E+01
-0.734E-03	0.150E+01
-0.741E-03	0.152E+01
-0.733E-03	0.154E+01
-0.698E-03	0.155E+01
-0.740E-03	0.157E+01
-0.767E-03	0.159E+01
-0.706E-03	0.161E+01
-0.780E-03	0.163E+01
-0.830E-03	0.165E+01
-0.787E-03	0.167E+01
-0.909E-03	0.169E+01
-0.143E-02	0.170E+01
-0.125E-02	0.172E+01
-0.145E-02	0.174E+01
-0.152E-02	0.176E+01
-0.129E-02	0.178E+01
-0.106E-02	0.180E+01
-0.111E-02	0.181E+01
-0.107E-02	0.183E+01
-0.107E-02	0.185E+01
-0.952E-03	0.187E+01
-0.976E-03	0.189E+01
-0.102E-02	0.191E+01
-0.104E-02	0.193E+01
-0.956E-03	0.195E+01
-0.910E-03	0.197E+01
-0.926E-03	0.199E+01

ρ'w'

-0.242E-02	0.114E+00
-0.247E-02	0.131E+00
-0.256E-02	0.150E+00
-0.252E-02	0.169E+00
-0.298E-02	0.186E+00
-0.204E-02	0.205E+00
-0.256E-02	0.224E+00
-0.240E-02	0.243E+00
-0.223E-02	0.260E+00
-0.265E-02	0.279E+00
-0.284E-02	0.298E+00
-0.250E-02	0.317E+00
-0.238E-02	0.336E+00
-0.215E-02	0.352E+00
-0.191E-02	0.371E+00
-0.170E-02	0.388E+00
-0.200E-02	0.407E+00
-0.186E-02	0.426E+00
-0.193E-02	0.445E+00
-0.801E-03	0.464E+00
-0.592E-03	0.483E+00
-0.987E-03	0.502E+00
-0.932E-03	0.521E+00
-0.246E-03	0.540E+00
-0.704E-03	0.560E+00
-0.450E-03	0.579E+00
-0.234E-03	0.595E+00
-0.149E-03	0.614E+00
0.406E-04	0.633E+00
-0.905E-06	0.652E+00
0.301E-04	0.671E+00
0.132E-03	0.693E+00
0.114E-03	0.710E+00
0.118E-03	0.729E+00
0.556E-04	0.748E+00
0.712E-04	0.767E+00
0.198E-03	0.786E+00
0.117E-03	0.805E+00
0.408E-04	0.824E+00
0.131E-03	0.843E+00
0.398E-04	0.862E+00
0.382E-04	0.881E+00
0.787E-05	0.900E+00
-0.816E-05	0.917E+00
0.384E-04	0.936E+00
0.601E-05	0.955E+00
0.229E-04	0.974E+00
-0.399E-04	0.990E+00
-0.369E-04	0.101E+01
-0.440E-04	0.103E+01
-0.473E-04	0.105E+01
-0.793E-04	0.107E+01
-0.560E-04	0.109E+01
-0.405E-04	0.110E+01
-0.558E-04	0.112E+01
-0.555E-04	0.114E+01
-0.418E-04	0.116E+01
-0.394E-04	0.118E+01
-0.459E-04	0.120E+01
-0.398E-04	0.122E+01
-0.375E-04	0.124E+01
-0.304E-04	0.125E+01
-0.462E-04	0.127E+01
-0.317E-04	0.129E+01
-0.303E-04	0.131E+01

-0.302E-04	0.133E+01
-0.674E-04	0.135E+01
-0.443E-04	0.137E+01
-0.621E-04	0.139E+01
-0.547E-04	0.140E+01
-0.389E-04	0.142E+01
-0.490E-04	0.144E+01
-0.679E-04	0.146E+01
-0.686E-04	0.148E+01
-0.581E-04	0.150E+01
-0.389E-04	0.152E+01
-0.541E-04	0.154E+01
-0.552E-04	0.155E+01
-0.614E-04	0.157E+01
-0.831E-04	0.159E+01
-0.576E-04	0.161E+01
-0.950E-04	0.163E+01
-0.908E-04	0.165E+01
-0.336E-03	0.167E+01
-0.762E-03	0.169E+01
-0.725E-03	0.170E+01
-0.355E-03	0.172E+01
-0.743E-04	0.174E+01
0.217E-03	0.176E+01
0.478E-03	0.178E+01
0.114E-02	0.180E+01
0.120E-02	0.181E+01
0.360E-03	0.183E+01
0.169E-03	0.185E+01
0.190E-04	0.187E+01
0.147E-04	0.189E+01
0.256E-05	0.191E+01
-0.207E-04	0.193E+01
-0.227E-04	0.195E+01
-0.138E-04	0.197E+01
-0.317E-04	0.199E+01

Fig. 5.26a

Prandtl data

9.22E-04	2.49E-01
1.07E-03	2.57E-01
1.81E-03	2.73E-01
1.84E-03	2.97E-01
1.56E-03	3.25E-01
1.24E-03	3.56E-01
9.78E-04	3.90E-01
1.08E-03	4.25E-01
9.59E-04	4.61E-01
7.35E-04	4.98E-01
5.07E-04	5.34E-01
3.26E-04	5.72E-01
3.40E-04	6.09E-01
8.97E-04	6.46E-01
8.52E-04	6.83E-01
6.50E-04	7.20E-01
4.51E-04	7.58E-01
2.93E-04	7.95E-01
1.84E-04	8.33E-01
1.13E-04	8.70E-01
6.83E-05	9.07E-01
4.06E-05	9.45E-01
2.39E-05	9.83E-01
1.39E-05	1.02E+00
8.06E-06	1.06E+00
4.65E-06	1.09E+00
2.62E-06	1.13E+00
1.45E-06	1.17E+00
7.82E-07	1.21E+00
4.20E-07	1.24E+00
2.63E-07	1.28E+00
1.70E-07	1.32E+00
1.28E-07	1.36E+00
9.43E-08	1.39E+00
7.61E-08	1.43E+00
5.77E-08	1.47E+00
3.96E-08	1.49E+00
2.19E-08	1.52E+00
2.43E-08	1.55E+00
1.99E-08	1.58E+00
1.81E-08	1.62E+00
1.42E-08	1.65E+00
1.01E-08	1.69E+00
7.73E-09	1.72E+00
4.34E-09	1.76E+00
5.40E-09	1.80E+00
5.05E-08	1.84E+00
9.22E-08	1.87E+00
1.01E-07	1.91E+00
8.30E-08	1.95E+00
4.48E-08	1.99E+00

Re shear stress

0.273E-02	0.134E+00
0.245E-02	0.157E+00
0.314E-02	0.180E+00
0.236E-02	0.200E+00
0.195E-02	0.223E+00
0.183E-02	0.243E+00
0.230E-02	0.263E+00
0.191E-02	0.283E+00
0.160E-02	0.306E+00
0.188E-02	0.329E+00
0.168E-02	0.349E+00
0.153E-02	0.371E+00
0.168E-02	0.391E+00
0.139E-02	0.414E+00
0.147E-02	0.437E+00
0.126E-02	0.457E+00
0.101E-02	0.480E+00
0.843E-03	0.503E+00
0.815E-03	0.526E+00
0.105E-02	0.549E+00
0.655E-03	0.571E+00
0.506E-03	0.594E+00
0.442E-03	0.617E+00
0.751E-03	0.640E+00
0.401E-03	0.660E+00
0.470E-03	0.683E+00
0.768E-03	0.706E+00
0.419E-03	0.726E+00
0.280E-03	0.749E+00
0.290E-03	0.769E+00
0.227E-03	0.791E+00
0.717E-04	0.814E+00
0.106E-03	0.837E+00
0.104E-03	0.860E+00
0.110E-03	0.883E+00
0.402E-04	0.906E+00
0.923E-04	0.929E+00
0.699E-04	0.951E+00
0.439E-04	0.974E+00
0.449E-04	0.994E+00
0.528E-04	0.102E+01
0.515E-04	0.104E+01
0.473E-04	0.106E+01
0.434E-04	0.109E+01
0.363E-04	0.111E+01
0.339E-04	0.113E+01
0.124E-04	0.115E+01
0.343E-04	0.118E+01
0.242E-04	0.120E+01
0.264E-04	0.122E+01
0.206E-04	0.125E+01
0.238E-04	0.127E+01
0.366E-04	0.129E+01
0.196E-04	0.131E+01
0.395E-04	0.134E+01
0.326E-04	0.136E+01
0.473E-04	0.138E+01
0.496E-04	0.140E+01
0.448E-04	0.143E+01
0.363E-04	0.145E+01
0.468E-04	0.147E+01
0.450E-04	0.149E+01
0.442E-04	0.152E+01
0.188E-04	0.154E+01
0.360E-04	0.156E+01
0.473E-04	0.158E+01
0.224E-04	0.161E+01
0.395E-04	0.163E+01
0.498E-04	0.165E+01
0.362E-04	0.167E+01
0.526E-04	0.169E+01
0.556E-04	0.172E+01
0.251E-04	0.174E+01
0.430E-04	0.176E+01
0.480E-04	0.179E+01
0.400E-04	0.181E+01
0.603E-04	0.183E+01
0.278E-04	0.185E+01
0.449E-04	0.187E+01
0.347E-04	0.190E+01
0.227E-04	0.192E+01
0.254E-04	0.194E+01
0.505E-04	0.197E+01
0.495E-04	0.199E+01

incompressible term

0.143E-02	0.134E+00
0.118E-02	0.157E+00
0.139E-02	0.180E+00
0.947E-03	0.200E+00
0.733E-03	0.223E+00
0.663E-03	0.243E+00
0.817E-03	0.263E+00
0.664E-03	0.283E+00
0.539E-03	0.306E+00
0.603E-03	0.329E+00
0.526E-03	0.349E+00
0.470E-03	0.371E+00
0.515E-03	0.391E+00
0.423E-03	0.414E+00
0.430E-03	0.437E+00
0.371E-03	0.457E+00
0.284E-03	0.480E+00
0.236E-03	0.503E+00
0.220E-03	0.526E+00
0.277E-03	0.549E+00
0.167E-03	0.571E+00
0.128E-03	0.594E+00
0.111E-03	0.617E+00
0.191E-03	0.640E+00
0.102E-03	0.660E+00
0.121E-03	0.683E+00
0.201E-03	0.706E+00
0.107E-03	0.726E+00
0.693E-04	0.749E+00
0.705E-04	0.769E+00
0.554E-04	0.791E+00
0.176E-04	0.814E+00
0.255E-04	0.837E+00
0.251E-04	0.860E+00
0.265E-04	0.883E+00
0.981E-05	0.906E+00
0.223E-04	0.929E+00
0.169E-04	0.951E+00
0.108E-04	0.974E+00
0.110E-04	0.994E+00
0.130E-04	0.102E+01
0.126E-04	0.104E+01
0.116E-04	0.106E+01
0.107E-04	0.109E+01
0.902E-05	0.111E+01
0.842E-05	0.113E+01
0.339E-05	0.115E+01
0.861E-05	0.118E+01
0.628E-05	0.120E+01
0.677E-05	0.122E+01
0.538E-05	0.125E+01
0.614E-05	0.127E+01
0.918E-05	0.129E+01
0.519E-05	0.131E+01
0.979E-05	0.134E+01
0.820E-05	0.136E+01
0.117E-04	0.138E+01
0.121E-04	0.140E+01
0.109E-04	0.143E+01
0.886E-05	0.145E+01
0.113E-04	0.147E+01
0.108E-04	0.149E+01
0.107E-04	0.152E+01
0.481E-05	0.154E+01
0.878E-05	0.156E+01
0.114E-04	0.158E+01
0.565E-05	0.161E+01
0.959E-05	0.163E+01
0.119E-04	0.165E+01
0.876E-05	0.167E+01
0.126E-04	0.169E+01
0.132E-04	0.172E+01
0.631E-05	0.174E+01
0.104E-04	0.176E+01
0.115E-04	0.179E+01
0.969E-05	0.181E+01
0.144E-04	0.183E+01
0.695E-05	0.185E+01
0.110E-04	0.187E+01
0.871E-05	0.190E+01
0.600E-05	0.192E+01
0.659E-05	0.194E+01

0.125E-04 0.197E+01
0.123E-04 0.199E+01

Fig. 5.26b

Prandtl

4.70E-03 2.23E-01
4.05E-03 2.30E-01
3.49E-03 2.45E-01
2.66E-03 2.65E-01
1.92E-03 2.91E-01
1.40E-03 3.19E-01
1.10E-03 3.48E-01
8.46E-04 3.79E-01
6.23E-04 4.11E-01
4.15E-04 4.44E-01
3.05E-04 4.76E-01
2.03E-04 5.09E-01
1.30E-04 5.42E-01
1.18E-04 5.75E-01
1.91E-04 6.08E-01
1.50E-04 6.41E-01
3.57E-04 6.74E-01
3.41E-04 7.07E-01
2.62E-04 7.40E-01
1.82E-04 7.73E-01
1.19E-04 8.06E-01
7.48E-05 8.39E-01
4.21E-05 8.72E-01
2.36E-05 9.05E-01
2.55E-05 9.38E-01
2.70E-05 9.71E-01
2.15E-05 1.00E+00
1.45E-05 1.04E+00
8.07E-06 1.07E+00
5.20E-06 1.10E+00
3.28E-06 1.14E+00
2.02E-06 1.17E+00
2.19E-06 1.20E+00
9.45E-04 1.23E+00
1.01E-03 1.25E+00
8.06E-04 1.27E+00
5.72E-04 1.28E+00
3.81E-04 1.30E+00
2.44E-04 1.32E+00
1.52E-04 1.35E+00
9.24E-05 1.37E+00
5.55E-05 1.39E+00
3.28E-05 1.42E+00
1.93E-05 1.44E+00
1.12E-05 1.47E+00
8.44E-06 1.49E+00
9.63E-06 1.52E+00
8.41E-06 1.54E+00
5.27E-06 1.57E+00
5.55E-06 1.59E+00
1.08E-05 1.62E+00
1.54E-05 1.64E+00
1.59E-05 1.67E+00
1.43E-05 1.69E+00
1.16E-05 1.71E+00
8.54E-06 1.74E+00
5.89E-06 1.76E+00
3.90E-06 1.79E+00
2.50E-06 1.81E+00
1.58E-06 1.84E+00
9.96E-07 1.86E+00
6.21E-07 1.89E+00
3.88E-07 1.91E+00
2.39E-07 1.94E+00
1.49E-07 1.96E+00
9.12E-08 1.99E+00

Re shear stress

0.138E-01 0.114E+00
0.148E-01 0.131E+00
0.125E-01 0.150E+00
0.142E-01 0.169E+00
0.138E-01 0.186E+00
0.150E-01 0.205E+00
0.152E-01 0.224E+00
0.145E-01 0.243E+00
0.153E-01 0.260E+00
0.160E-01 0.279E+00
0.156E-01 0.298E+00
0.151E-01 0.317E+00
0.132E-01 0.336E+00
0.143E-01 0.352E+00
0.131E-01 0.371E+00
0.160E-01 0.388E+00
0.130E-01 0.407E+00
0.127E-01 0.426E+00
0.150E-01 0.445E+00
0.123E-01 0.464E+00
0.125E-01 0.483E+00
0.115E-01 0.502E+00
0.118E-01 0.521E+00
0.903E-02 0.540E+00
0.797E-02 0.560E+00
0.750E-02 0.579E+00
0.760E-02 0.595E+00
0.841E-02 0.614E+00
0.565E-02 0.633E+00
0.758E-02 0.652E+00
0.588E-02 0.671E+00
0.415E-02 0.693E+00
0.537E-02 0.710E+00
0.405E-02 0.729E+00
0.372E-02 0.748E+00
0.404E-02 0.767E+00
0.369E-02 0.786E+00
0.240E-02 0.805E+00
0.252E-02 0.824E+00
0.228E-02 0.843E+00
0.173E-02 0.862E+00
0.162E-02 0.881E+00
0.113E-02 0.900E+00
0.118E-02 0.917E+00
0.112E-02 0.936E+00
0.818E-03 0.955E+00
0.751E-03 0.974E+00
0.644E-03 0.990E+00
0.556E-03 0.101E+01
0.566E-03 0.103E+01
0.597E-03 0.105E+01
0.551E-03 0.107E+01
0.624E-03 0.109E+01
0.614E-03 0.110E+01
0.608E-03 0.112E+01
0.639E-03 0.114E+01
0.565E-03 0.116E+01
0.678E-03 0.118E+01
0.678E-03 0.120E+01
0.591E-03 0.122E+01
0.750E-03 0.124E+01
0.685E-03 0.125E+01
0.685E-03 0.127E+01
0.777E-03 0.129E+01
0.741E-03 0.131E+01
0.892E-03 0.133E+01
0.747E-03 0.135E+01
0.887E-03 0.137E+01
0.942E-03 0.139E+01
0.924E-03 0.140E+01
0.882E-03 0.142E+01
0.962E-03 0.144E+01
0.970E-03 0.146E+01
0.960E-03 0.148E+01
0.111E-02 0.150E+01
0.112E-02 0.152E+01
0.111E-02 0.154E+01
0.107E-02 0.155E+01
0.114E-02 0.157E+01
0.119E-02 0.159E+01
0.111E-02 0.161E+01
0.123E-02 0.163E+01
0.134E-02 0.165E+01
0.129E-02 0.167E+01
0.155E-02 0.169E+01
0.236E-02 0.170E+01
0.212E-02 0.172E+01
0.230E-02 0.174E+01
0.235E-02 0.176E+01
0.197E-02 0.178E+01
0.160E-02 0.180E+01
0.167E-02 0.181E+01
0.160E-02 0.183E+01
0.159E-02 0.185E+01
0.141E-02 0.187E+01
0.145E-02 0.189E+01
0.152E-02 0.191E+01
0.155E-02 0.193E+01
0.141E-02 0.195E+01
0.135E-02 0.197E+01
0.137E-02 0.199E+01

incompressible term

0.564E-02 0.114E+00
0.587E-02 0.131E+00
0.476E-02 0.150E+00
0.532E-02 0.169E+00
0.499E-02 0.186E+00
0.522E-02 0.205E+00
0.509E-02 0.224E+00
0.466E-02 0.243E+00
0.480E-02 0.260E+00
0.486E-02 0.279E+00
0.467E-02 0.298E+00
0.436E-02 0.317E+00
0.375E-02 0.336E+00
0.399E-02 0.352E+00
0.361E-02 0.371E+00
0.436E-02 0.388E+00
0.346E-02 0.407E+00
0.335E-02 0.426E+00
0.384E-02 0.445E+00
0.314E-02 0.464E+00
0.319E-02 0.483E+00
0.288E-02 0.502E+00
0.291E-02 0.521E+00
0.224E-02 0.540E+00
0.197E-02 0.560E+00
0.184E-02 0.579E+00
0.188E-02 0.595E+00
0.208E-02 0.614E+00
0.140E-02 0.633E+00
0.186E-02 0.652E+00
0.143E-02 0.671E+00
0.100E-02 0.693E+00
0.130E-02 0.710E+00
0.975E-03 0.729E+00
0.903E-03 0.748E+00
0.977E-03 0.767E+00
0.904E-03 0.786E+00
0.591E-03 0.805E+00
0.618E-03 0.824E+00
0.555E-03 0.843E+00
0.428E-03 0.862E+00
0.399E-03 0.881E+00
0.282E-03 0.900E+00
0.293E-03 0.917E+00
0.277E-03 0.936E+00
0.205E-03 0.955E+00
0.189E-03 0.974E+00
0.163E-03 0.990E+00
0.142E-03 0.101E+01
0.147E-03 0.103E+01
0.157E-03 0.105E+01
0.146E-03 0.107E+01
0.166E-03 0.109E+01
0.164E-03 0.110E+01
0.163E-03 0.112E+01
0.168E-03 0.114E+01
0.148E-03 0.116E+01
0.176E-03 0.118E+01
0.175E-03 0.120E+01
0.152E-03 0.122E+01
0.193E-03 0.124E+01
0.176E-03 0.125E+01
0.175E-03 0.127E+01
0.199E-03 0.129E+01
0.188E-03 0.131E+01
0.226E-03 0.133E+01
0.187E-03 0.135E+01
0.222E-03 0.137E+01
0.236E-03 0.139E+01
0.231E-03 0.140E+01
0.219E-03 0.142E+01
0.241E-03 0.144E+01
0.241E-03 0.146E+01
0.240E-03 0.148E+01
0.276E-03 0.150E+01
0.279E-03 0.152E+01
0.277E-03 0.154E+01
0.266E-03 0.155E+01
0.290E-03 0.157E+01
0.313E-03 0.159E+01
0.292E-03 0.161E+01
0.320E-03 0.163E+01
0.330E-03 0.165E+01
0.303E-03 0.167E+01

0.331E-03	0.169E+01
0.491E-03	0.170E+01
0.407E-03	0.172E+01
0.451E-03	0.174E+01
0.458E-03	0.176E+01
0.377E-03	0.178E+01
0.301E-03	0.180E+01
0.310E-03	0.181E+01
0.294E-03	0.183E+01
0.292E-03	0.185E+01
0.258E-03	0.187E+01
0.264E-03	0.189E+01
0.275E-03	0.191E+01
0.278E-03	0.193E+01
0.254E-03	0.195E+01
0.240E-03	0.197E+01
0.244E-03	0.199E+01

Fig. 5.27

u/U_e data

0.696	0.126
0.714	0.140
0.783	0.177
0.843	0.211
0.872	0.249
0.882	0.286
0.897	0.323
0.921	0.360
0.933	0.397
0.941	0.434
0.949	0.469
0.957	0.509
0.973	0.543
0.980	0.583
0.984	0.620
0.983	0.657
0.981	0.694
0.987	0.731
0.996	0.769
0.997	0.806
0.998	0.843
0.998	0.880
1.000	0.917
1.000	0.954
1.000	0.991
1.000	1.031
1.000	1.066
1.000	1.106
1.001	1.143
1.000	1.180
1.000	1.217
1.001	1.254
1.001	1.291
1.002	1.329
1.002	1.366
1.003	1.403
1.004	1.440
1.005	1.477
1.005	1.514
1.006	1.546
1.006	1.551
1.006	1.586
1.006	1.623
1.007	1.660
1.008	1.697
1.008	1.734
1.008	1.771
1.009	1.809
1.009	1.846
1.008	1.883
1.008	1.923
1.004	1.960
1.001	1.997
0.999	2.034

n = 6

0.464159	0.01
0.521001	0.02
0.557426	0.03
0.584804	0.04
0.606962	0.05
0.625689	0.06
0.641972	0.07
0.65642	0.08
0.669433	0.09
0.681292	0.1
0.692201	0.11
0.702312	0.12
0.711744	0.13
0.72059	0.14
0.728923	0.15
0.736806	0.16
0.744289	0.17
0.751413	0.18
0.758215	0.19
0.764724	0.2
0.770968	0.21
0.776969	0.22
0.782747	0.23
0.788319	0.24
0.793701	0.25
0.798906	0.26
0.803947	0.27
0.808835	0.28
0.813579	0.29
0.818189	0.3
0.822672	0.31
0.827037	0.32
0.83129	0.33
0.835436	0.34
0.839482	0.35
0.843433	0.36
0.847293	0.37
0.851067	0.38
0.85476	0.39
0.858374	0.4
0.861914	0.41
0.865383	0.42
0.868783	0.43
0.872118	0.44
0.875391	0.45
0.878604	0.46
0.881758	0.47
0.884858	0.48
0.887904	0.49
0.890899	0.5
0.893844	0.51
0.896741	0.52
0.899593	0.53
0.9024	0.54
0.905164	0.55
0.907886	0.56
0.910568	0.57
0.913211	0.58
0.915817	0.59
0.918386	0.6
0.920919	0.61
0.923419	0.62
0.925884	0.63
0.928318	0.64
0.93072	0.65
0.933091	0.66
0.935433	0.67
0.937745	0.68
0.94003	0.69
0.942287	0.7
0.944517	0.71
0.946721	0.72
0.9489	0.73
0.951054	0.74
0.953184	0.75
0.955291	0.76
0.957374	0.77
0.959435	0.78
0.961475	0.79
0.963492	0.8
0.965489	0.81
0.967466	0.82
0.969422	0.83
0.971359	0.84
0.973277	0.85
0.975176	0.86
0.977057	0.87
0.97892	0.88
0.980765	0.89
0.982593	0.9
0.984404	0.91
0.986199	0.92
0.987978	0.93
0.98974	0.94
0.991488	0.95
0.993219	0.96
0.994936	0.97
0.996639	0.98
0.998326	0.99
1	1

n = 7

0	0
0.517947	0.01
0.57186	0.02
0.605963	0.03
0.631385	0.04
0.651836	0.05
0.669037	0.06
0.683934	0.07
0.697106	0.08
0.708934	0.09
0.719686	0.1
0.729552	0.11
0.738677	0.12
0.747172	0.13
0.755124	0.14
0.762603	0.15
0.769667	0.16
0.776362	0.17
0.782727	0.18
0.788796	0.19
0.794597	0.2
0.800155	0.21
0.80549	0.22
0.810622	0.23
0.815565	0.24
0.820335	0.25
0.824945	0.26
0.829404	0.27
0.833725	0.28
0.837915	0.29
0.841982	0.3
0.845936	0.31
0.849781	0.32
0.853525	0.33
0.857173	0.34
0.86073	0.35
0.864201	0.36
0.86759	0.37
0.870902	0.38
0.874139	0.39
0.877307	0.4
0.880407	0.41
0.883443	0.42
0.886418	0.43
0.889334	0.44
0.892193	0.45
0.894999	0.46
0.897753	0.47
0.900457	0.48
0.903113	0.49
0.905724	0.5
0.90829	0.51
0.910813	0.52
0.913294	0.53
0.915737	0.54
0.91814	0.55
0.920507	0.56
0.922837	0.57
0.925133	0.58
0.927395	0.59
0.929624	0.6
0.931822	0.61
0.933989	0.62
0.936126	0.63
0.938235	0.64
0.940315	0.65
0.942368	0.66
0.944395	0.67
0.946396	0.68
0.948371	0.69
0.950323	0.7
0.95225	0.71
0.954155	0.72
0.956037	0.73
0.957897	0.74
0.959736	0.75
0.961553	0.76
0.963351	0.77
0.965128	0.78
0.966886	0.79
0.968625	0.8
0.970346	0.81

0.972048 0.82
0.973733 0.83
0.9754 0.84
0.97705 0.85
0.978684 0.86
0.980302 0.87
0.981904 0.88
0.98349 0.89
0.985061 0.9
0.986617 0.91
0.988159 0.92
0.989686 0.93
0.9912 0.94
0.992699 0.95
0.994185 0.96
0.995658 0.97
0.997118 0.98
0.998565 0.99
1 1

n = 8

0 0
0.562341 0.01
0.613238 0.02
0.645119 0.03
0.66874 0.04
0.687656 0.05
0.703508 0.06
0.717195 0.07
0.729266 0.08
0.740083 0.09
0.749894 0.1
0.758882 0.11
0.767181 0.12
0.774895 0.13
0.782107 0.14
0.788881 0.15
0.795271 0.16
0.80132 0.17
0.807066 0.18
0.812539 0.19
0.817765 0.2
0.822768 0.21
0.827566 0.22
0.832178 0.23
0.836616 0.24
0.840896 0.25
0.845029 0.26
0.849025 0.27
0.852893 0.28
0.856643 0.29
0.860281 0.3
0.863814 0.31
0.867249 0.32
0.870591 0.33
0.873846 0.34
0.877018 0.35
0.880112 0.36
0.883131 0.37
0.88608 0.38
0.888962 0.39
0.89178 0.4
0.894536 0.41
0.897235 0.42
0.899878 0.43
0.902468 0.44
0.905006 0.45
0.907496 0.46
0.909939 0.47
0.912337 0.48
0.914691 0.49
0.917004 0.5
0.919277 0.51
0.921511 0.52
0.923708 0.53
0.925868 0.54
0.927994 0.55
0.930087 0.56
0.932147 0.57
0.934176 0.58
0.936174 0.59
0.938143 0.6
0.940083 0.61
0.941996 0.62
0.943882 0.63
0.945742 0.64
0.947576 0.65
0.949386 0.66
0.951173 0.67
0.952936 0.68
0.954676 0.69
0.956395 0.7
0.958092 0.71
0.959769 0.72
0.961425 0.73
0.963061 0.74
0.964679 0.75
0.966277 0.76
0.967857 0.77
0.96942 0.78
0.970965 0.79
0.972492 0.8
0.974004 0.81
0.975499 0.82
0.976978 0.83
0.978442 0.84
0.97989 0.85
0.981324 0.86
0.982743 0.87
0.984148 0.88
0.985539 0.89
0.986916 0.9
0.98828 0.91
0.989631 0.92
0.99097 0.93
0.992295 0.94
0.993609 0.95
0.99491 0.96
0.9962 0.97
0.997478 0.98
0.998744 0.99
1 1

Fig. 5.28a

u"/U

-.0035 1.8
-0.00212 0.112
-0.00193 0.397
-0.0003 0.682
-1E-05 0.966
2.98E-06 1.256
-0.00323 0.112
-0.00267 0.397
-2.3E-05 0.682
3.59E-05 0.966

v"/U

0.00148 0.112
0.00163 0.397
0.000553 0.682
8.47E-05 0.966
6.49E-05 1.256

w"/U

0.00106 0.112
0.00135 0.397
-0.00018 0.682
-2.5E-05 0.966

Fig. 5.28b

xy-plane

0.00143 0.134
0.00118 0.157
0.00139 0.18
0.000947 0.2
0.000733 0.223
0.000663 0.243
0.000817 0.263
0.000664 0.283
0.000539 0.306
0.000603 0.329
0.000526 0.349
0.00047 0.371
0.000515 0.391
0.000423 0.414
0.00043 0.437
0.000371 0.457
0.000284 0.48
0.000236 0.503
0.00022 0.526
0.000277 0.549
0.000167 0.571
0.000128 0.594
0.000111 0.617
0.000191 0.64
0.000102 0.66
0.000121 0.683
0.000201 0.706
0.000107 0.726
6.93E-05 0.749
7.05E-05 0.769
5.54E-05 0.791
1.76E-05 0.814
2.55E-05 0.837
2.51E-05 0.86
2.65E-05 0.883
9.81E-06 0.906
2.23E-05 0.929
1.69E-05 0.951
1.08E-05 0.974
1.1E-05 0.994
1.3E-05 1.02
1.26E-05 1.04
1.16E-05 1.06
1.07E-05 1.09
9.02E-06 1.11
8.42E-06 1.13
3.39E-06 1.15
8.61E-06 1.18
6.28E-06 1.2
6.77E-06 1.22
5.38E-06 1.25
6.14E-06 1.27
9.18E-06 1.29
5.19E-06 1.31
9.79E-06 1.34
8.2E-06 1.36
1.17E-05 1.38
1.21E-05 1.4
1.09E-05 1.43
8.86E-06 1.45
1.13E-05 1.47
1.08E-05 1.49
1.07E-05 1.52
4.81E-06 1.54
8.78E-06 1.56
1.14E-05 1.58
5.65E-06 1.61
9.59E-06 1.63
1.19E-05 1.65
8.76E-06 1.67
1.26E-05 1.69
1.32E-05 1.72
6.31E-06 1.74
1.04E-05 1.76
1.15E-05 1.79
9.69E-06 1.81
1.44E-05 1.83
6.95E-06 1.85
1.1E-05 1.87
8.71E-06 1.9
6E-06 1.92
6.59E-06 1.94
1.25E-05 1.97
1.23E-05 1.99

xz plane shear

0.00123 0.134
0.00128 0.157
0.000964 0.18
0.000963 0.2
0.000634 0.223
0.00055 0.243
0.000377 0.263
0.000295 0.283
0.000317 0.306
0.00055 0.329
0.000549 0.349
0.000412 0.371
0.000258 0.391
5.29E-05 0.414
3.2E-05 0.437
-4.6E-05 0.457
-0.00013 0.48
-0.00012 0.503
-0.00012 0.526

-0.00012	0.549
-0.00011	0.571
-0.00013	0.594
-0.00012	0.617
-9.9E-05	0.64
-7.6E-05	0.66
-0.00013	0.683
-8E-05	0.706
-7.6E-05	0.726
-5.2E-05	0.749
-7.8E-05	0.769
-0.00013	0.791
-1.1E-05	0.814
-7E-05	0.837
-2.2E-05	0.86
-2.8E-05	0.883
-1.1E-05	0.906
-1.5E-05	0.929
-1.2E-05	0.951
-5.8E-06	0.974
-6.5E-06	0.994
-1E-05	1.02
-8.2E-06	1.04
-5.2E-06	1.06
-7.7E-06	1.09
-4.4E-06	1.11
-5.6E-06	1.13
-8E-06	1.15
-7.5E-06	1.18
-8E-06	1.2
-8.5E-06	1.22
-7.1E-06	1.25
-7E-06	1.27
-8.1E-06	1.29
-7.1E-06	1.31
-3.9E-06	1.34
-7.9E-06	1.36
-4.6E-06	1.38
-4.5E-06	1.4
9.78E-08	1.43
-3.3E-07	1.45
-3.3E-06	1.47
-4.2E-06	1.49
-3.8E-06	1.52
-6.7E-06	1.54
-5E-06	1.56
-7.6E-06	1.58
-5.8E-06	1.61
-4.2E-06	1.63
-5.7E-06	1.65
-5.6E-06	1.67
-5E-06	1.69
-5.8E-06	1.72
-6.8E-06	1.74
-4E-06	1.76
-6.3E-06	1.79
-6.3E-06	1.81
-7.6E-06	1.83
-2.9E-06	1.85
-6.5E-06	1.87
-1.2E-05	1.9
-9.1E-06	1.92
-1E-05	1.94
-1.2E-05	1.97
-7E-06	1.99

xy-plane mohr

0.174E-02	.111
0.626E-03	.397
0.155E-03	.683
0.133E-04	.969
0.956E-05	1.254

xz-plane mohr

0.487E-02	.112
0.837E-03	.397
-0.164E-04	.682
0.670E-05	.966

Bibliography

1. Hirsch, C., *Numerical Computation of Internal and External Flows*, Vol. 2, John Wiley & Sons, New York, 1990.

2. Shang, J. S., and Scherr, S. J., "Navier Stokes Solution of the Flow Field Around a Complete Aircraft," AIAA Paper 85-1509, 1985.

3. Anderson, D. A., Tannehill, J. C., and Pletcher, R. H., *Computational Fluid Mechancs and Heat Transfer*, McGraw-Hill, New York, 1984.

4. Settles, G. S., and Dodson, L. J., "Supersonic and Hypersonic Shock/Boundary-Layer Interaction Database," *AIAA Journal*, Vol. 32, No. 7, July 1994.

5. Anderson, J.D., *Computational Fluid Dynamics: The Basics with Applications* (manuscript), Department of Aerospace Engineering, University of Maryland, College Park, MD, 1992.

6. Rose, W. C., and Childs, M.E., "Reynolds-Shear-Stress Measurements in a Compressible Boundary Layer Within a Shock-Wave-Induced Adverse Pressure Gradient," *Journal of Fluid Mechanics*, Vol. 65, Part 1, pp. 177-188, 1974.

7. Liou, W.W., and Shih, T.-H., "On the Basic Equations for the Second-Order Modeling of Compressible Turbulence," NASA TM 105277, October 1991.

8. Visbal, M., and Knight, D., "Evaluation of the Baldwin-Lomax Turbulence Model For Two-Dimensional Shock-Wave Boundary-Layer Interactions," AIAA Paper 83-1697, 1983.

9. Wilcox, D. C., "Comparison of Two-Equation Turbulence Models for Boundary Layers with Pressure Gradient," *AIAA Journal*, Vol. 31, No. 8, August 1993.

10. Rose, W. C., and Murphy, J. D., "Ratio of Reynolds Shear Stress to Turbulence Kinetic Energy in a Boundary Layer," *Physics of Fluids*, Vol. 16, No. 6, pp. 935-937, June 1973.

11. Clauser, F. H., "Turbulent Boundary Layers in Adverse Pressure Gradients," *Journal of the Aeronautical Sciences*, pp 91-108, February 1954.

12. Schetz, J. A., *Boundary Layer Analysis*, Prentice-Hall, Englewood Cliffs, NJ, 1993.

13. Tennekes, H., and Lumley, J. L., *A First Course in Turbulence*, MIT Press, Cambridge, MA, 1972.

14. Baldwin, B.S., and Lomax, H., "Thin Layer Approximation and Algebraic Model for Separated Turbulent Flows," AIAA Paper 78-257, 1978.

15. Hamed, A., and Shang, J.S., "Survey and Assessment of Validation Data Base For Shock-Wave Boundary-Layer Interactions in Supersonic Inlets," AIAA Paper 89-2939, 1989.

16. Munson, B.R., Young, D.F., and Okiishi, T.H., *Fundamentals of Fluid Mechanics*, John Wiley & Sons, New York, 1990.

17. Bowersox, R.D.W., "Aero 827 Class Notes," Air Force Institute of Technology, Wright-Patterson Air Force Base, OH, 1994.

18. Bowersox, R. D. W., and Schetz, J. A., "Compressible Turbulence Measurements in a High-Speed High-Reynolds-Number Mixing Layer," *AIAA Journal*, Vol. 32, No. 4, pp. 758-764, April 1994.

19. Schetz, J.A., *Foundations of Boundary Layer Theory for Momentum, Heat Transfer, and Mass Transfer*, Englewood Cliffs, N.J., 1984.

20. *Probe Catalog*, Omega Engineering, Inc., 1988.

21. Anderson, J. D., Jr., *Fundamentals of Aerodynamics*, Second Edition, McGraw-Hill, Inc., New York, 1991.

22. *Nicolet Systems Operation*, Nicolet, Madison, WI, 1991.

23. Volluz, R.J., *Handbook of Supersonic Aerodynamics*, Section 20, "Wind Tunnel Instrumentation and Opertions, NAVORD Report 1988, Vol. 6, 1961.

24. "Hot-Wire/Hot Film Anemometry," TSI Incorporated, St. Paul, MN, 1988.

25. "Instruction Manual--IFA 100 System/Intelligent Flow Analyzer," TSI Incorporated, St. Paul, MN, 1987.

26. Bowersox, R.D.W., "Compressible Turbulence in a High-Speed High-Reynolds Number Mixing Layer," PhD Dissertation, Virginia Polytechnic Institute and State University, VA, Department of Aerospace Engineering, September 1992.

27. McClure, W.B., "Plotter User's Manual," Department of Aeronautics, USAF Academy, March 1993.

28. Kovaszney, L.S.G., "The Hot-Wire Anemometer in Supersonic Flow," *Journal of Aeronautical Science*, Vol. 17, 1950, pp. 565-584.

29. Bowersox, R.D.W., "Thermal Anemometry, " in *Handbook of Fluid Dynamics* (Schetz, J.A. and Fuhs, W., eds.), John Wiley & Sons, 1995.

30. Kistler, A., "Fluctuation Measurements in a Supersonic Turbulent Boundary Layer," *Physics of Fluids*, 2, 220, 1959.

31. Bowersox, R.D.W., "MSHEaR User's Manual," Department of Aeronautics, Air Force Institute of Technology, Wright-Patterson AFB, Ohio, Summer 1994.

32. Waltrup, P.J., and Schetz, J.A., "Supersonic Turbulent Boundary Layer Subjected to Adverse Pressure Gradients," *AIAA Journal*, Vol. 11, No. 1, pp. 50-57, January 1973.

33. Sturek, W.B., and Danberg, J.E., "Supersonic Turbulent Boundary Layer in Adverse Pressure Gradient. Part I: The Experiment," AIAA Journal, Vol. 10, No. 4, pp. 475-480, April 1972.

34. Horowitz, P., and Hill, W., *The Art of Electronics*, Second Edition, Cambridge University Press, New York, 1989, p. 665.

35. White, F.M., *Viscous Fluid Flow*, Second Edition, McGraw-Hill, Inc., New York, 1991.

Vita

The author, the son of William and Wilma Dotter, was born in Beloit, Wisconsin on August 5, 1970. He graduated from Beloit Memorial High School in 1989, and from the United States Air Force Academy in June 1993, with a Bachelor's degree in aeronautical engineering. He entered the Air Force Institute of Technology in July 1993, and completed his Master's degree in December 1994.

REPORT DOCUMENTATION PAGE

Form Approved
OMB No. 0704-0188

1. AGENCY USE ONLY *(Leave blank)*	2. REPORT DATE	3. REPORT TYPE AND DATES COVERED
	December 1994	Master's thesis

4. TITLE AND SUBTITLE

COMPRESSIBLE TURBULENCE MEASUREMENTS IN A SUPERSONIC FLOW WITH ADVERSE PRESSURE GRADIENT

5. FUNDING NUMBERS

6. AUTHOR(S)

Jon W. Dotter, Second Lieutenant, USAF

7. PERFORMING ORGANIZATION NAME(S) AND ADDRESS(ES)

Air Force Institute of Technology, WFAFB, OH 45433

8. PERFORMING ORGANIZATION REPORT NUMBER

AFIT/GAE/ENY/94D-10

9. SPONSORING / MONITORING AGENCY NAME(S) AND ADDRESS(ES)

Dr. James McMichael/AFOSR/WPAFB, OH 45433

10. SPONSORING / MONITORING AGENCY REPORT NUMBER

11. SUPPLEMENTARY NOTES

12a. DISTRIBUTION / AVAILABILITY STATEMENT

Approved for public release; distribution unlimited

12b. DISTRIBUTION CODE

13. ABSTRACT *(Maximum 200 words)*

Mean flow and compressible turbulence measurements have been obtained upstream and within a shock boundary interaction and a compression ramp in Mach 3 flow. Compressible turbulence models have met with little success in the accurate prediction of high-speed flows involving complicated shock boundary interactions and adverse pressure gradients because of a crucial lack of experimental data. Data were collected using conventional Pitot and cone-static probes, single overheat cross-wire anemometry, multiple overheat cross-wire anemometry, and flow visualization techniques. Direct measurements of the total Reynolds shear stress were obtained using a turbulence transformation. Results indicate that compressibility effects, as evidenced by the density fluctuations, are large relative to the velocity fluctuations and should be accounted for rigorously in new turbulence models.

14. SUBJECT TERMS

Supersonic turbulent boundary layers, Reynolds-averaged Navier-Stokes equations, Shock boundary layers, Adverse pressure gradients

15. NUMBER OF PAGES
119

16. PRICE CODE

17. SECURITY CLASSIFICATION OF REPORT	18. SECURITY CLASSIFICATION OF THIS PAGE	19. SECURITY CLASSIFICATION OF ABSTRACT	20. LIMITATION OF ABSTRACT
Unclassified	Unclassified	Unclassified	UL